THE UNIVERSITY *of* EDINBURGH

Investigating the Molecular Mechanisms of Mutant *C9orf72* Human iPSC-derived Astrocyte-Mediated Motor Neuron Deficits

Maria Stavrou

BSc (Hons), MBBS, MRCP (Neuro)

A thesis submitted for the degree of

Doctor of Philosophy

2023

Supervisors

Siddharthan Chandran

Giles Hardingham

College of Medicine and Veterinary Medicine
University of Edinburgh, United Kingdom

Declaration

I, Maria Stavrou, declare that this thesis has been composed solely by myself and that it has not been submitted, in whole or in part, in any previous application for a degree. Except where stated otherwise by reference or acknowledgment, the work presented is entirely my own.

Validation of the pluripotency of iPSCs was performed by Dr Karen Burr and Jyoti Nanda. Samples for karyotyping were prepared by Dr Karen Burr, Dr Bhuvaneish T. Selvaraj and Jyoti Nanda. Maintenance of iPSC lines and derivation of motor neurons from iPSCs were conducted by Dr Karen Burr, Jyoti Nanda, Dr Bhuvaneish T. Selvaraj and Alessandra Cardinali. Bioinformatics was implemented by Drs Owen Dando and Xin He. Mass spectrometry analysis of isolated exosome and soluble factors was conducted by Dr Alfonso Bolado Carrancio (collaboration with Professor Margaret Frame's lab, Institute of Genetics and Cancer – IGC, University of Edinburgh). Reverse phase protein array (RPPA) was undertaken at the IGC RPPA facility by Kenneth Macleod (collaboration with Professor Neil Carragher's group, Institute of Genetics and Cancer, University of Edinburgh). Imaging of mitochondria labelled with MitoTracker Red CMXRos was carried out by Dr Justyna Cholewa-Waclaw at the Centre for Regenerative Medicine using Opera Phenix Plus high-content screening system.

Signature: Maria Stavrou

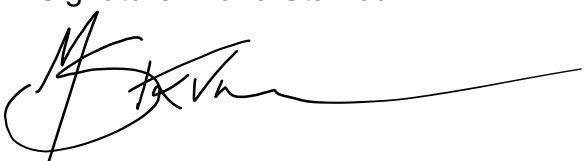

Date: 30/12/2022

Acknowledgements

I owe thanks and gratitude to many people for their unwavering help, mentorship, and guidance during the preparation of this work, as well as for offering me the autonomy to hypothesize and experiment.

In particular:

- My supervisors Siddharthan Chandran and Giles Hardingham.
- My bench supervisor Bhuvaneish T. Selvaraj.
- All members of the Chandran and Hardingham labs.
- The 1-year Rowling Scholars Scheme that unlocked for me the time required to drive and develop my research proposal and laid the foundations for securing independent funding for my PhD studies through the MRC Clinical Research Training Fellowship (August 2019 – August 2022).

Finally, I would like to thank my family and especially my wonderful partner Nicos for all his love and support, right from the very beginning, through every step along the way.

Lay Summary

How bad is it doctor? How long do I have? Why aren't there any treatments doctor? Those were the questions I was asked by a 35-year-old man on the day I conveyed the devastating diagnosis of Amyotrophic Lateral Sclerosis or ALS to him. The day when his life's path was irreversibly altered, the day when his roles as a partner, parent, professional, caregiver blurred into that of the patient. Within a year, this fit young man became wheelchair- and respirator-dependent, and six months after that he succumbed to the disease.

ALS is a degenerative and deadly neurological disorder, with 80% of patients dying within 5 years of diagnosis. The shocking pace of the disease results in a frightening journey of physical decline for the patients, who lose the ability to move their arms and their legs, speak, swallow and eventually, breathe.

Although important discoveries about ALS have been made, disappointingly, the knowledge has not yet turned into clinical breakthroughs to make a difference to our patients. To date no cure has been found. Why? Firstly, the brain is the most complex organ of the body and traditionally, drugs have been tested in animals rather than humans. As Alexander Pope said, 'the proper study of mankind is man'. Secondly, the brain cells that neighbour the nerve cells have long been neglected.

The building blocks of the brain are the nerve cells called neurons, but they do not live in isolation. They're surrounded by cells called glia (from the Greek word meaning 'glue') that are important for the growth and survival of neurons. Amongst the three types of glial cells, the astrocytes - named for their star-like shape - are the largest and most numerous brain cells in humans compared to all animal species. If the human brain were the night sky, the astrocytes would be the twinkling stars infusing it with brightness and vitality. Astrocytes are now in the neuroscience limelight. They regulate nerve cells and their environment by providing essential nutrients, cleaning up waste and helping to repair the damaged brain and spinal cord.

My research focuses on understanding the role of astrocytes in ALS. With the help of stem cell technology and scientific 'cookery', I studied 'human disease in a dish'. I compared astrocytes from healthy individuals with those from people with ALS carrying a specific gene mutation. This gene mutation is the most common genetic cause of ALS. I grew the healthy and ALS astrocytes with human motor neurons and examined their effects on the health of the neurons and on the movement and energy levels in mitochondria – the power supply to the motor neurons. We discovered that the movement of mitochondria, which travel up and down in nerve axons – the nerve axons are the long, thin structures in nerve cells in which electrical impulses are generated – is impaired when diseased ALS astrocytes are in direct, physical contact with healthy neurons.

Crucially, healthy astrocytes repaired the movement of mitochondria in nerve cells obtained from people with ALS. We showed that diseased astrocytes were not only responsible for hindering energy supply from the mitochondria in nerve cells, but that their own mitochondria were also defective. By boosting the mitochondria in those astrocytes, the nerve axons reverted to normal and the nerve cell's energy source was restored. This work has provided novel evidence that by manipulating astrocytes in ALS, we can protect the nerve cells and their connection to muscles from degeneration. Work is underway for identification of existing licensed medications that boost mitochondria in astrocytes that can rescue the nerve cells, aiming to slow, stop or even reverse the disease process.

Through our research and the ongoing support from people with ALS, I do think that the day we might be able to repair the damaged brain will come sooner than we think.

Abstract

Amyotrophic Lateral Sclerosis (ALS) is a progressive, incurable, and invariably fatal neurodegenerative condition characterised by loss of motor neurons (MNs). In addition, cellular abnormalities in ALS have long been known not to be restricted to MNs. Over the last two decades, there are multiple lines of evidence from pathology, genetics and experimental systems that implicate a central role for non-neuronal cells, astrocytes in particular, with ALS pathogenesis. This is not surprising given the intimate structural and functional association of astrocytes with, inter alia, the synapse and vasculature.

The finding that sporadic and familial ALS are largely phenotypically and pathologically indistinguishable highlights the value of studying familial ALS to shed mechanistic insight into this condition. Intronic hexanucleotide repeat expansion (G4C2) in the *C9orf72* gene is the commonest cause of inherited ALS and accounts for approximately 10% of sporadic ALS cases. Studies to date have largely focused on the consequences of *C9orf72* in MNs. In comparison, the cell autonomous and non-cell autonomous consequences of *C9orf72* in astrocytes are comparatively understudied and the underpinning molecular mechanisms remain grossly unexplored. One powerful strategy to interrogate the role of astrocytes in ALS is to harness genetic discoveries with human induced pluripotent stem cells (hiPSC) and gene editing technologies. The generation of paired gene-edited controls, where the only variable is the mutation of interest, allows causality to be assigned to any given phenotype.

Against this background, during my PhD I used multiple independent patient-derived induced pluripotent stem cell astrocytes and MNs, harbouring the *C9orf72* mutation along with paired gene-corrected controls and undertook a series of studies to investigate (1) astrocyte-mediated contact-dependent mechanisms through mixed-species RNA-Seq for determination of transcriptional dysregulation in wildtype primary rodent MNs induced by cocultured *C9orf72* astrocytes; and (2) astrocyte-mediated non-contact-dependent mechanisms by performing transcriptomic and proteomic analysis on MNs treated with astrocyte conditioned medium (ACM), and comprehensive profiling of ACM by mass spectrometry.

Importantly, the present study uncovers a hitherto unreported mechanism of axonal transport that relies on astrocyte-neuronal interaction. Although disrupted axonal transport, altered mitochondrial bioenergetics and astrocyte dyshomeostasis have been implicated in the aetiopathology of ALS, the role of astrocytes in regulating axonal transport and neuronal bioenergetic status is unknown. Here, it is shown that the astrocyte genotype directly regulates axonal transport. Specifically, in coculture, (i) C9-mutant astrocytes induce axonal transport deficits in control MNs and (ii) control astrocytes reverse the axonal deficit found in monocultures of C9-mutant MNs. Moreover, this work demonstrates cell and non-cell autonomous C9-mutant astrocyte effects on mitochondrial bioenergetic function. Finally, selective genetically mediated boosting of mitochondrial bioenergetic activity in C9-mutant astrocytes rescues astrocyte-mediated axonal transport deficits observed in coculture with control or C9-mutant MNs.

Collectively, these data suggest a novel role of astrocytes in regulating axonal transport which is mediated through astrocyte-neuronal metabolic crosstalk, providing evidence for astrocyte metabolism as a potential ALS therapeutic target.

Table of Contents

Table of Figures & Tables

Abbreviations

ACM – astrocyte conditioned medium
ALS – amyotrophic lateral sclerosis
AMPA – α-amino-3-hydroxy-5-methyl-4-isoxazolepropionic acid
APC – astrocyte progenitor cell
ASO – antisense oligonucleotide
ATP – adenosine triphosphate
BAC – bacterial artificial chromosome
BBB – blood brain barrier
BDNF – brain-derived neurotrophic factor
C9orf72 – chromosome 9 open reading frame 72
C9Δ – gene-corrected line
Cas9 – CRISPR-associated protein 9
cDNA – complementary DNA
CNS – central nervous system
CNTF – ciliary neurotrophic factor
CRISPR – clustered regularly interspaced short palindromic repeats
CSPG – chondroitin sulfate proteoglycans
DEGs – differentially expressed genes
DENN – differentially expressed in normal and neoplasia
DNA – deoxyribonucleic acid
DPR – dipeptide repeats
EAAT – excitatory amino acid transporter
EDTA – ethylenediaminetetraacetic acid
EGF – epidermal growth factor
ER – endoplasmic reticulum
fALS – familial Amyotrophic lateral sclerosis
FDA – food and drug administration
FGF2 – fibroblast growth factor 2
FTD – frontotemporal dementia
FUS – fused in sarcoma
G4C2 – GGGGCC

GAPDH – glyceraldehyde-3-phosphate dehydrogenase

GDNF – glial cell line-derived neurotrophic factor

GFAP – glial fibrillary acidic protein

GFP – green fluorescent protein

GLT-1 – glutamate type I transporter

GluR2 – glutamate receptor 2

gRNA – guide RNA

GTP – guanosine triphosphate

GTPase – guanosine triphosphatase

hESC – human embryonic stem cells

hiPSCs – human induced pluripotent stem cells

hnRNP – heterogeneous nuclear ribonucleoprotein

HRE – hexanucleotide repeat expansion

LDH – lactate dehydrogenase

MNs – motor neurons

mRNA – messenger RNA

MT – mitochondria

NFIA – nuclear factor I/A

NHEJ – nonhomologous end-joining

NPCs – neural progenitor cells

PBS – phosphate-buffered saline

PCR – polymerase chain reaction

pwALS – people with Amyotrophic lateral sclerosis

qRT-PCR – quantitative real-time PCR

RA – retinoic acid

RAN – repeat-associated non-ATG

RBP's – RNA-binding proteins

RIPA – radioimmunoprecipitation assay

RNA – ribonucleic acid

RNAse – ribonuclease

ROIs – regions of interest

rRNA – ribosomal RNA

S100B – S100 calcium-binding protein B

sALS – sporadic Amyotrophic lateral sclerosis

SNPs – single nucleotide polymorphisms

SOD1 – superoxide dismutase 1

TARDBP – transactive response DNA binding protein

TDP-43 – TAR DNA-binding protein 43

TGF-β – transforming growth factor β

tRNA – transfer ribonucleic acid

UPIs – ubiquitin-positive inclusions

UPP – ubiquitin proteasome pathway

UPR – unfolded protein response

WT – wildtype

ZFN – zinc finger nuclease

Chapter 1 Introduction

1.1 Disease epidemiology, Clinical Features and Current Management of Amyotrophic lateral sclerosis

Amyotrophic lateral sclerosis (ALS) is a progressive, incurable, and invariably fatal neurodegenerative condition characterised by loss of motor neurons (MNs) in the spinal cord, motor cortex and brainstem. There are about 5000 people living with ALS (pwALS) in the UK at any one time (Opie-Martin *et al.*, 2021). It is the most frequent neurodegenerative disease of mid-life, with a lifetime risk of 1 in 300 and a peak age of onset of about 60 years old ('The UK MND Research Institute', 2021). People with ALS have progressive voluntary muscle weakness involving the arms, legs, speech, swallowing and breathing (Rowland and Shneider, 2001). Currently the median survival time from ALS diagnosis is only 2-3 years, with death ensuing, most frequently, due to diaphragmatic weakness and consequent respiratory failure (Martin *et al.*, 2017). The median survival time from trial entry in the Pooled Resource Open-Access amyotrophic lateral sclerosis (ALS) Clinical Trials (PRO-ACT) database https://nctu.partners.org/ProACT was only 479 days (interquartile range 279–622) (Berry *et al.*, 2014).

Riluzole, a glutamate antagonist, is the only licensed drug in the UK for all ALS subtypes and prolongs survival by 2-3 months. It was approved by the Food and Drug Administration (FDA) in 1995 and by the National Institute for health and care Excellence (NICE) in 2001. In more recent years, Edaravone has been licensed in Japan, USA, Canada, and South Korea for the treatment of ALS. This drug has shown positive outcomes in reducing disease progression in a small subset of pwALS with specific characteristics, measured by the ALSFRS-R, a revised ALS functional rating score, commonly used in ALS trials (Wong *et al.*, 2021). At the end of September 2022, AMX0035 or Relyvrio which is a combination of two compounds, sodium phenylbutyrate and taurursodiol, was approved in the USA and Canada for treating ALS. The experimental therapy was tested on 137 participants who were recently diagnosed with the condition. Data from the Phase II clinical trial (CENTAUR) and its extension study demonstrated that (a) the mean rate of change in the ALSFRS-R

score was −1.24 points per month with the active drug and −1.66 points per month with placebo (difference, 0.42 points per month; 95% confidence interval, 0.03 to 0.81; P = 0.03) (Paganoni *et al.*, 2020) and (b) the survival of patients consistently on Relyvrio was prolonged by a mean of 6.9 months compared to those initially assigned to placebo. Given that this was a small trial for a clinical study with two-thirds of patients enrolled in the treatment group and one-third in the placebo group, which is not uncommon for ALS studies, a larger and longer Phase III trial called PHOENIX was conducted to confirm the efficacy of this therapy in 664 individuals with early ALS. Unfortunately, the PHOENIX trial did not meet its primary or secondary endpoints, and Relyvrio hasn't shown a meaningful effect on disease progression, lung function, or quality of life in ALS patients. As a result, Relyvrio has been taken off the market (Addendum: Relyvrio withdrawn, 2024).

Despite the disappointing results of the PHOENIX trial, over the last decade, significant progress has been made in understanding the molecular mechanisms of ALS. This has led to the emergence of several other investigational medicinal products that target critical pathways dysregulated in ALS pathology such as mitochondrial dysfunction, oxidative stress, RNA metabolism and proteostasis, neuroinflammation and others. Examples of promising candidates include masitinib and ultra-high dose methylcobalamin. Nevertheless, there is no evidence on significant efficacy on survival (Oki *et al.*, 2022), unless the treatments start prior to substantial impairment in functionality (Mora *et al.*, 2021). One particularly promising development in ALS treatment is the drug Tofersen (Qalsody). Tofersen specifically targets the SOD1 gene mutation, which is associated with about 15% of cases of familial ALS. Gene-silencing therapy with Tofersen uses an anti-sense oligonucleotide to downregulate or silence *SOD1* by binding to native mRNA sequences and reducing translation and subsequent toxic protein production (Miller *et al*., 2020). In a dose-escalating trial, intrathecal administration of Tofersen reduced cerebrospinal fluid concentrations of SOD1, in patients with ALS due to SOD1 pathologic variant. A subsequent trial confirmed these findings, showing that Tofersen treatment was associated with reduced disease progression in measures such as ALSFRS-R, vital capacity, and grip strength. These beneficial effects were observed in all patients who received Tofersen, with more significant reductions seen in those who started treatment early in the study (Miller *et al*., 2022). This treatment has already received

recommendations for approval in the European Union and has been granted accelerated approval by the FDA (Miller *et al*., 2022). This targeted approach offers exciting possibilities for the treatment of monogenic ALS.

ALS is the most common form of acquired motor neuron disease and is characterised by the presence of upper and lower motor neuron symptoms and signs, and disease progression; alternative diagnoses should be excluded (Talbot, 2009). A diagnosis relies on the interpretation of clinical history, physical examination and electrodiagnostic studies supported by the El Escorial/Awaji criteria. The Awaji criteria is an adaptation of the El Escorial criteria to better incorporate neurophysiologic data, improve diagnostic sensitivity and obviate diagnostic delay (Costa, Swash and De Carvalho, 2012). Other investigations are undertaken to exclude treatable conditions that mimic ALS. Extra-motor manifestations also contribute to ALS disease burden in a time-dependent manner. It is recognised that 50% of all pwALS will experience cognitive impairment, which is progressive, and out of those, 10-15% will meet the diagnostic criteria for ALS-Frontotemporal dementia (ALS-FTD) with apathy being a key feature (Bak, 2010; Burrell *et al.*, 2016).

Related forms of ALS exist that vary in prognosis and severity and can be crudely grouped into:

1. Progressive muscular atrophy – a progressive disorder that is clinically limited to lower motor neurons.
2. Primary lateral sclerosis – a progressive disorder that is clinically limited to upper motor neurons with duration of symptoms of at least four years since symptom onset.
3. Progressive bulbar palsy with cranial muscle involvement, predominantly the bulbar segment. Commonly, symptoms spread to involve other segments and patients eventually meet criteria for ALS.

This variability in disease presentation and heterogeneity in anatomic location complicate the diagnosis of ALS and collectively result in an average of 12.6 (SD +/- 2.6) months from first clinical symptom to diagnosis (Chiò *et al.*, 2013). Additionally, differences in clinical presentation exist within families of inherited ALS and/or among patients carrying the same pathogenic variant. Individuals carrying a *C9orf72*

expansion, for example, can remain asymptomatic, develop ALS, frontotemporal dementia (FTD), ALS with FTD or an atypical ALS phenotype (Al-Chalabi and Visscher, 2014; Rohrer *et al*., 2015). Approximately 30-50% of individuals carrying the *C9orf72* mutation remain asymptomatic throughout their lives (Murphy *et al*., 2017, Kortazar-Zubizarreta *et al*., 2023).

Furthermore, a comprehensive evaluation is crucial to rule out alternative diagnoses. The differential diagnosis includes conditions such as multifocal motor neuropathy (MMN), cervical radiculomyelopathy, benign fasciculations, inflammatory myopathies, post-polio syndrome, monomelic amyotrophy, hereditary spastic paraplegia, and spinobulbar muscular atrophy (Kennedy disease) (Williams 2013). Kennedy disease, an X-linked disorder due to an expanded CAG repeat in the androgen receptor gene, is characterized by progressive weakness and atrophy of facial, bulbar, and limb muscles. It is also associated with late-onset gynecomastia, defective spermatogenesis, and androgen resistance. Genetic testing for the androgen receptor gene can distinguish ALS from Kennedy disease (Chen *et al*., 2017).

Symptom-based management is the mainstay of treatment for ALS. In fact, given the devastating nature of the disease, multidisciplinary ALS clinics comprising of neurologists, specialist nurses, physiotherapists, speech and language therapists, respiratory experts, dieticians, social workers, and occupational therapists, have developed, with the goal to enhance the quality and quantity of life of pwALS. In the UK, in addition to Riluzole, two other interventions are widely implemented in ALS care. Percutaneous endoscopic gastrostomy (PEG) placement is used for symptomatic dysphagia to ensure sufficient caloric and fluid intake and decrease the risk of aspiration and choking. Although improvement in survival rates has not yet been demonstrated, possible positive effects on fast-progressing patients have been suggested (Ludolph *et al.*, 2020). Non-invasive ventilation is the standard of care for pwALS with respiratory insufficiency and there is evidence that it improves sleep-related symptoms and quality of life, and confers some survival advantage (Martin *et al.*, 2017).

1.2 Aetiology of Amyotrophic lateral sclerosis – Genetics

The cause of ALS is unknown in most cases. However, major pathological and genetic discoveries over the last decade have begun to transform our understanding of the aetiopathogenesis of ALS and related disorders such as frontotemporal dementia (FTD).

ALS is classified as familial (fALS) in the presence of a clear family history of the disease and sporadic (sALS) when this is absent. Although most cases are sporadic, approximately 10-15% are now classified as monogenic fALS, linked to more than 40 causative genes. More than half of these cases are attributed to highly penetrant causal variants in *C9orf72*, Cu/Zn superoxide dismutase (*SOD1)*, TAR DNA binding protein-43 (*TDP-43)* and Fused in sarcoma *(FUS)* (Borg *et al.*, 2021). The *C9orf72* hexanucleotide repeat expansion mutation is the commonest cause (Renton *et al.*, 2011) and is implicated in 40-50% of patients with hereditary ALS and 5-10% of cases with sporadic ALS (Byrne *et al.*, 2012). In the more recent population-based pedigree study by Ryan et al., 2019, it was demonstrated that the mean lifetime heritability of ALS in the *C9orf72* cohort was 52.3%, with the highest estimates recorded in mother-daughter pairings. Even in people without known pathogenic mutations, the lifetime risk of first-degree relatives to develop ALS was higher compared to the general population, accentuating the need to further decode ALS for identification of causative genes. It was concluded that genetic and non-genetic factors contribute equally to one's risk of developing ALS (Ryan *et al.*, 2019).

Aside from cases arising due to disease-causing variants in *SOD1* and *FUS* (< 3% of total ALS), all sporadic and familial ALS display a common pathological signature of mis-accumulation of TAR DNA binding protein 43 (TDP-43) protein, regardless of the mechanisms of disease onset. TDP43 is therefore a central player in ALS pathology. Neuropathologically, sporadic and familial ALS cases are characterised by abnormal cytosolic mislocalisation of ubiquitinated and hyperphosphorylated inclusions of TDP-43 in degenerating neurons and glia cells (Hasegawa *et al.*, 2008). Moreover, apparently sporadic cases have been identified to have gene variants causing familial ALS – the intronic hexanucleotide repeat expansions *C9orf72* are found in 10%, SOD1

mutation in 1-2%, TDP-43 mutation in 1% and FUS mutation in <1% (Su *et al.*, 2014). Genetic risk loci have also been exposed in sALS that include *ATXN2*, *UNC13A*, *SARM1*, *C21orf2*, *SCFD1* and *MOBP* (Borg *et al.*, 2021).

In addition to the common pathological signature of mis-accumulation of TDP43 aggregates, which is also associated with disease initiation, there is evidence for disruption of key common cellular pathways in both sporadic and inherited ALS. These include altered RNA metabolism, impaired protein proteostasis, dysregulated neuronal excitability/excitotoxicity, mitochondrial dysfunction, axonal transport defects, redox imbalance and neuroinflammation (Ling, Polymenidou and Cleveland, 2013; Endo, Komine and Yamanaka, 2016; Taylor, Brown and Cleveland, 2016).

Further, cellular abnormalities in ALS have long been known not to be restricted to MNs. Over the last two decades, there are multiple lines of evidence from pathology, genetics and experimental systems that implicate a central role for non-neuronal cells, astrocytes in particular, with ALS pathogenesis. This is not surprising given the intimate structural and functional association of astrocytes with, *inter alia*, the synapse and vasculature (Fig 1.1).

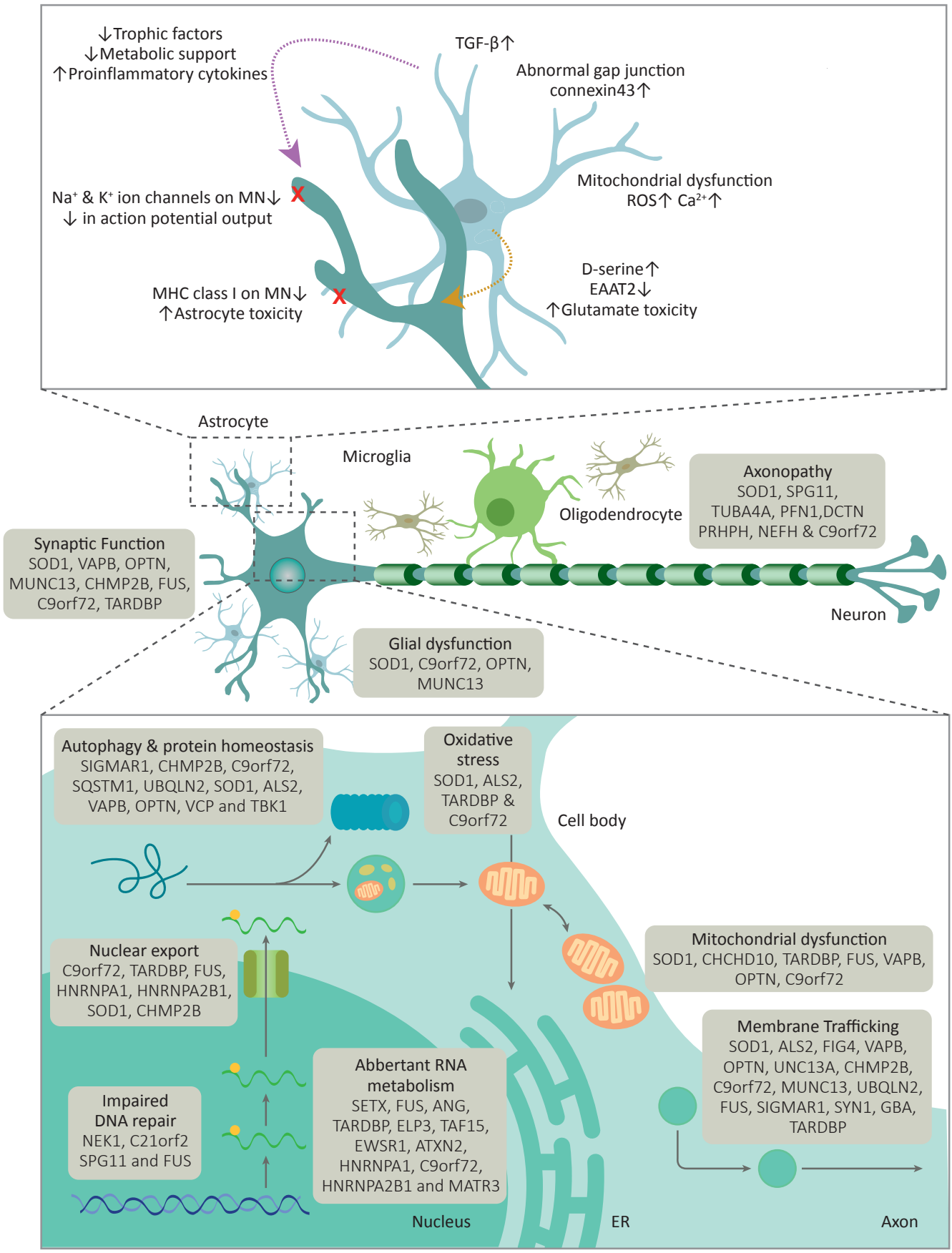

Figure 1.1 The pathophysiology of ALS with a focus on astrocyte involvement [adapted from (Hardiman et al., 2017; Yamanaka and Komine, 2018), with modifications]. ER = endoplasmic reticulum.

1.3 *C9orf72*-mediated Amyotrophic lateral sclerosis

The pathogenic hexanucleotide (GGGGCC) repeat expansion in the non-coding region of chromosome 9 open reading frame 72, *C9orf72*, is the first large non-coding repeat expansion linked to several neurodegenerative conditions including ALS, frontotemporal dementia (FTD), Primary lateral sclerosis (PLS), Progressive muscular atrophy (PMA), Huntington's disease and Alzheimer's disease, with the latter four phenotypes being rarer presentations (Snowden *et al.*, 2012; Kohli *et al.*, 2013). The significant clinical, genetic, and pathological intersections between ALS and FTD has led to the recognition that the two diseases form a broad neurodegenerative continuum.

This expansion mutation is the commonest genetic cause of ALS, accounting for approximately 40% of fALS and 5-10% of sporadic cases (Umoh *et al.*, 2016). It is reported in 1 in 10 of every ALS case among European-ancestry populations, and according to the Scottish register, the *C9orf72* mutation applies to 11 % of the Scottish population (Cleary *et al.*, 2016; Murphy *et al.*, 2017).

Almost all individuals inherit the G4C2 hexanucleotide repeat expansion in an autosomal dominant manner from a heterozygous parent. The expansion is located at the non-coding region between exons 1a and 1b – the gene contains 11 exons – and gives rise to three coding variants (Fig 1.2).

In the normal population, the repeat size varies between 2 and 25, whereas in ALS patients the expansion size ranges between 600 to 5000 repeats. A repeat length of > 30 repeats is commonly used as a diagnostic criterion for pathogenic expansions, but there is lack of consensus on clear cut-off values on minimum hexanucleotide repeats for disease manifestation (DeJesus-Hernandez *et al.*, 2011; Rohrer *et al.*, 2015). Additionally, due to the hexanucleotide repeat instability in somatic cells – somatic mosaicism – the repeat size frequently varies from tissue to tissue and amongst central nervous regions (Van Mossevelde *et al.*, 2017). This leads to discrepant expansion sizes when measured in peripheral blood and the CNS (van Blitterswijk *et al.*, 2015).

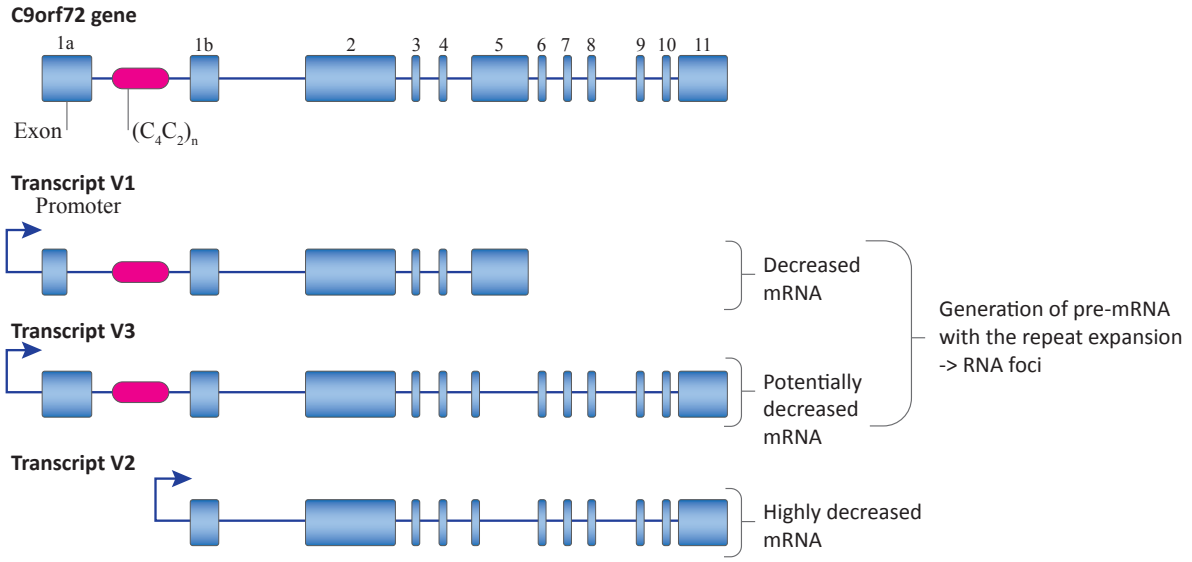

Figure 1.2 The C9orf72 gene and transcripts. A schematic diagram of the *C9orf72* gene and its three transcript variants. The site of the G4C2 repeat region is shown in red and exons are shown in blue. Transcripts V2 and V3 encode the long form of the C9orf72 protein, whereas transcript V1 encodes the short form [adapted from (Haeusler, Donnelly and Rothstein, 2016), with modification].

The mutation shows age-dependent incomplete penetrance, with some patients developing disease in their twenties and a small portion of healthy carriers over the age of 80. According to Murphy et al., 2017, family history does not affect *C9orf72* penetrance, signifying incomplete or lost family history in many sporadic cases. The genetic phenomenon of anticipation – described in trinucleotide repeat disorders such as myotonic dystrophy and Huntington's disease, where a decreasing age of onset and disease severity in succeeding generations is associated with an increased size of expansion – is debated in *C9orf72* ALS/FTD, with conflicting reports on the relationship between the age of onset, symptom severity and repeat expansion length (Gijselinck *et al.*, 2016; Fournier *et al.*, 2019; Jackson *et al.*, 2020). All in all, the expansion's precise size does not provide prognostic information relating to age of onset and disease severity in *C9orf72* repeat expansion carriers.

The G4C2 repeat imparts both loss-of-function and gain-of-function mechanisms that affect neuronal, glial, and immune cell function. These include: (1) loss-of-function, also known as haploinsufficiency, associated with diminished transcription of the *C9orf72* coding region and suppressed protein levels, and (2) gain-of-function through

toxicity from RNA foci and dipeptide repeats. These mechanisms are addressed in detail in the sections below (1.3.1; 1.3.2; 1.3.3). Increasing evidence from experimental models support that toxicity and loss-of-function mechanisms act synergistically to cause the neurodegenerative phenotypes seen in C9-FTD/ALS.

1.3.1 Physiological functions of *C9orf72* and loss-of-function mechanisms

Since the discovery of the *C9orf72* mutation in 2011, there has been intense investigation around the physiological functions of the C9ORF72 protein and its relevance to disease.

The gene *C9orf72* is transcribed into three RNA variants through alternative splicing, which results in the production of 2 different protein isoforms. The G_4C_2 repeat expansion is either located at the first intron of variant 1 and 3 **or** at the promoter region of variant 2. Variants 2 and 3 are translated into the same protein isoform with an estimated molecular weight of ~54kD (C9 long isoform), and variant 1 is translated into a shorter protein isoform with an estimated molecular weight of ~24kD (C9 short isoform) (DeJesus-Hernandez *et al.*, 2011). In variant 2, the location of the hexanucleotide repeat expansion (HRE) in the promoter region has been proposed to affect the expression of the variant. For variants 1 and 3, the HRE is included in the respective pre-mRNA. In physiological conditions, the long isoform demonstrated diffuse cytoplasmic expression and co-localised with lysosomes whereas the short isoform localised at the nuclear membrane and interacted with Importin-1 and RAN-GTPase, two major proteins of nucleocytoplasmic transport (Xiao *et al.*, 2015), implicating its role in this fundamental biological mechanism that affects every aspect of health and disease.

Despite the high conservation of the *C9orf72* human gene in primates and across different species – implying its important biological functions – Chen at al., 2017, reported that the pathological hexanucleotide repeat expansion was only found in humans, chimpanzees and gorillas and not in other vertebrates (Chen and Zhang, 2017). These are species with higher levels of dexterity and a greater index of opposability. Humans and higher-order primates possess a fast-conducting monosynaptic corticomotoneuronal tract, which is crucial for their advanced fine motor

skills and various dexterous abilities (Yang and Lemon, 2003). On the contrary, rodent forelimb movements are mostly controlled by a *disynaptic* cortico-reticulospinal pathway (Alstermark et al., 2004). Such genomic conservation indicates the role of the *C9orf72* hexanucleotide region in the development of the cortico-motor-neuronal pathway for voluntary motor dexterity.

In humans, *C9orf72* transcripts were detected in most tissues and importantly in the central nervous system (DeJesus-Hernandez *et al.*, 2011; Renton *et al.*, 2011; Rizzu *et al.*, 2016) with highest prevalence in a subset of myeloid cells (CD14+ monocytes, oesinophils and neutrophils). Expression was enriched to a lesser extent in macrophages, followed by lymphoid cells and the cells of the CNS. These outcomes were corroborated with transcriptomic analyses in the rodent model demonstrating highest expression in myeloid cells, macrophages, microglia and dendritic cells (Atanasio *et al.*, 2016; O'Rourke *et al.*, 2016). Collectively, this evidence shows the fundamental role of C9orf72 in innate and adaptive immunity responses (Rizzu *et al.*, 2016).

Bioinformatic studies indicated that C9orf72 has high homology to the differentially expressed in normal and neoplastic (DENN) protein family and is therefore suggested to act as a guanine nucleotide exchange factor (GEF) for specific Rab GTPases. Rab GTPases (Rabs) are either turned on by specific guanine nucleotide exchange factors GEFs or turned off by GTPase-activating proteins (GAPs) and ultimately control all aspects of intracellular vesicle trafficking in eukaryotes, by recruiting effector molecules (kinases, motors, phosphatases and other adaptor proteins) when they are bound to GTP in their active form (Stenmark, 2009). This prediction was confirmed by accumulating evidence denoting the interaction between the C9ORF72 protein and multiple Rabs – implicated in endoplasmic reticulum-Golgi transport, and endosomal-lysosomal and autophagosomal-lysosomal pathways – in cell culture models and human post-mortem tissue (Farg *et al.*, 2014; Sellier *et al.*, 2016; Aoki *et al.*, 2017; Frick *et al.*, 2018; Yang, Jiao and Shen, 2020). Further evidence on the regulatory role of C9orf72 in autophagy comes from studies suggesting its association with Unc-51-like kinase 1 (ULK1) autophagy initiation complex (Webster *et al.*, 2016), while knockdown of the C9ORF72 protein in neuronal cell lines impaired endocytosis and led to the accumulation of autophagosomes (Farg *et al.*, 2014). It has also been

reported that C9ORF72 forms a stable tripartite protein complex with Smith-Magenis chromosome region 8 (SMCR8) and WDR41 (WD20 repeat domain 41) and is implicated in autophagy and endosomal trafficking, by binding to Rabs (Sellier *et al.*, 2016; Sullivan *et al.*, 2016; Yang *et al.*, 2016).

Additional roles of the C9ORF72 protein have also been reported. It regulates axonal actin dynamics by modulating cofilin phosphorylation through activation of small GTPases Arf6 and Rac1. Importantly, cofilin phosphorylation was enhanced in *C9orf72*-depleted mouse motor neurons, induced pluripotent stem cell-derived motor neurons and post-mortem brain tissue from C9-ALS patients (Sivadasan *et al.*, 2016). The G4C2 HRE was recently demonstrated to interact with mitochondrial intermembrane space protein AIFM1, leading to its translocation from the cytosol to the mitochondrial intermembrane space where it interacts with TIMMDC1 (translocase of inner mitochondrial membrane domain containing 1) and the prohibitin complex to stabilize the assembly of OXPHOS complex I. The mitochondrial complex I function were shown to be defective in iPSC-derived motor neurons from C9-ALS patients, indicating that *C9orf72* haploinsufficiency causes defective mitochondrial function in ALS (Wang *et al.*, 2021).

The pathogenicity of haploinsufficiency has been further supported by the consistent demonstration of decreased *C9orf72* transcripts and protein levels in different regions of post-mortem brain tissue and blood from *C9orf72* HRE carriers, and by locomotor deficits accompanied by motor neuron degeneration reported in knockdown zebrafish models and *C. elegans* (Therrien *et al.*, 2013; Smeyers, Banchi and Latouche, 2021). Several mechanisms have been postulated for the suppression in C9orf72 expression including: (1) production of complex secondary structures such as G-quadruplex or R-loop structures consisting of a DNA: RNA hybrid and a displaced DNA strand, by the HRE, which hinder RNA polymerase transcription and cause abortive transcription of *C9orf72* (Haeusler, Donnelly and Rothstein, 2016); (2) epigenetic modifications through hypermethylation of the *C9orf72* promoter leading to transcriptional downregulation of the promoter (Gijselinck *et al.*, 2016; Van Mossevelde *et al.*, 2017) or histone trimethylation (Belzil *et al.*, 2013). Notably, *C9orf72* promoter hypermethylation can also be viewed as neuroprotective through suppression of toxic RNA foci and DPR formation (McMillan *et al.*, 2015; Xi *et al.*, 2015).

Nevertheless, two independently reported cases with homozygosity of the mutation, where neither the clinical phenotype nor the pathology was more severe compared to heterozygous ones, argue against the sole role of haploinsufficiency in disease pathogenesis. Transcripts from expansion-containing alleles were clearly detectable in the homozygous cases (Cooper-Knock *et al.*, 2013; Fratta *et al.*, 2013). Further, with the exception of one patient harbouring a *C9orf72* splice site mutation in exon 5 (F. Liu *et al.*, 2016), no coding mutations have been discovered in the *C9orf72* gene (Harms *et al.*, 2013).

In contrast to findings in zebrafish and *C. elegans* models described above, rodent *C9orf72* null studies, have yielded inconclusive outcomes for loss of function as a possible aetiology for C9 ALS-FTD. Stereotactic intracerebroventricular administration of antisense oligonucleotides against mouse *C9orf72* decreased mRNA levels by 30-40% throughout the CNS of mice compared to controls, but did not cause behavioural, motor or pathological features consistent with ALS/FTD (Lagier-Tourenne *et al.*, 2013). Neural-specific ablation of *C9orf72* in mice using the Cre/loxP system, significantly reduced body weight but again did not cause motor neuron degeneration or deterioration in motor function (Koppers *et al.*, 2015). Finally, *C9orf72*-deficient mice (lacking C9orf72 in all tissues) exhibited an inflammatory phenotype with lymphadenopathy, splenomegaly, autoimmunity, and reduced survival, with defects of lysosomal function and altered immune responses in macrophages and microglia. There were no overt neurodegenerative phenotypes such as neuronal degeneration, gliosis, increased ubiquitination and TDP-43 mislocalisation (O'Rourke *et al.*, 2016; Sudria-Lopez *et al.*, 2016).

It is important to note that many mouse models exhibiting *only* gain-of-function mechanisms [discussed further in section 1.3.4] again didn't display phenotypes consistent with neurodegeneration (Jiang *et al.*, 2016), with the exception of overexpression models (Chew *et al.*, 2015; F. Liu *et al.*, 2016; Lee *et al.*, 2018a). More recently, the generation of combined gain- and loss-of-function models highlighted the contribution of C9orf72 loss of function in disease development. Taken together, these data not only preclude the possibility that *C9orf72* haploinsufficiency contributes to neurodegeneration in conjunction with gain-of-function mechanisms, genetic and

environmental factors, but they also highlight the role of C9orf72 in proteostasis, proper immune system function and autoimmunity.

The loss of C9orf72 in mice and consequent disruption of lysosomal trafficking is compatible with the extensive data described above, that C9orf72 is a member of the DENN family and regulates endosomal trafficking events and autophagy through interaction with Rabs. In C9 ALS/FTD human induced motor neurons, haploinsufficiency in *C9orf72* levels impaired vesicle trafficking, lowered lysosomal numbers, increased glutamate receptors and impaired DPR protein clearance, leading to neurodegeneration via excitotoxicity (Shi *et al.*, 2018). Consistent with these findings, *C9orf72* loss in a gain-of-function mouse model of C9 ALS/FTD exacerbated motor impairment in a dose-dependent manner, indicating the importance of *C9orf72* haploinsufficiency *in vivo* and that C9-HRE-mediated pathogenic mechanisms may act in synergy to drive neurodegeneration (Shao *et al.*, 2019).

C9orf72 may also have anti-inflammatory effects, an idea supported by (1) the upregulation of microglia-activation genes upon ASO-knock-down of C9orf72 in mice (Lagier-Tourenne *et al.*, 2013); (2) microglial dysfunction with abnormal endocytic pathway and increased levels of inflammatory cytokines (IL-1b and IL-6) in *C9orf72 null* mice (O'Rourke *et al.*, 2016); (3) failure of suppression of STING/type 1 Interferon-mediated inflammation in *C9orf72* -/- mouse myeloid cells and (4) enhanced type 1 Interferon signature in samples (blood-derived macrophages, whole blood and brain tissue) from people with C9 ALS/FTD compared to sporadic cases (McCauley *et al.*, 2020). These data suggest that loss of C9ORF72 protein contributes in a non-cell autonomous manner to the neurodegeneration in C9 ALS/FTD, by diminishing the ability of microglia to clear aggregated proteins and/or by modifying immune responses. Moreover, Burberry et al., 2020, discovered that suppression of gut microflora with broad-spectrum antibiotics and intestinal flora transplantation in *C9orf72* KO mice abolished autoimmune and inflammatory phenotypes, proposing the role of C9orf72 function to innate immune activation and regulation of pathological inflammatory responses (Burberry *et al.*, 2020). On a clinical level, the hypothesis that autoimmunity or dysregulation of the immune system contributes to the pathogenesis and development of ALS and other neurodegenerative conditions has been considered for decades. Interestingly, two studies showed that C9 HRE carriers are

significantly more likely to have been diagnosed with systemic autoimmune disease prior to their neurological diagnosis, indicating a role of *C9orf72* in immunity regulation. Both studies were limited by small sample sizes (Miller *et al.*, 2016; Fredi *et al.*, 2019).

1.3.2 Gain-of-function mechanisms

Gain of function comprises of expression of abnormal bidirectionally transcribed RNAs from both the sense $(G_4C_2)_n$ and the antisense $(G_2C_4)_n$ DNA strand, containing the repeat expansion (Zu *et al.*, 2013). These expanded RNAs either aggregate in the nucleus into secondary structures called *RNA foci* and/or are translated into *aggregation-prone toxic homopolymeric proteins* via repeat associated non-ATG translation, called dipeptide repeats (DPRs).

This unconventional translation of sense and antisense expanded RNAs produces five DRPs: (1) glycine-alanine (GA), glycine-arginine (GR) and glycine-proline (GP) from the sense transcript; (2) proline-arginine (PR), proline-alanine (PA), and glycine-proline (GP) from the anti-sense transcript (Zu *et al.*, 2013). The arginine-containing DPRs are the most toxic species, a property that has been demonstrated in human cell lines, mice and particularly in drosophila models, although neurotoxic effects have also been exhibited with poly-GA (Y. Zhang *et al.*, 2014; Jovičič *et al.*, 2015; Freibaum and Taylor, 2017).

DPR products have been detected as ubiquitin- and p62-positive, but TDP43-negative neuronal cytoplasmic and intranuclear inclusions in various C9-ALS/FTD patient brain regions, including areas such as the cerebellum and occipital and parietal lobes that are considered to be less involved in the disease, and more rarely in the spinal cord. Several studies supported an association between the severity of neurodegeneration and TDP43 pathology (both more prominent in the motor cortex and spinal cord) rather than the burden of DPR deposition in human tissue (greatest in the cerebellum), raising controversy regarding the role of DPRs in disease pathogenesis. Nevertheless, Saberi et al., 2018, found that one of the proteins, poly-GR DPR anatomically correlated to disease-affected regions and colocalised with TDP43 deposits in dendrites in motor regions of C9-ALS CNS, confirming its contribution to

disease pathogenesis (Saberi *et al.*, 2018). Some studies have also raised the possibility of RNA foci and DPR inclusions preceding and driving TDP43 pathology (Proudfoot *et al.*, 2014; Vatsavayai *et al.*, 2016).

RNA foci were visualised in post-mortem derived material from *C9orf72* patients, with the use of fluorescent in situ hybridisation with fluorophore-tagged probes against the repeats. Sense and anti-sense RNA foci were predominantly present in motor neurons and less frequently interneurons, of the frontal and motor cortices, cerebellum, hippocampus and spinal cord and were also detected in non-neuronal cells such as astrocytes, microglia and oligodendrocytes in smaller proportions (Cooper-Knock *et al.*, 2013; Lagier-Tourenne *et al.*, 2013; Mizielinska *et al.*, 2013). They have also been identified in other patient-derived cells including circulating white blood cells, primary fibroblasts and induced pluripotent stem cells (Zhao *et al.*, 2020). Most RNA foci cluster in the nucleus, but cytoplasmic and occasionally perinuclear (around the edge of the nuclear membrane) aggregates were also observed in various cell types form C9-ALS patients (neurons, astrocytes, white blood cells and fibroblasts) (Cooper-Knock *et al.*, 2013; Mizielinska *et al.*, 2013; Swinnen and Robberecht, 2014; Swinnen *et al.*, 2018). The perinuclear location supports the involvement of RNA in nucleocytoplasmic shuttling defects, a fundamental pathway for ALS and FTD amenable to pharmacotherapeutic intervention. RNA foci were also observed in neurons containing p62- or TDP-43 inclusions (Mizielinska *et al.*, 2013).

An association between the distribution and burden of RNA foci and the clinical phenotype has not yet been established and contradictory observations have been reported to date, signifying the need for additional studies (Barker *et al.*, 2017). Mizielinska et al., 2013, initially showed a significant and inverse relationship between the abundance of sense RNA foci in the frontal cortex and age of disease onset in a cohort of 8 C9-FTD patients (Mizielinska *et al.*, 2013). Conversely, in a larger patient cohort of *C9orf72* expansion carriers (18 pure ALS, 16 FTD/ALS and 26 FTD patients), DeJesus-Hernandez et al., 2017, observed a positive correlation between increased abundance of antisense RNA foci in the frontal cortex and delayed age of disease onset. Also, the RNA foci burden was not associated to clinico-pathological features, implying that they are not the sole contributor to disease pathogenesis (DeJesus-Hernandez *et al.*, 2011).

The hypothesis of HRE-induced toxicity, involving RNA foci and DPRs, proposes three main mechanisms.

***Firstly*,** the accumulation of these RNA foci in the nucleus leads to sequestration of RNA-binding proteins (RBP's) with consequent alterations in their physiological functions and disruption in critical processes of RNA metabolism including mRNA maturation (alternative polyadenylation and splicing), regulation of mRNA stability and translation and degradation. The interaction between the *C9orf72* repeat mRNA and RBP's, such as nucleolin, Pur-α, the heterogeneous nuclear ribonucleoprotein group (hnRNPs) - hnRNPA3 and hnRNPH, ADARB2, SRSF1, SRSF2, and ALYREF - has been demonstrated in human post-mortem tissue, and in *in vitro* and *in vivo* models (Cooper-Knock *et al.*, 2013; Xu *et al.*, 2013; Haeusler, Donnelly and Rothstein, 2016). Sequestration of hnRNPH by RNA foci reduced its splicing efficiency on TARBP2, one of its known RNA targets, indicating disruption in its normal function (Lee *et al.*, 2013). Additionally, overexpression of Pur-a, a RBP that has been implicated in transcriptional control and cytoplasmic RNA localisation, rescued RNA foci-induced neurodegeneration in a *Drosophila* model expressing 30 interrupted G4C2 repeats and mouse neuronal cell lines (Xu *et al.*, 2013). Two translation products of the C9 HRE, poly-GR and poly-PR were also found to avidly bind to hydrogel droplets and when exogenously applied on astrocyte cultures, they migrated to the nucleus and associated to the nucleoli, with consequential impediments on RNA biogenesis (splicing changes and defects in rRNA maturation) and cell death (Kwon *et al.*, 2014). Further, these two arginine-rich dipeptide repeats were shown to induce toxic translational arrest after interacting with ribosomal proteins (Kanekura *et al.*, 2016; Moens *et al.*, 2019). However, despite the significant findings regarding the effects of these dipeptide repeats, the literature lacks comprehensive information regarding the concentrations of DPR used in these studies. Determining the physiologically relevant concentrations of poly-GR and poly-PR is crucial for accurate disease modelling. By using concentrations observed in patients, we can better replicate the disease environment and gain a more comprehensive understanding of the pathological mechanisms underlying ALS. This knowledge not only enhances our understanding of the disease but also paves the way for more effective disease modelling and the development of targeted therapeutic strategies.

It has been contemplated that the clinico-pathological heterogeneity in C9 ALS-FTD could be ascribed to the discrepant sequestration of RBP's between brain regions and patients (Mizielinska and Isaacs, 2014). This role of RBP's is further supported by post-mortem tissue evidence from C9 ALS/FTD patients of extensive changes in alternative splicing events, implying that malfunction or mislocalisation of RBPs could cause these transcriptional irregularities (Cooper-Knock *et al.*, 2015; Prudencio *et al.*, 2015; Conlon *et al.*, 2016). Overall, the functional mechanisms of RBP's and downstream consequences of their sequestration in disease pathology remain to be illuminated.

***Secondly*,** recruitment of nucleolin by G4C2 RNA repeats induces nucleolar stress as denoted by the more fractured appearance of the nucleolus and the dispersion of nucleolin staining in patient lymphocytes and fibroblasts carrying the C9 HRE (Haeusler, Donnelly and Rothstein, 2016). Nucleolin was found to be mislocalised from its normal nuclear sites and there were rRNA maturation defects, which could affect a series of downstream processes involved in the biogenesis and functionality of ribosomes. A recent study showed nucleolar shrinkage in the spinal motor neurons of C9-ALS and sporadic ALS patients that was independent to principal pathological changes such as TDP-43 mis-localisation and RNA foci, suggesting that nucleolar dysfunction is likely to be upstream in pathogenesis (Aladesuyi Arogundade *et al.*, 2021).

The ***third mechanism*** of HRE-mediated toxicity is nucleocytoplasmic transport impairment, which may underlie the nuclear depletion and cytoplasmic accumulation of TDP43 in ALS/FTD. This critical pathogenic event has also been implicated in normal ageing as well as other neurodegenerative disorders such as Alzheimer's and Huntington's disease. Nucleocytoplasmic trafficking disruption has been shown in two *Drosophila* models but the relative contribution of expanded G_4C_2 RNA versus DPRs or other mechanisms were not elucidated. In the first study, Freibaum et al., 2015, used a comprehensive, unbiased genetic screen in transgenic *Drosophila* lines expressing 8, 28 or 58 G_4C_2-repeat-containing transcripts and identified 18 modifier genes that encoded components of the nuclear pore complex, coordinated nucleocytoplasmic trafficking (export of nuclear RNA and import of nuclear proteins) and interacted with the G_4C_2-repeat (Freibaum *et al.*, 2015). This was associated with

defective RNA export and nuclear RNA retention phenotype that was observed both in their *Drosophila* model and in C9-ALS induced pluripotent stem-cell-derived neurons. The second study discovered RANGAP, a key factor involved in the regulation of nuclear import and export, bound to G_4C_2 RNA that was mislocalised in *Drosophila*, C9-ALS human iPSC-derived neurons and in post-mortem brain tissues (motor cortex). The consequential impairment of import of nuclear proteins such as the GTP-binding nuclear protein Ran, was reversed by antisense oligonucleotides and small molecules (TMPyP4) that destabilised the HRE G-quadruplexes (K. Zhang *et al.*, 2015). Moreover, transient overexpression of poly-GR/PR in human cell lines disrupted nucleocytoplasmic transport via induction of stress granule assembly and localisation of key factors (Ran, Nups and Karyopherins) into stress granules. It has been speculated that such downregulation of nucleocytoplasmic transport and subsequent halting in protein synthesis, may represent an immediate cellular coping mechanism in response to acute stress, whereas chronic compromise as in neurodegenerative conditions can be potentially deleterious. In fact, inhibiting stress granule formation with ataxin-2 ASOs, ameliorated nucleocytoplasmic transport defects and neurodegeneration in the *Drosophila* model and iPSCs (K. Zhang *et al.*, 2018).

1.3.3 Other mechanisms

Separately, DPR-protein mediated toxicity has also been associated with impaired activity of the ubiquitin-proteasome system that normally controls protein homeostasis in the endoplasmic reticulum (ER), leading to accumulation of misfolded proteins in the ER and ER stress (Y. J. Zhang *et al.*, 2014). More recently, DPRs have been implicated in damaging the IP3 receptor-mediated calcium signalling between ER and mitochondria by disrupting VAPB-PTPIP51 ER-mitochondria tethering proteins, through activation of GSK3β rather than physical interaction, in cultured rat cortical neurons. GSK3β is a known negative regulator of the VAPB-PTPIP51 interaction (Hartopp *et al.*, 2022). ER-mitochondria contact perturbations were also illustrated in C9-iPS derived neurons and in transgenic mice expressing a mutant human *C9orf72* gene containing the expanded repeat (Gomez-Suaga *et al.*, 2022).

1.3.3.a Axonal Transport defects

To maintain their homeostasis and survival, neurons rely extensively on the axonal transport of membranous organelles and macromolecules. Axonal transport dysfunction is heavily linked to the pathogenesis of ALS, described initially in patients (Sasaki and Iwata, 1996) and further elaborated in animal models of ALS (Williamson and Cleveland, 1999; Hafezparast *et al.*, 2003; Selvaraj *et al.*, 2012). Human genetic studies in ALS have also identified pathogenic mutations in genes that are involved in axonal transport machinery *DCTN1*, *KIF5A, TUBA4A, PFN1* and have unequivocally shown that defective intracellular trafficking can in fact trigger ALS (Münch *et al.*, 2004; Smith *et al.*, 2014; Nicolas *et al.*, 2018). Further, *in vivo* and cellular studies have shown axonal transport impairments are also conserved in key ALS mutations such as SOD1, TDP43 and FUS, and in other age-related neurodegenerative disorders (Wang *et al.*, 2013; De Vos and Hafezparast, 2017a; Sleigh *et al.*, 2019). Intriguingly, introduction of dynein mutants – a protein involved in retrograde axonal transport – in SOD1G93A ALS mice attenuated motor neuron degeneration and significantly improved survival of the mice (Kieran *et al.*, 2005; Teuling *et al.*, 2008), suggesting manipulation of axonal transport as a therapeutic target in ALS.

In *C9orf72*-ALS, the investigation of axonal transport disruption as a potential disease mechanism, is a new and emerging field. Mehta et al., 2021, established that human induced pluripotent stem cell (hiPSC)-derived MNs harbouring the C9 mutation exhibit dysfunctional mitochondrial motility. This phenotype was rescued in the gene-corrected lines and after genetic manipulation of mitochondrial biogenesis in mutant neurons. Importantly, these findings were corroborated through neuropathological analysis of C9-ALS post-mortem spinal cord tissue, where reduced expression of mitochondrial encoded transcripts in the ventral horn motor and not dorsal horn neurons, was shown (Mehta *et al.*, 2021). Another group observed that exogenous addition of arginine-containing DPRs (Poly-PR/GR) on control iPSC-derived MNs and in the drosophila model *in vivo*, reproduced this impairment in bidirectional axonal transport of cargo (mitochondria and RNA granules), through physical interaction with microtubules and molecular motors – kinesin-1 and cytoplasmic dynein (Fumagalli *et al.*, 2021). Collectively, the above studies and others using *C9orf72* human iPS

cellular platforms (Abo-rady *et al.*, 2020) showed pathological DPRs and RNA but no reduction in overall *C9orf72* mRNA and protein levels, suggesting that the transport impairment is due to gain-of-toxic-function disease mechanisms.

1.3.4 Animal models and human induced pluripotent stem cell models of *C9orf72* ALS/FTD

Animal models of C9-ALS have proved challenging to generate due to the long gene sequence length. This was overcome through the generation of transgenic mice utilizing bacterial artificial chromosome (BAC) vectors, which can carry large inserts such as C9orf72 and in fact four groups published on the generation of *C9orf72* repeat expansion BAC transgenic mice (Balendra and Isaacs, 2019). Transgenic mice with high repeat expansion levels exhibited the pathological hallmarks of C9-ALS, including nuclear RNA foci and cytoplasmic RAN translation aggregates. Nonetheless, discrepancies were reported in expression levels with the expansion size dropping to >500 repeats in some cases. Overall, the majority failed to show robust C9-ALS/FTD pathology and neurodegeneration. Interestingly, the *C9orf72* BAC transgenic mouse model used by Liu et al (2016) recapitulated many aspects of ALS such as neuronal loss, muscle denervation, paralysis, decreased survival, cortical and hippocampal degeneration (Y. Liu *et al.*, 2016); however, the rate of penetrance in the animals caused variability in its phenotypic expression, particularly across sexes (Lutz, 2018).

Ensuing attempts by two independent groups to replicate these phenotypes of reduced survival and motor deficits originally described by Liu and colleagues were not successful (Mordes *et al.*, 2020). Nevertheless, in the consequent publication of Nguyen et al., 2020, the phenotypes detected in the cohorts of C9-BAC mice established at the University of Bern and University of Rochester Medical Centre were those of reduced survival, weight loss, neurodegeneration and accumulation of RNA foci and RAN proteins, compatible with ALS/FTD-related pathology (Nguyen *et al.*, 2020). These varying outcomes across studies and institutions are likely attributed to methodological differences in characterising rodent behavioural phenotypes, weight

loss and grip strength; handling and environmental factors; and the background of mice.

Two more recent transgenic mouse models overexpressing GFP-GR100 or GFP-PR28 – arginine-rich GR and PR reported to be highly toxic amongst the five dipeptide repeats – displayed neurodegeneration, behavioural and/or motor deficits and reduced survival but TDP43 pathology was not demonstrated (Y. J. Zhang *et al.*, 2018; Hao *et al.*, 2019).

Several groups have also engineered mouse models with loss of function mutations, including two germline knockout models and the generation of a conditional allele using the Cre-LoxP system to induce Cre-mediated inactivation of C9orf72 in cell subtypes. In these models, motor phenotypes, reduced survival and hallmarks ALS pathologies such as TDP43 cytoplasmic inclusions or gliosis were not detected (Koppers *et al.*, 2015; Dickinson *et al.*, 2016; O'Rourke *et al.*, 2016). Instead, the mice developed splenomegaly, lymphadenopathy and defective immune responses and microglial dysfunction, supporting the role of C9orf72 in proper immune system, macrophage, and microglial function.

Although transgenic mice have undoubtedly served as preclinical models to examine experimental therapies over the years, they are often poorly characterised, have evolutionarily less advanced CNS and shorter lifespan – complicating the replication of late-onset human neurodegenerative conditions – and the majority rely on non-physiological expression of disease-related proteins. This is well-highlighted by recent studies describing important transcriptomic differences between mouse models of neurodegenerative disease and human post-mortem samples (Chen *et al.*, 2020). Moreover, they have limited translatability due to dissimilar environmental contributions and differences in the genome, particularly in non-coding DNA. Given the significant clinical heterogeneity in ALS, it is now widely accepted that epigenetic and environmental factors can modulate the disease onset, course and severity and this diversity cannot be captured in transgenic disease models (Vasta *et al.*, 2022).

Human induced pluripotent stem cells (hiPSCs) constitute a useful and complementary system for studying the *C9orf72* mutation. Studies using iPSC-derived

motor neurons and astrocytes from C9-ALS/FTD patients have substantiated that C9orf72 is associated with autophagy, altered proteostasis, dysregulation in calcium signalling, mitochondrial function, DNA damage, excitotoxicity, cell death and that C9 astrocytes display a toxic phenotype that drives/contributes to neuronal degeneration (Meyer *et al.*, 2014a; Varcianna *et al.*, 2019; Zhao *et al.*, 2020). Crucially, some of these findings have been confirmed in post-mortem tissue samples (Dafinca *et al.*, 2016; Selvaraj *et al.*, 2018; Mehta *et al.*, 2021). Refer to section 1.5.

1.4 Astrocytes in ALS

1.4.1 Physiological functions of astrocytes

Astrocytes, derived from the Greek word άστρον (meaning "star" due to their star-like shape), are the most abundant cells in the brain. While Michael von Lenhossék is often credited with coining the term "astrocyte" in 1895, the existence of these cells was first reported by Otto Deiters in 1865. Additionally, Camillo Golgi provided detailed illustrations of astrocytes in 1872. Initially, astrocytes were regarded primarily as supporting cells with structural and trophic functions, filling the gaps between neuronal networks. Nevertheless, it is now clearly evident that astrocytes are strategic cells for controlling neuronal activity and are crucial for maintenance of CNS homeostasis and metabolic support at all levels of organisation including: (1) molecular – ion and neurotransmitter homeostasis and regulation of pH; (2) cellular and network homeostasis – neurogenesis, neuronal guidance, control of synapse number and synaptic transmission; (3) organ homeostasis – regulation of the blood brain barrier and glymphatic system (Verkhratsky and Nedergaard, 2018). Moreover, astrocytes are pivotal regulators of synapses either through contact-dependent mechanisms or by secreting soluble factors, thereby shaping synapse formation, strength and function of both excitatory and inhibitory synapses (Mauch *et al.*, 2001; Christopherson *et al.*, 2005; Eroglu *et al.*, 2009; Fuentes-Medel *et al.*, 2012; de Majo *et al.*, 2020). They ensheath the neuronal synapses and this complex of astrocyte processes with the pre- and post-synaptic clefts forms the ‘tripartite synapse’, explained below (Araque *et al.*, 1999).

The term “astrocytes” comprises a heterogeneous group of cells which are morphologically and molecularly distinct. While both human and rodent brains harbour the two main classes of astrocytes – protoplasmic and fibrous – significant interspecies differences exist in size and complexity of cellular architecture. Human protoplasmic and fibrous astrocytes are larger, have more complex arborisation and are more efficient in calcium signalling (Oberheim *et al.*, 2009). This more extensive overlap in humans, with protoplasmic astrocytes contacting up to 2 million synapses versus 120000 synapses in the mouse, could potentially have an important role in neurodegenerative disease progression where increased physical cellular proximity allows the seeding and fast dissemination of protein aggregates such as amyloid-beta, tau and a-synuclein. Additionally, there is enhanced glia communication and provision of more efficient homeostatic and metabolic support for neurons (Finkbeiner, 1992; Nualart-marti, Solsona and Fields, 2013).

Interlaminal and varicose astrocytes, are two other astrocyte-specific populations, which project interlaminar fibres spanning the cortical layers, and are found only in human and higher-order primate brains. These cells are implicated in human-specific cognitive functions (Oberheim *et al.*, 2009) and their involvement has been described in Down’s syndrome and Alzheimer’s disease (Colombo, Quinn and Puissant, 2002; Colombo *et al.*, 2005).

Notably, human astrocytes retained their larger size and complexity when transplanted into the rodent brain, indicating that these features are intrinsically driven (X. Han *et al.*, 2013). They also contributed to enhanced long-term potentiation, learning and memory in chimeric mice (X. Han *et al.*, 2013) further underscoring the importance of increased astrocytic structural complexity in coordinating higher-order cognitive processing in humans (Oberheim *et al.*, 2009). Taken together, these findings suggest specialisation of astrocytes in the human brain that may contribute to cognitive capabilities unique to humans.

i. Astrocytes in CNS Homeostasis

Neurotransmitter and ion homeostasis

Some of basic astrocytic homeostatic functions include buffering of ions such as K+, Na+ and H+, as well as regulation of neurotransmitters, mainly GABA and glutamate, at the synaptic cleft. As such, they modulate neuronal excitability and network activity. Glutamate is the primary excitatory neurotransmitter in the CNS and has important roles in learning, memory, and synaptic plasticity. Nevertheless, excess glutamate at the synapse can cause excitotoxic neuronal death. The clearance of excessive extracellular glutamate is dependent upon astrocytic glutamate transporters after impulse transmission (Jia *et al.*, 2015; Karki *et al.*, 2015). Astrocytes express two types of Na+-dependent high-affinity glutamate transporters, also referred to as excitatory amino acid transporters in humans (EAAT) – EAAT1 and EAAT2 (Anderson and Swanson, 2000). The taken-up glutamate is rapidly converted to glutamine by glutamine-synthase inside the astrocytes and recycled back to neurons at the pre-synaptic terminals for glutamate resynthesis. This glutamate-glutamine cycle is essential for the rapid and efficient clearance of glutamate from the synaptic cleft and prevention of excitotoxicity, as well as maintenance of normal synaptic function.

Neurovascular coupling

Neurovascular coupling refers to the coupling between neuronal activity and cerebral blood flow – increased energy demand in neurons during activity stimulates cerebral blood flow and enhances the supply of energy substrates (Blinder *et al.*, 2013). This function is orchestrated by astrocytes, which are ideally positioned between the neurons and the brain microvasculature and enwrap both the vessels (vascular smooth muscle cells, endothelial cells and pericytes) and neuronal synapses via their end-feet processes (Liebner *et al.*, 2018). The astrocyte-vessel interaction is extensive, and it is estimated that 99.7% of the brain vasculature is in direct contact with astrocyte processes (Mathiisen *et al.*, 2010; McConnell *et al.*, 2019) Consequently, astrocytes conduct information bidirectionally between blood vessels and neurons (Presa *et al.*, 2020). They sense neuronal activity at the synapse and respond by coordinating the delivery of oxygen, glucose, and other essential nutrients with the metabolic requirements of the nervous system. Also, they are coupled via gap junctions forming an electrical syncytium and allowing the spread and

amplification of signals across neuronal networks (Giaume and Liu, 2012). Specifically, synaptic release of neurotransmitters such as glutamate and ATP triggers IP_3-dependent calcium rise at the astrocytic end-feet processes, which leads to the release of vasoactive signals that can induce both vasodilation and vasoconstriction, thereby driving neurovascular coupling. This variability of response seems to be determined by early versus late developmental stages (Stackhouse and Mishra, 2021), the type of astrocyte receptor activated and resultant Ca2+ signal amplitude (Tran, Peringod and Gordon, 2018; McConnell *et al.*, 2019). Additionally, variable signalling mechanisms have been proposed to act between arterioles and capillaries (Mishra *et al.*, 2016).

Metabolic Homeostasis

Astrocytes play a pivotal and complex role in CNS metabolic homeostasis. With their end-feet wrapped around the cerebral vasculature allowing the uptake of metabolic substances directly from the blood stream and by expressing high concentrations of high-capacity glucose transporters, GLUT1, astrocytes act as the predominant route for glucose entry into the CNS (McConnell *et al.*, 2019; Beard *et al.*, 2022). The astrocyte-neuron lactate shuttle (ANLS) hypothesis (Bélanger, Allaman and Magistretti, 2011) postulates that astrocytes respond to glutamatergic activation by increasing their rate of glucose utilisation and pushing glucose predominantly through the glycolytic pathway, to produce lactate and pyruvate as metabolic substrates. These are then shuttled to nearby neurons to serve as the predominant fuel source for neuronal oxidative phosphorylation. This pathway is regulated by neuronal activity, allowing the provision of metabolic support to be closely coupled to neuronal need (Bélanger, Allaman and Magistretti, 2011). Astrocytes are also the exclusive source of glycogen in the adult brain. Glycogen has a key role as an energy buffer in brief increases in energy demands such as during hippocampus-regulated memory formation, by rapidly delivering the energy substrate lactate to neurons through monocarboxylate transporters (Matsui *et al.*, 2017).

While both neurons and astrocytes are capable of fully oxidizing glucose to lactate, astrocytes exhibit a significantly higher rate of glycolysis. This metabolic activity in astrocytes leads to the conversion of a substantial amount of glucose into lactate,

which is subsequently released into the extracellular space (Belanger et al., 2011). The uptake of glucose and the release of lactate by astrocytes are known to be stimulated by glutamate, as demonstrated by multiple independent research groups (Pellerin and Magistretti, 2012). In the presence of glutamate, astrocytes experience an increase in glucose uptake and glycolysis, while neurons exhibit inhibition of these processes. This intriguing observation suggests that neurons rely on alternative metabolites, other than glucose, for their energy requirements. Consequently, this creates a favourable environment for neurons to utilize lactate as an energy substrate, completing the ANLS pathway (Dienel, 2012). A study by Jiwaji *et al*. provided further evidence that the ANLS pathway can be modulated by neuronal activity by illustrating that sustained neuronal activity increased rates of glucose utilisation and lactate production in mouse and human astrocytes and drove expression of metabolic genes (Jiwaji *et al.*, 2017).

Interestingly the role of astrocytic mitochondrial function and metabolism in CNS health and disease, is an emerging field. It is well-established that astrocytes use glycolysis as their main mechanism of energy production, whereas in neurons, the predominant mode of energy production is oxidative phosphorylation. In fact, the *in vivo* energy demands of astrocytes could be fulfilled in the absence of oxidative phosphorylation, with an observed increase in lactate production in conditional Cox10 mouse mutants, intact viability and absence of glial or neuronal cell loss (Cox10 is part of the cytochrome c oxidase complex and required for complex IV function), indicating that astrocytes are glycolytic (Supplie *et al.*, 2017).

Nevertheless, there is strong evidence postulating the role of astrocyte TCA cycle in biosynthetic processes rather than oxidative phosphorylation. Functional astrocyte mitochondria are crucial for glutamate regulation and metabolism. After glutamate uptake from the synaptic cleft, its conversion to glutamine is dependent on glutamate dehydrogenase enzyme, which is essentially found in astrocyte mitochondria. Therefore, it has been proposed that dysfunctional astrocyte mitochondria likely have dysregulated glutamate uptake and metabolism, resulting in excitatory neurotoxicity in neurons. Miro1 is a component of the mitochondrial motor/adaptor complex found in astrocytic processes, is a sensor of extracellular calcium and facilitator of mitochondrial transport and mitophagy. Following mitochondrial stress, Miro1 is

degraded, which facilitates the clearance of damaged mitochondria. Defective proteostasis of Miro1 in Parkinson's disease astrocytes led to mitophagy dysfunction and Ca^{2+} imbalance (López-Doménech *et al.*, 2021). Further, toxic fatty acids are produced by neurons and transferred to astrocytes in ApoE-positive lipid particles. In the astrocytes, they're metabolised via mitochondrial β-oxidation in response to neuronal activity and this in turn activates the detoxification gene expression programs (Rose *et al.*, 2020; Bantle *et al.*, 2021).

Astrocytes also serve as the primary cell type responsible for the clearance of damaged mitochondria from neurons, through a process called transmitophagy, which is thought to begin in neurons and be completed in astrocytes (Bantle *et al.*, 2021). Finally, they can transfer healthy mitochondria to axons in the context of injury. This transfer is regulated by CD38 and is completed in a calcium-dependent manner (Cheng *et al.*, 2020a).

Astrocyte metabolic impairments have been described in several human-specific neurodegenerative diseases including ALS (Nagai *et al.*, 2007a; Allen, Hall, Castelli, *et al.*, 2019), Parkinson's (Schmidt *et al.*, 2011; Jiang *et al.*, 2013) and Alzheimer's disease (Allaman *et al.*, 2010; Le Douce *et al.*, 2020).

ii. Astrocytes in CNS signalling

Synapse homeostasis

The tight structural interaction between the astrocyte processes and the synapse at the 'tripartite synapse' complex has important functional consequences on synaptic activity. Astrocytes are essential for formation, selective elimination, function, and plasticity of synapses, throughout development and adulthood.

The initial discovery of the synaptogenic role of astrocytes was made using purified retinal ganglion cells, where addition of astrocyte conditioned medium enhanced synapse formation (Ullian *et al.*, 2001). More recently, this was described in cultured human cerebral cortical spheroids (Sloan *et al.*, 2018). Major astrocyte-secreted synaptogenic factors have been identified over the years that control different aspects of excitatory and inhibitory synapse development, maturation, and plasticity. These

include thrombospondins and pentraxin3 which have been postulated to be concomitantly secreted (Christopherson *et al.*, 2005; Fossati *et al.*, 2019); two members of the secreted protein acidic and rich in cysteine (SPARC) family proteins, Hevin (also known as SPARC-like1/SPARCL1) and SPARC (Kucukdereli *et al.*, 2011); glypicans 4 and 6 (Allen *et al.*, 2012); cholesterols (Mauch *et al.*, 2001); cytokines including TNF-α and TGF-β (Diniz *et al.*, 2012) and others (Fossati, Matteoli and Menna, 2020).

Elimination of redundant, non-functional synapses allows synaptic refinement and strengthening of the remaining inputs to reach a mature, precise neural circuit during development. In the mature nervous system, synapse "clearing" events continue through experience- and memory-dependent structural synaptic plasticity, but the number of events declines with age (Jung and Chung, 2018). Astrocytes actively contribute to these neuronal-activity-dependent synapse elimination processes by phagocytosing unwanted synapses through the MEGF10 and MERTK pathways, distinct phagocytic pathways to those associated with microglial function (Allen, 2014; Stogsdill *et al.*, 2017).

Astrocytes are not electrically excitable; however, they shape neuronal signalling via the expression of metabotropic and ionotropic-sensing receptors (Pasti *et al.*, 1997; Perea and Araque, 2005). Calcium transients are induced within astrocytes in response to neuronal activity (Cornell-bell *et al.*, 1990; Stobart *et al.*, 2018; Lines *et al.*, 2020). Similarly, co-imaging of Ca^{2+} transients in astrocytes and neurons following mouse whisker stimulation demonstrated that neuronal and glial calcium waves operate in synchrony during sensory tasks (Stobart *et al.*, 2018). Specifically, neurotransmitters released at the pre-synaptic cleft bind to G-protein coupled astrocyte receptors, eliciting the activation of the phospholipase C (PLC)/inositol 1,4,5-trisphosphate (IP3) cascade and resulting in elevation of intracellular Ca2+. This signal is propagated to adjacent astrocytes, evoking calcium waves (Scemes and Giaume, 2006; Agulhon *et al.*, 2008). Further evidence is required to elucidate whether the propagation of astrocytic calcium waves (1) originates with the gap-junction-coupled astroglial network, (2) is achieved by the calcium-dependent paracrine release of ATP which activates IP3-mediated calcium rise in neighbouring astrocytes in a feed-forward manner (Guthrie *et al.*, 1999), (3) is the product of the

linear summation of neighbouring neuronal activity or (4) represents the combination of the aforementioned mechanisms (Nett, Oloff and Mccarthy, 2002; Kanemaru *et al.*, 2014; Bazargani and Attwell, 2016; Guerra-Gomes *et al.*, 2018; Arizono *et al.*, 2020). Nevertheless, it is now well-established that activity-dependent cytosolic calcium elevation in astrocytes induces the release of neuroactive molecules, also known as gliotransmitters, such as ATP, D-serine and glutamate, which bind to neurons and modulate neuronal activity (Guthrie *et al.*, 1999; Bezzi and Volterra, 2001; Covelo and Araque, 2018).

The role of oligodendrocytes and microglia in CNS homeostasis.

Oligodendrocytes

Oligodendrocytes play a pivotal role in the CNS by generating myelin sheaths that ensheath axons. The myelination of axons significantly enhances the speed and efficiency of electrical signal transmission. Myelin sheaths constitute the white matter, which comprises approximately half of the human brain mass (Herndon *et al*., 1998). The synthesis of myelin demands a considerable amount of energy, which is likely facilitated by increased levels of mitochondrial respiration (Edmond *et al*., 1987; Fünfschilling *et al*., 2012, Diaz *et al*., 2012). In addition to their myelinating function, oligodendrocytes provide crucial metabolic support to neurons and their axons by delivering essential nutrients and substrates. This metabolic support is thought to occur through mechanisms such as the lactate shuttle and glucose transport. However, the precise conditions under which these processes operate remain incompletely understood (Fünfschilling *et al*., 2012; Lee *et al*., 2012). Moreover, oligodendrocytes are instrumental in maintaining ion homeostasis by regulating extracellular potassium ions levels during neuronal signaling (Larson *et al*., 2018).

Given their critical functions in myelination and metabolic support of neurons, any impairment in oligodendrocyte function can precipitate a variety of neurological disorders. Some of these include the Pelizaeus-Merzbacher disease, multiple sclerosis, vanishing white matter disease, multiple system atrophy, and progressive multifocal leukoencephalopathy (Han *et al.*, 2022).

Microglia

Microglia, another type of glial cells along with oligodendrocytes and astrocytes, play many pivotal roles in maintaining metabolic homeostasis. Unlike other glial cells, microglia are the innate immune cells of the CNS, and their most important roles in this context are immune surveillance and the regulation of inflammation processes. Microglia are responsible for maintaining the health of the CNS tissue and stand as the first responders to any injury or infection of the brain and spinal cord (Kreutzberg, 1996). In a way, microglia behave similarly to macrophages and adapt their metabolism once an infection is discovered (Davalos *et al*. 2005). Once microglia discover an infection, they rapidly change their metabolism from primarily oxidative phosphorylation to glycolysis, which enables them to achieve a dramatic morphological change along with a high increase in their numbers and gene transcription (Savage *et al*., 2019). This change in metabolism is of the same variation that macrophages and tumour cells perform, and is named the Warburg effect (Warburg, 1956). Once the change has happened, microglia can assume many phenotypes out of which some release high amounts of anti-inflammatory cytokines to combat the infection, and others clear the debris of affected cells.

Aside from the immune response, microglia play other important roles in maintaining the metabolic homeostasis of the CNS. Those roles are modulating neuronal activity by altering hormonal signaling, synaptic pruning in the early stages of neuronal development, and removing cell debris and dysfunctional synapses by phagocytosis (Gomez-Nicola and Perry, 2015). Microglia can also affect insulin signaling pathways and glucose uptake by neurons, impacting overall energy homeostasis (Greenhill, 2023). Dysregulation of microglial function can lead to the development of numerous neurodegenerative diseases, such as Alzheimer's, Huntington's, Parkinson's, multiple sclerosis, Rett syndrome, schizophrenia, and many others (Gao *et al.*, 2023).

1.4.2 Astrocytes in neurodegeneration

As reported in the previous section, astrocytes play a crucial role in central nervous system functioning, particularly with respect to synaptic activity, neurotransmitter regulation, ion balance, and metabolism (Vasile, Dossi and Rouach, 2017). It is not

surprising that given these extensive roles maintaining a healthy milieu for neuronal survival and activity, the dysfunction or loss of astrocytes contributes to neurodegeneration. In fact, astrocyte dysfunction has been implicated in the onset and progression of Alzheimer's disease (AD), Parkinson's disease (PD), Huntington's disease (HD), Multiple Sclerosis (MS), and Amyotrophic Lateral Syndrome (ALS) [Reviewed in (Phatnani and Maniatis, 2015)].

Many studies have shown that reactive astrocytes exhibit a loss of function and a concurrent gain of toxic function in neurodegenerative diseases. It is now becoming increasingly recognised that the exact function of reactive astrocyte states occurs on a spectrum, characterised by specific gene expression signatures and functions, and is dependent on the pathological context and stage of disease (Escartin *et al.*, 2021). Reactive astrocytes have been found to be ubiquitous throughout the central nervous system of individuals with neurodegenerative diseases, and it is therefore believed that they are partly responsible for the neuronal losses that are central to the pathology of these diseases (Li *et al.*, 2019). In the SOD1 ^{G93A} ALS mouse model, selective knock-out of three factors that induce neurotoxic/reactive astrocytes, IL1α, TNFα and C1q, led to a much slower deterioration in performance and prolonged the overall lifespan, highlighting the importance of gliosis as a major contributor in disease pathogenesis and a potential ALS therapeutic target (Guttenplan *et al.*, 2020).

Recently, the additional role of astrocytes in regulating brain metabolic homeostasis has been elucidated in various studies, particularly with respect to mitochondrial metabolism (Rose *et al.*, 2020). The intercellular transport of mitochondria between astrocytes and neurons appears to be bidirectional. Under physiological and pathological conditions, neurons release their damaged mitochondria to astrocytes for degradation and recycling, a process called transmitophagy (Davis *et al.*, 2014; Morales *et al.*, 2020; Lampinen *et al.*, 2022). Specifically, Lampinen et al., 2022, demonstrated enhanced internalisation of neuronal mitochondria in astrocytes from AD mice, in human iPSC-derived astrocytes from a symptomatic AD patient and *in vivo* in the mouse hippocampi, whilst Morales et al., 2020, provided evidence of neuroglial transmitophagy in the context of Parkinson's disease.

Conversely, astrocytes donate healthy mitochondria to neurons in injurious or neurodegenerative environments. In particular, after transient cerebral ischaemia in mice there was increased entry of astrocytic mitochondria into adjacent neurons with subsequent improved pro-survival signalling and amelioration in motor deficits (Hayakawa *et al.*, 2016). This astrocytic release of functional mitochondria was associated to CD38-cyclic ADP-ribose-mediated calcium signalling, whereas siRNA-suppression of this pathway reduced extracellular mitochondrial transfer and negatively impacted functional neurological outcomes. Moreover, hiPSC-derived astrocytes from healthy individuals were able to prevent degeneration of dopaminergic neurons that were exposed to rotenone to model Parkinson's disease. Researchers found that neurons internalized healthy mitochondria that were released into the media by wild-type astrocytes (Cheng *et al.*, 2020a). Notwithstanding, these supportive roles can be disrupted in injury, aging and neurodegeneration, where astrocytic activation can cause intrinsic mitochondrial dysfunction, impacting neuronal health through a gain of inflammatory function (release of proinflammatory cytokines) but also through a loss of supportive function such as antioxidant and trophic support (dysregulation of calcium homeostasis and excess generation of reactive oxygen species) [Reviewed in (Gollihue and Norris, 2020)].

Similarly, astrocytes have been implicated in ALS and there has been an intense focus on investigating the different mechanisms that underlie astrocytic dysfunction and how this contributes to MN degeneration in ALS.

1.4.3 Astrocytes in ALS with a focus on *C9orf72*-ALS

Initial evidence from pathological studies suggested that defects in glutamate uptake by astrocytes were due to focal loss of EAAT2 transporter in affected brain regions in sporadic and familial ALS cases (Rothstein *et al.*, 1995). Furthermore, the mis-accumulation SOD1 protein in astrocytes in the spinal cord of SOD1 ^{G85R} mice provided additional evidence for astrocytic involvement in ALS (Bruijn *et al.*, 1997). Studies from the Cleveland group using chimeric mice, where wild type non-neuronal/glial cells (that did not express the pathogenic/mutant SOD1 protein) delayed degeneration and prolonged the survival of SOD1 mutant-expressing motor neurons,

were pivotal in demonstrating the concept of non-cell autonomous neurodegeneration (Clement *et al.*, 2003). Astrocytic or microglial ablation of the mutant SOD1 transgene slowed down disease progression and improved survival in mice (using floxed SOD1 ^{G37R} or SOD1 G^{85R} mice with Cre-recombinase), further validating that interactions between motor neurons and glial cells constitute one of the key mechanisms in ALS pathogenesis (Yamanaka *et al.*, 2008; Wang, Gutmann and Roos, 2011).

Cervical spinal cord transplantation and engraftment of mutant SOD1 astrocyte precursor cells in wild-type mice induced neuronal degeneration with corresponding motor behavioural deficits (Papadeas *et al.*, 2011), whereas transplantation of healthy astrocyte precursors into the spinal cord of mutant SOD1 rats was neuroprotective with slower disease progression and longer survival (Lepore *et al.*, 2008). Moreover, chronic infusions of mutant SOD1 astrocytic secreted factors resulted in MN degeneration and neuromuscular dysfunction in healthy rats (Ramírez-Jarquín *et al.*, 2017), while in *in vitro* studies there was accelerated death of either human embryonic stem-cell derived or iPS cell-derived MNs when they were either cocultured with primary human astrocytes expressing the mutant SOD1 protein or treated with the conditioned medium from those cells (Nagai *et al.*, 2007b; Di Giorgio *et al.*, 2008; Marchetto *et al.*, 2008).

Importantly, non-cell autonomy has also been established in sporadic ALS that accounts for most ALS cases. Human stem cell-derived astrocytes from patients with sporadic disease can be directly toxic to wild-type MNs, a finding that has been demonstrated *in vitro* (Haidet-Phillips *et al.*, 2011) and *in vivo* (Qian *et al.*, 2017). Collectively, these results indicate a shared mechanism leading to neuronal degeneration between fALS and sALS through astrocyte-mediated toxicity. The contribution of astrocyte TDP43 dysfunction in ALS remains to be elucidated. Astrocytes expressing ALS-causing mutations in TDP43 have been shown to either trigger/exacerbate or have no influence on neuronal survival (Fritz *et al.*, 2013; Haidet-Phillips *et al.*, 2013; Serio *et al.*, 2013; Tong *et al.*, 2013; Rojas *et al.*, 2014).

Mechanistically, several molecules have been associated to astrocyte-driven toxicity in ALS experimental models including; (1) Excess glutamate at the synaptic cleft due to defective EAAT2 function leading to post-synaptic overstimulation and neuronal

excitotoxicity (Rothstein *et al.*, 1995; Bruijn *et al.*, 1997; Pardo *et al.*, 2006); (2) Increased levels of D-Serine, an essential co-agonist for NMDA receptors that determines the excitability of glutamatergic neurons, have been reported in the spinal cords of people with sporadic and familial ALS, as well as the mSOD1 mouse model (Sasabe *et al.*, 2012); (3) A number of released astrocytic factors have been considered to be potentially toxic including proinflammatory cytokines, complements, prostaglandins and reactive oxygen species (Nagai *et al.*, 2007a; Di Giorgio *et al.*, 2008; Marchetto *et al.*, 2008; Haidet-Phillips *et al.*, 2011). Specifically, upregulation of interferon (IFN)-stimulated genes was demonstrated in astrocytes surrounding the MNs in the spinal cords of SOD1 mouse model at a pre-symptomatic stage, while reduction or deletion of the IFN-receptor 1 prolonged the survival period of the mice (Wang, Yang and Zhang, 2011). Mutant, adult astrocytes cultured from the spinal cords of 2-month old SOD1 mice exhibited upregulation of inflammatory and reactive factors and upon coculture with hES-cell derived HB9::GFP MNs, they promoted ALS-like degeneration and intracellular protein aggregation through the release of TGF-β1, which in turn activated the mTOR signalling pathway and disrupted autophagy (Tripathi *et al.*, 2017). The astrocyte-derived neurotoxic factors in SOD1-ALS ACM have been postulated to induce MN death by causing hyperexcitability that leads to calcium overload and oxidative stress (Fritz *et al.*, 2013).

Astrocytes lose their homeostatic functions and hence ability to provide neuronal support in ALS. In patients and murine models, ALS astrocytes downregulated major histocompatibility complex 1 (MHC1) on MNs, thus making them more susceptible to astrocyte-mediated demise (Song *et al.*, 2016). In another study, TNF receptor 1 (TNFR1) signalling was identified as a major promoter of glial cell derived neurotrophic factor (GDNF) synthesis/release in astrocytes, an agent that confers protection to neurons. Elimination of TNFR1 from SOD1-ALS mice abolished astrocytic GDNF and accelerated neurodegeneration, indicating that the TNFR1-GDNF astrocytic pathway may represent a therapeutic target for ALS (Brambilla *et al.*, 2016). Astrocyte networks formed by gap junctions including connexins play a critical role in the regulation of extracellular pH and glutamate levels, and in the exchange for glucose, lactate, ions and second messengers. The gap junction protein Connexin 43 – the main Connexin in astrocytes – was found to be upregulated in hiPSC-derived astrocytes and in the spinal cords of people with sporadic ALS and SOD1 mice, and

was suggested to induce neuronal toxicity through increases in intracellular calcium (Almad *et al.*, 2016).

Metabolic support from astrocytes is also impaired in ALS. Mitochondria in SOD1-expressing astrocytes showed defective respiratory function and increased superoxide radical formation (Cassina *et al.*, 2008). Similarly, human primary astrocytes expressing mutated SOD1 demonstrated proinflammatory activity with increase in ROS production, likely mediated by NOX2. The antioxidant apocynin reversed these effects and rescued MN survival (Marchetto *et al.*, 2008). Other groups have provided evidence of diminished metabolic support associated with defects in the lactate shuttling between astrocytes and neurons and decreased lactate provision to MNs, as well as calcium dysregulation in the SOD1 astrocytes, where oxidative stress induced excess calcium release from the endoplasmic reticulum and altered SNARE-dependent vesicular exocytosis (Ferraiuolo *et al.*, 2011; Kawamata *et al.*, 2014; Madji Hounoum *et al.*, 2017).

Recently, more research has been focusing on the effect of astrocytes in *C9orf72*-mediated ALS. Several studies examined C9orf72-astrocyte contact-dependent effects through physical astrocyte-neuronal coculture assays (Meyer *et al.*, 2014b; Zhao *et al.*, 2020), and through treatment of MNs with astrocyte conditioned medium (ACM) (Madill *et al.*, 2017; Birger *et al.*, 2019; Varcianna *et al.*, 2019).

In the study by Meyer *et al.* (2014), human i-astrocytes (directly differentiated from patient fibroblast using transcription factors) harbouring the *C9orf72* mutation were cocultured with control MNs for 4-5 days and led to around 60-80% of MNs dying while surviving MNs exhibited fewer and shorter neurites. This drop in viability was not rescued upon addition of healthy ACM, thereby postulating that this outcome was not secondary to insufficient production of neurotrophic factors by astrocytes. Importantly, they also found that C9 i-astrocytes induced similar neurotoxicity when compared to those derived from other ALS subtypes (Meyer *et al.*, 2014b). More recently, in work by Zhao *et al*. (2020), human iPSC-derived C9 astrocytes exhibited intracellular RNA aggregates/foci and dipeptide repeats – consistent with C9 ALS pathology – that were abolished with complete correction of the hexanucleotide repeat expansion with CRISPR-Cas9 genome editing. Upon culture with C9 astrocytes, human iPSC-derived

control MNs exhibited functional impairments as reflected by decreased magnitude of Na^+ and K^+ currents through voltage-gated channels and a subsequent progressive loss of action potential output. This effect was reversed with control or gene-corrected astrocytes, confirming that the C9 mutation is responsible for this non-cell autonomous motor neuron pathophysiology. Moreover, transcriptomic analysis on C9 astrocytes revealed dysregulation in genes involved in pathways including ionotropic glutamate receptor signalling, ribosomal RNA processing, synaptic transmission, and cell adhesion. These results support the known function of astrocytes in regulating neurotransmission and RNA metabolism and confirm that these processes are disrupted in C9 astrocytes. Surprisingly, and in contrast to previous studies, no reduction in MN survival was observed after coculture with C9 astrocytes (Zhao *et al.*, 2020).

In 2017, Madill *et al*. treated iPSC-derived MNs from healthy individuals with the ACM from three C9-ALS patients and three controls and reported a significant reduction in neuronal viability. Additionally, they cultured HEK293T cells with ACM from patient and control astrocytes, and autophagy was subsequently activated through starvation. Cells treated with C9-ALS ACM showed lower levels of LC3-II, suggesting a reduction in the autophagic flux. This was accompanied by an increase in p62 puncta (presumably awaiting degradation) and higher SOD1 expression. They concluded that C9-ACM may disrupt the balance between autophagosome expression and degradation and proposed one potential astrocyte-related mechanism involving autophagy inhibition (Madill *et al.*, 2017). In conformity, a more recent *in vitro* study demonstrated that mouse MNs cultured with ACM from astrocytes directly converted from *C9orf72* patient fibroblasts, displayed a reduction in neurite outgrowth and survival (Varcianna *et al*., 2019). This was associated with the secretion of fewer exosomes from C9-mutant i-astrocytes relative to those secreted by healthy astrocytes. Moreover, exosomal RNA analysis identified downregulation of miR-494-3p – a negative regulator of semaphorin 3A, which is a target involved in axonal maintenance. Treatment of MNs with a mimic, in the presence of C9 ACM significantly reduced the levels of semaphorin 3A in neurons and increased neurite branching and survival. Results were validated in post-mortem tissue (Varcianna *et al.*, 2019). This is of interest given that disrupted RNA homeostasis is implicated in ALS and exosome cargo includes RNA species.

Although this field is still in its infancy, mass spectrometric analysis of the astrocyte secretome identified diminished antioxidant properties of the C9-mutated conditioned medium as indicated by downregulated secretion of antioxidant proteins (SOD1 and SOD2) that are typically released by wild-type astrocytes, thereby contributing to neuronal oxidative stress and ensuing neurodegeneration (Birger *et al.*, 2019). Nevertheless, SOD1 isoform is normally distributed throughout the cytoplasm and nucleus and SOD2 isoform is in the mitochondrial matrix. This poses concern on whether the proteins detected via mass spectrometry were due to apoptosis rather than active secretion. Together with recent interactome-based approaches, this highlights the value of a comprehensive and unbiased approach, including conventional proteomics, to identify and dissect the impact of astrocyte-mediated signals on neurons.

Given the significant association between dysfunctional energy metabolism and disease progression in ALS, Allen *et al*. (2019a) used a phenotypic metabolic profiling technique to measure the rate of reduced nicotinamide adenine dinucleotides (NADH) from 91 potential energy substrates and identify defects of any metabolic pathways in astrocytes. It was shown that *C9orf72*- and sporadic-ALS-induced astrocytes have diverse metabolic profiles and diminished metabolic flexibility (ability to utilise alternative metabolites) compared to those from healthy controls, which negatively impacted cell survival under times of cellular stress such as bioenergetic starvation (Allen, Hall, Woof, *et al.*, 2019a). The decrease of metabolic flexibility involved disruptions in adenosine, fructose, and glycogen metabolism, as well as in the membrane transport of mitochondrial specific energy substrates.

To explore defects in other astrocytic metabolic pathways, Allen *et al*. 2019, conducted a follow-up study in which they focused on impairments in adenosine metabolism in induced astrocytes from C9 and sporadic ALS patients. This yielded a novel finding that adenosine deaminase (ADA), a ubiquitous enzyme that is crucial for purine homeostasis, is downregulated in diseased i-astrocytes. Importantly, inhibition of ADA in control i-astrocytes alone, was sufficient to decrease MN survival in a coculture setting. Furthermore, stimulation of this pathway with inosine supplementation led to an increase in ATP and bioenergetic flux in astrocytes, in addition to a reduction in MN

toxicity. Together, these results indicate that efficient adenosine deamination is important for the supportive role of astrocytes and accumulation of adenosine enhances neurotoxicity in both C9 ALS and sALS (Allen, Hall, Castelli, *et al.*, 2019).

1.5 ALS modelling and human iPSCs

1.5.1 Challenges in modelling ALS

Post-mortem brain and spinal cord tissues have provided essential pathological information for ALS and have been utilised to isolate neurons and glial cells for several *in vitro* studies. However, due to the irreversible changes post-mortem tissues may have undergone during the process of death, they have limited utility in studying ALS and so are not suitable for examining biological changes during the initial disease stages. Additionally, their availability is limited by regulatory and ethical constraints; the resulting cultures are often diverse, with various cell types demanding extensive tissue processing and strict culture conditions (Mattson and Rychlik, 1990; Slanzi *et al.*, 2020). Having said that, it remains crucial to confirm findings from *in vitro* and experimental animal models in human brain and spinal cord tissue in order to advance our knowledge of ALS pathogenic mechanisms and identify potential therapeutic targets. This is possible due to recent developments in tissue banking, providing high-quality tissue for neurodegenerative research in addition to advanced tools including proteomics, metabolomics, mRNA microarrays, and genomics.

Given ethical and practical limitations in studying CNS function in humans and primates, rodents have been extensively used as a model for mammalian brain function and disease, providing valuable insights into disease pathophysiology. This is appropriate because humans share approximately 97.5% DNA sequence homology with mice. Rodent and human brains exhibit similar overall anatomical connectivity and comparable gross brain structures underlying core circuitry responsible for key functions, including motor function, sensation, and simple cognitive skills. In addition, rodent and human nervous systems exhibit a similar range of cell types. These include neuronal and non-neuronal types (oligodendrocytes, astrocytes, and microglia), displaying roles and functions broadly analogous to their human equivalents.

Nonetheless, there is an emerging understanding that future research requires a more detailed consideration of interspecies differences. Rodents have evolutionarily less advanced CNS structures compared to humans, and their shorter lifespans do not allow accurate replication of late-onset, age-related phenotypes in neurodegenerative conditions. This is also well highlighted by recent studies describing important transcriptomic differences between mouse models of neurodegenerative disease and human post-mortem samples (Chen *et al.*, 2020; Zhou *et al.*, 2020).

Mice are the most commonly used species for modelling ALS and have provided important insights into disease pathogenesis and a platform for therapeutics screening (Philips and Rothstein, 2015; Picher-Martel *et al.*, 2016; Tosolini and Sleigh, 2017; Lutz, 2018). Nevertheless, drugs that have success in transgenic mouse models typically fail to translate into effective disease-modifying therapies in humans during clinical trials, highlighting their inherent limitations (Philips and Rothstein, 2015; Tosolini and Sleigh, 2017). Most transgenic ALS rodent models depend on the overexpression of the protein of interest, often leading to accelerated phenotypes. For example, the most commonly used *SOD1*^{G93A} model carries approximately 25 copies of the human transgene (Shibata, 2001; De Giorgio *et al.*, 2019), and transgenic mice overexpress wild-type human *TARDBP* by 1.2 to 2-fold more than the endogenous gene level. On the other hand, rodent models that express the gene/mutation at physiological levels exhibit slower and less severe disease progression but more closely recapitulate ALS-causing mutations, allowing the examination of early-disease processes and biomarkers (De Giorgio *et al.*, 2019). Also, the predominant limitation of the SOD1 genetic models is that TDP43 pathology, which is present in about 97% of ALS subtypes, is not detected, indicative of discrepant disease mechanisms. Finally, clinical heterogeneity is evident amongst ALS patients signifying multiple disease modifiers, including genetic, epigenetic, and environmental factors, which are difficult to recapitulate in transgenic animal models.

1.5.2 Advantages and limitations of the hiPS-cellular system in ALS and gene editing technologies

Animal models continue to provide key insights into underpinning molecular disease mechanisms. Nevertheless, due to their limitations, they should be complemented with hiPSC models of disease. It is difficult to study certain ALS genotypes or sporadic ALS because few animal and *in vitro* models incorporate all or even most of the pathogenesis. However, the iPSC lines produced from ALS patient samples allow researchers to study specific genetic backgrounds and sporadic ALS (Lee *et al.*, 2018b; Selvaraj *et al.*, 2018; Zhao *et al.*, 2020; Mehta *et al.*, 2021). The use of iPSCs in studying sporadic ALS is especially valuable due to the involvement of pathogenic mechanisms that may not be present in genetic forms and cannot be studied in transgenic animal models (Fujimori *et al.*, 2018).

A key advantage of iPSCs is the ease and efficiency of producing a homologous cell population with a patient's genetic background, providing an unlimited supply of differentiated cells with disease-specific relevance. ALS patient-derived iPSCs have high translational capacity because they recapitulate disease-related protein expression levels and through the hiPSC technology, key pathological signatures have been reproduced across a spectrum of neurodegenerative disease models (Selvaraj *et al.*, 2012; Serio *et al.*, 2013; Burkhardt *et al.*, 2016; Hall *et al.*, 2017; Zhao *et al.*, 2020). For instance, when patient-derived mutant iPSCs were differentiated into functional motor neurons, they had higher levels of TDP-43 and displayed lower survivability compared to controls (Bilican *et al.*, 2012). As was implemented in the prementioned study, the same patient-derived iPSC line had the potential to be differentiated into multiple cell types, and expansive growth in protocols for doing so have emerged (Maury *et al.*, 2015; Douvaras *et al.*, 2017). These cell lines are also an efficient method for identifying candidate molecules and therapeutic targets (Egawa *et al.*, 2012; Fujimori *et al.*, 2018). A ground-breaking report in 2018 used both sporadic and familial induced pluripotent stem cell-derived motor neuron phenotypes to identify putative neuroprotective medicines. Ropinirole, a medicine licensed for use in Parkinson's disease was found to be highly effective in reversing disease phenotypes. This opens up the possibility of repurposing Ropinirole, an approach that appears as

a cost- and time-effective strategy for the development of therapeutic options in ALS (Fujimori *et al.*, 2018).

Gene editing has increased the effectiveness of studying iPSCs and has overcome a major limitation associated with this model, which is the line variability at genetic, epigenetic, transcriptional and functional levels complicating the identification of underpinning molecular pathomechanisms (Cahan and Daley, 2013). Evidence from whole genome sequencing has suggested that any two hiPSC lines may have more transcriptional disparities than human iPSCs compared to human ESCs (Bock *et al.*, 2011). A disease-related mutation, therefore, can result in an exaggerated or hidden phenotype, leading to inaccurate comparisons between patient and control cell lines (Sandoe and Eggan, 2013). Gene editing technology uses nucleases to target DNA sequences and induce double-stranded breaks, joining DNA at new points, resulting in an edited genome. This allows investigation of specific genes or gene mutations in relevant disease pathologies.

Gene editing in hiPSC-based systems of monogenetic diseases has therefore been ground-breaking with the generation of gene-corrected/isogenic controls, where the only variable is the mutation of interest, allowing causality to be ascribed to a given phenotype (Beurdeley *et al.*, 2013; Ran *et al.*, 2013). The newest tool is CRISPR/Cas9, which is known to be faster, easier, and more efficient than the previously used methods [zinc finger nucleases (ZFNs), transcription activator-like effector nucleases (TALENs)], although there is a risk of off-target effects that may cause genetic instability and disrupt the function of otherwise normal genes (Ran *et al.*, 2013; Sander and Joung, 2014; Selvaraj *et al.*, 2018). Several solutions have been identified to overcome the challenges encountered with CRISPR/Cas9 and provide solid genotype-phenotype correlations, including the paired nicking strategy, where the Cas9 nuclease is replaced with a nickase version of Cas9 and paired with two single-guided RNAs that each cleaves one strand. This has been shown to reduce off-target activity by 50-1500 fold in cell lines (Ran *et al.*, 2013). Other solutions to enhance target specificity and minimise mutagenesis include engineered smaller-sized versions of Cas9 and truncation/alteration of the single-guide RNA either at the 3' or 5' ends or by addition of 2 guanine nucleotides to its 5' end (X. H. Zhang *et al.*, 2015; Kleinstiver *et al.*, 2016).

In *C9orf72*-ALS, two methods have been predominantly implemented to generate gene-corrected lines with the CRISPR-Cas9 method. These are the non-homologous end-joining (NHEJ) mechanism, which involves deletion of the G4C2 repeat region (Selvaraj *et al.*, 2018) and the homology-directed repair, where the excised region is replaced with a donor template carrying the wild-type repeat size, thus having the advantage of preserving the architecture of the locus (Ababneh *et al.*, 2020). Importantly, NHEJ was undertaken in vivo in two *SOD1*-ALS transgenic mouse models and led to the prevention of ALS-like pathology. Although this genome editing strategy can be associated with off-target effects, large deletions and hence genomic instability – all of which are significant safety concerns – the authors concluded that these events are predictable and can be overcome through careful selection of the cleavage sites (Deng *et al.*, 2021). Such findings highlight the translational capacity of CRISPR/Cas9 genome editing.

Using three independent *C9orf72* patient lines with gene-corrected pairs, generated via the CRISPR-Cas 9 technology (NHEJ mechanism), the Chandran group has shown; (1) selective human MN vulnerability to AMPA-receptor-mediated excitotoxicity that is mutation-dependent (Selvaraj *et al.*, 2018); (2) that C9-mutant astrocytes recapitulate key aspects of disease including nuclear RNA foci and that upon physical contact with MNs they cause them to undergo progressive loss of action potential output due to reductions in the magnitude of voltage-gated Na+ and K+ currents. This effect is reversed with control or gene-corrected astrocytes, confirming that the C9 mutation is responsible for the non-cell autonomous MN pathophysiology (Zhao *et al.*, 2020); (3) reduced neurite outgrowth and dysfunctional mitochondrial motility and bioenergetic function in C9-MNs with rescue of the phenotypes in the gene-corrected lines (Mehta *et al.*, 2021).

One important consideration when using iPSCs for age-related conditions is that iPSCs more closely represent fetal cells rather than adult or aged cells. Thus, if the onset of the disease depends on the aging process, as in ALS, additional methods are required to address the discrepancies between the advanced age of onset of neurodegenerative conditions and the fetal-equivalent maturation state of iPSC-derived cells and recapitulate clinical pathophysiological states (Devine and Patani,

2017). Induction of aging through the addition of progerin in hiPSC-based Parkinson's disease model, induced an aged phenomenon and dopamine-specific phenotypes, such as neuromelanin accumulation, loss of dendrites, oxidative stress and Lewy-body precursor inclusions, generating a more representative disease model (Miller *et al.*, 2013). Introducing excitotoxins, proteasome inhibitors, and inducers of oxidative stress or DNA damage constitute other methods that have been employed to experimentally manipulate aging *in vitro* (Richard and Maragakis, 2015). Additionally, to circumvent this limitation, recent studies have shown that neurons and astrocytes directly converted/reprogrammed from fibroblasts, without the addition of pluripotency factors, retain the ageing features of the donors' fibroblasts at a transcriptional and functional level (Victor *et al.*, 2018; Gatto *et al.*, 2021). However, the field still requires further exploration with a systematic and comprehensive multifaceted approach to address the various cellular and molecular stages and hallmarks of ageing including genomic instability, epigenetic alterations, loss of proteostasis, mitochondrial defects, cellular senescence, altered intercellular communication and others, in a standardised and reproducible manner.

Mutations can also randomly appear during the reprogramming or passaging steps in the development of iPSC cell lines (Gore *et al.*, 2011). This has led to the introduction of karyotyping as a standard post-reprogramming procedure. Routine genetic screening is also recommended to establish that no deleterious point mutations are present that may impact the ALS phenotypes.

Finally, like other *in vitro* methods, hiPSC models, cannot fully recapitulate the *in vivo* environment due to the lack of 3D structure and function. With the recent advances in 3D organoid modelling, studying intercellular interactions and circuit dynamics is now feasible, providing a physiologically relevant preclinical model which helps to capture the complexity of the human brain development, function, and disease and to revolutionise drug discovery. Recently, Pereira et al. 2021, produced sensorimotor organoid cultures that contained functional neuromuscular junctions between the motor neurons and skeletal muscle, which were impaired in organoids derived from people with ALS (Pereira *et al.*, 2021). Several challenges remain to be addressed including model reproducibility; detailed characterisation of cell subtypes at all stages of the organoid culture; determination of the degenerative versus developmental

contributions to the phenotypes; and deciphering the interactions of a multitude of mechanisms in a structurally highly complex model. In any case, limitations of all scientific methods, including iPSCs, make it crucial to substantiate experimental findings with human data in post-mortem tissue (Selvaraj *et al.*, 2018; Mehta *et al.*, 2021).

1.6 Aims of studies

Against this background, I will undertake a series of studies to investigate the cell- and non-cell autonomous consequences of the *C9orf72* mutation on hiPSC-derived astrocytes.

(1) [Chapter 3] – Investigation of **astrocyte-mediated <u>non-contact dependent</u> mechanisms (astrocyte conditioned medium; ACM)** in *C9orf72*-mediated ALS.

Examination of ACM effects on neurons: This section focuses on the molecular effects of *C9orf72,* and gene-corrected (C9Δ) hiPSC-derived astrocyte conditioned medium (ACM) on neurons, utilizing a fully humanised model, through:

a. Transcriptomic analysis of ACM-treated human embryonic stem cell derived (hESC)-derived *HB9*::GFP MNs to identify gene expression changes and pathways affected by the conditioned medium.
b. Reverse phase protein array on ACM-treated hESC *HB9*::GFP MNs to provide insights into protein expression and post-translational modifications.

Proteomic analysis of ACM: In a complementary analysis, comprehensive proteomic profiling of the ACM itself using mass spectrometry is conducted for characterisation of the protein composition of the ACM and identification of potential factors that mediate its effects on neurons.

(2) [Chapter 4] – Investigation of **astrocyte-mediated <u>contact-dependent</u> mechanisms** through the mixed species model.

This chapter analyses transcriptomic alterations in wildtype primary rodent MNs induced by cocultured hiPSC-derived *C9orf72* astrocytes using mixed species RNA-Seq.

(3) [Chapter 5] – Investigation of the effects of astrocyte genotype on axonal mitochondrial transport and neuronal mitochondrial bioenergetics through implementation of astrocyte-neuronal physical cocultures.

This chapter explores how boosting astrocyte metabolism with selective PGC1α pathway manipulation in *C9orf72* astrocytes can rescue the axonal mitochondrial transport deficit.

Chapter 2 METHODS & MATERIALS

2.1 Generation of iPSC lines and gene-corrected control iPSC lines

Dermal fibroblasts from three *C9orf72* ALS/FTD patients (C9-1, C9-2, C9-3) harbouring the G_4C_2 repeat expansion in the *C9orf72* gene were acquired and reprogrammed under full Ethical/Institutional Review Board approval at the University of Edinburgh. Gene-edited controls were generated via CRISPR/Cas9 technology, as previously described by our group (Selvaraj *et al*., 2018; Zhao *et al*., 2020; Mehta *et al*., 2021). Over the course of this study, karyotypes of all iPSC lines were examined using the conventional Giemsa banding chromosomal analysis, conducted by The Doctors Laboratory Ltd, London. Exclusion of mycoplasma contamination was ascertained through monthly testing of iPSC culture supernatants using the Venor®GeM Classic detection kit (11-1050, Minerva Biolabs GmbH).

Details of human iPSC control and C9orf72 lines

Line	Reprogramming method	Repeat length	Sex	Ethnicity	Age of onset (years)	Age at skin biopsy (years)	Disease duration (months)	Diagnosis	Family history
C9-1	Sendai	c. 750	Female	Dutch	38	39	31	ALS/FTD (pm confirmed)	ALS/FTD
C9-2	Retroviral	c. 638	Male	Caucasian	52	58	72	ALS	Mother-dementia
C9-3	Retroviral	c. 960	Male	Dutch	65	67	36	ALS	ALS/FTD

Table 2.1: Details of human iPSC control and C9orf72 lines.

2.2 Motor neuron (MN) generation from parental and gene-edited human iPSCs

Spinal motor neuron (MN) differentiation was performed using an established protocol with minor modifications, yielding a highly enriched and electrophysiologically mature neuronal culture, devoid of glia, with approximately 60% of cells being positive for islet-1 and islet-2 homeobox MN markers one week post-plating (Mehta *et al.*, 2021) (

Appendix). Induced pluripotent stem cells (iPSCs) were dissociated into single cells using 1X Accutase® (Sigma-Aldrich) and neuralised as a suspension culture utilizing dual-SMAD inhibition with SB-431542 (20 µM; Tocris Bio-Techne), LDN-193189 (0.1 µM; Selleckchem), and potentiation with the Wnt-agonist, CHIR-99021 (3 µM; Tocris Bio-Techne) in N2/B27 medium, which consists of 0.5X Neurobasal™ (Gibco Thermo Fisher Scientific), 0.5X Advanced DMEM/F12 (Gibco Thermo Fisher Scientific), 1X Antibiotic–Antimycotic (Gibco Thermo Fisher Scientific), 1X GlutaMAX™ (Gibco Thermo Fisher Scientific), 100 µM beta-mercaptoethanol (Gibco Thermo Fisher Scientific), 1X B-27™ supplement (Gibco Thermo Fisher Scientific), 1X N-2 supplement (Gibco Thermo Fisher Scientific), and 10 µM l-ascorbic acid (Sigma-Aldrich).

On day 2, neural spheres were simultaneously patterned to spinal cord identity by treatment with retinoic acid (RA, 0.1 µM; Sigma-Aldrich) and smoothened agonist (SAG, 0.5 µM; Sigma-Aldrich), promoting caudalisation and ventralisation, respectively, along with SB-431542, LDN-193189, and CHIR-99021 in N2/B27 medium for an additional 5 days. On day 7, spheres were maintained in culture with RA and SAG, supplemented with recombinant human brain-derived neurotrophic factor (BDNF, 10 ng/ml; R&D Systems Bio-Techne) in N2/B27 medium to generate MN progenitors. From day 9, MN progenitors were cultured in the day 7 medium with the addition of DAPT (10 µM; Tocris Bio-Techne), an inhibitor of Notch signaling, for an additional 5 to 7 days.

At days 14 to 16, MN spheres were dissociated using 0.05% Trypsin–EDTA (Gibco Thermo Fisher Scientific), and cells were plated as a monolayer onto dishes coated with laminin from Engelbreth-Holm-Swarm murine sarcoma basement membrane (5 µg/ml; Sigma-Aldrich), fibronectin human plasma (10 µg/ml; Sigma-Aldrich), and Matrigel® (1:20), which had been pre-treated with poly-l-ornithine bromide (100 µg/ml; Sigma-Aldrich). On day 0, MN spheres were dissociated and cultured in motor neuron neurotrophic factor (MN-NF) medium, which contains 1X Neurobasal, 1X Antibiotic–Antimycotic, 1X GlutaMAX™, 1X MEM Non-Essential Amino Acids solution (Gibco Thermo Fisher Scientific), 100 µM beta-mercaptoethanol, 1X B-27™ supplement, 1X N-2 supplement, RA (1 µM), ascorbic acid (2.5 µM), BDNF (10 ng/ml), recombinant human glial-derived neurotrophic factor (GDNF, 10 ng/ml; R&D Systems Bio-Techne),

recombinant human ciliary neurotrophic factor (CNTF, 10 ng/ml; R&D Systems Bio-Techne), and animal-free recombinant human insulin-like growth factor-1 (IGF-1, 10 ng/ml; PeproTech), along with 25 µM uridine/5-fluoro-2′-deoxyuridine (U/FDU).

From day 2 onwards, the medium was regularly changed every 2 to 3 days and supplemented with uridine/5-fluoro-2′-deoxyuridine (1 µM; Sigma-Aldrich) for at least one-week post-plating, to eliminate residual proliferating cells.

2.3 Astrocyte generation from parental and gene-edited human iPSCs

Astrocytes were generated from iPSCs using established lab protocols and were characterised through expression of astrocyte-specific markers and implementation of functional assays (glutamate uptake assay and calcium imaging) as previously described (Zhao *et al*., 2020) (

Appendix).

Specifically, iPSCs were neuralised and subsequently converted into spheres following the established protocols described in the previous section. The spheres were then cultured in motor neuron (MN) maturation medium for a duration of 2 to 4 weeks. Following this maturation phase, the spheres were chopped and cultured in NSCR EL20 medium for an additional 4 to 6 weeks to induce astrogliogenesis. At the conclusion of this conversion phase, the medium was switched to NSCR EF20 medium to support the proliferation of astrocyte progenitor cells (APCs) within the spheres.

The resulting astrospheres were dissociated into single cells using the Papain Dissociation System (Worthington Biochemical) and plated onto 6-well plates coated with Matrigel (BD Biosciences, diluted 1:80) at a density of 7.5 × 10^5 cells per well. These cells were subsequently differentiated into astrocytes by transitioning the medium to AstroMed CNTF medium for a period of 2 weeks. Throughout the astrocyte generation process, the media were changed every 2 to 3 days to ensure optimal growth conditions.

The NSCR EF20 medium comprised Advanced DMEM/F12 (Invitrogen), 1% N2 supplement (Invitrogen), 1% B-27 supplement (Invitrogen), 1% penicillin/streptomycin (Invitrogen), 1% GlutaMAX solution (Invitrogen), 20 ng/ml fibroblast growth factor 2 (FGF-2; PeproTech), and 20 ng/ml epidermal growth factor (EGF; R&D Systems). The AstroMed CNTF medium consisted of Neurobasal medium (Invitrogen), 2% B-27 supplement (Invitrogen), 1% non-essential amino acids (NEAA; Invitrogen), 1% penicillin/streptomycin (Invitrogen), 1% GlutaMAX (Invitrogen), and 10 ng/ml ciliary neurotrophic factor (CNTF; R&D Systems).

2.4 Cocultures of MNs and astrocytes

Astrocyte progenitor cells were dissociated into single cells and plated on Matrigel-coated plates (Matrigel 1:80 diluted, BD Biosciences) in astrocyte differentiation medium to differentiate progenitors into mature astrocytes over 2 weeks. Astrocyte

differentiation medium contains Neurobasal medium (Invitrogen), 2% B-27 supplement (Invitrogen), 1% NEAA (Invitrogen), 1% penicillin/streptomycin (Invitrogen), 1% GlutaMAX (Invitrogen), and 10 ng/ml ciliary neurotrophic factor (CNTF; R&D Systems). At 2 weeks, MN spheres (day 16) were dissociated into single cells using the Trypsin/EDTA and plated on astrocyte monolayers in MN-NF medium (1X Neurobasal, 1X Antibiotic–Antimycotic, 1X GlutaMAX™, 1X MEM Non-Essential Amino Acids solution [11140–035, Gibco™ Thermo Fisher Scientific], 100 µM beta-mercaptoethanol, 1X B-27™ supplement, 1X N-2 supplement, RA [1 µM], ascorbic acid [2.5 µM], BDNF [10 ng/ml], recombinant human glial-derived neurotrophic factor [GDNF, 10 ng/ml; 212-GD, R & D Systems® Bio-Techne], recombinant human ciliary neurotrophic factor [CNTF, 10 ng/ml; 257-NT, R & D Systems® Bio-Techne], and animal-free recombinant human insulin-like growth factor-1 [IGF-1, 10 ng/ml; AF-100–11, PeproTech®]).

Astrocyte-MN cocultures and MN monocultures were maintained for 2 weeks prior to performing experiments. MN-NF medium was changed every 2–3 days and supplemented with uridine/5-fluoro-2′-deoxyuridine (1 µM, U/FDU; U3003 and F0503, Sigma-Aldrich®) for at least 1-week after plate-down to remove residual proliferating cells.

Plate	Density of astrocytes	Density of neurons
96-well plate (89626, ibidi)	$4x10^4$ cells/well	$4x10^3$ cells/well
µ-*Slide* 8-well plate (80826, ibidi GmbH)	$12x10^4$ cells/well	$10x10^3$ cells/well
Seahorse XF24 V28 cell culture plate	$5x10^4$ cells/well	$5x10^4$ cells/well

Table 2.2 Density of neurons and astrocytes in physical cocultures

2.5 Axonal Transport Studies

Astrocyte-MN cocultures were generated on µ-*Slide* 8-well plates as described above. MN monocultures were also produced by plating MNs on laminin/fibronectin/matrigel-

coated µ-slide 8-well ibidi dishes at a density of $5x10^4$ cells per well [laminin (5 µg/ml; L2020, Sigma-Aldrich), fibronectin human plasma (10 µg/ml; F2006, Sigma-Aldrich), and Matrigel (1:20)-coated dishes that had been pre-treated with poly-L-ornithine bromide (100 µg/ml; P3655, Sigma-Aldrich)]. At plate-down, the MNs were sparsely transduced with lentivirus expressing mitoDsRed2 as follows:

a) MN Monocultures: Multiplicity of infection (MOI) of 0.5-1, adjusted to obtain 1-2 labelled cells per field of view, as previously described (Mehta *et al.*, 2021).
b) Astrocyte-MN cocultures: mitoDsRed2 lentivirus was added at MOI 10 to approximately 10,000 MNs (per well; on µ-*Slide* 8-well plates) and MNs were selectively transduced prior to being transferred onto fully differentiated astrocytes.

Live imaging of mitochondrial axonal transport was undertaken at 14 days post MN plate-down at 63 X magnification (Plan-Apochrat 1.40 NA oil DIC M27 objective, Carl Zeiss) using an Axio Observer Z1 inverted motorised microscope (Carl Zeiss). The microscope was equipped with a Cy3 FL filter-set (Carl Zeiss), Zen 2011 z-stack, time lapse and Definite Focus modules (Carl Zeiss), and an S1 Environmental System (Carl Zeiss) incubation chamber for temperature control at 37 °C and 5% CO_2 flow. Time-lapse imaging of mitochondria in axons was conducted as previously described (Mehta *et al.*, 2021). For all conditions, measurements were acquired from the proximal portion of the axon and the axonal segments selected for recording, were at least 100 µm from the cell soma, to avoid the axon hillock – the part of the axon at the juncture with the cell body. Images were acquired at a capture rate of 0.2 Hz for 5 minutes, covering a ~ 100 µm stretch of axon and a small z-stack, if required. Motile mitochondria were defined as those travelling at or above the cut-off speed of 0.1 µm/s (Fumagalli *et al.*, 2021). Time lapse images were used to generate videos, exported from the Zeiss software and further analysis was implemented in Fiji. Kymographs were generated and analysed using KymoToolBox ImageJ plugin (Zala *et al.*, 2013) to determine the numbers of static (≤ 0.1 µm/s) *versus* bidirectionally motile mitochondria (either towards or away from the soma). A minimum of 5 axons (n) were imaged per condition per biological replicate (N, where N=3). The percentage of motile mitochondria (labelled with mitoDsRed2) relative to the total number of mitochondria was quantified in a 100 µm stretch of axon in *C9orf72* and gene-edited MNs. For

calculating the mean speed of motile mitochondria in each segment measured, only mitochondria with a speed higher than 0.1 microns per second over the recorded section of time (5 minutes) were included in the analysis. The average speed of those mitochondria per axon was taken forward.

2.6 Metabolic profiling of astrocytes & neurons (seahorse assay)

The following cell densities were used for the seahorse assay:

a) Astrocyte monocultures: APCs were plated on Matrigel-coated V7 Seahorse plates (100777-004, Agilent) at a density of 50,000 cells per well to ascertain a highly confluent cellular monolayer. They were cultured in CNTF medium for differentiation into astrocytes over 2 weeks.
b) MN monocultures: MNs were plated on polyethyleinimine (2.2 mg/ml in 0.1 M borate buffer, pH 8.4; 408727 and B3545, Sigma-Aldrich®)-treated V28 Seahorse plates (100882-004, Agilent). The plates were subsequently coated overnight with laminin/Matrigel®/fibronectin as described in (Mehta *et al.*, 2021). Neuronal density was at 50,000 cells per well.
c) Astrocyte-MN cocultures: described in Section 2.4.

The standard Agilent Seahorse XF Cell Mito Stress protocol was modified depending on the condition and the experiments were conducted at 14 days post MN plate down using a Seahorse XFe24 Analyzer (Agilent). This reader can simultaneously measure (1) the oxygen consumption rate (OCR), an excellent read-out for mitochondrial respiratory activity and the current choice experiment to examine underlying mitochondrial dysfunction and (2) the extracellular acidification rate (ECAR), a read-out that correlates with lactate excretion per unit time after its conversion to pyruvate and therefore the rate of anaerobic glycolysis. Culture medium was exchanged for low-buffering capacity Seahorse XF Base Medium (102,353, Agilent) supplemented with 1X Glutamax™, 10 mM glucose (Sigma-Aldrich®) and 2 mM pyruvate (Sigma-Aldrich®), adjusted to pH 7.35 ± 0.5 at 37 °C with 1M sodium hydroxide. The cells were equilibrated for 30 minutes at 37 °C with no CO_2, prior to being inserted in the machine. OCR and ECAR were measured basally and after sequential addition of specific mitochondrial inhibitors as illustrated in the table below. FCCP dose was

optimised for astrocyte and neuronal monocultures (tested doses for neurons – 0.125 µM, 0.25 µM, 0.5 µM; tested doses for astrocytes – 0.125 µM, 0.25 µM, 0.5 µM, 1 µM) and the concentration adopted that maximised the OCR response.

DRUG	TARGET	ASTROCYTE MONOCULTURES	MN MONOCULTURES	ASTROCYTE-NEURONAL COCULTURES
Oligomycin (Sigma-Aldrich®)	F_1F_0 ATP synthase inhibition	1.5 µM	3 µM	3 µM
Carbonyl cyanide 4-(trifluoromethoxy)phenylhydrazone (FCCP; Cayman Chemical, Cambridge Bioscience)	Increases proton leak; uncouples mitochondria	1 µM	0.5 µM	0.5 µM
Antimycin/rotenone (Sigma-Aldrich®)	Complex III/Complex I inhibitors	0.5 µM	3 µM	3 µM
2-deoxy-D-glucose (D6134, Sigma-Aldrich®)	Terminates glycolysis	100 mM	100 mM	100 mM

Table 2.3 Drugs targeting the mitochondrial bioenergetic machinery and their concentrations

The protocol involved a 3 min mixing, 2 min wait, 3 min measure cycle (total duration of each cycle was 8 min). Three measurements/cycle were obtained basally (before drug injections; total duration of 24 min) and three measurements were taken after each drug addition, (first: oligomycin; second: FCCP; third: antimycin/rotenone; fourth: 2-deoxy-D-glucose). Five individual wells were used per condition in each plate, with experiments repeated in three independent plate-downs from different MN differentiations ($N = 3$). In astrocyte and MN monocultures, the measured OCR ($[O_2]$/time) was normalised to total protein content using the bicinchoninic acid assay (23225, Pierce™ Thermo Fisher Scientific) (Connolly *et al.*, 2018). For astrocyte-neuronal cocultures, neuronal counts were estimated through neuron-specific staining [immunocytochemistry with SMI-312 at 1:1000 (837904, BioLegend®)]. Data were visualised in, and imported from, Seahorse Wave Desktop software (version 2.6.0.31, Agilent). **Basal respiration,** which represents the net sum of all processes in the cell capable of consuming O_2, including mitochondria and other oxidases, was calculated by subtracting non-mitochondrial respiration (i.e., the minimum OCR value after antimycin/rotenone addition) from the OCR value right before oligomycin injection. **Maximal respiration** was calculated by subtracting non-mitochondrial respiration from the highest OCR measurement after FCCP injection. **ATP-linked**

respiration was calculated by subtracting the oligomycin rate from baseline cellular OCR. **Basal ECAR** was represented by the value immediately prior to the addition of oligomycin. **Respiratory-inhibited maximal glycolysis** was inferred by subtracting the ECAR value immediately after the injection of 2-deoxy-D-glucose from the ECAR value immediately prior to the injection of 2-deoxy-D-glucose. In physical astrocyte-neuronal cocultures, the basal, the ATP-linked and maximal respiration of neurons was obtained after subtraction of corresponding astrocyte values.

2.7 Mitochondrial staining for determination of mitochondrial membrane potential

Astrocyte-MN cocultures were generated on 96-well plates as described above. MN monocultures were also produced by plating MNs on laminin/Matrigel/fibronectin-coated 96-well plates at a density of 10,000 cells per well. Neurons were labelled and demarcated from astrocytes either at plate-down with transduction with lentivirus expressing GFP or immunostained after fixation with MN-marker SMI312 at 1:1000 (837904, BioLegend®). After 14 days, astrocyte-MN cocultures and MN monocultures were incubated with 100 nM of potentiometric dye MitoTracker Red CMXRos (Thermo Fisher) for 45 minutes at 37°C (Dafinca *et al.*, 2016). This is a membrane-permeant, lipophilic, cationic fluorescent probe that is sequestered in the mitochondrial membrane of living cells and its accumulation is dependent on mitochondrial potential (Connolly *et al.*, 2018). The covalent binding of the dye to the polarised inner mitochondrial membrane permits its retention during washing and fixation of cells and makes it suitable for fluorescence microscopy. The cells were then washed with PBS and fixed in 4% PFA. Fluorescence was visualised using Opera Phenix Plus high-content screening system at 40X magnification (OperaPHX/OPRTCLS Water Immersion Objective 40x: NA 1.1, WD 0.62 mm (field of view: approx. 323 µm x 323 µm). Flatfield correction was automatically performed by Harmony Software during image acquisition. Harmony or Signals Image Artist was used for image analysis.

2.8 Lentiviral overexpression of PGC1α

PGC1α overexpression lentivirus that was previously generated by our lab (Mehta *et al.*, 2021), was transduced in human-iPSC derived astrocytes (*C9*-mutant) at a multiplicity of infection (MOI) of 5.

2.9 Proteomic studies of astrocyte-conditioned medium (astrocyte secretome)

2.9.1 Secretome isolation protocol

Astrocyte progenitor cells were dissociated into single cells and plated on Matrigel-coated 10-cm plates (Thermo Fisher, cell culture-treated surface) in astrocyte differentiation medium, for differentiation into mature astrocytes over 2 weeks. Two plates were required for each line per biological replicate at 80-90% cell confluency for secretome isolation. Fully mature astrocytes were washed three times in pre-warmed PBS and maintained in serum- and phenol red-free medium without exogenous proteins for 24h. The medium was subsequently collected in a pre-chilled 50 ml Falcon tube and centrifuged at 400 x $g_{(av)}$, 10 min, 4°C to remove cells. The cell pellet was discarded, and the supernatant was re-centrifuged at 1000 x $g_{(av)}$, 10 min, 4°C to remove cellular debris. The supernatant (clarified conditioned medium) was then filtered through a sterile 0.22-µm filter unit into a fresh, pre-chilled Falcon tube.

Exosome preparation: Exosomes were isolated from conditioned medium by ultracentrifugation at 100,000 x $g_{(av)}$ for 90 min at 4 °C using a SW41 rotor and Beckman Coulter Ultracentrifuge after initial collection, centrifugation, and filtration through a 0.22 µm filter to remove cell debris as described above. The supernatant was then removed, and the exosome pellet was resuspended in 300 µl DEBC treated PBS and stored in -80°C.

Soluble factor preparation: The supernatant (exosome-free medium) obtained following ultracentrifugation, was concentrated using a 20-ml MWCO Pierce protein concentrator (Thermo Fisher Scientific) to a final volume of 100µl – 150µl through centrifugation at 3000 x $g_{(av)}$, 45-60 min, 4°C.
The exosome and protein fractions were reduced, alkylated and digested with trypsin using the in-solution digest approach. Peptides were desalted and purified using C18

StageTips and analysed in an Orbitrap Fusion™ Lumos™ Tribrid™ Mass Spectrometer at the Institute of Genetics and Cancer (collaboration with Dr Alfonso Bolado – Professor Margaret Frame's group).

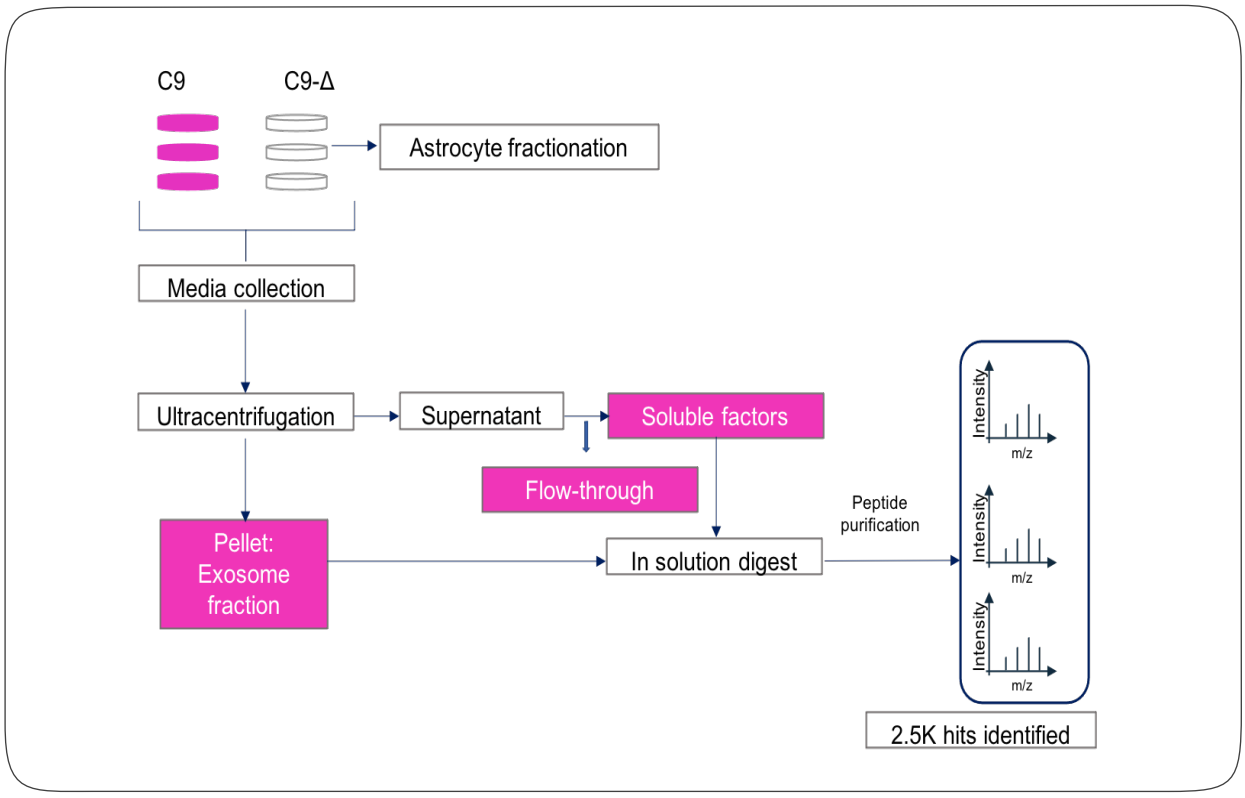

Figure 2.1 Outline of secretome and exosome preparation.

2.9.2 Mass Spectrometry Data Analysis

The mass spectrometry (MS) data analysis was conducted with Dr Alfonso Bolado, a postdoctoral researcher in Professor Frame's laboratory at the Institute of Genetics and Cancer, University of Edinburgh. Label-free quantitative analysis of MS data was performed with MAXQUANT Software (version 1.6.2.10). Label-free quantification (LFQ) values were normalised by total cell lysate. The calculated LFQ values were used for further statistical analysis using the Perseus software. The 'protein groups' result files of all biological replicates were uploaded as a matrix. Potential contaminants, reversed protein entries, and proteins that were only identified by modified peptides, were excluded. Hits that were not identified in at least two biological replicates of either group were discarded.

LFQ values were Log2 transformed, normalized by z-score, and missing values were imputed from a normal distribution. Missing values were imputed in the Log2 Z-scored matrix, specifically for samples where x - 1 valid values were found in at least one group, where x represents the number of biological replicates, and the groups refer to the conditions (gene-corrected isogenic or mutant). Hits with less than x - 1 valid values in at least one group were discarded. The imputation was performed using the Perseus software via the "Processing -> Imputation -> Replace missing values from normal distribution" function. This method allows Perseus to shrink the distributions by a factor of “0.3” (width) and downshift them by “1.8” (downshift) standard deviations, utilizing each column's (biological sample) average and standard deviation to maintain the variances among samples. Other imputation methods were not considered, as this approach is considered robust and accounts for differences among each sample; the downsize employed ensures that the imputed values do not produce statistically false positive results.

Unsupervised hierarchical clustering was performed based on uncentred Pearson correlation using Cluster 3.0. Distances between hits were computed using a complete-linkage matrix. Clustering results were visualized using Java TreeView (version 1.1.1).

To analyse protein enrichment, the log2 transformed LFQ intensities of different replicates were grouped by categorical annotation, and the Benjamini-Hochberg procedure with FDR ≤ 0.05 was implemented. Proteins exhibiting significant results at an FDR ≤ 0.05 and a fold change higher than 1.5 compared to the other group were considered as enriched proteins. Enriched proteins were visualized by volcano plots, delineating the calculated differences of means against the -log2 transformed p-values. Proteins categorized as “enriched” were analysed based on their number of unique peptides. Only proteins identified by at least two unique peptides in all samples of the enriched group were considered. Hits were clustered by cellular compartment (STRING analysis). The proteins described as extracellular hits (GO terms: secretory granule, vesicle, extracellular region part, extracellular space) were further analysed to identify potentially affected pathways/functions.

Additionally, all samples were processed on the same day and analysed using three technical replicates to ensure consistency and reliability in the results.

2.10 Mixed species physical coculture experiment

Mixed species coculture experiments were performed using mouse MNs and hiPSC-derived astrocytes (1 x control, 1 x *C9orf72* and its corresponding gene-corrected pair). The mixed species RNA-Seq approach allows the investigation of bidirectional juxtacrine signalling mechanisms by profiling contact-dependent transcriptomic changes in both cell types involved, MNs and astrocytes, simultaneously. This is attributed to the evolutionary divergence of mRNAs between rodents and humans that facilitates *in silico* segregation of mRNA in this mixed species experimental paradigm (Qiu *et al.*, 2018).

2.10.1 Isolation and enrichment of embryonic mouse MNs from the lumbar spinal cord of individual mouse embryos

Embryonic MNs (E13.5) were obtained from wild type mice (typically 2 litters were required per biological experiment per plate down). Ventrolateral parts of the spinal cord were dissected from the mouse embryos, stored in HBSS, and kept on ice. Tissues were trypsinised (0.1% trypsin) for 15 minutes at 37°C. Trypsin digestion was arrested by adding 0.1% trypsin inhibitor. Tissues were mechanically triturated to form a single-cell suspension and transferred to a p75-^{NTR} panning plate for selective enrichment of MNs. This was followed by addition of depolarisation solution (sterile filtered solution of 30 mM potassium chloride, 0.8% sodium chloride and 2 mM calcium chloride in water; stored at room temperature). Potassium chloride-mediated depolarisation and the consequential opening of voltage-gated calcium channels, leads to calcium influx, reorganisation of the actin cytoskeleton and detachment of the cells from the antibodies (Wiese *et al.*, 2010). About 5,000-15,000 MNs were isolated and enriched from one embryonic spinal cord. MNs were plated on confluent mature astrocyte monolayers for cocultures on 12-well plates in MN-NF maturation medium (*circa* 300,000 astrocytes and 50,000 – 75,000 mouse MNs per well, depending on yield of mouse MNs). MN monocultures were also produced. Media were changed

every 2-3 days, and all cultures were maintained for 7 days. Astrocyte monocultures, used as control, were also switched to MN-NF maturation medium.

2.10.2 Quantitative reverse transcription PCR

Total RNA was extracted with a RNeasy Mini Kit (Qiagen, 74106) according to the manufacturer's instructions, followed by genomic DNA removal using the on-column DNase method (79254, Qiagen®). 250 ng of RNA was reverse transcribed to cDNA using the DyNAmo™ cDNA Synthesis Kit (10748908, Thermo Fisher Scientific). Subsequently cDNA was diluted 1:10. Real-time reverse transcription quantitative PCR (RT-PCR) reactions were implemented in triplicates with a DyNAmo ColorFlash SYBR Green qPCR kit (10442308, Thermo Fisher Scientific) and cycling was conducted using a C1000TM Thermal Cycler with a CFX96 Real-time System (Bio-Rad). qPCR started with initial 3 min denaturation at 95 °C followed by 40 cycles of 95 °C denaturation and 60 °C (murine GAPDH) or 62 °C (18s rRNA, GFAP, murine Synapsin 1) annealing temperature for 30 sec each. The data were visualised and exported using Maestro 1.1 software (Bio-Rad). Primers were synthesised by Sigma-Aldrich®. Primers were designed to only amplify targets from a single species and were validated by qPCRs with cDNA generated from pure mouse or human cultures.

2.10.3 Immunocytochemistry

For validation through immunocytochemistry, monocultures of mouse MNs and hiPSC-derived astrocytes, and cocultures of mouse MNs with hiPSC-derived astrocytes, were generated on 30-mm glass coverslips. 7 days post mouse MN plate-down, cells were washed once with phosphate-buffered saline (PBS; 10010, Gibco™ Thermo Fisher Scientific) and incubated with warm 4% paraformaldehyde (AGR1026, Agar Scientific) for 20 min at room temperature. After fixation, cells were washed three times with PBS, followed by permeabilisation – incubation for 10 min at room temperature with PBS containing 0.2% Triton X-100 (T8787, Sigma-Aldrich®). Thereafter, they were incubated for 1 h at room temperature in 6% normal goat serum blocking buffer (S-1000, Vector Laboratories) in PBS. Primary antibodies were subsequently diluted in blocking buffer and cells were incubated in primary antibody

overnight at 4 °C. The next day, cells were washed three times with PBS and incubated with the appropriate Alexa Fluor-conjugated secondary antibody (Alexa Fluor® range, Thermo Fisher Scientific) at room temperature for 1h, with the samples protected from light. After washing with PBS, 4′,6-diamidino-2-phenylindole (DAPI, 1 µg/ml diluted in PBS; 10236276001, Roche) was applied for nuclear counterstaining for a further 10 min. Coverslips were then washed with PBS, and mounted onto glass slides (12362098, Thermo Fisher Scientific) with FluorSave™ Reagent (345789, Millipore). Images were acquired from random positions of the coverslips, using an Axio Observer Z1 inverted motorised microscope (Carl Zeiss). Primary antibodies used in this study were: SMI-312 at 1:1000 (837904, BioLegend®), β-III-Tubulin at 1:1000 (T8660, Sigma), GFAP at 1:500 (Z0334, Dako), S100β at 1:1000 (Z0311, Dako).

2.10.4 RNA extraction, RNA sequencing and transcriptomic analysis

Total RNA was extracted from mouse MNs, mature hiPSC-derived astrocytes and cocultures of mouse MNs with hiPSC-derived astrocytes (1 x control, 1 x *C9orf72* and its corresponding gene-corrected pair) at 7 days post mouse MN plate down, using the RNeasy® Mini kit (74104, Qiagen®), following the manufacturer's instructions. RNA samples were assessed for concentration (NanoDrop ND-100 Spectrometer, NanoDrop Technologies) and quality (Agilent 2200 TapeStation, Agilent Technologies) before library preparation. Library preparation and sequencing were carried out by Edinburgh Genomics (Edinburgh, UK).

For mixed-species transcriptomic analysis of rodent-human cocultures, separation of RNA-Seq reads and assignment to their true species of origin was performed using Sargasso, based on a published protocol (Qiu *et al.*, 2018). Sequencing was performed at a depth of 60M reads for monocultures and 150M reads for coculture samples. Reads were mapped to the primary assemblies of the human (hg38) and mouse (mm10) reference genomes. Alignment was performed with the short RNA-Seq read mapper, STAR (Dobin *et al.*, 2013). Tables of per-gene read counts were generated from the mapped reads with the featureCounts tool (Liao, Smyth and Shi, 2014). Differential expression analysis was then performed using the R package

DESeq2 (Love, Huber and Anders, 2014). Human astrocytes in coculture with mouse motor neurons were compared with astrocyte monocultures (for mutant, gene-corrected, and control astrocytes) to discover differentially expressed astrocytic genes induced or repressed by neurons (at a Benjamini-Hochberg false discovery rate of 0.05). Similarly mouse motor neurons in coculture with mutant, gene-corrected, and control human astrocytes were compared with neurons in monoculture to discover differentially expressed neuronal genes induced or repressed by astrocytes. Gene ontology (GO) analysis was performed on the differentially expressed genes to identify putatively altered pathways or processes, using the R package topGO (Alexa, Rahnenführer and Lengauer, 2006).

2.11 Investigation of molecular effects of astrocyte-conditioned medium on neurons (humanised model)

2.11.1 Generation of MN monocultures

Human embryonic stem cell derived *HB9*::GFP MNs were plated on laminin/ fibronectin/matrigel-coated plates as follows:

a) For Reverse phase protein array, 500,000 cells were plated per well on 12-well plates (Thermo Fisher, cell culture-treated surface) and two wells were required per condition per biological experiment (N, where N=3). Requirements as per protocol – 100 µl of each sample at 2 mg/ml concentration.
b) For RNA sequencing, 100,000 cells were plated per well on 24-well plates (Thermo Fisher, cell culture-treated surface) and two wells were required per condition per biological experiment (N, where N=3). Requirements as per protocol – ≥ 0.5 µg per sample.

Dissociated MNs were cultured in MN-NF medium. MN-NF medium at plate-down and upon addition of astrocyte conditioned medium (ACM), was supplemented with uridine/5-fluoro-2′-deoxyuridine (1 µM, U/FDU; U3003 and F0503, Sigma-Aldrich®) for at least 1-week post plate-down to remove residual proliferating cells. Addition of ACM to MNs took place 48 hours post MN plate-down. MN monocultures were also maintained as controls and MN-NF medium was changed regularly every 2-3 days.

2.11.2 Conditioning the medium

To prepare ACM, hiPSC-derived astrocytes (1 x *C9orf72* and its corresponding gene-corrected pair) were generated on Matrigel-coated 10-cm plates (Thermo Fisher, cell culture-treated surface) in astrocyte differentiation medium, as described above, at 80-90% cell confluency. Two plates of astrocytes per line were prepared for each biological experiment.

Astrocyte monocultures were gently washed with PBS and switched to MN-NF maturation medium (10 ml for each 10-cm plate). Seventy-two hours later, media were collected, centrifuged to remove cellular debris, and added fresh on pre-plated MNs. The MNs were incubated with 50% ACM (1 ml for 12-well plates and 500 µl for 24-well plates) and 50% fresh MN-NF maturation medium with double concentration growth factors. The following incubation periods were implemented:

a) Reverse phase protein array: 7-day treatment with media changes every 72 hours; 24-hour incubation on Day 6 post MN plate down; 2-hour incubation on Day 7 post MN plate down.
b) RNA Sequencing: 24-hour incubation on Day 6 post MN plate down.

2.11.3 Reverse phase protein array

To determine the proteomic effects of ACM on wild-type MNs, Reverse phase protein array (RPPA) was performed on ACM-treated MNs at 3 time-points – 2 hours (for elucidation of immediate and specific phosphorylation events); and over 24 hours and 7 days (for identification of secondary signalling cascades). RPPA is a pathway profiling approach which allows simultaneous analysis of many phosphorylated, cleaved, or total proteins using a pre-specified panel of antibodies against various signalling pathways (c. 120 antibody spots per sample). RPPA sample preparation was performed as previously described by our group (Johnstone *et al.*, 2019).

Cells were plated on 12-well plates as described above. Media was removed and cells were washed with ice cold PBS whilst kept on ice. All excess PBS was aspirated. Freshly prepared lysis buffer was added to cells at 75-100 ul per well [1% Triton X-100, 50 mM HEPES, pH 7.4, 150 mM NaCl, 1.5 mM $MgCl_2$, 1 mM EGTA, 100 mM NaF, 10 mM Na pyrophosphate, 1 mM Na_3VO_4, 10% glycerol, containing freshly added protease and phosphatase inhibitors (Roche Applied Science, Cat. 05056489001 and 04906837001, respectively)]. Cells were scraped, transferred in 1.5 ml tubes, and incubated on ice for 20 min with occasional vortexing. They were subsequently centrifuged at 14,000 rpm for 10 minutes at 4°C. The supernatant was collected, and the cell pellet was discarded. Cellular protein concentration was determined by

Bradford protein assay using Coomassie Plus Protein Assay (ThermoFisher) and BSA protein standard (2 mg/ml) (ThermoFisher). Absorbance was read in flat-bottomed 96 well plates with 595nm filter plate reader (FLUOstar Omega, BMG Labtech, Aylesbury, UK). Protein concentrations were adjusted to 2mg/ml with lysis buffer. Protein concentrations at or less than 1 mg/ml were left undiluted. Samples were heated to 80°C for 3 minutes and then printed as a concentration series in replicates. Multiple exposure and curve fitting parameters were performed to ensure protein abundance measurements were conducted in the linear range to obtain a single value. Established protocols were followed for the preparation of the Nitrocellulose slide format RPPA (Macleod, Serrels and Carragher, 2017). 120 intracellular signalling molecules were examined which were considered ideally suited to elucidate mechanisms of action by ACM on neurons (Table 2.3).

Table 2.4 Antibodies used in RPPA study

Antibody	Supplier	Catalog Number	Species
FAK1	Cell Signaling Technologies	3285	rabbit
FAK1 P Y397	Cell Signaling Technologies	3283	rabbit
CamKII P Thr286	Cell Signaling Technologies	3361	rabbit
HSP27 (HSPB1) P Ser78	Cell Signaling Technologies	2405	rabbit
IkB-alpha	Cell Signaling Technologies	4812	rabbit
MEK1/2	Cell Signaling Technologies	9122	rabbit
MEK1/2 P Ser217/221	Cell Signaling Technologies	9154	rabbit
PARP	Cell Signaling Technologies	9542	rabbit
PKC (pan) P Ser660 (beta-2)	Cell Signaling Technologies	9371	rabbit
PKC substrate P (R/K)X(S*)(Hyd)(R/k)	Cell Signaling Technologies	2261	rabbit
PKC-zeta	Cell Signaling Technologies	9372	rabbit
PKC-zeta/lambda P Thr410/403	Cell Signaling Technologies	9378	rabbit
IGF-1R beta P Tyr1162,Tyr1163	Invitrogen (Biosource)	44-804G	rabbit
ErbB-1/EGFR	Cell Signaling Technologies	2232	rabbit
ErbB-2/Her2/EGFR P Tyr1248/Tyr1173	Cell Signaling Technologies	2244	rabbit
ErbB-3/Her3/EGFR	Cell Signaling Technologies	4754	rabbit
ErbB-3/Her3/EGFR P Tyr1289	Cell Signaling Technologies	4791	rabbit
Stat5	Invitrogen (Biosource)	44-368G	rabbit
Stat5 P Tyr694	Cell Signaling Technologies	9351	rabbit
EGFR P Tyr1173	Cell Signaling Technologies	4407	rabbit
Stat3 P Tyr705	Cell Signaling Technologies	9138	mouseIgG1
IkB-alpha P Ser32	Cell Signaling Technologies	2859	rabbit
S6 Ribosomal protein P Ser235,Ser236	Cell Signaling Technologies	2211	rabbit
p44/42 MAPK (ERK1/2)	Cell Signaling Technologies	9102	rabbit
p44/42 MAPK (ERK1/2) P Thr202/Thr185,Tyr204/Tyr187	Cell Signaling Technologies	4370	rabbit

Src	Cell Signaling Technologies	2109	rabbit
Akt	Cell Signaling Technologies	9272	rabbit
Akt P Ser473	Cell Signaling Technologies	4060	rabbit
PARP cleaved Asp214	Cell Signaling Technologies	9541	rabbit
beta-actin	Cell Signaling Technologies	4970	rabbit
NFkB p65 Ser536	Cell Signaling Technologies	3033	rabbit
c-Myc	Cell Signaling Technologies	5605	rabbit
E-Cadherin	Cell Signaling Technologies	3195	rabbit
4E-BP1 P Ser65	Cell Signaling Technologies	9451	rabbit
4E-BP1 P Thr37,Thr46	Cell Signaling Technologies	2855	rabbit
beta-Catenin	Cell Signaling Technologies	9562	rabbit
beta-Catenin P Ser33,Ser37,Thr41	Cell Signaling Technologies	9561	rabbit
beta-Catenin P Thr41,Ser45	Cell Signaling Technologies	9565	rabbit
PTEN	Cell Signaling Technologies	9552	rabbit
Ubiquitin (P4D1)	Cell Signaling Technologies	3936	mouseIgG1
Tsc-2 (Tuberin) P Thr1462	Cell Signaling Technologies	3617	rabbit
Tsc-2 (Tuberin)	Cell Signaling Technologies	3612	rabbit
GSK-3-alpha/beta P Ser21/Ser9	Cell Signaling Technologies	9331	rabbit
p53 P Ser15	Cell Signaling Technologies	9284	rabbit
p38 MAPK PThr180,Tyr182	Cell Signaling Technologies	9211	rabbit
p38 MAPK	Cell Signaling Technologies	9212	rabbit
mTOR P Ser2448	Cell Signaling Technologies	2971	rabbit
mTOR	Cell Signaling Technologies	2972	rabbit
c-Myc P Thr58,Ser62	Epitomics	1203-1	rabbit
S6 Ribosomal protein p Ser240,Ser244	Cell Signaling Technologies	2215	rabbit
S6 Ribosomal Protein	Cell Signaling Technologies	2217	rabbit
Stat1 P Tyr701	Cell Signaling Technologies	9171	rabbit

Src (family) P Tyr416	Cell Signaling Technologies	2101	rabbit
Smad2/3 P Ser465/Ser423,Ser467/Ser425	Cell Signaling Technologies	8828	rabbit
Smad1/5 P Ser463/Ser465	Cell Signaling Technologies	9516	rabbit
AMPK alpha	Cell Signaling Technologies	2532	rabbit
AMPK alpha P Thr172	Cell Signaling Technologies	2535	rabbit
Bcl-2	Epitomics	1017-1	rabbit
Bcl-xl	Abcam/Epitomics	ab32370	rabbit
Bid	Abcam/Epitomics	ab32060	rabbit
Bim P Ser69	Cell Signaling Technologies	4585	rabbit
Caspase 3	Cell Signaling Technologies	9662	rabbit
Caspase 3 cleaved	Cell Signaling Technologies	9664	rabbit
p53	Cell Signaling Technologies	9282	rabbit
CREB	Cell Signaling Technologies	9197	rabbit
GSK-3-beta P Ser9	Cell Signaling Technologies	9336	rabbit
TBK1/NAK	Cell Signaling Technologies	3504	rabbit
GSK-3-beta	Cell Signaling Technologies	9315	rabbit
Ki-67 (Annexin II, p36)	Beckton Dickinson	610968	mouseIgG1
PKC-alpha	Beckton Dickinson	610108	mouseIgG2b
Stat1	Cell Signaling Technologies	9176	mouseIgG1
Tuberin P S1387	Cell Signaling Technologies	5584	rabbit
SQSTM1 (p62)	Cell Signaling Technologies	8025	rabbit
PLC-gamma1	Cell Signaling Technologies	2822	rabbit
Smad2 P Ser465,Ser467	Cell Signaling Technologies	3108	rabbit
Tau	Abcam/Epitomics	ab32057	rabbit
Smad3 P Ser423,Ser425	Cell Signaling Technologies	9520	rabbit
Stat3	Cell Signaling Technologies	12640	rabbit
Tau Phospho/non Phos ser 305	Epitomics	2368-1	rabbit
NFkB p105/p50	GeneTex	GTX110585	rabbit
Calmodulin	Calbiochem	NB12	mouseIgG1
IGF-1R beta	Cell Signaling Technologies	3027	rabbit

Profilin (C56B8)	Cell Signaling Technologies	3246	rabbit
Rock1 (C8F7)	Cell Signaling Technologies	4035	rabbit
EGFR (D38B1) XP ®	Cell Signaling Technologies	4267	rabbit
Arf6 (D12G6)	Cell Signaling Technologies	5740	rabbit
4E-BP1	Cell Signaling Technologies	9452	rabbit
4E-BP1 P Ser65 (174A9)	Cell Signaling Technologies	9456	rabbit
4E-BP1 P Thr37,Thr46	Cell Signaling Technologies	9459	rabbit
Akt P Ser473	Cell Signaling Technologies	9271	rabbit
Akt P Thr308	Cell Signaling Technologies	9275	rabbit
EGFR P Y992	Cell Signaling Technologies	2235	rabbit
mTOR (7C10)	Cell Signaling Technologies	2983	rabbit
YAP1 [EP1674Y]	Abcam	ab52771	rabbit
Histone H2A.X P Ser139 [EP854(2)Y]	abcam	ab81299	rabbit
Eph1A [EPR1786]	abcam	ab133598	rabbit
EphB3 [EPR8280]	abcam	ab133742	rabbit
EphB2 [EPR10072(B)]	abcam	ab150411	rabbit
RhoA (67BC)	Cell Signaling Technologies	2117	rabbit
Histone H2A.X	Cell Signaling Technologies	2595	rabbit
Smad2 (C86F7)	Cell Signaling Technologies	3122	rabbit
Caveolin-1 (D46G3) XP R	Cell Signaling Technologies	3267	rabbit
Cofilin P Ser3 (C77G2)	Cell Signaling Technologies	3313	rabbit
YAP P Ser127	Cell Signaling Technologies	4911	rabbit
EphA2 P Ser897	Cell Signaling Technologies	6347	rabbit
Smad1 (D59D7)	Cell Signaling Technologies	6944	rabbit
EphA2 (D4A2)	Cell Signaling Technologies	6997	rabbit
Stat3 P Ser727	Cell Signaling Technologies	9134	rabbit
TGF beta (56E4)	Cell Signaling Technologies	3709	rabbit
c-Abl P Y245	Cell Signaling Technologies	2868	rabbit
c-Abl P Y412 (247C7)	Cell Signaling Technologies	2865	rabbit

c-Abl	Cell Signaling Technologies	2862	rabbit
CamKII alpha (22B1) P Thr286	Abcam	ab2724	mouseIgG1
beta-Tubulin	Abcam	ab6046	rabbit
PKC-alpha P Thr638	Abcam	ab32502	rabbit
p90 S6 kinase (Rsk1-3)	Santa Cruz	sc-231	rabbit
PKC-gamma P Thr514	GeneTex	GTX25778	rabbit
mTOR P Ser2481	Millipore (Upstate)	09-343SP	rabbit

2.11.4 RNA Extraction, RNA Sequencing and transcriptomic analysis of MNs

Total RNA was extracted from human embryonic stem cell derived *HB9*::GFP MNs treated with ACM for 24 hours (as described in the previous sections), using the RNeasy® Mini kit (74104, Qiagen®), according to the manufacturer's instructions. RNA samples were evaluated for concentration (NanoDrop ND-100 Spectrometer, NanoDrop Technologies) and quality (Agilent 2200 TapeStation, Agilent Technologies) before library preparation.

Library preparation and sequencing were carried out by the Source Bioscience Sequencing team Cambridge, UK. For each sample, cDNA was converted to a sequencing library using the TruSeq stranded mRNA-seq library. Barcoded libraries were pooled and sequenced on an Illumina HiSeq 4000 using 75 base paired end reads to generate at least 46 million raw reads per sample. The reads were mapped to the primary assembly of the human (hg38) reference. Again, read alignment was performed with the STAR tool, and tables of per-gene read counts were generated from the mapped reads with the featureCounts tool. Differential gene expression analysis was performed using the R package DESeq2 (with differentially expressed genes determined at a Benjamini-Hochberg false discovery rate of 0.05), and gene ontology (GO) analysis with the R package topGO.

Subsequent analysis (Wu and Smyth, 2012), where commonly and concordantly differentially expressed genes between different comparisons were examined, involved the following thresholds:

a) Average Fragments Per Kilobase of transcript per Million mapped reads [FPKM] *per-comparison* > 1; genes with an FPKM < 1 were disregarded
b) Adjusted p-value in the respective comparisons < 0.05
c) Fold change thresholds
    i. Lenient
        – 50% FC for C92 ACM Vs MNs & C92D ACM Vs MNs
        – 10 % FC for C92 Vs C92D ACM
    ii. Stringent
        – 100% FC for C92 ACM Vs MNs & C92D ACM Vs MNs
        – 20 % FC for C92 Vs C92D ACM

2.12 Statistical analysis

Statistical testing of the RNA-seq data is described in previous sections. Other statistical analysis was performed using SPSS® Statistics or Prism version 8.4.0 (GraphPad Software). Data are presented as mean ± standard error of mean. Data were initially determined to be parametric or non-parametric before applying the appropriate statistical analysis, with false discovery rate (FDR) correction for multiple comparisons, as stated in the legends [$^{*}p < 0.05$, $^{**}p < 0.01$, $^{***}p < 0.001$]. Throughout the study, independent biological replicates are defined as independently performed experiments.

Chapter 3 Investigation of astrocyte-mediated non-contact dependent mechanisms in *C9orf72*-mediated ALS

3.1 Introduction

The first piece of evidence of effects of mutant astrocyte conditioned medium (ACM) in ALS comes from Nagai and colleagues in 2007 who showed that MN death was triggered by soluble toxic factors released from mutant SOD1 astrocytes, with toxicity being mediated through a Bax-dependent mechanism (Nagai *et al.*, 2007a). Conditioned medium derived from mutant SOD1-expressing astrocytes also caused death of primary mouse spinal cord neurons by inducing hyperexcitability (Fritz *et al.*, 2013), whilst C9-mutant ACM impaired neuronal viability through potential disruption of the balance between autophagosome expression and degradation (Madill *et al.*, 2017). Birger et al., performed mass spectrometric analysis on C9-ALS hiPSC-derived ACM and detected deficiencies in SOD1 and SOD2 proteins compared to controls, indicatory of diminished antioxidant capacity (Birger *et al.*, 2019). The SOD1 isoform is distributed through the cell cytoplasm and the SOD2 isoform is in the mitochondrial matrix. This observation may suggest that the detected proteins in the astrocyte secretome could be a result of apoptosis rather than active secretion. However, it is important to consider the possibility of non-canonical secretion mechanisms that may facilitate the release of these proteins under pathological conditions. Such mechanisms could include the release of proteins via membrane vesicles or exosomes, or through direct membrane rupture during cellular stress.

Other studies demonstrated that C9-induced astrocytes not only secreted fewer extracellular vesicles than healthy individuals, but they also induced neurite outgrowth deficits and reduced survival. Consequent isolation and analysis of exosomal fraction RNA identified downregulation of several miRNAs in mutant ACM implicated in regulating axonal maintenance and growth (Varcianna *et al.*, 2019). This is of interest given that disrupted RNA homeostasis is implicated in ALS, and exosome cargo includes RNA species. Together with interactome-based approaches, this emphasises the value of comprehensive and unbiased approaches, such as conventional proteomics, to identify and dissect the non-contact mediated effects of

C9 and C9Δ human iPSC-derived astrocytes on neurons and the responsible astrocyte-derived soluble factors (Ikiz *et al.*, 2015; Iguchi *et al.*, 2016; Westergard *et al.*, 2016).

To determine the impact of C9 and C9Δ ACM on neuronal health at a molecular level, (a) a completely humanised model was implemented; and (b) unbiased transcriptomic studies and reverse phase protein array on ACM-treated MNs were performed at selected time-points. Furthermore, to begin to identify potential mediators, mass spectrometric analysis of the ACM was undertaken.

3.2 Transcriptomic analysis on ACM-treated human embryonic stem cell–derived *HB9*::GFP MNs

To probe the neuronal cellular processes mediated by *C9orf72*-ACM, RNA sequencing was undertaken on wild-type human embryonic stem cell–derived (hESC) *HB9*::GFP MNs treated with ACM from mutant and gene-corrected astrocytes (C9-2 astrocyte pair) for 24 hours. Samples from MN monocultures were also collected as controls (

Appendix). Triplicates were produced for each condition.

The aim was to explore to what extent gene expression changes were induced in MNs by ACM, and how those transcriptional alterations were potentially different between astrocyte genotypes. This could generate different classes of genes:

- Those affected by both types of ACM (mutant: C9-2 and gene-corrected: C9-2Δ) to a similar degree (ACM-specific).
- Those affected by one ACM genotype but not the other (genotype-specific).
- Those affected by both ACM and genotype.

The heatmap demonstrated a clear separation of samples in two clusters – MNs in their own medium against MNs incubated with either mutant or gene-corrected ACM. Principal component analysis (PCA) expectedly showed grouping of biological replicates (represented by different shapes) and of conditions (represented by different colours). Importantly, it confirmed the previous observation, with strong clustering of the MN samples treated with either C9-2 or C9-2Δ ACM – there was only 1%

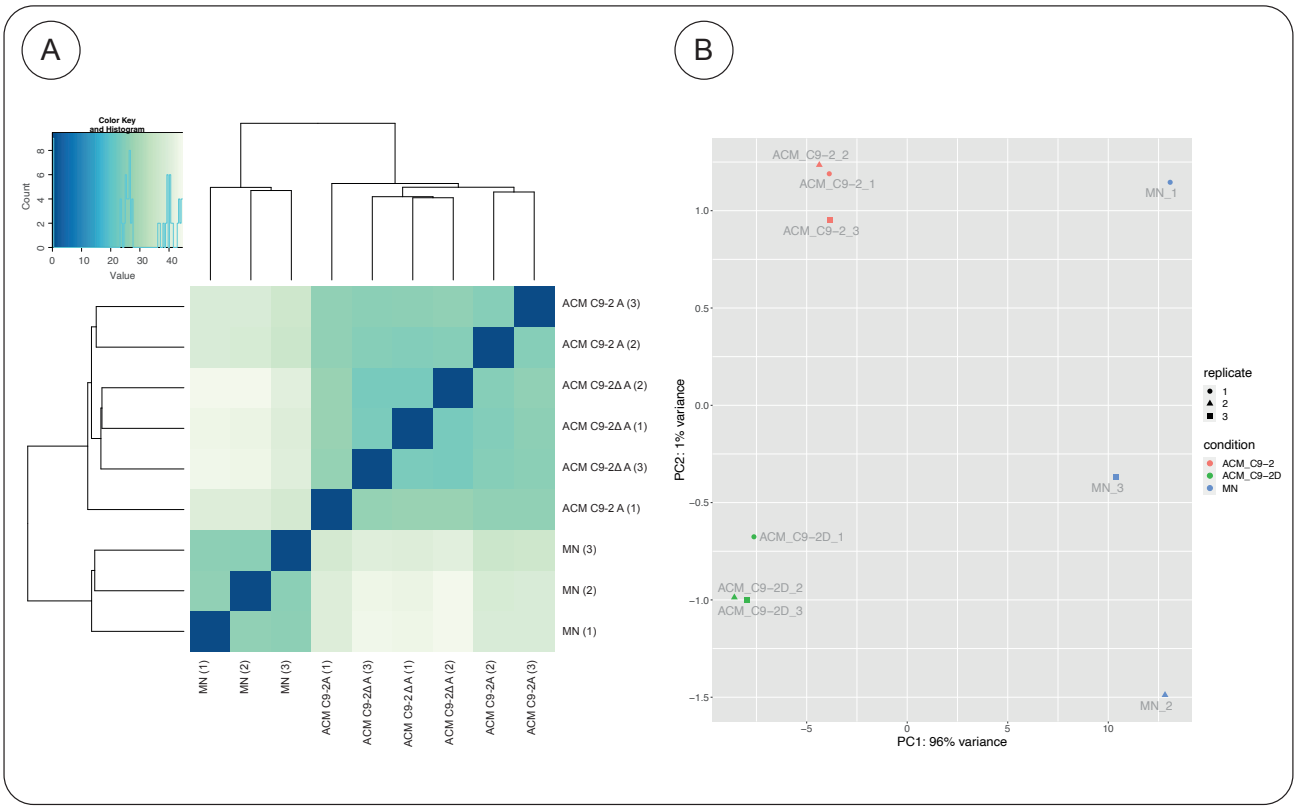

Figure 3.1 (A) Heat map and dendrogram depicting hierarchical clustering of RNA Sequencing reads of MNs cultured in their own medium and MNs treated with either mutant or gene-corrected ACM. Right upper corner legend: Colours in the heatmap represent the Euclidean distance between samples, after between-sample normalisation of RNA-Seq read counts followed by a variance-stabilising transformation. (B) Principal component analysis showing strong clustering of the ACM-treated MN samples (only 1% genotype-driven variance) and a 96% variance between MNs in their own medium and ACM-cultured neurons. (MNs = motor neurons; ACM = astrocyte conditioned medium).

genotype-driven variance – and a 96% variance between MNs in their own medium *versus* ACM-cultured neurons. These results indicated that the *major* transcriptomic variation in MNs was likely induced by addition of ACM in general, rather than by the C9 genotype (Fig 3.1).

The samples (3 biological replicates) within each condition were more homogeneous compared to transcriptomic profiling previously undertaken by our group (Zhao *et al.*, 2020). Given that differential gene expression is determined by the difference in mean expression between conditions compared to the variability within each condition, this intraclass homogeneity led to thousands of statistically significant differentially expressed genes with small fold changes when applying established filtering criteria adjusted p-value < 0.05 and retention of genes with mean Fragments Per Kilobase of transcript per Million mapped reads (FPKM) *per comparison* > 1. Thus, the following fold change thresholds were introduced to capture changes in gene expression of putative biological relevance.

Fold change thresholds:

Loose

- 50%-FC for “C9-2 ACM Vs MNs” & “C9-2Δ ACM Vs MNs”
- 10%-FC for “C9-2 Vs C9-2Δ ACM”

Stringent

- 100%-FC for “C9-2 ACM Vs MNs” & “C9-2Δ ACM Vs MNs”
- 20%-FC for “C9-2 Vs C9-2Δ ACM”

The smaller fold change cut-off for “C9-2 Vs C9-2Δ ACM” in both cases, is attributed to the reduced fold change magnitudes between these two conditions (Fig 3.2).

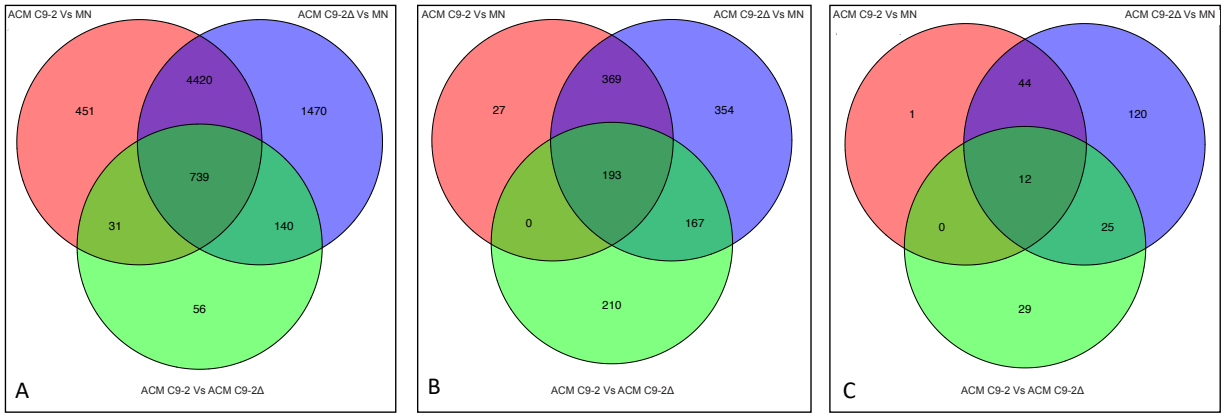

Figure 3.2 Venn diagram depicting identification of differentially expressed genes (DEGs) between the three comparisons – “C9-2 ACM Vs MNs”, “C9-2Δ ACM Vs MNs”, “C9-2 ACM Vs C9-2Δ ACM”. The filtering criteria implemented in A, B & C are average FPKM per-comparison > 1 (i.e., to appear in the ACM C9-2 Vs MNs circle, the average FPKM across the 6 ACM C9-2 and MN samples must be > 1) and adjusted p-value in the respective comparisons < 0.05.

(A) No fold change criteria.

(B) Loose criteria: 50%-FC for “C9-2 ACM Vs MNs” & “C9-2Δ ACM Vs MNs”; 10%-FC for “C9-2 Vs C9-2Δ ACM”.

(C) Stringent criteria: 100%-FC for “C9-2 ACM Vs MNs” & “C9-2Δ ACM Vs MNs”; 20%-FC for “C9-2 Vs C9-2Δ ACM”.

In each graph, the red circle represents the total number of significantly DEGs between C9-2 ACM Vs MNs in their own medium; the blue circle represents the significantly DEGs between C9-2Δ ACM Vs MNs; the green circle represents the significantly DEGs between C9-2 ACM Vs C9-2Δ ACM (upregulation in the C9-2 ACM signifies downregulation in the C9-2Δ ACM and vice versa); the top purple section portrays genes that are significantly affected by both ACMs to a similar degree but not the genotype; the olive-green section in the middle includes the genes that are significantly affected by both ACM and genotype; the light green section at the bottom indicates the genotype-driven DEGs.

The “loose criteria fold change threshold” provided an appropriate set of genes that could be taken forward for GO analysis whilst imposing *some* thresholds to remove the genes with marginal fold changes that are unlikely to be biologically important. Using this approach 369 genes were differentially expressed by both ACM types to a similar degree, 193 genes were affected by both the ACM treatment and the *C9orf72* genotype, and 210 genes were differentially regulated by the genotype only.

The selection of fold change cut-offs in our RNA sequencing analysis was a critical aspect of our study, particularly given that these data are novel and there was no prior literature to guide our decisions. The following factors were considered in determining the cut-offs, particularly the loose criteria threshold:

1. Exploratory Nature of the Study: Since this was an initial investigation into the effects of ACM treatment on human embryonic stem cell-derived motor neurons, we aimed to adopt a broad approach to capture a wide range of gene expression changes. The loose criteria threshold was intentionally chosen to maximize the identification of differentially expressed genes that could provide insights into the underlying biological processes involved.

2. Selection of Thresholds: The initial thresholds were chosen based on a combination of biological relevance and practical considerations. We aimed to identify changes that could be biologically significant, even if they were modest. The decision to set a 50%-fold change for comparisons between ACM-treated motor neurons and controls was based on the understanding that significant biological effects can arise from even small shifts in gene expression, especially in complex neuronal environments.

3. Statistical Stringency: We applied an adjusted p-value of < 0.05 along with the fold change cut-offs to ensure that identified genes were statistically significant. This combination allowed us to filter for meaningful expression changes while accounting for the variability inherent in biological data. The loose criteria were set to ensure that we captured a broader spectrum of genes, which is essential in an exploratory analysis.

4. Variability in Gene Expression: Early analyses revealed variability in gene expression levels across biological replicates. This variability informed our decision to use smaller fold change thresholds for comparisons between C9-2 and C9-2Δ ACM, where we anticipated that differences might be subtle. The goal was to avoid excluding potentially important genes based solely on stringent cut-offs.

5. Iterative Evaluation: The process of establishing these thresholds was iterative. After conducting initial RNA sequencing analyses with the chosen thresholds, we reviewed the results to assess the distribution of gene expression changes and their biological implications. Based on these observations, we refined our criteria and adjusted ensure that the chosen thresholds effectively captured relevant differences while remaining manageable for downstream analyses.

Subsequent Gene ontology analysis was performed on those differentially expressed genes (DEGs) and revealed upregulation of sets of genes that are associated with rather generic functions such as: cell division (upregulated pathway in MNs to a similar degree after treatment with both ACM types when compared to MNs in the own medium) [Fig 3.3 A]; positive regulation of receptor recycling and cell migration (upregulated pathways in MNs after C92Δ ACM treatment) [Fig 3.4 A]; extracellular matrix organisation (upregulated in MNs treated with both ACM types compared to MNs alone, but expression was even higher in treatment with C9-2Δ ACM compared to C9-2 ACM) [Fig 3.5 B]. This highlights one of the limitations of GO enrichment analysis where heavily annotated, multifunctional genes can drive the generation of non-specific results of potentially limited biological relevance (Fig 3.3; Fig 3.4; Fig 3.5).

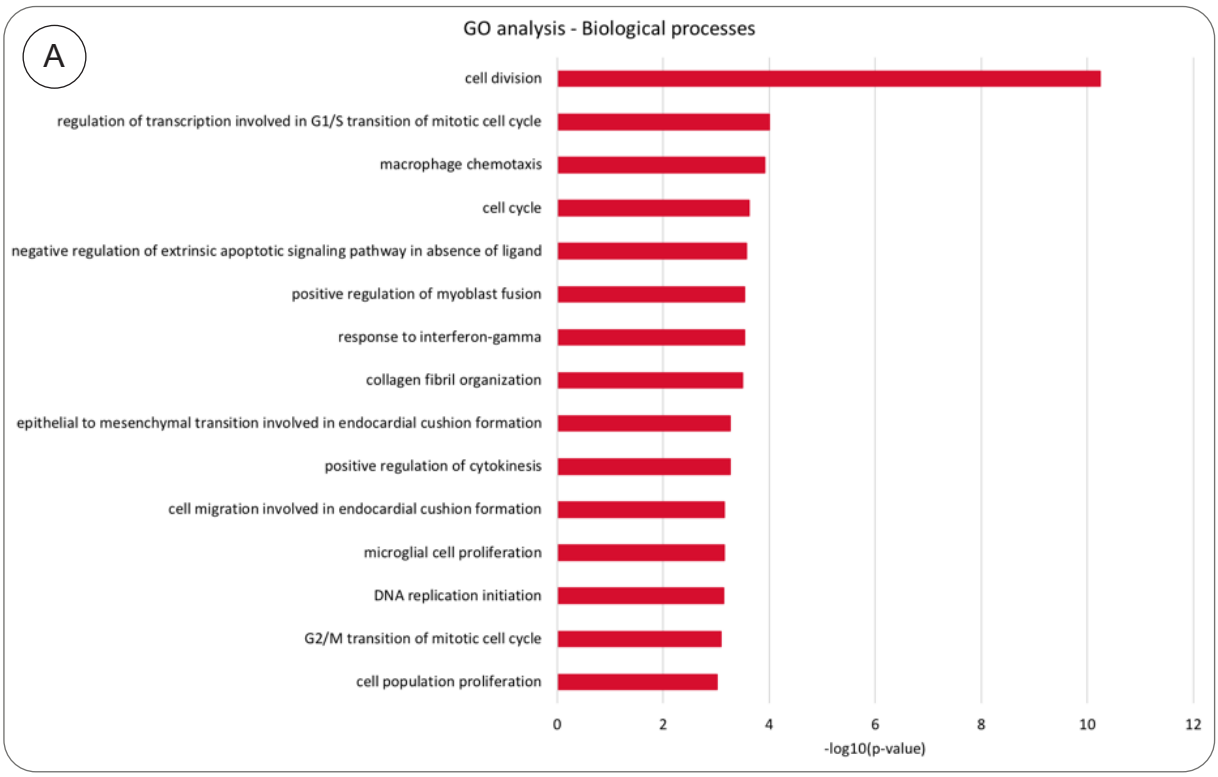

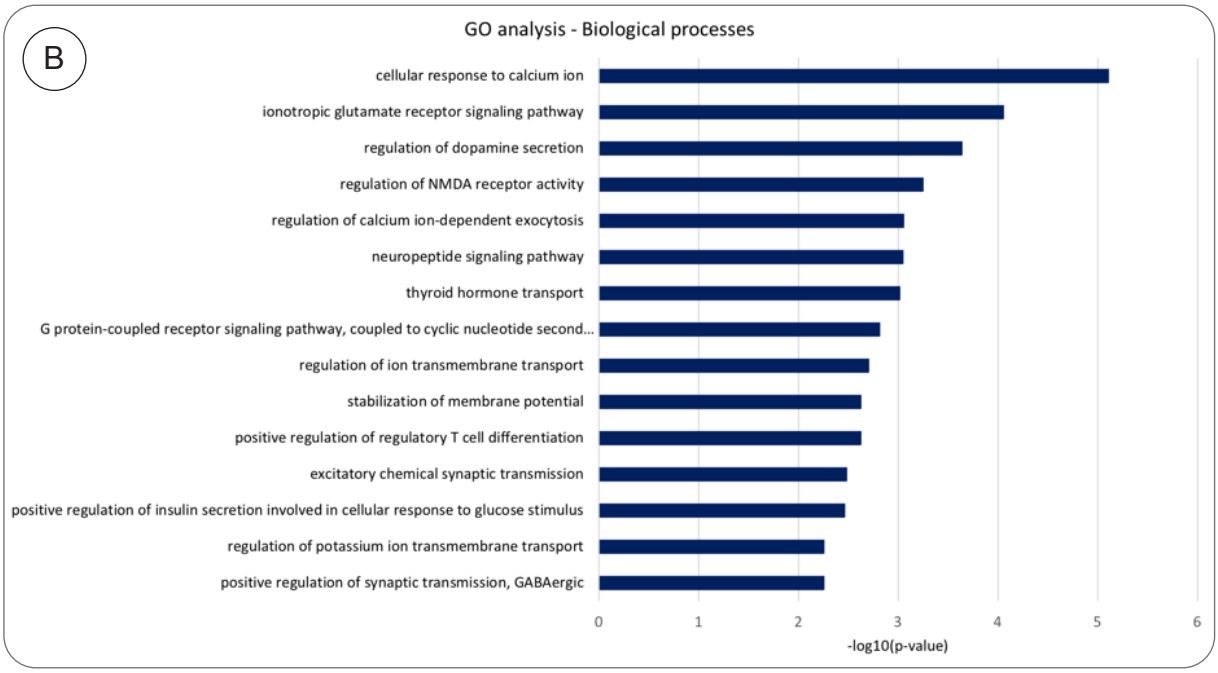

Figure 3.3 Gene ontology analysis for biological processes on "ACM-specific" genes that identified putatively up- and downregulated altered pathways or processes. These genes are affected by both types of ACM (C9-2 and C9-2Δ) to a similar degree when compared to MNs in their own medium.
(A) Upregulated pathways in MNs after C9-2 and C9-2Δ ACM treatment.
(B) Downregulated pathways in MNs after C9-2 and C9-2Δ ACM treatment.

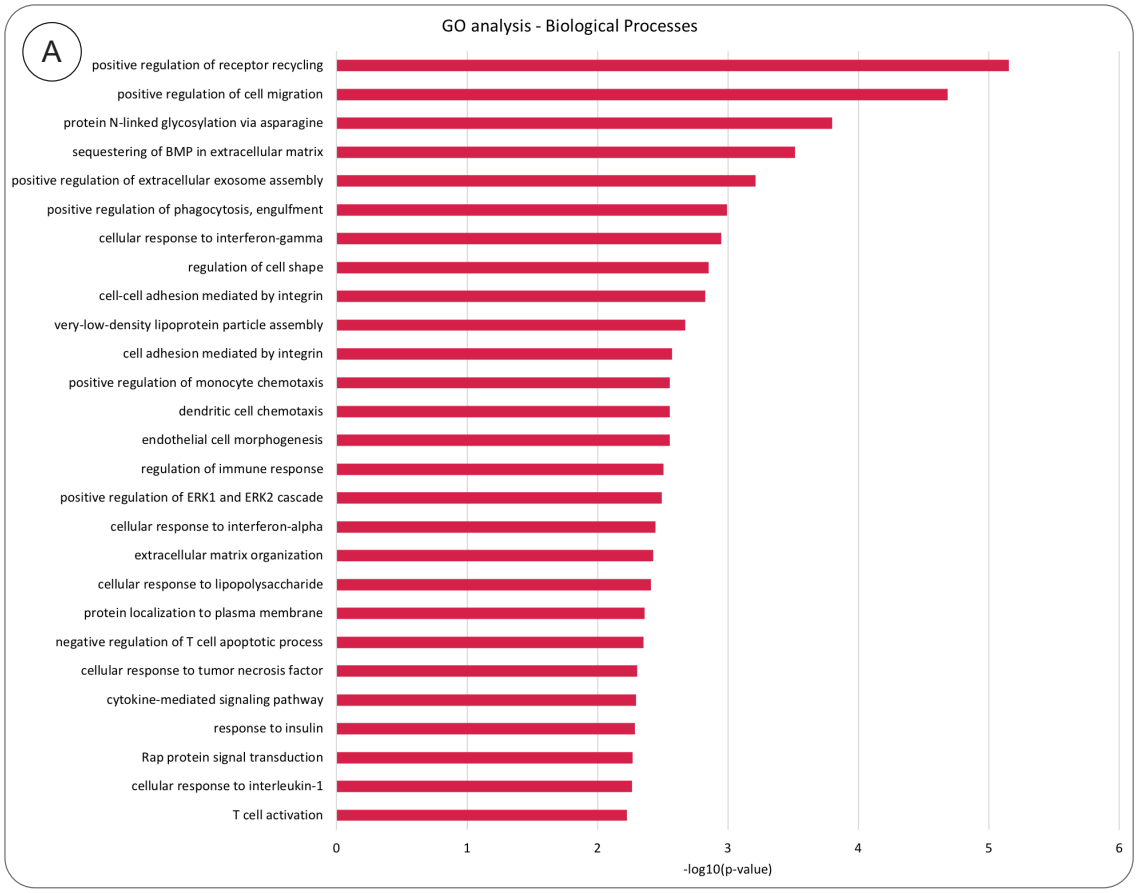

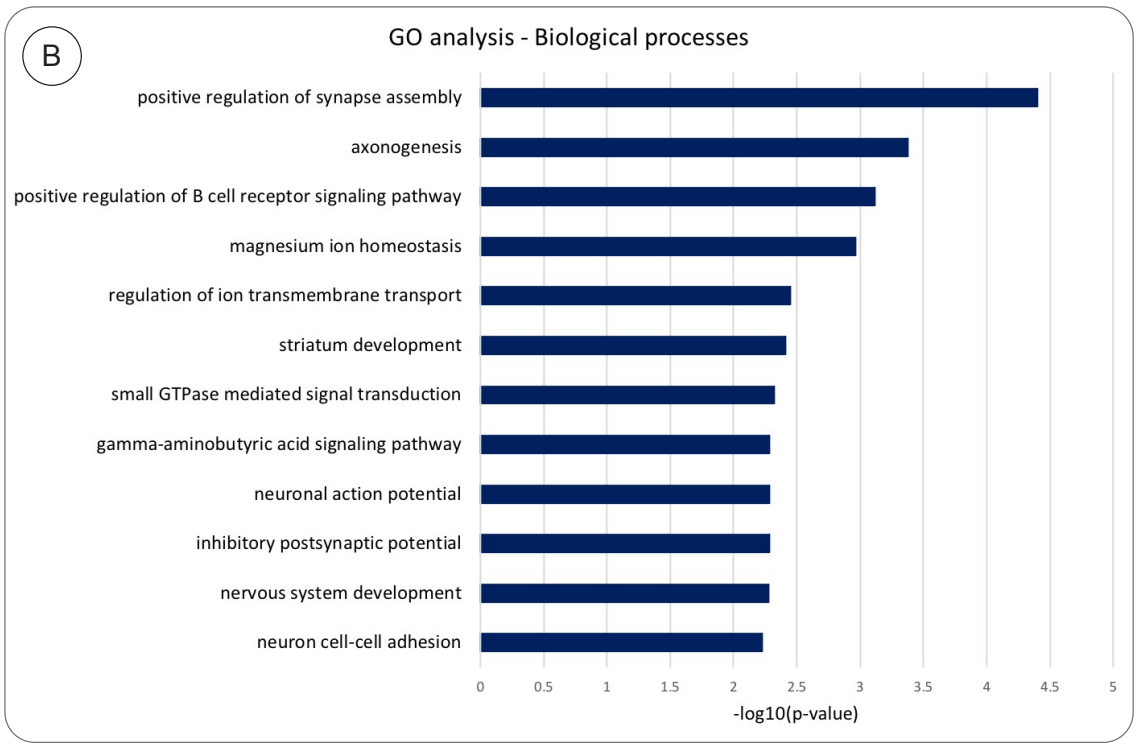

Figure 3.4 Gene ontology analysis for biological processes on "genotype-specific" genes that identified putatively up- and downregulated altered pathways or processes. These genes have significant differential expression upon MN treatment with C9-2 ACM when compared to C9-2Δ ACM. (A) Upregulated pathways in MNs after C9-2Δ ACM treatment (and corresponding downregulation after C9-2 ACM treatment). (B) Downregulated pathways in MNs after C9-2Δ ACM treatment (and corresponding upregulation after C9-2 ACM treatment).

A

Effect of ACM	Effect of Genotype	Total number of DEGs
UP in ACM-treated MNs	Higher expression in treatment with C9-2 ACM compared to C9-2Δ ACM	1 gene
UP in ACM-treated MNs	Higher expression in treatment with C9-2Δ ACM compared to C9-2 ACM	182 genes (GO analysis – figure below)
DOWN in ACM-treated MNs	Lower expression in treatment with C9-2Δ ACM compared to C9-2 ACM	10 genes
DOWN in ACM-treated MNs	Lower expression in treatment with C9-2 ACM compared to C9-2Δ ACM	0 genes

B

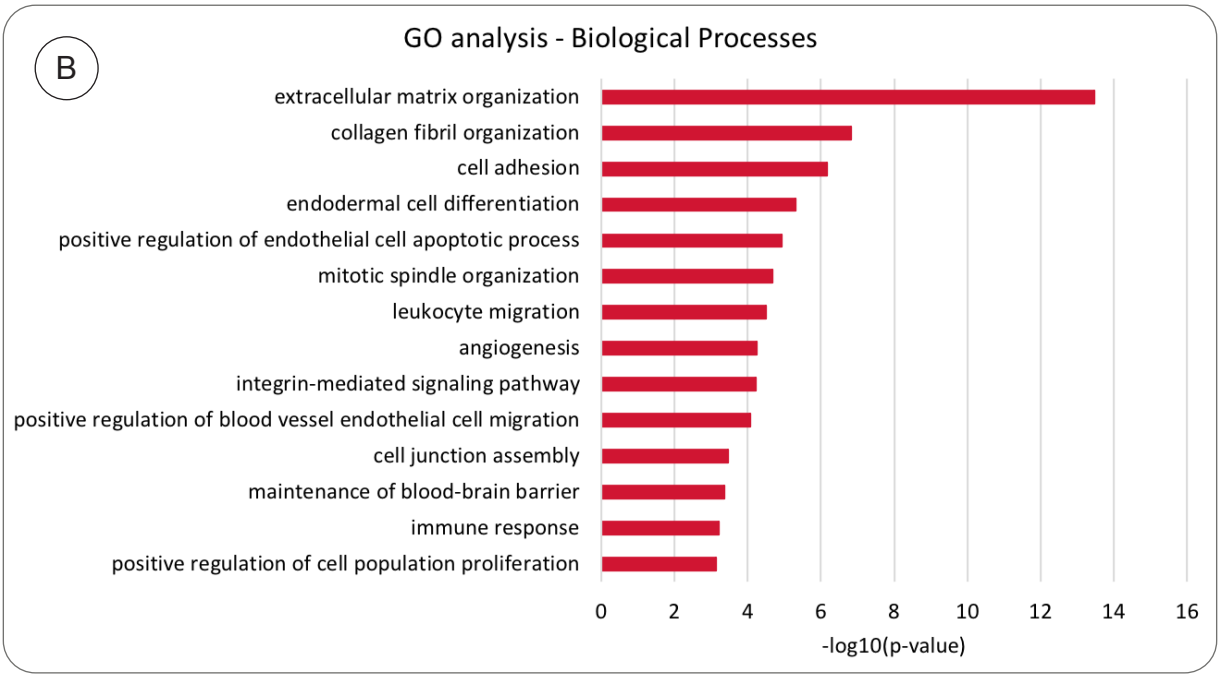

Figure 3.5 (A) Table illustrating the DEGs that are either upregulated or downregulated upon exposure to both types of ACM with additional genotype-driven impact.
(B) Gene ontology analysis for biological processes on genes that are upregulated in MNs treated with both ACM types compared to MNs alone, but their expression is even HIGHER in treatment with C9-2Δ ACM compared to C9-2 ACM.

3.3 Reverse phase protein array on ACM-treated human embryonic stem cell-derived *HB9*::GFP MNs

Reverse phase protein array (RPPA) technology was used to determine protein expression and phosphorylation signatures in WT hESC-derived *HB9*::GFP MNs after treatment with ACM from astrocytes harbouring the *C9orf72* mutation and their corresponding gene-corrected controls (C9-2 & C9-2Δ astrocytes). RPPA represents a highly sensitive and precise tool, which incorporates a pre-specified panel of validated, high-quality antibodies for quantification of specific proteins and their post-translational modifications in biological specimens (Johnstone *et al.*, 2019) and is established in our lab. Circa 120 candidate antibody spots per sample were selected. Selection of antibodies was based on their biological relevance to signalling pathways of interest (such as extracellular matrix signalling), support of their applicability and importance in the scientific literature (Table 2.3; Methods and Materials).

Conditioned medium was generated by incubating fully mature astrocytes – after astrocyte progenitor cells were differentiated into astrocytes for 14 days – with MN-NF maturation medium (80-90% cell confluency, equivalent to 5-6x10^6 astrocytes per 10-cm plate). Conditioned medium was subsequently collected every 72 hours, centrifuged to remove cellular debris, and added fresh on pre-plated MNs. Confluent monocultures of WT hESC-derived *HB9*::GFP neurons were treated with 50% ACM (equivalent to 1 ml for 12-well plates) and 50% fresh MN-NF maturation medium with double concentration growth factors. The following treatment timepoints were implemented for C9-mutant and C9Δ-gene-corrected ACM (one astrocyte pair – the C9-2 pair – was taken forward):

(1) 2 hours on Day 7 post-MN plate down for elucidation of immediate and specific phosphorylation events,
(2) over 24 hours [incubation at Day 6 post-MN plate down] **and**
(3) over 7 days with media changes every 72 hours for identification of secondary signalling cascades.

Three biological replicates were collected per condition per timepoint. MN monocultures were also maintained as controls, where MN-NF medium was changed regularly every 2-3 days. MN samples were collected for analysis at 7 days.

Phosphorylation analysis comprised of normalisation of phosphorylated and total proteins to loading control (β-actin), followed by calculating ratios of phosphorylated/total cellular protein levels using those normalised values. For each selected protein/pathway, per-condition averages were calculated over the three replicates in each condition and represented in bar charts. The values were plotted as log2 fold changes (FCs) of the average for one condition, divided by the average for the other – for example, "average for the C9-2-mutant ACM treatment"/ "average for MNs" (Fig 3.6).

Overall, genotype-mediated log2 FCs of protein expression (phosphorylation status) on MNs when comparing treatment with either C92-mutant ACM or C92Δ-isogenic ACM across the three timepoints, were small at <0.4 (Fig 3.6 C). The highest expression fold changes in MNs upon addition of C9-2-mutant ACM against MNs in their own medium, were observed in the following pathways: CamKii P Thr286/calmodulin *at 2 and 24 hours, and 7 days* (log2FC of 1, 1.3 and 1.6, respectively) *and* p44/42 MAPK (ERK1/2) P Thr202/Thr185, Tyr204/Tyr187 divided by p44/42 MAPK (ERK1/2) *at 7 days* (log2FC of 2.4) (Fig 3.6 A). Conversely, C9-2Δ-isogenic ACM induced expression fold changes of <1 in MNs in comparison to MNs alone at 2 and 24 hours (Fig 3.6 B). The highest fold changes were detected at 7 days in: (1) p44/42 MAPK (ERK1/2) P Thr202/Thr185, Tyr204/Tyr187 divided by p44/42 MAPK (ERK1/2) – log2 FC 2.5, (2) CamKii P Thr286/calmodulin – log2FC 1.3, (3) 4E-BP1 PSer65 divided by 4E-BP1 – log2FC 1.2 (Fig 3.6 B).

A

C9-2-mutant ACM treatment
Vs MNs alone for 2 hours
Log2 FC
1.0
0.5
0.0
-0.5
CamKii P Thr286
MEK1/2 P Ser217/221
IGF-1R beta P Tyr1162,Tyr1163
Stat5 P Tyr694
S6 Ribosomal protein p Ser240,Ser244
S6 Ribosomal protein P Ser235,Ser236
p44/42 MAPK (ERK1/2) P Thr202/Thr185,Tyr204/Tyr187
Akt P Ser473
GSK-3-alpha/beta P Ser21/Ser9
GSK-3-beta P Ser9
p38 MAPK PThr180,Tyr182
mTOR P Ser2448
Smad2/3 P Ser465/Ser467/Ser425
Smad1/5 P Ser463/Ser465
4E-BP1 PSer65
4E-BP1 P Thr37,Thr46
YAP P Ser127

C9-2-mutant ACM treatment
Vs MNs alone for 24 hours
Log2 FC
1.0
0.5
0.0
-0.5
CamKii P Thr286
IGF-1R beta P Tyr1162,Tyr1163
p44/42 MAPK (ERK1/2) P Thr202/Thr185,Tyr204/Tyr187
p38 MAPK PThr180,Tyr182
S6 Ribosomal protein p Ser240,Ser244
S6 Ribosomal protein P Ser235,Ser236
4E-BP1 P Thr37,Thr46
YAP P Ser127
Stat5 P Tyr694
mTOR P Ser2448
GSK-3-alpha/beta P Ser21/Ser9
Smad1/5 P Ser463/Ser465
Smad2/3 P Ser465/Ser467/Ser425
4E-BP1 PSer65
Akt P Ser473
GSK-3-beta P Ser9
MEK1/2 P Ser217/221

C9-2-mutant ACM treatment
Vs MNs alone for 7 days
Log2 FC
2.0
1.0
0.0
-1.0
p44/42 MAPK (ERK1/2) P Thr202/Thr185,Tyr204/Tyr187
CamKii P Thr286
4E-BP1 P Thr37,Thr46
Stat5 P Tyr694
S6 Ribosomal protein p Ser240,Ser244
S6 Ribosomal protein P Ser235,Ser236
IGF-1R beta P Tyr1162,Tyr1163
p38 MAPK PThr180,Tyr182
4E-BP1 PSer65
Smad2/3 P Ser465/Ser467/Ser425
Smad1/5 P Ser463/Ser465
Akt P Ser473
GSK-3-alpha/beta P Ser21/Ser9
mTOR P Ser2448
MEK1/2 P Ser217/221
YAP P Ser127
GSK-3-beta P Ser9

B

C9-2Δ-isogenic ACM treatment
Vs MNs alone for 2 hours
Log2 FC
0.4
0.0
-0.4
CamKii P Thr286
4E-BP1 P Thr37,Thr46
IGF-1R beta P Tyr1162,Tyr1163
p44/42 MAPK (ERK1/2) P Thr202/Thr185,Tyr204/Tyr187
mTOR P Ser2448
S6 Ribosomal protein p Ser240,Ser244
S6 Ribosomal protein P Ser235,Ser236
YAP P Ser127
Stat5 P Tyr694
Akt P Ser473
Smad2/3 P Ser465/Ser467/Ser425
GSK-3-alpha/beta P Ser21/Ser9
p38 MAPK PThr180,Tyr182
Smad1/5 P Ser463/Ser465
4E-BP1 PSer65
MEK1/2 P Ser217/221
GSK-3-beta P Ser9

C9-2Δ-isogenic ACM treatment
Vs MNs alone for 24 hours
Log2 FC
0.6
0.3
0.0
-0.3
p44/42 MAPK (ERK1/2) P Thr202/Thr185,Tyr204/Tyr187
CamKii P Thr286
IGF-1R beta P Tyr1162,Tyr1163
S6 Ribosomal protein P Ser235,Ser236
4E-BP1 P Thr37,Thr46
p38 MAPK PThr180,Tyr182
S6 Ribosomal protein p Ser240,Ser244
Stat5 P Tyr694
Akt P Ser473
mTOR P Ser2448
4E-BP1 PSer65
GSK-3-beta P Ser9
Smad2/3 P Ser465/Ser467/Ser425
GSK-3-alpha/beta P Ser21/Ser9
YAP P Ser127
Smad1/5 P Ser463/Ser465
MEK1/2 P Ser217/221

C9-2Δ-isogenic ACM treatment
Vs MNs alone for 7 days
Log2 FC
2.0
1.0
0.0
-1.0
p44/42 MAPK (ERK1/2) P Thr202/Thr185,Tyr204/Tyr187
CamKii P Thr286
4E-BP1 P Thr37,Thr46
Stat5 P Tyr694
S6 Ribosomal protein P Ser235,Ser236
4E-BP1 PSer65
S6 Ribosomal protein p Ser240,Ser244
IGF-1R beta P Tyr1162,Tyr1163
mTOR P Ser2448
Smad1/5 P Ser463/Ser465
Akt P Ser473
Smad2/3 P Ser465/Ser467/Ser425
p38 MAPK PThr180,Tyr182
GSK-3-alpha/beta P Ser21/Ser9
MEK1/2 P Ser217/221
GSK-3-beta P Ser9
YAP P Ser127

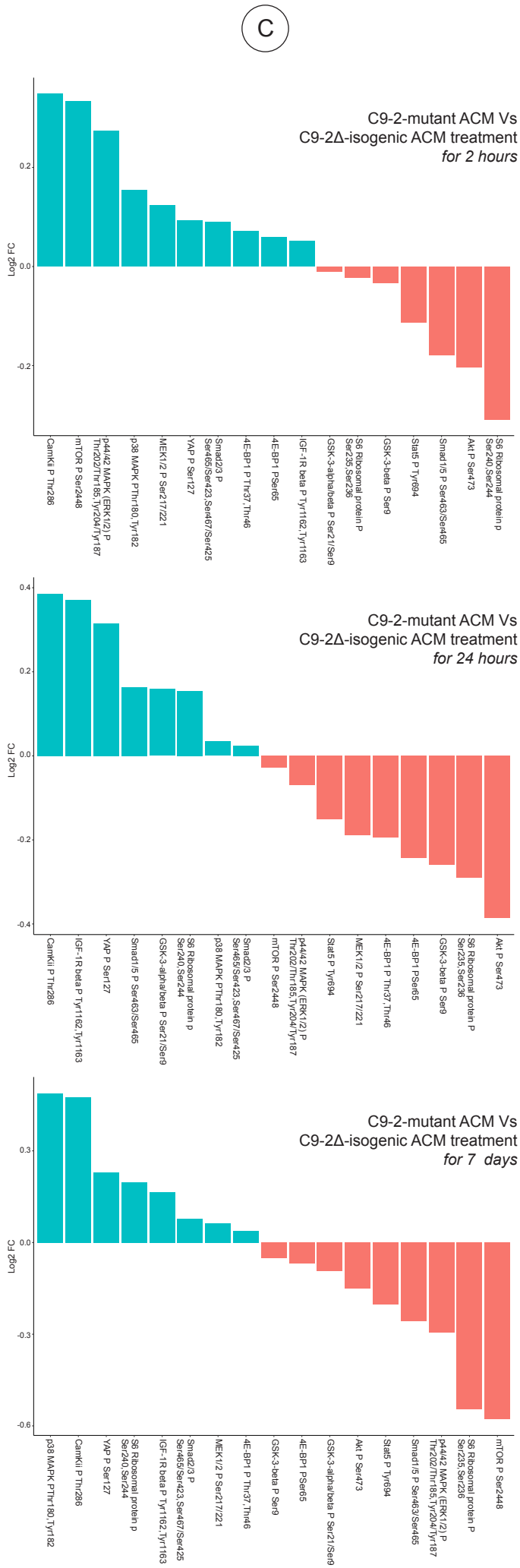

Figure 3.6 Bar charts on phosphorylation protein status depicting log2 fold changes (FCs) between the conditions in decreasing order, with positive log2 FCs in blue and negative log2 FCs in red. For each time-point (2 hours, 24 hours, 7 days):

(A) Comparison between C9-2 ACM Vs MNs (upregulated pathways after treatment with C9-2 ACM compared to MNs in their own medium are represented in blue).

(B) Comparison between C9-2Δ ACM Vs MNs (upregulated pathways after treatment with C9-2Δ ACM compared to MNs in their own medium are represented in blue).

(C) Comparison between C9-2 ACM Vs C9-2Δ ACM (upregulated pathways after treatment with C9-2 ACM compared to treatment with C9-2Δ ACM are represented in blue).

For a more comprehensive representation of the protein pathways affected by either the C9-genotype or ACM or both at the 3 timepoints, the *magnitude* of the log2 fold change between the C9 and C9Δ genotypes (i.e. the absolute log2FC between genotypes, a strictly non-negative value, which measures the "size" of the difference in effect between genotype ACMs) was plotted *versus* the magnitude of the log2 fold change between C9Δ ACM and MN (i.e. the absolute log2FC in C9Δ ACM Vs MN, which measures the "size" of the effect due to the C9Δ ACM). The points are coloured according to the difference between these two absolute values – blue points are more affected by genotype, red points are more affected by ACM, and grey points are similarly affected by both (Fig 3.7).

Lastly, t-tests were performed on selected pathways, for comparisons between C9-2 ACM, C9-2Δ ACM or MNs at each timepoint (2-hour, 24-hours, and 7-days) using the original expression values (i.e., three replicates per condition) (Table 3.1). In C9-2 ACM Vs MNs, it was found that 6/17 protein pathways were significantly different at 2 hours, 3/17 protein pathways at 24 hours and 8/17 pathways at 7 days. In C9-2Δ ACM Vs MNs, 4/17 protein pathways were significantly differentially expressed at 2 hours, 1/17 protein pathway at 24 hours and 8/17 pathways at 7 days. However, in C9-2 ACM Vs C9-2Δ ACM, only 5/17 were significantly different at 7 days and none at the other two earlier timepoints.

In conclusion, these outcomes suggest that effects on neuronal protein expression (phosphorylation status) are driven by exposure to astrocyte conditioned medium irrespective of genotype. Given these small or modest effects, independent of genotype, further studies were not pursued.

A

2-hour treatment
Genotype
Vs ACM

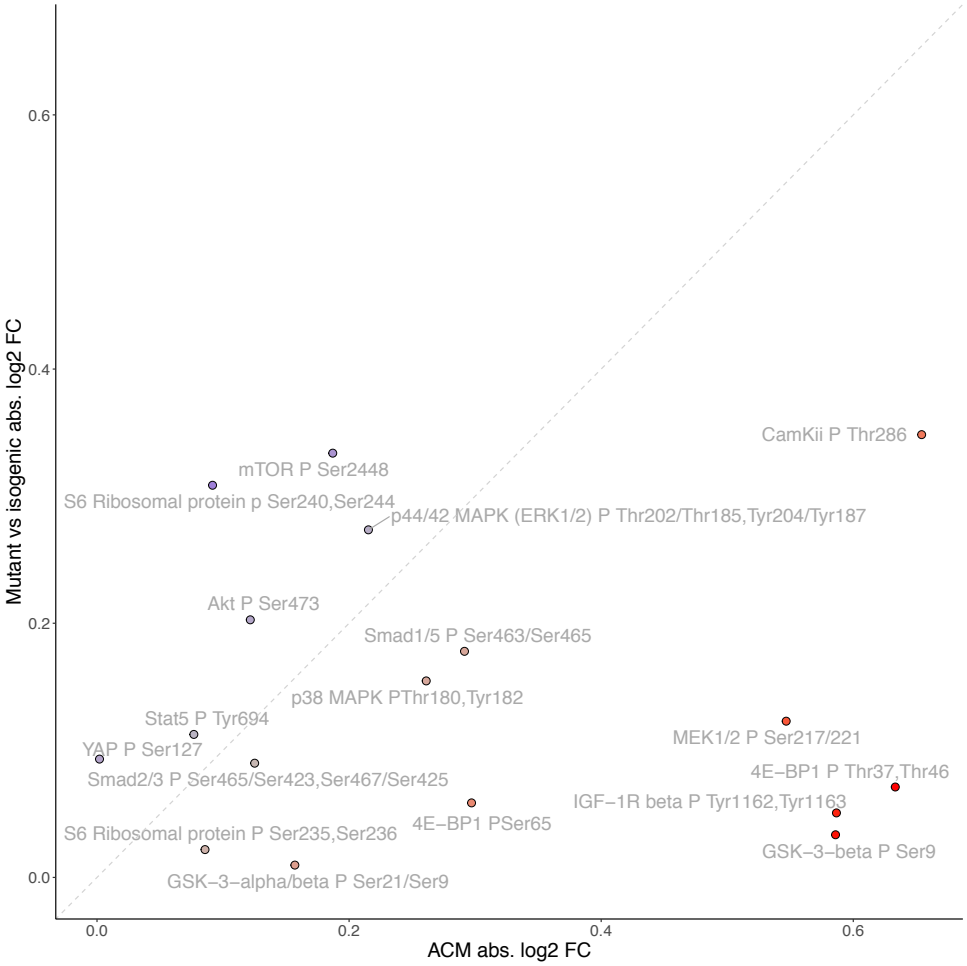

B

24-hour treatment
Genotype
Vs ACM

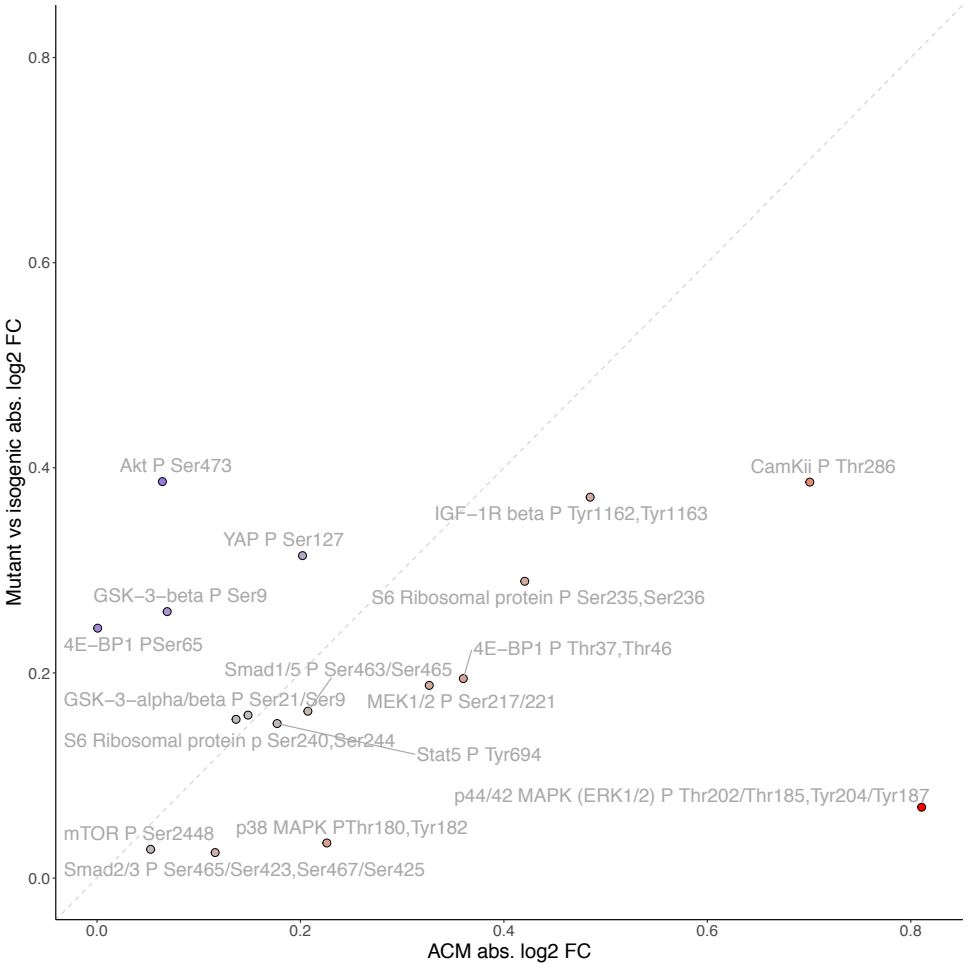

C

7-day treatment
Genotype
Vs ACM

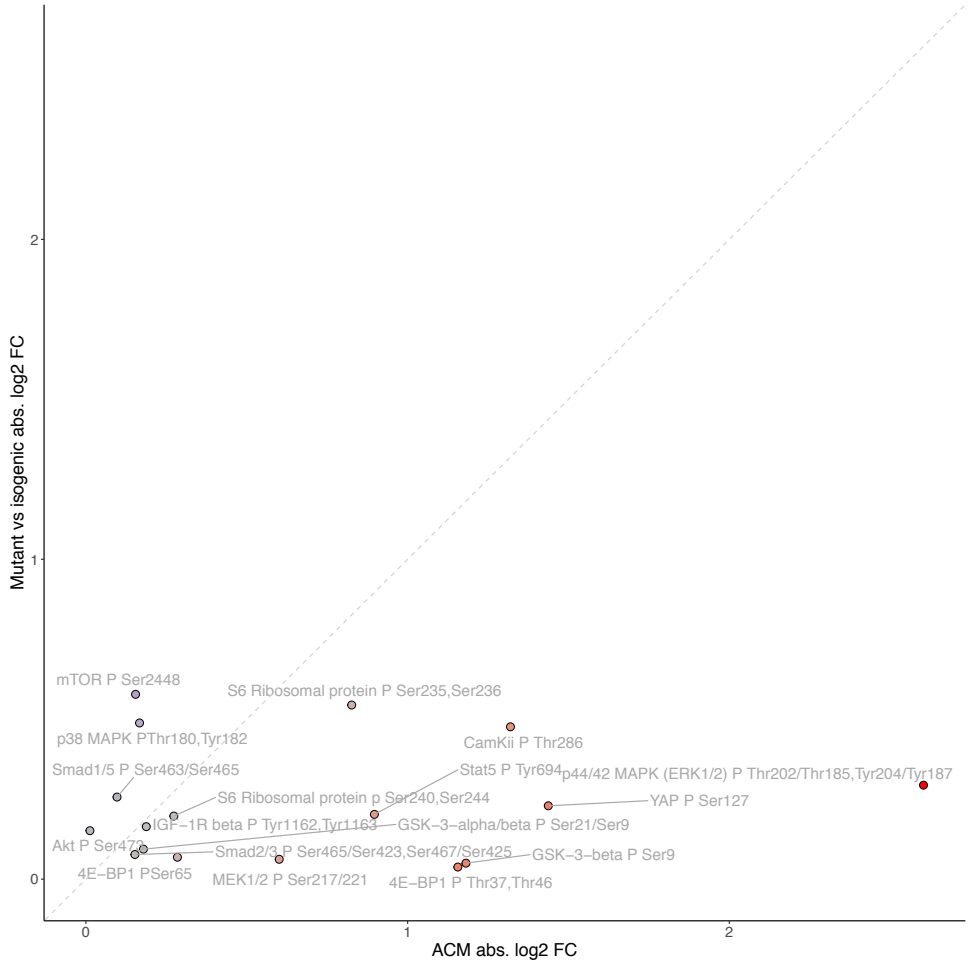

Figure 3.7 (A-C) Scatter plots displaying the absolute log2 FCs between C9 and C9Δ genotypes Vs the absolute log2 FCs in ACM Vs MN. The x-axis represents the ACM influence, and, on the x-axis, there are the absolute values (i.e., the magnitude) of the log2 FCs of C9-2Δ ACM Vs MNs. The values on the y-axis are the absolute values of the log2 fold changes of C9-2 ACM Vs C9-2Δ ACM. The colours indicate the size and direction difference between these two log2 FCs – blue points are more affected by genotype, red points are more affected by ACM, and grey points are similarly affected by both.

Comparison	CamKii P Thr286 divided by calmoduli n	MEK1/2 P Ser217/22 1 divided by MEK1/2	IGF-1R beta P Tyr1162,Tyr 1163 divided by total	Stat5 P Tyr694 divided by Stat5	S6 Ribosomal protein p Ser240,Ser24 4 divided by total	S6 Ribosomal protein P Ser235,Ser236 divided by total	p44/42 MAPK (ERK1/2) P Thr202/Thr185,Tyr2 04/Tyr187 divided by p44/42 MAPK (ERK1/2)	Akt P Ser473 divided by Akt	GSK-3 alpha/beta P Ser21/Ser9 divided by GSK-3-beta	GSK-3-beta P Ser9 divided by GSK-3-beta	p38 MAPK PThr180,Tyr1 82 divided by p38 MAPK	mTOR P Ser2448 divided by mTOR	Smad2/3 P Ser465/Se r423,Ser4 67/Ser425 divided by Smad2 (C86F7)	Smad1/5 P Ser463/Se r465 divided by SMAD1	4E-BP1 PSer65 divided by 4E-BP1	4E-BP1 P Thr37,Thr 46 divided by 4E-BP1	YAP P Ser127 divided by YAP1 [EP1674Y]	sig_count
C92 ACM Vs MN 2hr	0.042647	0.04834	0.00815497	0.138772	0.333459396	0.717447921	0.105147214	0.071070469	0.72270938	0.149547	0.650823065	0.034155	0.534743	0.077434	0.023515	0.01086	0.639031	6
C9 2Δ ACM Vs MN 2hr	0.174535	0.023025	0.00127518	0.641934	0.727320664	0.651690846	0.55250049	0.541112942	0.70185745	0.171973	0.383728253	0.296017	0.182204	0.189567	0.031812	3.29E-05	0.993267	4
C92 ACM Vs C9 2Δ ACM 2hr	0.2492	0.456147	0.5967838	0.499969	0.267520802	0.8575867	0.365755959	0.361374047	0.97590513	0.824525	0.490880486	0.102478	0.273781	0.30169	0.544888	0.41238	0.560048	0
C92 ACM Vs MN 24hr	0.030254	0.029379	0.02325223	0.854972	0.168745294	0.603722221	0.2462792	0.077908077	0.9777336	0.330471	0.266749942	0.886728	0.212431	0.796287	0.063743	0.12672	0.701784	3
C9 2Δ ACM Vs MN 24hr	0.161056	0.106538	0.21283985	0.380836	0.556014901	0.062980976	0.031687206	0.829215542	0.74637898	0.892953	0.608495899	0.844812	0.121976	0.459799	0.997679	0.152717	0.423419	1
C92 ACM Vs C9 2Δ ACM 24hr	0.219832	0.305976	0.21040872	0.469329	0.375501802	0.205413426	0.869818125	0.303678173	0.58341944	0.629141	0.925738075	0.923608	0.629697	0.530056	0.361905	0.332886	0.308386	0
C92 ACM Vs MN 7 days	0.001156	0.026223	0.02937031	0.003421	0.050794946	0.166541582	1.19E-04	0.233554555	0.53246075	0.069449	0.189917977	0.010509	0.413434	0.439293	0.068175	0.00136	0.041377	8
C9 2Δ ACM Vs MN 7 days	0.010139	0.022273	0.07184188	0.015706	0.198695485	0.005759053	9.54E-04	0.911371176	0.66293249	0.07307	0.491322851	0.183373	0.068867	0.534509	0.017527	3.72E-04	0.034131	8
C92 ACM Vs C9 2Δ ACM 7 day	0.023923	0.695854	0.15670653	0.220366	0.15787379	0.006565903	0.06295927	0.052290793	0.36074726	0.148379	0.032411757	0.007822	0.389949	0.156084	0.386935	0.505732	0.021637	5

Table 3.1 t-tests were performed on selected pathways, for comparisons between C9-2 ACM, C9-2Δ ACM or MNs at each timepoint (2-hour, 24-hours and 7-days) using the original expression values (i.e., three replicates per condition).

3.4 Proteomic analysis of astrocyte conditioned medium

To begin to identify major proteins secreted by hiPSC-derived *C9orf72* astrocytes and their corresponding gene-corrected controls, comprehensive profiling of the whole astrocyte secretome (soluble factors/proteins and exosomes) was performed by unbiased mass spectrometric (MS) analysis on the 3 independent astrocyte pairs, in collaboration with Professor Margaret Frame, Institute of Genetics & Cancer, University of Edinburgh. Astrocyte progenitor cells were dissociated into single cells and plated onto 10-cm plates at 5-6x10^6 in EGF- and FGF2-containing medium. This medium was switched into astrocyte differentiation medium after 24 hours, for differentiation into astrocytes (14 days). Two plates were required for each condition at 80-90% cell confluency for secretome isolation; at least three biological replicates were studied in each case. The steps for isolation of soluble factors and exosomes are described in the 'Methods & Materials' section in detail.

Hierarchical clustering portrayed grouping of the mutant samples and grouping of the gene-corrected samples indicating that the observed differential peptide expression was likely driven by the *C9orf72* mutation (Fig 3.8).

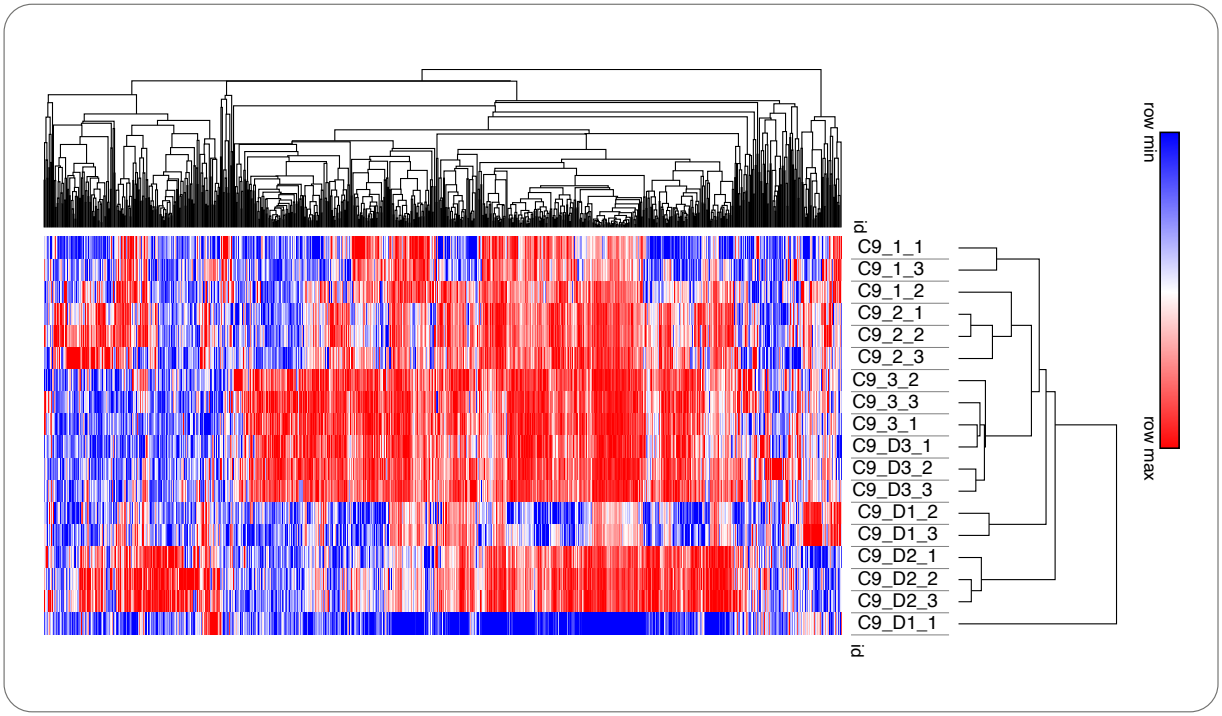

Figure 3.9 Mass spectrometric analysis of the astrocyte secretome – Hierarchical clustering. There is clustering of the mutant and gene-corrected lines, indicating that the observed differential peptide expression is likely driven by the *C9orf72* mutation.

A total of 2,500 hits from the soluble factor fraction and 59 hits from the exosome fraction were identified. Those were ranked and prioritised as follows to allow the detection of statistically significant and "biologically relevant" hits:

1. Candidates must have significant differential expression in the 3 independent mutant lines when compared to gene-corrected controls.
   (p-value < 0.05; fold change ≥ 1.5)
2. Candidates must be dysregulated in the same direction across all 3 lines.
3. Proteins categorised as "enriched" were analysed based on the number of their unique peptides. Only proteins identified by at least two unique peptides in each sample were considered.
4. Hits were clustered by cellular compartment (STRING analysis) – extracellular hits (GO terms: secretory granule, vesicle, extracellular region part, extracellular space).

Following implementation of the above stringent filtering criteria, enriched soluble factors/proteins from the mutant astrocyte secretome – 42 in total – belonged to pathways associated with axon guidance, cytoskeleton organisation, regulation of cell adhesion and inflammation, all of which have been implicated in neurodegeneration (Fawcett, Oohashi and Pizzorusso, 2019; Tran *et al.*, 2020). These included chondroitin sulphate proteoglycans, IGF and NFkβ signalling, and activation of the Smad-signalling cascade by TGFβ (Fig 3.9).

Additionally, **four hits were upregulated in the C9Δ astrocyte secretome across the 3 pairs** and included: alpha-2-macroglobulin [A2M] (fold change 1.5, MS/MS count 3535); Dickkopf WNT signalling pathway inhibitor 3 [DKK3] (fold change 1.7, MS/MS count 262); caeruloplasmin [CP] (fold change 1.56, MS/MS count 600); KCTD12 (fold change 1.56, MS/MS count 195). Although A2M and DKK3 have been implicated in Alzheimer's disease (AD) – A2M facilitates the clearance of β-amyloid deposits and inheritance of its deletion confers increased risk for AD (Blacker *et al.*, 1998), whilst DDK3 downregulation enhanced synapse integrity and memory in the hAPP-J20 AD mouse model (Nuria *et al.*, 2022) – their role has not been described in the context of ALS and were not considered biologically relevant.

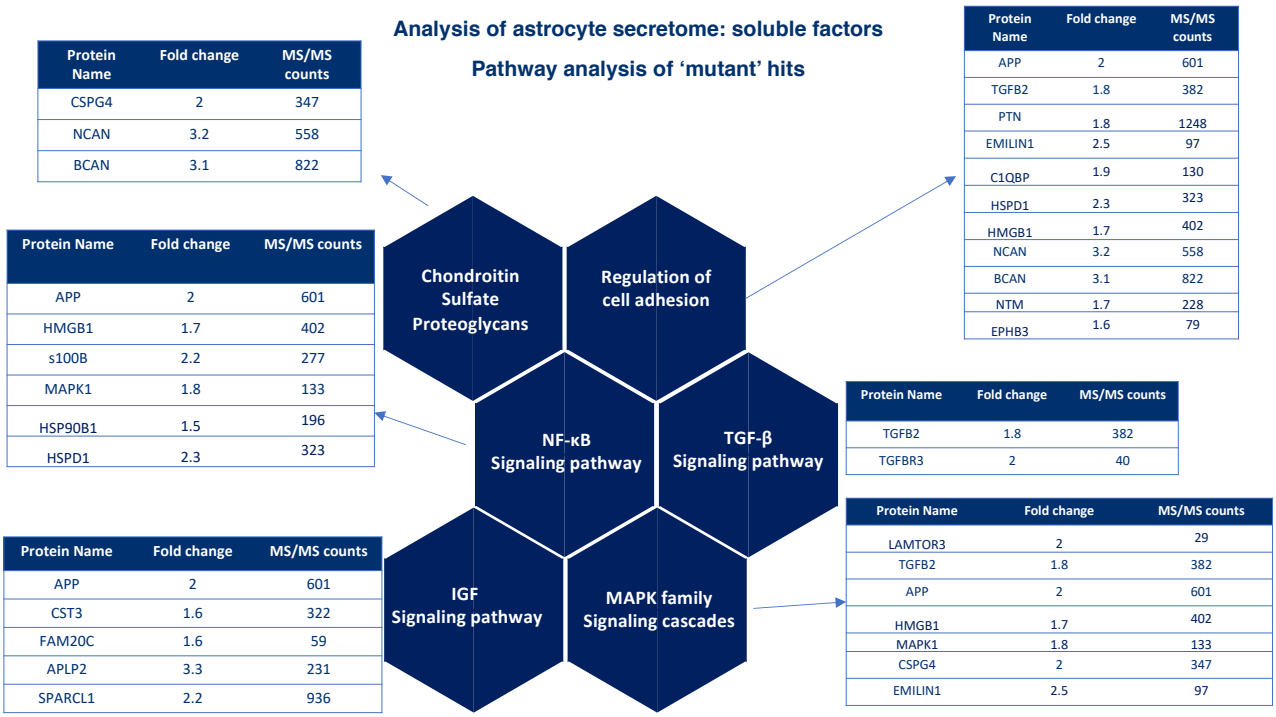

Figure 3.12 Analysis of astrocyte secretome – soluble factors. Pathway analysis of "mutant" hits. Enriched pathways in statistically significant C9-mutant differentially expressed proteins.

Chondroitin sulfate proteoglycans (CSPGs) were selected for further validation by immunoblot due to (1) enrichment of three members of this family in the mutant astrocyte secretome, (2) their high fold changes and (3) their association in acute CNS traumatic injuries and neurodegenerative disorders (Siebert, Conta Steencken and Osterhout, 2014; Tran *et al.*, 2020). Consequent validation by immunoblot of conditioned medium confirmed mutant-dependent upregulation of CSPGs including neurocan, brevican and CSPG4 (Fig 3.10).

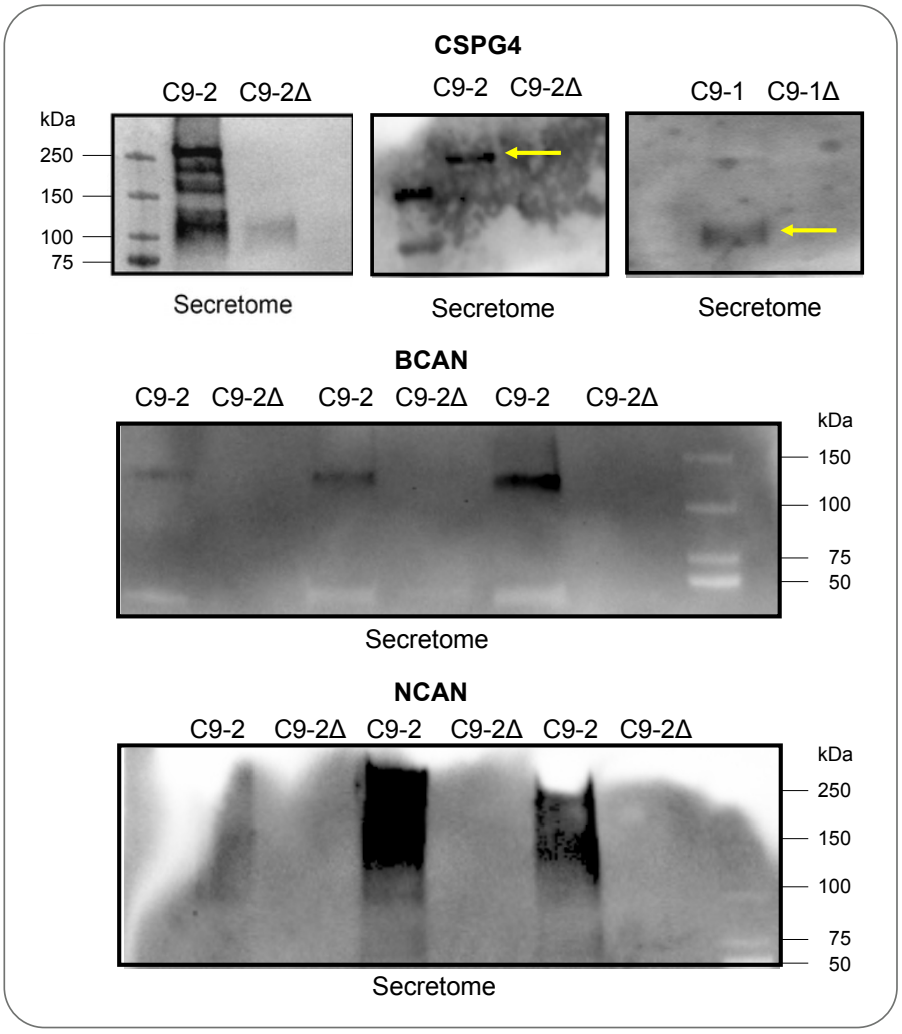

Figure 3.15 Western blot validation of mass spectrometric data. Validation by immunoblot of conditioned medium confirmed mutant-dependent upregulation of CSPGs including neurocan, brevican and CSPG4.

Lastly, after application of the filtering criteria on the 59 exosome hits, 18 of those were described to have an exosomal location; 14 were upregulated in gene-corrected lines and 4 were upregulated in the mutant ones (Table 3.2). Amongst those, thrombospondin 2 and glypican 6 were identified in the gene-corrected samples, which are known to modulate synaptic plasticity (Wang, Guo and Huang, 2012; Goldman *et al.*, 2015).

Gene Name	Exosomal location	Content	Upregulation
A2M	Y	Protein	Mutant
C4A	Y	Protein	Mutant
C4B	Y	Protein	Mutant
COL5A1	Y	Protein	Isogenic
IL11	Y	Protein	Isogenic
IL1RAP	Y	Protein	Isogenic
LIF	Y	Protein	Isogenic
MCAM	Y	Protein	Isogenic
RAB27A	Y	Protein	Isogenic
SEPP1	Y	Protein	Isogenic
SERPINE1	Y	Protein	Isogenic
THBS2	Y	Protein	Isogenic
C5orf46	Y	Protein	Isogenic
HAPLN3	Y	Protein	Isogenic
PRSS23	Y	Protein	Isogenic
SDC1	Y	Protein	Isogenic
SPON1	Y	Protein	Mutant
GPC6	Y	Protein	Isogenic

Table 3.4 This table presents a summary of exosomal proteins. Fourteen proteins were upregulated in the gene-corrected astrocyte conditioned medium and four proteins were upregulated in the mutant astrocyte conditioned medium.

3.5 Discussion

To better understand the complex extracellular signalling mediated by astrocytes harbouring the C9 mutation, a catalog of astrocyte-secreted proteins is an essential starting point for further research. This field is still in infancy. There are several technical challenges in developing effective protocols for global secretome analysis. These include the cell culture technique and yield of cells, the sample purity, and the optimization of protein-free media conditions, such as the length of serum-free incubation and cell washing procedures. Downstream sample processing and analytical methods are equally important.

In this project, published protocols on secretome isolation (Smith *et al.*, 2017; Sarvi *et al.*, 2018) were adapted to the hiPSC model. hiPSC-derived astrocytes were cultured on 10-cm plates at 80-90% confluency and protein concentrations of approximately 1µg/µl were obtained – an acceptable concentration for mass spectrometric analysis. To improve the sample purity, increase proteomic coverage and acquire low abundance proteins, sample pre-treatment was performed 24 hours prior to ACM collection, with three washings with PBS and removal of serum albumin and exogenous proteins from the medium. This approach effectively removed most serum proteins, as determined by the reduction of such proteins in mass spectrometric analysis.

The label-free quantitative proteomic technique was implemented to determine the relative amounts of proteins in biological samples. This method is based on spectral counting which translates to a measurement of the final protein concentration in the sample, rather than relying on sample labelling with stable isotopes. Tagging proteins can affect their normal activity, ability to interact with other proteins and distribution (Zhu, Smith and Huang, 2010). For instance, Tandem Mass Tags (TMT) labelling is a widely used technique that allows for the simultaneous quantification of multiple samples in a single mass spectrometry run. While TMT labelling can enhance the sensitivity and accuracy of protein quantification, it was not utilised in this study to avoid potential alterations in protein behaviour that could arise from the tagging process.

Finally, the detection of proteins of low biological significance was addressed by obtaining biological triplicates across the three pairs and applying stringent filtering criteria. The criteria were also useful for distinguishing between non-secreted cytosolic proteins in the ACM due to cell death and proteins secreted by non-conventional mechanisms.

In conclusion, this study used a global and unbiased strategy for secretome analysis through mass spectrometry and offered detailed and comprehensive characterisation of the conditioned medium from C9 and C9Δ hiPSC-derived astrocytes through identification of specific and biologically relevant proteins that are known to be secreted. Additionally, in contrast to other studies, three, independent, mutant *C9orf72* lines with their corresponding CRISPR/Cas9-mediated gene-corrected pairs were used. Having gene-corrected controls, where the only variable is the mutation of interest, allows causality to be assigned to any given phenotype and overcomes the transcriptional heterogeneity across iPSC lines.

Protein enrichment analysis of C9-mutant secreted factors revealed three members of the chondroitin sulfate proteoglycan family (CSPG4, neurocan [NCAN] and brevican [BCAN]) and proteins belonging to IGF, NFkβ and TGFβ signalling cascades. These signalling pathways have been linked to the pathogenesis of neurodegenerative disease (von Bernhardi *et al.*, 2015; Li, Sibon and Dijkers, 2018; Caldwell *et al.*, 2020). CSPG4 is known to be predominantly expressed in perivascular cells such as pericytes and plays a crucial role in maintaining the integrity of the blood-brain barrier and regulating cerebrovascular functions. Transcriptomic analyses of murine (He *et al*., 2018) and human brain (Yang *et al*., 2022) have highlighted CSPG4's expression in pericytes, providing insights and implying its contributions to the development of neurological diseases, such as Alzheimer's. In addition to their role in cerebrovascular functions, pericytes have been shown to interact closely with astrocytes in the CNS. These interactions involve the formation of pericyte-astrocyte gap junctions, which allow for the exchange of signaling molecules and nutrients between the two cell types (Peppiatt et al., 2006). Given the proximity and functional interactions between pericytes and astrocytes, it is plausible to suggest that CSPG4 expression in pericytes may have implications for astrocyte activation and astrogliosis in neurodegenerative diseases.

Astrogliosis is a key component of the multi-cellular response observed in neurodegenerative disorders including ALS. Understanding the distinction between mutation or disease-induced changes from reactive responses to chronic disease is important in defining distinct mechanisms that may be neuroprotective or may drive disease progression. A defining feature of this response is the production of extracellular matrix (ECM) including chondroitin sulphate proteoglycans (CSPGs) (Fawcett, Oohashi and Pizzorusso, 2019; Liddelow and Sofroniew, 2019; Tran *et al.*, 2020, 2021). It is of interest, noting findings in the current study and previous published work from our group of disrupted axonal transport of C9 MNs (Mehta *et al.*, 2021), that CSPGs through activation of the RhoA/ROCK signalling pathway, have been implicated in disrupting microtubule assembly and impairing axonal transport (Blanquie and Bradke, 2018). Future work could involve evaluation of the effects of CSPGs on axonal transport and neuronal physiological properties in the context of C9-ALS. For example, treatment of wild-type MNs with CSPG4, NCAN and BCAN separately and combined (through implementation of a dose-response approach). If any of the conditions recapitulate structural or physiological toxicity, manipulation experiments by addition of neutralising antibodies to C9-mutant ACM (start by blocking one target protein at a time and then multiple simultaneously) could be undertaken, followed by assessment for neuronal functions.

Considering the identified chondroitin sulfate proteoglycans (CSPG4, neurocan [NCAN], and brevican [BCAN]) in the secretome of C9-mutant astrocytes, it is noteworthy to consider the role of galectin-3 in the context of CSPG regulation. Galectin-3 is a member of the galectin family of proteins known for its ability to bind to β-galactoside-containing glycoconjugates, including CSPGs. This interaction has been implicated in various cellular processes, including cell adhesion, migration, and modulation of the extracellular matrix (ECM) (Pereira *et al.*, 2019).

Research has shown that galectin-3 can sequester CSPGs, potentially influencing their availability and activity within the extracellular environment. By binding to CSPGs, galectin-3 may affect their interactions with other signaling molecules and receptors, thereby modulating cellular responses. This raises important considerations regarding

the interplay between galectin-3 and CSPGs in the context of neurodegenerative diseases.

Given the findings in our study and the known roles of CSPGs in astrogliosis and neuroinflammation, future investigations could explore the therapeutic potential of targeting galectin-3 as a means of modulating CSPG activity. For instance, assessing the effects of galectin-3 inhibition on the secretion of CSPGs by C9-mutant astrocytes could provide insights into its role in astrocyte activation and the broader implications for neurodegenerative pathologies.

Furthermore, evaluating whether galectin-3 treatment alters the effects of CSPGs on neuronal function could offer valuable information on the mechanisms underlying CSPG-related toxicity. This approach could involve co-culture experiments where wild-type motor neurons are exposed to both CSPGs and galectin-3, assessing for any protective or detrimental effects on neuronal health and function.

In summary, considering the potential role of galectin-3 in sequestering CSPGs adds an important dimension to our understanding of the complex extracellular signaling mediated by astrocytes harbouring the C9 mutation. Incorporating this perspective could lead to new avenues for therapeutic intervention targeting the interactions between galectin-3 and CSPGs in the context of neurodegenerative diseases.

Future experiments are also warranted to explore the association between the intracellular proteome – with subcellular protein distribution – in hiPSC-derived astrocytes [*C9orf72* and gene-corrected (C9Δ) astrocytes from three independent patient lines] by mass spectrometry, and the existing astrocyte secretome dataset. Such profiling will generate a baseline reference library of intracellular and secreted proteins in cultured C9 and C9Δ astrocytes and this “omics” data integration will further facilitate the study of astrocyte functions in C9-ALS, and the determination of molecular mechanisms in astrocyte-neuron communication.

Exosomes constitute one of the major types of secreted extracellular vesicles and have emerged as a new and important intercellular communication process. Since they derive from specific cells, they carry disease-specific

proteins/miRNAs/mRNAs/lipids/metabolites and constitute an excellent source for biomarker discovery. In ALS, exosomes have been implicated as potential vehicles of (1) key proteins such as TDP-43, SOD1, FUS, DPRs and aberrant hexanucleotide repeat expansions in *C9orf72* ALS and (2) miRNAs associated with disease onset and progression (Chen *et al.*, 2021). With regards to astrocyte-derived exosomes in ALS, they have been shown to efficiently transport the mutated, misfolded SOD1 protein to spinal neurons, causing their death. Additionally SOD1-expressing astrocytes activated unconventional secretory pathways and increased their exosomal release, a mechanism that was considered to be compensatory and protective (Basso *et al.*, 2013). On the contrary, Varcianna et al., 2019, identified decreased secretion of extracellular vesicles by C9-iAstrocytes with subsequent transcriptomic analysis depicting specific downregulation miR-494-3p involved in axonal maintenance (Varcianna *et al.*, 2019). Overall, the specific cargos in exosomes derived from astrocytes are grossly unexplored. Moreover, the field suffers from lack of standardisation of isolation methodologies and the implementation of new techniques without detailed comprehensive analysis.

This study has characterised astrocyte-derived exosomes in *C9orf72* ALS with the use of a completely humanised model, the advantage of gene-corrected pairs and mass spectrometric analysis that allows unbiased and more detailed profiling of exosomal components compared to alternative methods of exosome characterisation (Jalaludin, Lubman and Kim, 2021). The identified exosomal proteins should be further validated by immunoblot. Next experiments should comprise of (1) investigating changes in the neuronal morphological (axonal/neurite outgrowth) and physiological phenotypes after treatment with exosomes from C9-mutant and gene-corrected samples; (2) identification of astrocyte exosome-induced neuronal transcriptomic alterations through RNA-Seq to detect pathways mediating the phenotypes; (3) exosomal isolation from the three mutant *C9orf72* lines with their corresponding CRISPR-Cas9-mediated gene-corrected pairs, followed by RNA extraction and implementation of RNA Seq for exosome transcriptome profiling to obtain information about expression levels and dynamics of exosomal RNAs, and understand their physiological function.

The present study did not include a comparison of Gene Ontology (GO) terms between the transcriptomic profiles of motor neurons treated with astrocyte-conditioned

medium (ACM) and the differential proteome of astrocyte-derived exosomes. Future investigations should focus on identifying overlapping GO terms to elucidate shared signaling pathways and biological processes, which may clarify how astrocyte exosomes modulate neuronal responses in the context of neurodegenerative diseases.

The addition of whole ACM was not sufficient to induce C9orf72-genotype-driven changes to wild type neurons (human embryonic stem cell derived *HB9*::GFP MNs) at a transcriptomic and proteomic level. Intriguingly, upon treatment with astrocyte conditioned medium (from both genotypes) there was downregulation in the expression of GRIN3A, GRIN1, GRIA2, GRIN2B, NLGN1 genes, which belong to "ionotropic glutamate receptor signalling pathway" and "regulation of NMDA receptor activity" GO terms. These findings contrast with previously published and well-established functions of astrocytes, which activate NMDARs through the secretion of glutamate and D-serine thus modulating synaptic plasticity (Hardingham and Bading, 2003; Han *et al.*, 2013). Astrocytes have been shown to increase the size of NMDAR-mediated synaptic currents in neurons compared to neuronal monocultures with specific potentiation of synaptic GluN2B receptor activity (Hahn, Wang and Margeta, 2015).

Interestingly, the results also indicate that mutant ACM (C9-2A ACM) stimulates the expression of synaptic genes, which is contrary to the expectation that mutant ACM would inhibit synaptic function. Several plausible explanations may account for this unexpected observation:

1. Compensatory Mechanisms: The upregulation of synaptic genes in response to mutant ACM may reflect a compensatory mechanism by motor neurons (MNs) attempting to counteract the detrimental effects of the mutant environment. In the face of stress or neurotoxic signals, cells may activate protective pathways, including those involved in synaptic plasticity and repair.

2. Altered Cell-Cell Interactions: The presence of mutant ACM may change the dynamics of cell signaling and communication between motor neurons. This altered interaction could lead to the activation of pathways that promote synaptic gene expression, potentially as part of an adaptive response to maintain synaptic integrity.

3. Context-Dependent Responses: It is possible that the context in which the mutant ACM is applied influences its effects on gene expression. Factors such as the timing of treatment, the specific composition of the ACM, and the developmental stage of the MNs could all play crucial roles in determining the outcome of synaptic gene expression.

4. Non-Canonical Pathways: Non-canonical signaling pathways might be activated in response to the mutant ACM, contributing to the upregulation of synaptic genes. These pathways may not be fully understood and could represent novel mechanisms of cellular response in the context of ALS.

In summary, while the stimulation of synaptic genes by mutant ACM deviates from expected outcomes, it opens avenues for further investigation into the underlying mechanisms, including compensatory responses and non-canonical signalling pathways. Understanding these processes could provide valuable insights into the pathology of ALS and potential therapeutic targets.

The overall genotype-mediated log2 fold changes (FCs) of protein expression and phosphorylation status were relatively small (<0.4) across all time points when comparing the two ACM treatments. This suggests that while there are detectable changes in protein expression, the overall magnitude of these changes is modest.

The most pronounced fold changes were observed in specific pathways upon addition of C9-2-mutant ACM (compared to MNs in their own medium). Notably, the phosphorylation of CamKii at Thr286/calmodulin increased progressively over time (log2FC of 1, 1.3, and 1.6 at 2 hours, 24 hours, and 7 days, respectively). This indicates a sustained activation of the CamKii pathway, which is crucial for calcium signaling, synaptic plasticity, and neuronal survival. The progressive increase in phosphorylation suggests that MNs may be responding adaptively to the presence of the C9-2-mutant ACM, potentially enhancing signalling mechanisms involved in neuron function and protection. The data also show a significant increase in the phosphorylation status of p44/42 MAPK (ERK1/2) at 7 days (log2FC of 2.4). This pathway is well-recognized for its role in cell survival, proliferation, and differentiation. The strong activation of this pathway indicates that MNs are likely engaging protective signalling mechanisms in response to the stressor presented by the C9-2-mutant

ACM. Such activation could be interpreted as a neuroprotective response aimed at counteracting potential degeneration or cellular stress induced by the mutant environment.

In contrast, treatment with C9-2Δ-isogenic ACM resulted in fold changes of less than 1 in MNs compared to MNs in their own medium at 2 and 24 hours. This indicates a lack of significant activation of the pathways measured during these time points. The results suggest that the isogenic ACM does not elicit a robust signalling response in MNs, which may imply that it is less effective at modulating or supporting neuronal health compared to the C9-2-mutant ACM. At 7 days, the highest fold changes for p44/42 MAPK, CamKii, and 4E-BP1 were observed with the C9-2Δ-isogenic ACM, with log2FCs of 2.5, 1.3, and 1.2, respectively. This late increase suggests that while immediate responses to the isogenic ACM might be minimal, there may be delayed effects that warrant further investigation. The increase in 4E-BP1 phosphorylation, which is involved in protein synthesis regulation, indicates a potential shift in metabolic or translational activity in response to the treatment.

Next steps will involve a multi-faceted approach to further explore the signaling pathways activated by C9-2-mutant and C9-2Δ-isogenic ACM treatments in motor neurons (MNs). Firstly, a detailed cross-referencing of the dataset with genes previously implicated in motor neuron homeostasis and pathology will be conducted, particularly focusing on p44/42 ERK1/2 and other key genes linked to ALS and related neurodegenerative conditions. This will entail leveraging existing literature to identify relevant gene expression profiles and signaling pathways that may correlate with the current findings.

Additionally, the analysis will be expanded to include functional assays assessing the impact of the identified pathways on neuronal survival, synaptic plasticity, and overall cellular health. These may include cell viability assays, calcium imaging to evaluate calcium signaling dynamics, and electrophysiological recordings to measure synaptic function in response to both ACM treatments.

Time-course experiments will also be performed to monitor the temporal dynamics of protein expression and phosphorylation changes beyond the initial 7-day period. This may reveal delayed responses and long-term adaptations of MNs to the treatments.

Furthermore, experiments aimed at identifying dysregulated signalling pathways in wild type MNs following ACM treatment will be repeated after optimising the 'generation of conditioned medium' protocol. Next steps could involve testing longer conditioning periods (> 72 hours) while avoiding cell stress. Centrifugal concentration of conditioned medium will also be employed to determine protein concentration prior to treating MNs (Allen *et al.*, 2012; Caldwell *et al.*, 2020). To corroborate the current astrocyte secretome dataset, the astrocyte conditioned medium could be separated into exosomes, secreted factors and flow-through, following the established protocol (Section 2.9.1 – Methods and Materials). Each component could then be added to MNs for further analysis. Unbiased transcriptomic studies can be repeated on treated MNs at 24 hours, while proteomic studies and reverse phase protein array at 3 time-points – 2 hours (for elucidation of immediate and specific phosphorylation events) and over 24 hours and 7 days (for identification of secondary signalling cascades). Prioritised pathways will be ranked based on (a) statistical confidence in their degree of differential expression (b) degree of fold change, (c) biological relevance and support in the literature. These pathways can then be modelled/manipulated in iPSC-cellular models using genetic or pharmacological methods in control and/or C9-mutant ALS MNs to assess for morphological and physiological outcomes (Zhao *et al.*, 2020).

Finally, neuron-astrocyte cocultures will be implemented using transwell inserts, rather than transferring ACM from astrocytes to neurons. This approach mitigates potential modifications to the cultured medium due to environmental changes and allows for the continuous delivery of fresh astrocyte medium to the neurons, preserving intact secreted factors, while avoiding cellular physical contact (Cheng *et al.*, 2020b).

Chapter 4 Investigation of astrocyte-mediated contact-dependent mechanisms through the mixed species model

4.1 Introduction

Signalling between different cell types is central to many biological processes in the brain. Additionally, the influences between cell types are rarely unidirectional so it is valuable to be able to profile both cell types simultaneously. Achieving artifact-free physical separation of cell types to study them is challenging – for example physical dissociation of cultures and FACS sorting may induce stress to cells and gene expression artifacts, often suffers some degree of impurity and generally allows the analysis of only a single cell type. The implementation of the mixed species RNA-Seq approach of coculturing distinct cell types from different species (human and mouse in this case) facilitates the substitution of physical cell sorting by in silico RNA-seq read sorting and enables the investigation of bidirectional juxtracrine signalling mechanisms through concurrent transcriptional profiling of both cell types involved (MNs and astrocytes). This is possible because of the evolutionary divergence of mRNA sequences (Qiu *et al.*, 2018). In this chapter, the astrocyte-neuronal molecular cross talk is analysed by implementing physical cocultures of human astrocytes (C9 – mutant and C9Δ – gene-corrected) with rodent neurons and using mixed species RNA-Seq to investigate astrocytic effects on neurons.

4.2 Analysis of transcriptomic alterations in mouse MNs due to hiPSC-derived C9orf72 astrocytes.

A mixed species coculture assay system was set up wherein embryonic spinal cord MNs from wild-type mice, devoid of astrocytes, (Wiese *et al.*, 2010) (Fig 4.1) were cocultured with Control, *C9orf72* and gene-edited (C9Δ) hiPSC-derived astrocytes (from one pair) for 7 days. Following RNA extraction, quantitative RT-PCR using species-specific primers was performed as a quality control step, to estimate the proportion of mouse MNs (mMNs) and human astrocytes in the coculture experiments. This demonstrated that 10-60% cells in the coculture were mMNs and was corroborated by the percentage depletion of human GFAP expression in cocultures

when compared to the astrocyte monocultures. Hence, the model was amenable for interspecies RNA Sequencing (Fig 4.2).

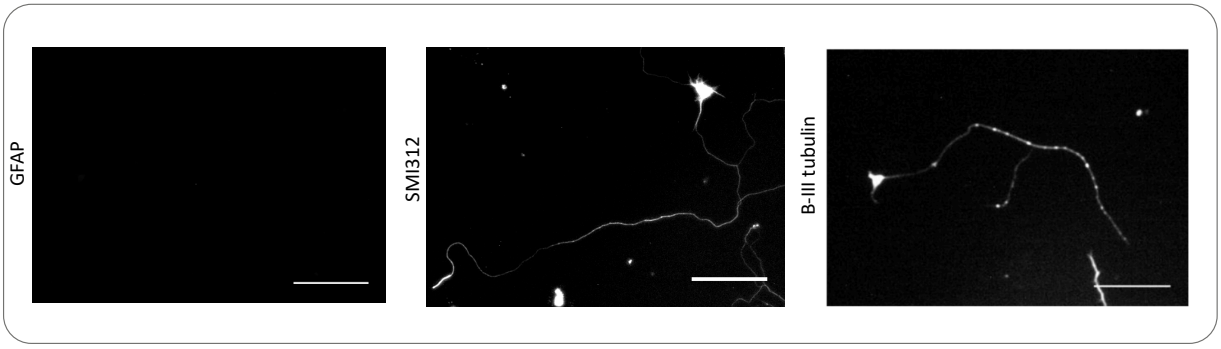

Figure 4.1 Validation of mouse MNs (mMNs) via immunostaining. Enriched primary mMNs isolated from E13.5 embryos showing neuronal markers SMI312 and βIII-tubulin and absence of astrocytes (negative for GFAP immunostaining). Scale bar 100µm.

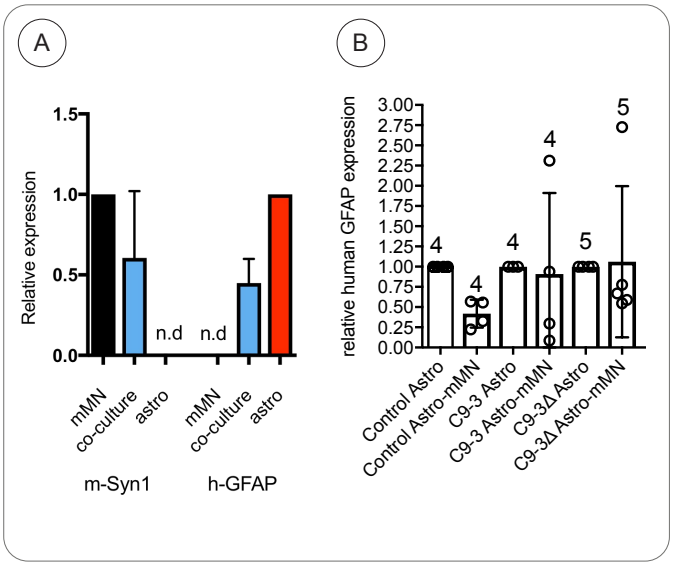

Figure 4.2 (A) Relative expression (qRT-PCR) of murine Synapsin1 and human GFAP in mMNs, human astrocytes and coculture conditions showing detectable levels of RNA from both cell types in the coculture set-up, thus, amenable for mixed species RNA-seq.
(B) Relative expression (qRT-PCR) of human GFAP in human astrocyte monocultures and coculture conditions demonstrating GFAP depletion in cocultures.

RNA sequencing was performed on hiPSC-derived astrocyte monocultures from control, 1 x *C9orf72* and its paired *C9orf72* gene-corrected (C9Δ) iPSC lines, and upon coculture with mouse MNs. Sequencing was performed at 60M reads for monocultures and 150M reads for coculture samples. Sequencing reads were mapped and segregated to human and mouse genomes using SARGASSO, in collaboration with Dr Dando (Hardingham lab).

Principal Component Analysis (PCA) showed two clusters of samples (left Vs right) (Fig 4.3).

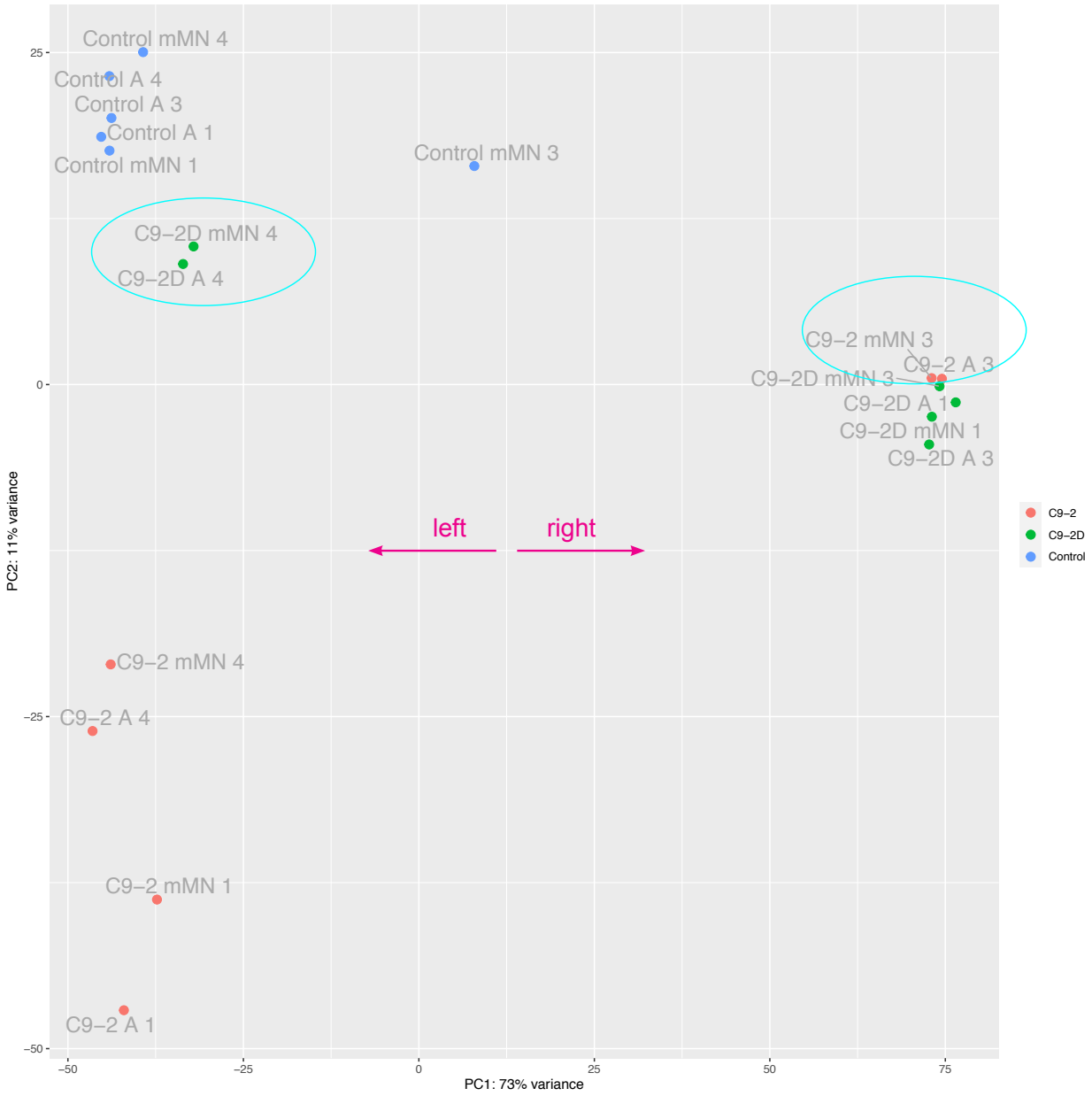

Figure 4.3 Principal component analysis (PCA) showed two cluster of samples (left Vs right).

Each cluster was compared to the hiPSC-derived astrocyte RNA seq dataset from previous published work (Zhao *et al.*, 2020). There was higher association of the original RNA-Seq astrocyte data with the group on the left of the PCA plot as depicted by a higher correlation coefficient, indicative of transcriptomic differences between the two sets (left Vs right) (Fig 4.4).

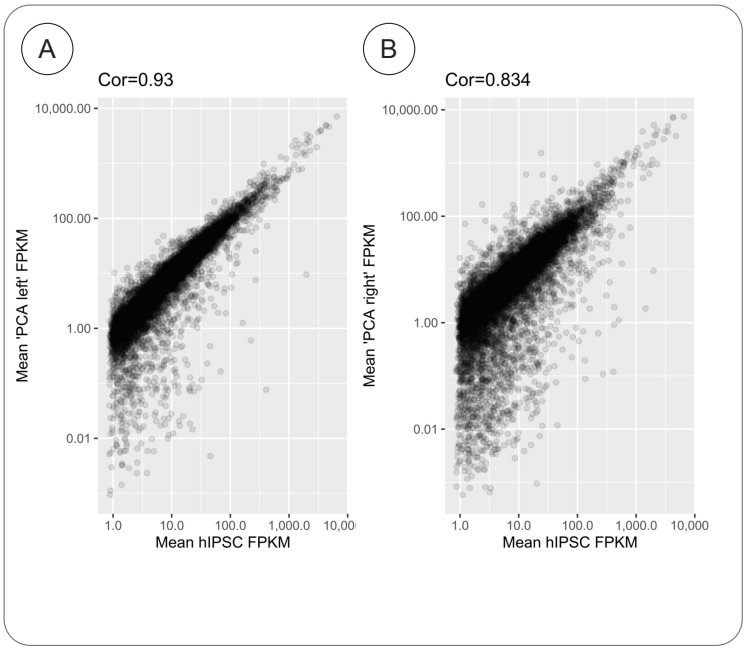

Figure 4.4 Comparison of gene expression between samples on 'left' & 'right' on PCA plot with original hiPSC-derived astrocyte transcriptome data.

There is a higher correlation of the hiPSC data with samples on the 'left of the PCA plot (A) compared to (B), which represents the 'right' side of the PCA plot. This indicates transcriptomic differences between 'left' and 'right' samples.

To ascertain the aetiology of these transcriptional discrepancies, an investigation for off-target cell contamination was undertaken by using well-established marker genes for human neurons and endothelial cells (Fig 4.5 A, B). The hiPSC astrocyte data was again compared to the samples on the left and right of the PCA plot. No distinct differences were identified. Nonetheless, there was increased expression of AQP4, SLC4A4 and SPARCL1 – astrocyte markers associated with astrocyte differentiation and maturity – in the samples on the right (Fig 4.5 C).

These findings were further validated by examining the expression of immature/fetal and mature astrocyte-specific signature genes in selected samples using established gene profiles (Cahoy *et al.*, 2008; Y. Zhang *et al.*, 2014) (Fig 4.6 A). In conclusion, the sample cluster on the 'right' of the PCA plot was considered to have a more mature signature compared to the one on the 'left' and to the hiPSC astrocyte data (Fig 4.6 B, C).

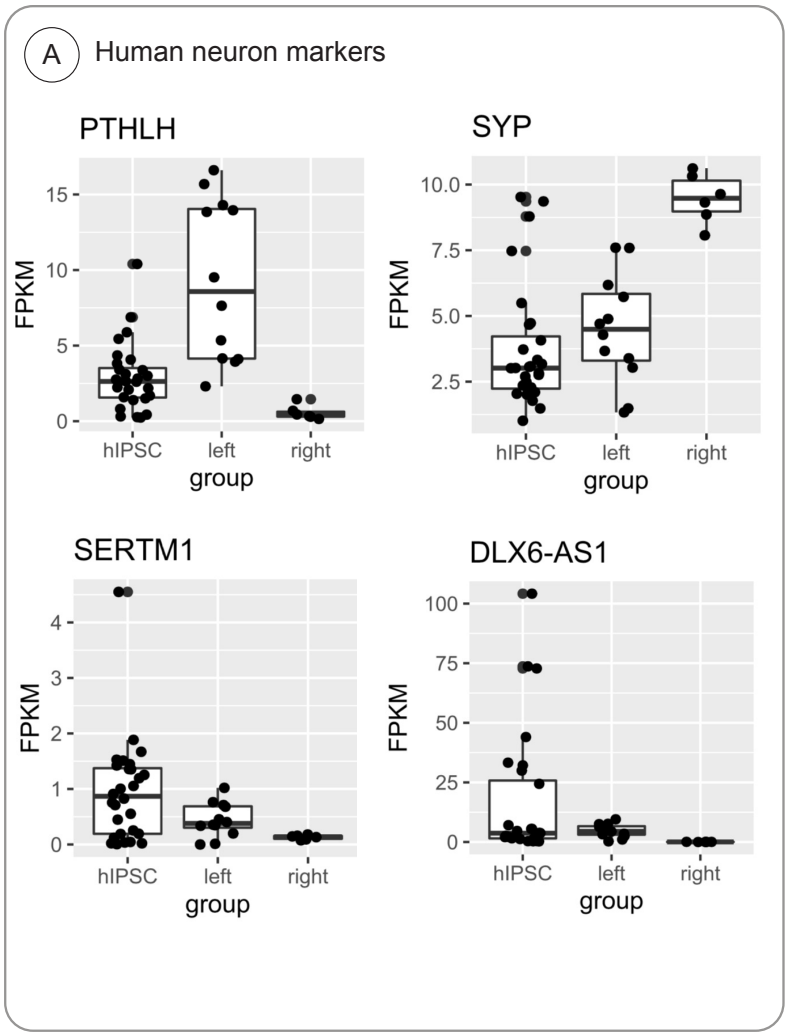

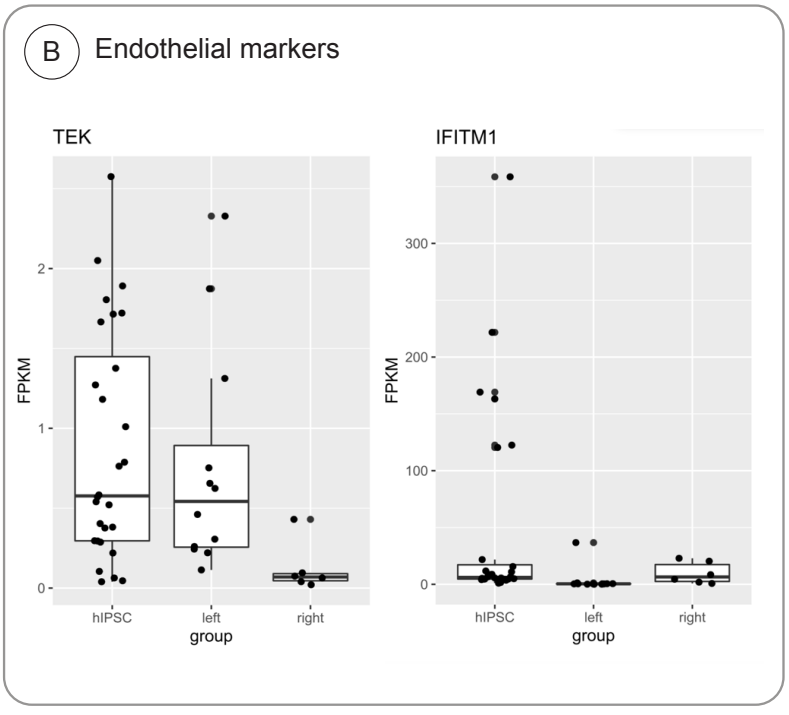

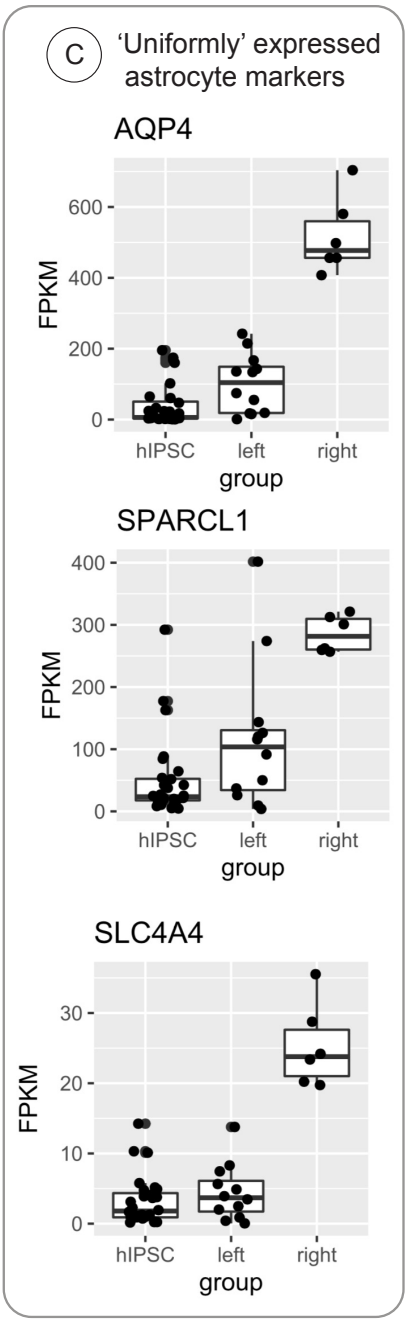

Figure 4.5 Investigation for off-target cell contamination with well-established marker genes for (A) human neurons and (B) endothelial cells. The original hiPSC astrocyte data (Zhao et al., 2019) was compared to the samples on the left and right of the PCA plot. No distinct differences were identified. (C) There was increased expression of AQP4, SLC4A4 and SPARCL1 in the sample on the 'right'. These are astrocyte markers associated with differentiation and maturity.

A

Gene name	Fetal	Mature	
HGF	+	+	- = <1 fpkm
AQP4	++	++++	"+" = 1-5 fpkm
BMPR1B	+	+++	"++" = 5-25 fpkm
PLCD4	-	+	"+++" = 25-75 fpkm
PHKG1	-	-	"++++" = > 75 fpkm
CBS	++	+	
PAQR6	+	+++	
ALDH1L1	-	++	
CCDC80	+	+	
FMO1	-	-	
SLC30A10	-	+	
PPP1R3C	+	+++	
ENTPD2	-	-	
EGFR	++	++	
OTX1	++	+	
ATP13A4	+	+++	
KCNN3	+	++	
PTX3	++	-	
TNC	+++	-	
SOX9	++++	+++	
ABCD2	+	++	
LRIG1	++	+++	
GLI1	-	-	
GLI2	+	-	
OTX1	++	+	
RFX4	++	++	
DBX2	-	+	
SLC14A1	-	+++	
GDPD2	++	++	
EGFR	++	++	
PAX6	++	++	

B Genes associated with astrocyte maturity

C92 A 'outlier' on the right of PCA plot	C92Δ A 'outlier' on the left of PCA plot
AQP4	AQP4
BMPR1B	BMPR1B
PLCD4	PLCD4
PAQR6	PAQR6
ALDH1L1	ALDH1L1
SLC30A10	SLC30A11
PPP1R3C	PPP1R3C
EGFR	EGFR
KCNN3	KCNN3
ABCD2	ABCD2
LRIG1	LRIG1
DBX2	DBX2

Highest expression

Lowest expression

Upregulation of 7 astrocyte maturity markers in the C92 A 'outlier'
Upregulation of 5 astrocyte maturity markers in the C92Δ A 'outlier'

C Genes expressed by fetal astrocytes / APC stage

	C92 A 'outlier' on the right of PCA plot	C92Δ A 'outlier' on the left of PCA plot
OTX1	Low	High
CBS	High	Low
PTX3	Low	High
TNC	Low	High
SOX9	Low	High
GLI1	Low	High
OTX1	Low	High

Figure 4.6 (A) Analysis of expression of immature/fetal and mature astrocyte-specific signature genes in selected samples (C92 A 'outlier' on the right of the PCA plot & C92Δ A 'outlier' on the left of the PCA plot) using established gene profiles. (B) 7 astrocyte maturity markers were upregulated in the C92 A 'outlier' and 5 astrocyte maturity markers were upregulated in the C92Δ A 'outlier'.
(C) The sample cluster on the right of the PCA plot was considered to have a more mature astrocyte signature with lower expression of fetal astrocytic genes compared to the one on the left.

Taking into consideration the higher correlation of the “left” sample cluster with the published hiPSC-derived astrocyte data, those samples were taken forward for examination of intercellular (astrocyte-neuronal) transcriptional effects. Transcriptional changes were detected in mouse motor neurons when cocultured with control, mutant and gene-corrected astrocytes (on separate analysis for each condition). However, in view of the between-sample variability of neuronal gene expression in cocultures with control, mutant and gene-corrected astrocytes, probably attributed to the heterogeneous states of astrocyte maturity and as depicted by principal component analysis, no statistically significant differentially expressed genes were identified across the 3 conditions (Fig 4.7 B). Neuron-induced transcriptional changes in the astrocytes were observed to a lesser extent suggesting that the ratio of neurons:astrocytes was too low for induction of a substantial effect (Fig 4.7).

A

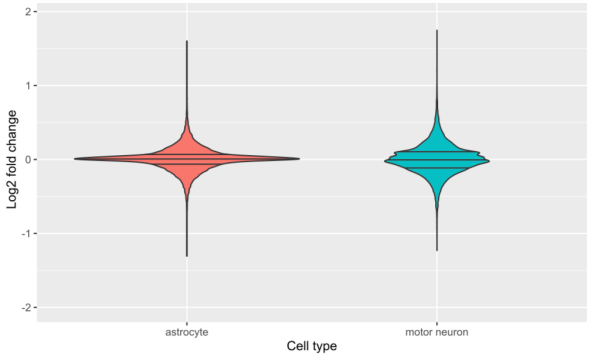

B

Comparison	Upregulated	Downregulated	D.E.total
Astrocyte-induced transcriptional changes in MNs			
Control co-culture vs MN monoculture	123	394	517
C9 mutant co-culture vs MN monoculture	62	57	119
C9 isogenic co-culture vs MN monoculture	314	243	557
Cocultures on left of PCA plot vs MN monocultures	**1**	**0**	**1**
Neuron-induced transcriptional changes in astrocytes			
Control co-culture vs astrocyte monoculture	128	63	191
C9 mutant co-culture vs astrocyte monoculture	18	11	29
C9 isogenic co-culture vs astrocyte monoculture	36	15	51
Cocultures on left of PCA plot vs astrocyte monocultures	**164**	**136**	**300**

Figure 4.7 Inter-cell effects – Differential expression analysis of cocultures & monocultures.

(A) Violin plot illustrating the distribution of neuro-induced transcriptional changes in astrocytes (red plot) and the astrocyte-induced differentially expressed genes in neurons (green plot).

(B) Table demonstrating the larger number of total dysregulated genes in neurons compared to astrocytes. The between sample variability in astrocyte maturity led to considerable differences in the neuronal genes affected by astrocytes across conditions and the detection of only one statistically significant differentially expressed neuronal gene.

4.3 Discussion

In summary, a mixed species coculture experimental paradigm was established that enables the evaluation of transcriptional alterations induced by ALS-diseased astrocytes on neurons. This was verified by the detection of astrocytic and neuronal transcripts in the isolated RNA of the cocultures.

Transcriptomic analysis and consequent comparison and characterisation of the dataset with validated markers of astrocyte maturity, revealed heterogeneity in human astrocyte maturation states which inevitably influenced astrocytic effects on neuronal gene expression. Additionally, the samples on the "left" of the PCA plot that demonstrated a strong fetal signature, were more compatible with the previously published hiPSC-derived astrocyte RNA Seq data. This exposes one of the known limitations of the hiPSC cellular system in that it does not integrate cellular aging into the disease modelling paradigm and iPSC-derived phenotypic cells exhibit immature functional characteristics akin to their respective embryonic or fetal cells (Lapasset *et al.*, 2011; Patterson *et al.*, 2012). Although iPSC-based disease modelling of ALS and other neurodegenerative disorders has offered unprecedented insight into the underpinning molecular and cellular mechanisms of neurodegeneration, it is important to integrate this approach with complementary model systems to enhance the translational yield of preclinical testing. Recent studies have also shown that astrocytes derived through direct conversion of fibroblasts into induced neuroprogenitors cells (iNPCs), without the use of pluripotency factors, retain age-related features (Varcianna *et al.*, 2019; Gatto *et al.*, 2021). This may be a reliable tool for capturing the molecular sequelae of both cellular aging and the non-cell autonomous mechanisms of the disease.

The physiological responses of neurons to signals originating from healthy and ALS-diseased astrocytes and vice versa, involve changes in gene expression that are not yet fully understood. This mixed species approach obviates the need for physical sorting of cocultured cells and enables the comprehensive, simultaneous transcriptomic analysis of human astrocytes and mouse neurons, due to the evolutionary divergence of homologous sequences at the nucleotide level.

Future studies should include additional quality control before the implementation of RNA sequencing through qPCR analysis for astrocyte maturity markers such as AQP4, BMPR18, ALDH1L1, ABCD2. Homogeneous samples should be taken forward. The effect of iPSC passage number on maturity and presence of potential contaminating cells (such as neurons) in hiPSC-derived astrocyte cultures at higher passage numbers should also be determined. Further, samples should be collected from the other two independent, mutant *C9orf72* lines with their corresponding CRISPR-Cas9-mediated gene-corrected pairs and a minimum of three independent biological replicates are required per condition. This will address inter-mouse variability and maximise the sensitivity and accuracy of DEG identification and quantification, for valid biological interpretation of the results.

An important consideration when interpreting data from a mixed species coculture platform is whether any of the inter-cellular transcriptional changes are driven by the different animal species. Single species coculture samples should also be obtained, to assess whether the genes induced by human astrocyte activity in mouse neurons and in reverse, do not derive from the difference in the species of origin. Qiu et al., tested the expression of mouse astrocytic genes (induced by rat neuronal activity), the induction of which could be tracked in a single-species experiment because their expression was more than 10-fold higher in astrocytes than in neurons. All astrocytic genes were indeed stimulated in a single-species mouse neuron-astrocyte coculture but not in the neuronal monocultures, indicating that having neurons from a different species doesn't result in spurious effects of synaptic activity on astrocyte gene expression (Qiu *et al.*, 2018).

Chapter 5 - Investigation of the effects of astrocyte genotype on axonal mitochondrial transport and neuronal mitochondrial bioenergetics

5.1 Introduction

Axonal transport of cargo such as mitochondria, is essential for neuronal function and survival (Sleigh *et al.*, 2019; Guillaud *et al.*, 2020; Han *et al.*, 2020). Moreover, genetic and *in vivo* evidence suggest a potential causative link between dysregulated axonal transport and neurological disorders such as ALS (Sleigh *et al.*, 2019). Indeed, abnormalities of mitochondria function and motility are described in ALS including human autopsy and cellular studies of *C9orf72*-ALS (Dafinca *et al.*, 2016; Lopez-gonzalez *et al.*, 2016; Onesto *et al.*, 2016; Fujimori *et al.*, 2018; Fumagalli *et al.*, 2021; Mehta *et al.*, 2021). To date, these studies have largely focused on the intraneuronal consequences of genetic mutations on axonal transport.

Astrocytes, oligodendrocytes and Schwann cells are all involved in supporting axons through the lactate shuttle mechanism (Bélanger, Allaman and Magistretti, 2011; Domènech-Estévez *et al*., 2015; Rinholm *et al*., 2011). Oligodendrocytes in the CNS (Rinholm *et al*., 2011) and Schwann cells in the PNS (Domènech-Estévez et al., 2015) express MCT1, which facilitates the transport of lactate to neurons and supports axonal energy demands. The downregulation of the MCT1 transporter in oligodendrocytes has been implicated in the development of ALS (Lee et al., 2013), while the role of Schwann cell-mediated lactate transport in ALS progression is still unknown.

Astrocytes not only contribute to neuronal homeostasis through the lactate shuttle, but they also provide glycogen to neurons and have the potential to regulate axonal mitochondrial transport (Bélanger, Allaman and Magistretti, 2011; Brown and Ransom, 2007; Beard *et al.*, 2022). Various astrocytic metabolic mechanisms have been implicated in ALS (Clement *et al.*, 2003; Yamanaka *et al.*, 2008; Tefera and Borges, 2016). These include reduced expression of the glutamate reuptake transporter EAAT2 causing downregulation of the glutamate-glutamine cycling and hyperexcitability (Lin *et al.*, 1998), defects in the astrocyte-neuronal lactate shuttling

(Yamanaka and Komine, 2018) and altered membrane transport of mitochondrial specific energy substrates (Allen, Hall, Woof, *et al.*, 2019b). Whilst the wider metabolic role of astrocytes in modulating neuronal homeostasis is well-studied, the role of astrocytes in specifically regulating axonal mitochondrial transport and neuronal bioenergetic status in ALS, is unknown.

Against this background, using multiple independent patient C9-mutant iPSC-derived astrocytes (C9-A) and corresponding gene-corrected controls (C9Δ-A), the role of astrocytes in regulating MN axonal transport was examined. It was shown that C9Δ-A positively regulate axonal mitochondrial transport in mutant MNs, whereas C9-A impair fast axonal transport of mitochondrial cargo in control MNs. It was demonstrated that C9-astrocyte-mediated deficits on axonal transport are driven by changes in neuronal mitochondrial bioenergetics. Furthermore, it was established that C9-A display cell autonomous defective bioenergetics and critically, that selective genetic enhancement of astrocyte mitochondrial function reverses C9-mutation-dependent MN axonal transport deficits. Together, these findings suggest a novel role of astrocytes in regulating axonal transport and highlight the importance of astrocytic metabolism in the context of C9-ALS.

5.2 Astrocyte genotype regulates axonal mitochondrial transport

Three patient-derived human induced pluripotent stem cell (hiPSC) astrocyte lines carrying the C9ORF72 mutation (C9) were used, along with their isogenic gene-corrected control with the C9ORF72 mutation removed (C9Δ), which was generated using CRISPR/Cas9. Highly enriched spinal cord patterned astrocytes and motor neurons (MNs) were generated as described previously (Selvaraj *et al.*, 2018; Zhao *et al.*, 2020). Both C9 and C9Δ patient-derived MNs (C9-MN or C9Δ-MN) were studied in isolation or in co-culture with the three pairs of C9 and C9Δ-derived astrocytes (C9-A or C9Δ-A). This allowed for the assessment of cell-autonomous and astrocyte-derived non-cell autonomous effects of the C9ORF72 mutation on MN mitochondrial function.

Two established features of mitochondrial axonal transport were measured: the proportion and average velocity of motile mitochondria (anterograde movement).

Control MNs (C9Δ-MNs or human embryonic stem cell-derived *HB9*::EGFP [hESC *HB9*::EGFP MNs]) were selectively labelled with mito-dsRed2 for measuring axonal transport and then co-cultured with C9-A. It was found that co-culturing control MNs with mutant astrocytes led to a reduction in both the percentage and speed of motile mitochondria in MNs (Fig 5.1 A, B, C, E; Fig 5.2 A-B), when compared to monocultures of control MNs. Significantly, both mitochondrial transport phenotypes were reversed when control MNs (C9Δ-MNs or hESC *HB9::*EGFP MNs) were co-cultured with control C9Δ-A (Fig 5.1 A, B, C, E; Fig 5.2 A-B).

It was next examined whether co-cultures of mutant MNs with mutant astrocytes would result in greater axonal transport deficits, noting earlier reports of cell-autonomous axonal transport impairments in C9-MNs (Fumagalli *et al.*, 2021; Mehta *et al.*, 2021). Indeed, in comparison with isolated C9-MNs, a significant reduction in the speed of motile mitochondria was observed when C9-MNs were co-cultured with C9-A; the percentage of motile mitochondria, on the other hand, was not affected (Fig 5.1 D, F). Importantly, co-culture of C9-MNs with control C9Δ-A resulted in the rescue of both axonal transport deficits (% motility and mean speed of mitochondria) to wildtype levels (Fig 5.1 B, D, F). These data recapitulate previous findings of cell-autonomous axonal transport deficits associated with the C9ORF72 mutation on MNs and reveal that, in co-culture, the MN axonal transport phenotype is determined by the genotype of the astrocyte and not the neuron.

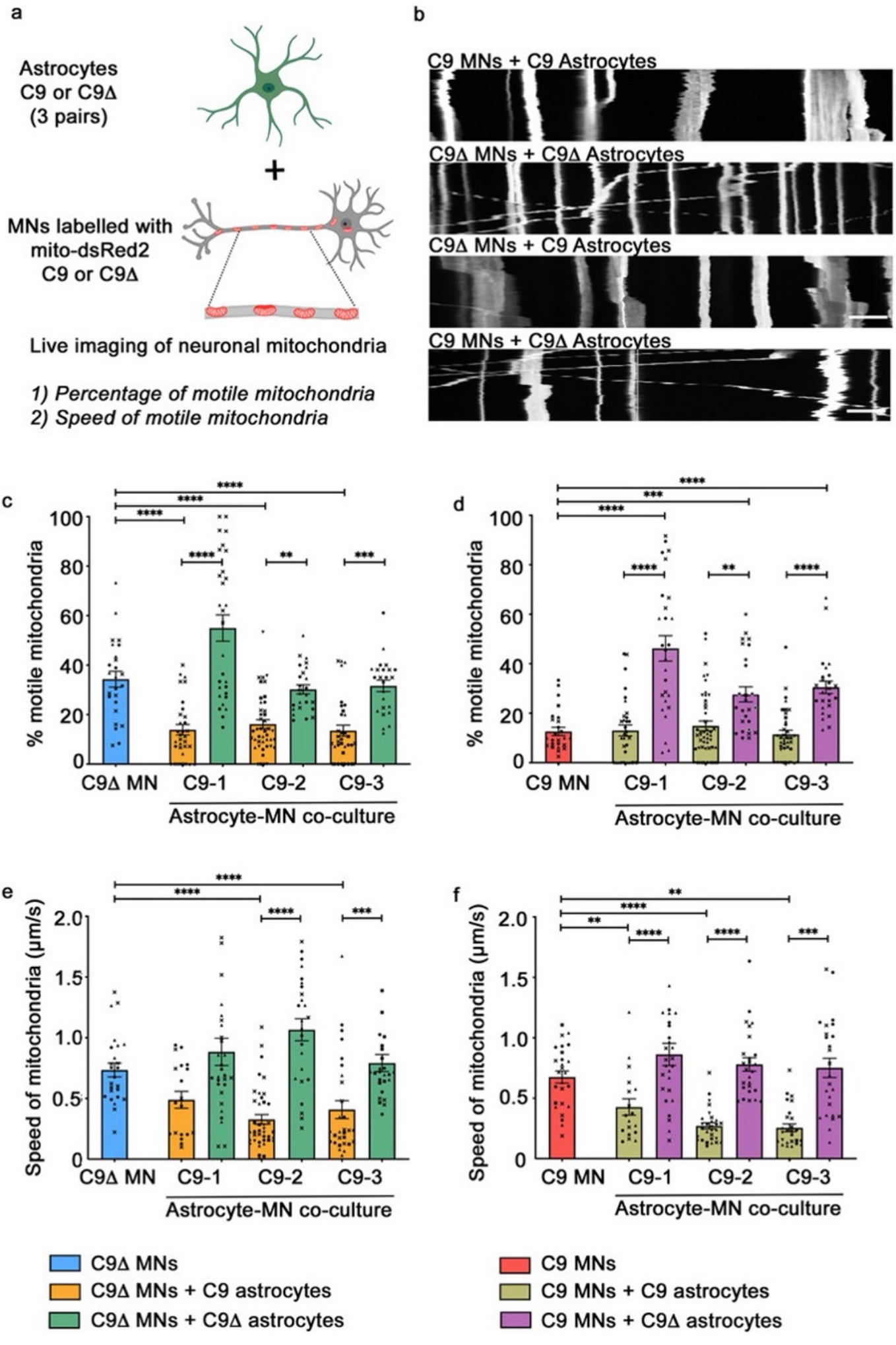
a
Astrocytes
C9 or C9Δ
(3 pairs)
+
MNs labelled with
mito-dsRed2
C9 or C9Δ
Live imaging of neuronal mitochondria
1) Percentage of motile mitochondria
2) Speed of motile mitochondria
b
C9 MNs + C9 Astrocytes
C9Δ MNs + C9Δ Astrocytes
C9Δ MNs + C9 Astrocytes
C9 MNs + C9Δ Astrocytes
c
% motile mitochondria
C9Δ MN
C9-1
C9-2
C9-3
Astrocyte-MN co-culture
d
% motile mitochondria
C9 MN
C9-1
C9-2
C9-3
Astrocyte-MN co-culture
e
Speed of mitochondria (µm/s)
C9Δ MN
C9-1
C9-2
C9-3
Astrocyte-MN co-culture
f
Speed of mitochondria (µm/s)
C9 MN
C9-1
C9-2
C9-3
Astrocyte-MN co-culture
C9Δ MNs
C9Δ MNs + C9 astrocytes
C9Δ MNs + C9Δ astrocytes
C9 MNs
C9 MNs + C9 astrocytes
C9 MNs + C9Δ astrocytes

Figure 5.1 Effects of astrocytes on mitochondrial transport in motor neurons in physical co-cultures. **(a)** Schematic diagram of motor neuron and astrocyte physical co-culture platform to assess mitochondrial transport in MNs. **(b)** Kymographs depicting mitochondrial transport in motor neurons upon co-culture with astrocytes; scale bar = 10 µm. **(c&d)** Quantification of the percentage of motile mitochondria (labelled with mitoDsRed2) and **(e&f)** mean speed of motile mitochondria in a 100 µm stretch of proximal axon in hiPSC-derived C9-MN and gene-corrected paired controls, co-cultured with either C9-A or gene-corrected paired controls from the three independent patient lines [(mutant astrocytes represented by C9-A; mutant motor neurons by C9-MN; gene-corrected astrocytes by C9Δ-A; gene-corrected motor neurons by C9Δ-MN); **x**,●,▲,■,▼ (1^{st}/2^{nd}/3^{rd}/4^{th}/5^{th} biological experiment – respectively)]. Data are represented as mean ± SEM. n ≥ 5 axons per independent plate-down (biological experiment), N ≥ 3 independent plate-downs. p-values (*<0.05; **<0.01; ***<0.001; ****<0.0001) determined by Kruskal Wallis test followed by a Dunn's post hoc test. One-way ANOVA for data in graphs: (c) - [$F(6, 202) = 28.22$, $p < 0.0001$], (d) - [$F(6, 218) = 22.83$, $p < 0.0001$], (e) - [$F(6, 186) = 13.91$, $p < 0.0001$], (f) - [$F(6, 171) = 18.17$, $p < 0.0001$].

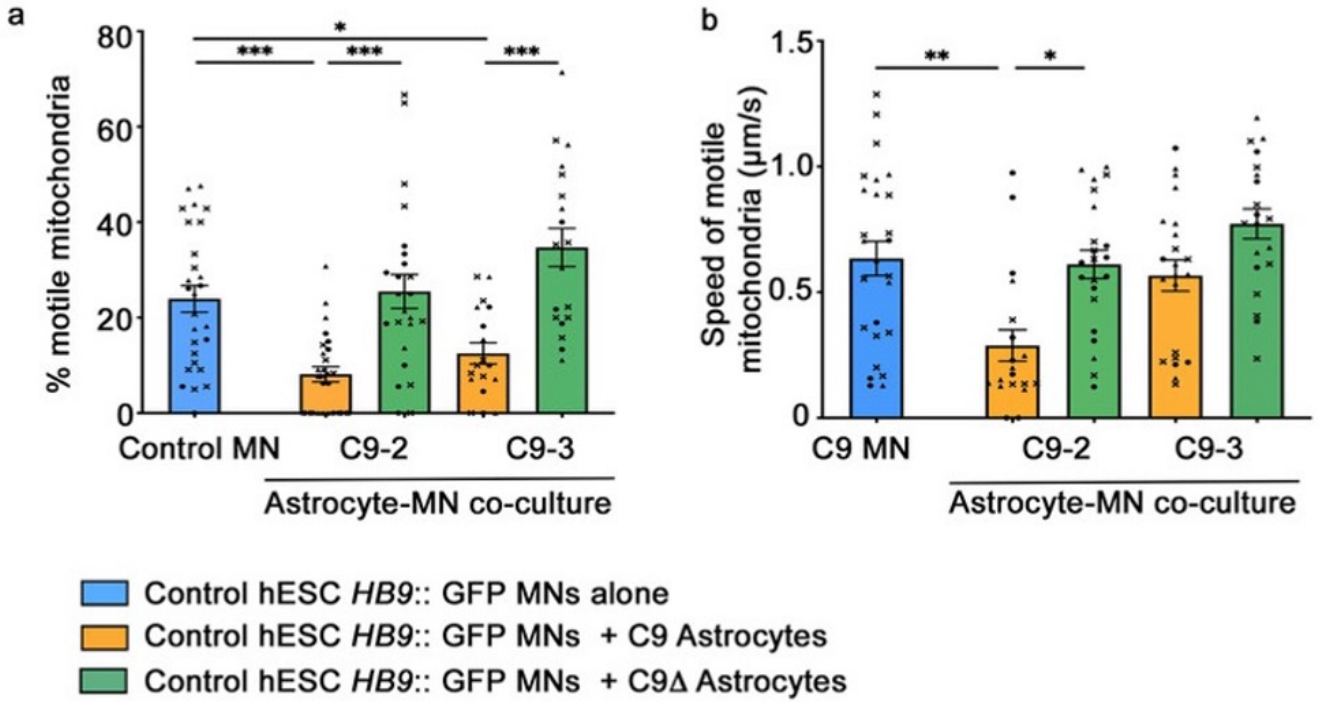

Figure 5.2 Effects of astrocytes on mitochondrial transport in neurons in physical co-cultures.
(a&b) Quantification of the percentage of motile mitochondria (labelled with mitoDsRed2) and mean speed of motile mitochondria in a 100 µm stretch of proximal axon in control hESC *HB9*::GFP MNs co-cultured with either C9-astrocytes or gene-corrected astrocyte controls (C9Δ-A) from two independent patient lines. **x, ●, ▲, ■, ▼** ($1^{st}/2^{nd}/3^{rd}/4^{th}/5^{th}$ biological experiment – respectively. Data are represented as mean ± SEM. n ≥ 5 axons per independent plate-down, N ≥ 3 independent plate-downs (biological replicates). P-values (*<0.05; **<0.01; ***<0.001; ****<0.0001) determined by Kruskal Wallis test followed by a Dunn's post hoc test. One-way ANOVA for data in graphs: (a) - [F (4, 110) = 13.01, p <0.0001], (b) - [F (4, 104) = 7.163, p <0.0001].

5.3 *C9orf72* astrocytes impair mitochondrial bioenergetics in MNs

In view of the role of astrocytes in regulating brain energy homeostasis (Bélanger, Allaman and Magistretti, 2011), the direct effect of astrocytes on mitochondrial bioenergetics in motor neurons (MNs) was next examined using the Seahorse assay in co-cultures. Oxygen consumption rates (OCR) were first compared between monocultures and co-cultures. It was found that the mitochondrial OCR of MN monocultures and MNs co-cultured with astrocytes was nearly 8-fold higher than that of astrocytes alone (Fig 5.3 A), implicating that any significant change in OCR values in astrocyte-MN co-cultures is principally driven by MNs. Impairment in basal and maximal mitochondrial respiration was confirmed in monocultures of C9-MNs, with a reversal noted in C9Δ-MNs (Fig 5.3 C-D) (Mehta *et al.*, 2021).

It was observed that co-cultures with astrocytes, regardless of the genotype, enhanced basal and maximal respiration compared to MN monocultures, despite comparable neuronal densities (Fig 5.3 B-D). Crucially, significant reductions in basal and maximal respiration were found when either C9-MNs or C9Δ-MNs were co-cultured with C9-A in comparison to co-culture with C9Δ-A (Fig 5.4 A-B). These data indicate that neuronal mitochondrial bioenergetic function is modulated by the astrocyte genotype.

To further validate the effect of astrocyte co-culture on neuronal mitochondrial function, MN mitochondrial membrane potential (steady-state level) was next measured using MitoTracker Red CMXRos, which accumulates in mitochondria in a potential-dependent manner (Dafinca *et al.*, 2016; Connolly *et al.*, 2018). MNs were labelled using lentiviruses expressing GFP or identified using immunostaining with the neuron-specific marker SMI312 post-fixation. Quantification of the mean fluorescence intensity (normalized to to the region of interest) of MitoTracker in MNs (monocultures) showed that reduced mitochondrial membrane potential was observed in the C9-MN line compared to its paired gene-corrected control (Fig 5.4 C). In co-culture with C9-A, a significant reduction in the mitochondrial membrane potential of C9-MN or C9Δ-MNs was noted. Importantly, this deficit was reversed in co-culture with their corresponding C9Δ-A (Fig 5.4 D). Taken together, these findings demonstrate for the first time that perturbations in the mitochondrial bioenergetics of control and mutant

MNs are directly mediated by astrocytes harbouring the C9ORF72 mutation upon co-culture.

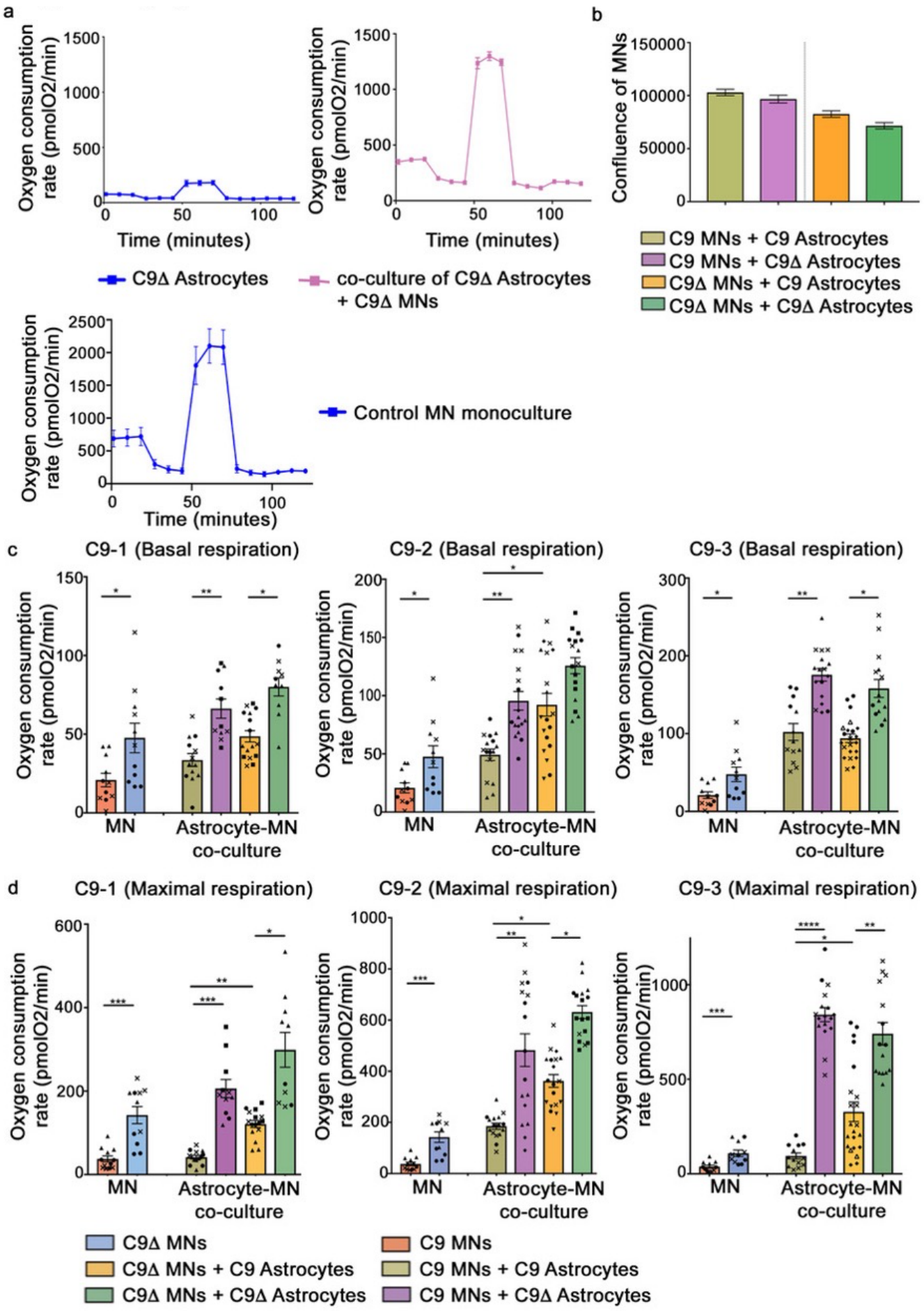

Figure 5.3 (a) Testing the feasibility of implementation of the seahorse assay to examine the impact of C9-A on neuronal mitochondrial respiratory activity. The mitochondrial OCR of MN monocultures and MNs co-cultured with astrocytes were nearly 8-fold higher than astrocytes alone (plated cell densities for: astrocytes – 200,000 cells; MNs – 200,000 cells; astrocyte-neuronal co-cultures – 200,000 cells of each cell type).
(b) Neuronal confluence in subsequent co-culture experiments was determined by neuron-specific staining via SMI-312 immunocytochemistry; (N=2) **(c-d)** Co-cultures with astrocytes, regardless of the genotype, enhanced basal and maximal respiration compared to MN monocultures.
Plated cell densities for: MNs – 50,000 cells; astrocyte-neuronal co-cultures – 50,000 cells of each cell type. **x**, ●, ▲, ■, ▼ (1^{st}/2^{nd}/3^{rd}/4^{th}/5^{th} biological experiment – respectively). Data are represented as mean ± SEM; n ≥ 3 wells per line per experiment, with experiments repeated in three independent cultures from different differentiations (N = 3). P-values (*<0.05; **<0.01; ***<0.001; ****<0.0001) determined by Mann Whitney U non-parametric test for comparison between the MN monocultures and by Kruskal Wallis test followed by a Dunn's post hoc test for comparisons between the astrocyte-neuronal co-cultures.

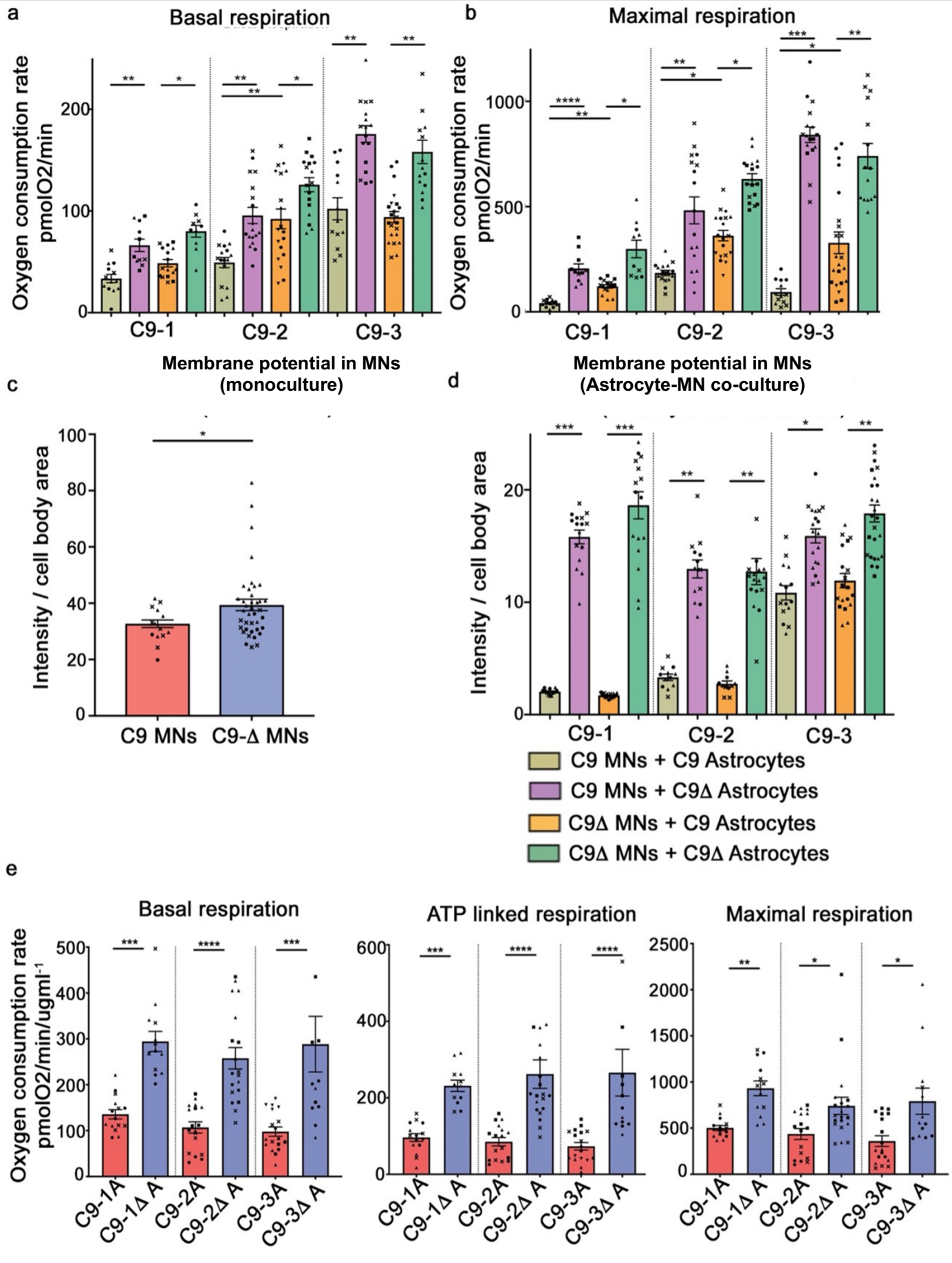
a
Basal respiration
Oxygen consumption rate pmolO2/min
C9-1
C9-2
C9-3
b
Maximal respiration
Oxygen consumption rate pmolO2/min
C9-1
C9-2
C9-3
c
Membrane potential in MNs (monoculture)
Intensity / cell body area
C9 MNs
C9-Δ MNs
d
Membrane potential in MNs (Astrocyte-MN co-culture)
Intensity / cell body area
C9-1
C9-2
C9-3
C9 MNs + C9 Astrocytes
C9 MNs + C9Δ Astrocytes
C9Δ MNs + C9 Astrocytes
C9Δ MNs + C9Δ Astrocytes
e
Basal respiration
ATP linked respiration
Maximal respiration
Oxygen consumption rate pmolO2/min/ugml-1
C9-1A
C9-1Δ A
C9-2A
C9-2Δ A
C9-3A
C9-3Δ A

Figure 5.4 C9ORF72 astrocytes impair mitochondrial bioenergetics in MNs.

(a-b) Quantification of the oxygen consumption rate (OCR) as measured by the Seahorse Analyzer denoting basal and maximal FCCP-uncoupled mitochondrial respiration for physical neuronal-astrocyte co-cultures of hiPSC-derived astrocytes (from the three-independent patient-derived C9orf72 lines) and hiPSC-derived MNs (C9-mutant/gene-corrected pair). **x**, ●, ▲ ($1^{st}/2^{nd}/3^{rd}$ biological experiment – respectively). Data are represented as mean ± SEM; n ≥ 3 wells per condition per experiment, with experiments repeated in at least three independent plate downs (N ≥ 3).
P-values (*<0.05; **<0.01; ***<0.001; ****<0.0001) determined by Kruskal Wallis test followed by a Dunn's post hoc test. One-way ANOVA for data in graphs: (a) - [F (11, 175) = 30.99, p <0.0001], (b) - [F (11, 175) = 44.73, p <0.0001].

(c) Quantification of the mean fluorescence intensity of MitoTracker in hiPSC-derived MNs (C9-mutant/gene-corrected pair) shows reduced mitochondrial membrane potential (MMP) in the patient line (*, p < .05, Mann Whitney U non-parametric test); N = 3 independent differentiations; **x**, ●, ▲ ($1^{st}/2^{nd}/3^{rd}$ biological experiment – respectively); automated analysis n = 19–40 wells analysed per genotype per biological experiment with >20 MNs per well.

(d) Physical co-cultures of hiPSC-derived astrocytes (from the three-independent patient-derived C9orf72 lines) and hiPSC-derived MNs (C9-mutant/gene-corrected pair) shows reduced MMP in co-cultures with C9-astrocytes with reversal with C9Δ astrocytes. P-values (*<0.05; **<0.01; ***<0.001; ****<0.0001) determined by Kruskal Wallis test followed by a Dunn's post hoc test. N = 3 independent differentiations; **x**, ●, ▲ ($1^{st}/2^{nd}/3^{rd}$ biological experiment – respectively); automated analysis n = 6-12 wells analysed per condition per biological experiment with >20 MNs per well. One-way ANOVA [F (11, 182) = 67.96, p <0.0001]. **(e)** C9ORF72 astrocytes, when compared to their corresponding gene-edited controls, display defective bioenergetics (diminished capacity to produce ATP). Quantification of the oxygen consumption rate (OCR) as measured by the Seahorse Analyzer, normalised to the amount of total protein, denoting basal, ATP-linked, and maximal FCCP-uncoupled mitochondrial respiration for C9ORF72 astrocytes and gene-corrected paired controls across the three independent pairs. **x,** ●, ▲, ■, ▼ ($1^{st}/2^{nd}/3^{rd}/4^{th}/5^{th}$ biological experiment – respectively). Data are represented as mean ± SEM; n ≥ 3 wells per condition per experiment, with experiments repeated in at least three independent plate downs (N ≥ 3). P-values (*<0.05; **<0.01; ***<0.001; ****<0.0001) determined by Kruskal Wallis test followed by a Dunn's post hoc test.

5.4 Boosting astrocyte metabolism with selective PGC1α pathway manipulation in *C9orf72* astrocytes rescues the axonal mitochondrial transport deficit

Having established that MN mitochondrial bioenergetics are directly modulated by astrocytes, the impact of the C9ORF72 mutation in isolated astrocytes on mitochondrial bioenergetics was next examined using the Seahorse assay. It was revealed that C9-A, compared to their paired gene-corrected controls, displayed significantly reduced basal, ATP-linked, and maximal respiration (Fig 5.4 E). Therefore, it was hypothesized that bioenergetic deficits in C9-A are responsible for their non-cell autonomous effects on axonal transport in MNs.

To test this hypothesis, transcriptional co-regulator peroxisome proliferator-activated receptor gamma co-activator 1-alpha (PGC1α) was overexpressed in C9-A using lentivirus, which significantly increased OCR in isolated C9-astrocyte cultures (Fig 5.5). PGC1α is a central inducer of mitochondrial biogenesis and metabolism in cells (Wu *et al.*, 1999; Lin, Handschin and Spiegelman, 2005). Transduced C9-A were then co-cultured with either C9-MNs or C9Δ-MNs, and it was found that the deficits in mitochondrial motility and speed were rescued (Fig 5.6 A-E).

In summary, it was uncovered that in C9ORF72-ALS, the rescue of mitochondrial bioenergetics in astrocytes with PGC1α is sufficient to reverse axonal transport deficits in C9ORF72 MNs, revealing that non-cell autonomous metabolic regulation of axonal transport occurs via astrocytes.

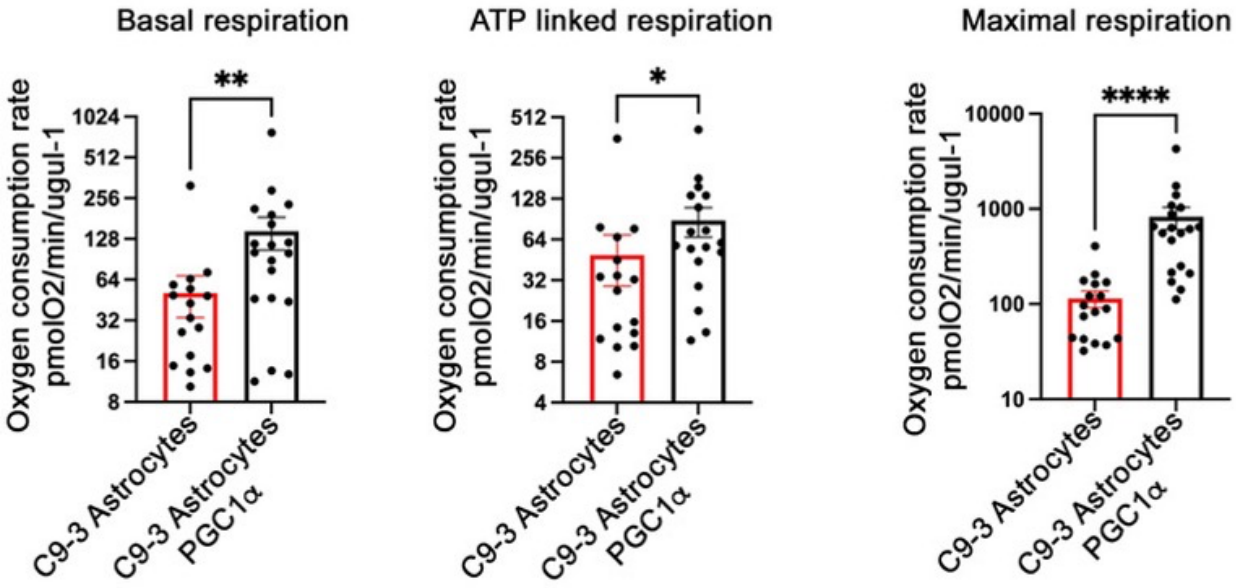

Figure 5.3 Boosting astrocyte metabolism with selective PGC1α pathway manipulation in C9 astrocytes increases basal, ATP-linked and maximal respiration. Data are represented as mean ± SEM; n ≥ 3 wells per line per experiment, with experiments repeated in three independent cultures from different differentiations (N = 3). P-values (*<0.05; **<0.01; ***<0.001; ****<0.0001) determined by Mann Whitney U non-parametric test.

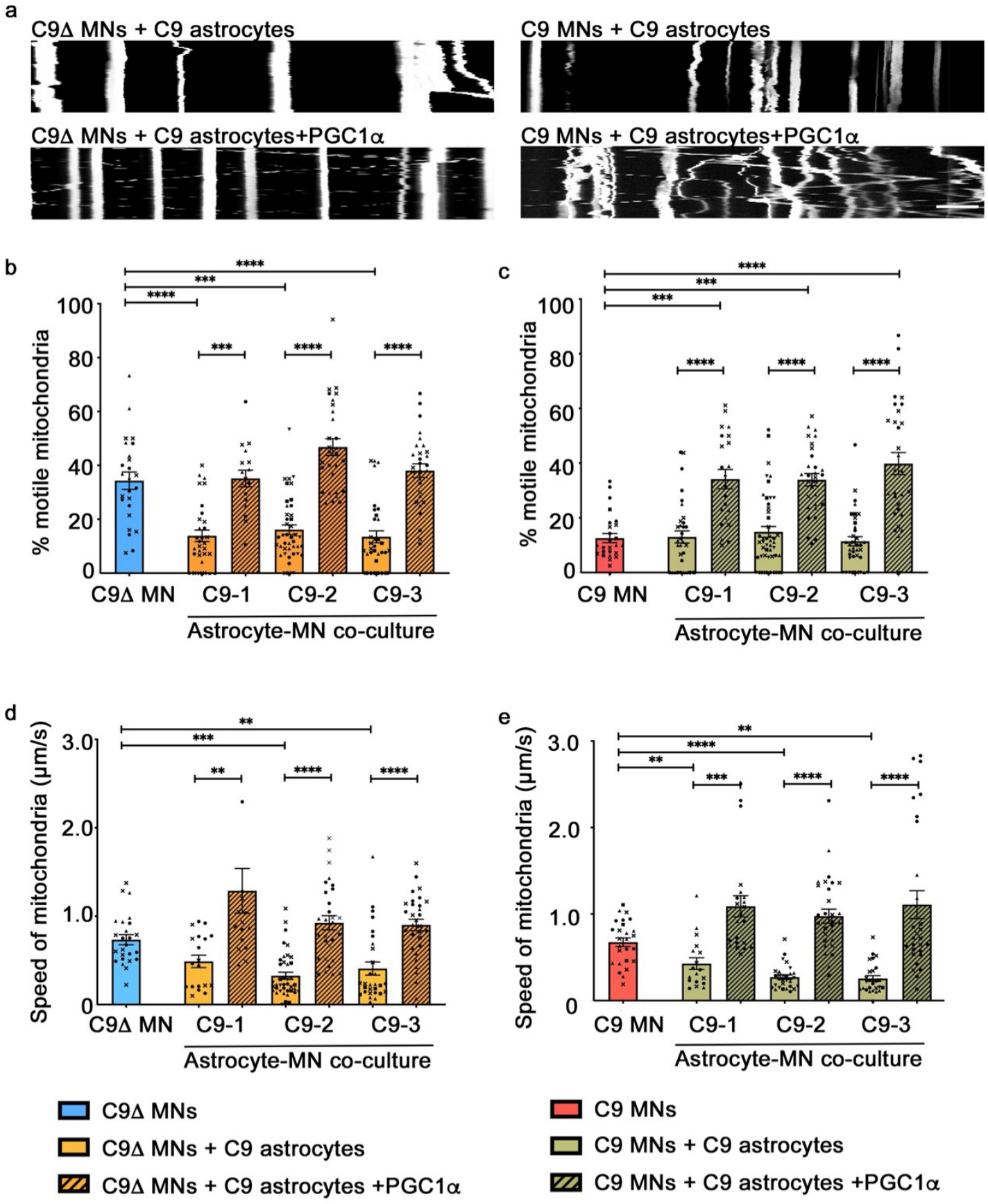
a
C9Δ MNs + C9 astrocytes
C9 MNs + C9 astrocytes
C9Δ MNs + C9 astrocytes+PGC1α
C9 MNs + C9 astrocytes+PGC1α
b
% motile mitochondria
C9Δ MN
C9-1
C9-2
C9-3
Astrocyte-MN co-culture
c
% motile mitochondria
C9 MN
C9-1
C9-2
C9-3
Astrocyte-MN co-culture
d
Speed of mitochondria (µm/s)
C9Δ MN
C9-1
C9-2
C9-3
Astrocyte-MN co-culture
e
Speed of mitochondria (µm/s)
C9 MN
C9-1
C9-2
C9-3
Astrocyte-MN co-culture
C9Δ MNs
C9Δ MNs + C9 astrocytes
C9Δ MNs + C9 astrocytes +PGC1α
C9 MNs
C9 MNs + C9 astrocytes
C9 MNs + C9 astrocytes +PGC1α

Figure 5.4 Boosting astrocyte metabolism with selective PGC1α pathway manipulation in C9 astrocytes rescues the neuronal mitochondrial transport deficit. **(a)** Kymographs depicting mitochondrial transport in motor neurons upon co-culture with astrocytes overexpression PGC1a; scale bar = 10 µm. **(b&c)** Quantification of the percentage of motile mitochondria (labelled with mitoDsRed2) and **(d&e)** mean speed of motile mitochondria in a 100 µm stretch of proximal axon in hiPSC-derived C9-MNs and gene-corrected paired controls, cocultured with either C9-A with or without PGC1α overexpression from the three independent patient lines. **x**, ●, ▲, ■ (1^{st}/2^{nd}/3^{rd}/4^{th} biological experiment – respectively).

Data are represented as mean ± SEM; n ≥ 5 axons per independent plate-down, N ≥ 3 independent plate-downs (biological replicates). P-values (*<0.05; **<0.01; ***<0.001; ****<0.0001) determined by Kruskal Wallis test followed by a Dunn's post hoc test. One-way ANOVA for data in graphs: (b) - [F (6, 199) = 30.33, p <0.0001], (c) - [F (6, 221) = 24.66, p <0.0001], (d) - [F (6, 181) = 14.73, p <0.0001], (e) - [F (6, 173) = 17.53, p <0.0001].

5.5 Discussion

In this chapter, using *C9orf72*-patient stem cell derived astrocytes and MNs, a novel role of astrocytes in regulating axonal transport in MNs has been established. Specifically, the cell and non-cell autonomous C9-astrocyte effects on mitochondrial bioenergetic function are demonstrated, as well as direct evidence that selective manipulation of astrocytes can rescue axonal transport in C9-MNs.

Axonal transport dysfunction is heavily linked to the pathogenesis of ALS, described initially in patients (Sasaki and Iwata, 1996) and further elaborated in animal models of ALS (Williamson and Cleveland, 1999; Hafezparast *et al.*, 2003; Selvaraj *et al.*, 2012). Human genetic studies in ALS have also identified pathogenic mutations in genes that are involved in axonal transport machinery *DCTN1*, *KIF5A, TUBA4A, PFN1* (Münch *et al.*, 2004; Smith *et al.*, 2014; Nicolas *et al.*, 2018; Burk and Pasterkamp, 2019). Further, in vivo, and cellular studies have shown axonal transport impairments are also conserved in key ALS mutations such as SOD1, TDP43 (Wang *et al.*, 2013; De Vos and Hafezparast, 2017b), *C9orf72* (Fumagalli *et al.*, 2021; Mehta *et al.*, 2021). Intriguingly, introduction of dynein mutants – a protein involved in retrograde axonal transport – in SOD1G93A ALS mice attenuated motor neuron degeneration and significantly improved survival of the mice (Kieran *et al.*, 2005; Teuling *et al.*, 2008), suggesting manipulation of axonal transport as a therapeutic target in ALS.

Thus far, axonal transport deficits reported in ALS have been attributed to cell-autonomous dysfunction. However, this study shows the regulation of axonal transport through astrocyte mediated non-cell autonomous mechanisms. Interestingly, in addition to the impairment in the percentage of motile mitochondria, C9-astrocytes also affect the speed/velocity of those motile mitochondria; this contrasts with the cell-autonomous deficits observed in C9-MNs where speed of motile mitochondria was unaffected. This observation suggests that mitochondrial motility (% motile mitochondria) and speed of motile mitochondria are regulated by distinct astrocyte-dependent cellular mechanisms. Further studies are necessary to explain the specific mechanisms by which *C9orf72* astrocytes contribute to astrocyte-mediated regulation of axonal transport. The pathological mechanisms of the C9ORF72 mutation remain unclear, but three processes are implicated: loss of normal protein function, toxic

dipeptide repeats (DPRs) and RNA foci formation. To elucidate these mechanisms, co-culture experiments should be undertaken involving MNs with either C9ORF72 knockout (KO) astrocytes or control astrocytes engineered to overexpress DPRs or RNA foci. Mitochondrial percentage motility and velocity can be assessed using mito-dsRed2 labelling and live-cell imaging, while mitochondrial function can be evaluated via Seahorse XF technology.

The relevance of these findings to genetic TDP43 and sporadic ALS is crucial for determining whether this represents a convergent dysfunction across the disease spectrum. Since TDP-43 pathology unifies sporadic and genetic forms**,** it would be prudent to first investigate whether astrocyte-mediated mitochondrial transport dysfunction extends to genetic TDP-43 ALS. This can be achieved through the generation of hiPSC-derived astrocytes from TDP-43 mutation carriers and KO astrocytes, which will be co-cultured with MNs, for assessing axonal transport dysregulation in TDP-43 models. Depending on the outcomes, experiments should be broadened to sporadic disease.

Additionally, it is important to investigate intracellular calcium concentrations in MNs cocultured with C9 or C9Δ astrocytes, as dysregulated calcium signalling is known to significantly impact mitochondrial function and dynamics. The measurement of axonal ATP levels in live cell cultures also warrants consideration. Techniques such as bioluminescent ATP assays or genetically encoded ATP indicators offer the potential to assess ATP levels in real-time, thereby providing deeper insights into the energy dynamics within the axons of motor neurons. Such methodologies could further illuminate the interplay between astrocytic function, mitochondrial bioenergetics, and axonal transport.

In this study, to further explore the impact of astrocytes on neuronal mitochondrial function in a physical coculture setting, the mitochondrial membrane potential in MNs was assessed at steady-state levels using MitoTracker Red CMXRos (Dafinca et al., 2016; Connolly et al., 2018). MitoTracker Red CMXRos serves as a reliable indicator of mitochondrial membrane potential by accumulating in active mitochondria, where its fluorescence intensity is directly proportional to the membrane potential. However, it is essential to acknowledge that TMRM (Tetramethylrhodamine, methyl ester) is

recognized for its superior sensitivity to FCCP-induced Δψ depolarization when compared to MitoTracker. A recent study by Desai et al. (Desai *et al.*, 2024) highlights that the sensitivity to depolarizing agents is ranked as TMRM ≫ MitoTracker Red CMXRos > MitoGreen. Given these insights, this experiment should be repeated with TMRM.

Intraneuronal trafficking of cargo is not limited to mitochondria. RNA, RNP complexes, proteins, and other organelles such as lysosomes are all dependent on axonal transport for long-distance distribution from the cell body to the distal axon process. The specific types of cargo that C9ORF72 astrocytes modulate in motor neurons (MNs) should thus be determined, particularly whether the axonal transport impairment is specific to mitochondrial cargo or encompasses additional organelles. Using live-cell imaging techniques, such as fluorescent microscopy, the dynamics of mitochondrial, lysosomal, and RNA-protein (RNP) complex transport along axons can be tracked.

The human brain consumes c.20% of the body's energy despite accounting for only 2% of body mass. This high metabolic demand of the human brain reflects the energy demands of active and resting neurons, their networks and plasticity. Motor neurons are especially energy demanding on account of their length, with axons projecting up to a metre to synapse with skeletal muscle. Astrocyte-neuronal metabolic coupling through glutamate-stimulated aerobic glycolysis and the glutamate-glutamine cycle, is central to supporting the energy demands of neurons (Magistretti and Pellerin, 1999; Ortinski *et al.*, 2010). Such homeostasis is critical for the regulation of neuronal mitochondrial metabolism through maintenance of substrate supply for oxidative phosphorylation, the effective clearance of glutamate from the synaptic cleft and the rapid removal of ammonia generated by neurotransmission. Importantly, although astrocytes are not reliant on mitochondrial oxidative phosphorylation for their energy production, key physiological processes including calcium and glutamate regulation and metabolism, modulation of Ca2+-dependent processes such as gliotransmission, fatty acid oxidation, trans-mitophagy and production of antioxidants are dependent on functional mitochondria (De Miranda *et al.*, 2018; Mouton-Liger *et al.*, 2018; Sliter *et al.*, 2018; Russo *et al.*, 2020). Here, we identified that C9-astrocytes have broad impairments in both glycolysis and mitochondrial bioenergetics. These findings are

consistent with a recent study demonstrating that C9-astrocytes have reduced metabolic flexibility (i.e., ability to use alternative metabolites to meet energy demands) and deficits in adenosine, fructose, and glycogen metabolism (Allen, Hall, Woof, *et al.*, 2019b). Multiple lines of evidence implicate astrocytic mitochondrial dysfunction in Parkinson's disease (Sliter *et al.*, 2018; Chen *et al.*, 2022) and other neurodegenerative diseases – beta-amyloid peptides induced oxidative stress in astrocytes and subsequent neurotoxicity through activation of NADPH oxidase (Abramov, Canevari and Duchen, 2004) and mitochondria in SOD1-expressing astrocytes showed severe impairment in oxygen consumption (Cassina *et al.*, 2008).

The Chandran group and others have previously described cell-autonomous mitochondrial bioenergetic deficit in C9-MNs that leads to impairment in axonal transport (Fumagalli *et al.*, 2021; Mehta *et al.*, 2021). The present study uncovers a hitherto unreported mechanism of axonal transport that relies on astrocyte-neuronal interaction. The mechanistic basis of how C9-mutant astrocytes cause altered axonal transport is unknown. One potential explanation is reduced transfer of metabolites such as pyruvate or lactate from astrocytes to neurons through mono-carboxylate transporters, leading to impaired axonal ATP generation (Rouach *et al.*, 2008). However, this is improbable in the current experimental paradigm since the mitochondrial bioenergetics profile was assessed in the presence of saturating amounts of pyruvate.

An alternative possibility is that astrocytes are enhancing neuronal mitochondrial function independent of exchange of metabolites. It has been shown that dynamic inter-mitochondrial transfer between mammalian cells upregulates aerobic respiration (Spees *et al.*, 2006; Chuang *et al.*, 2017). Indeed, intercellular transfer has been demonstrated between astrocytes and neurons (Gao *et al.*, 2019) and shown to be neuroprotective in an *in vivo* ischemic stroke model (Hayakawa *et al.*, 2016). Multiple mechanisms of intercellular mitochondrial transfer have been described involving tunneling nanotubes (Wang and Gerdes, 2015), extracellular vesicles containing mitochondria (Amari and Germain, 2021) and GAP junctions (Liu *et al.*, 2021; Norris, 2021). In this context, it is important to determine whether astrocytic mitochondrial transfer is disrupted by: (a) investigating whether healthy/gene-corrected hiPSC-derived astrocytes can donate functional mitochondria to rescue ALS mutant MNs,

potentially offering a novel cellular therapy, and (b) identifying the mechanisms of intercellular mitochondrial transfer – such as tunnelling nanotubes, extracellular vesicles, or gap junctions – through pharmacological or genetic approaches. Fluorescently labelled mitochondria can be employed to track astrocyte-neuronal dynamic exchanges, with fluorescence-activated cell sorting (FACS) utilised to confirm transfer.

In summary, non-cell autonomous signalling between astrocytes and neurons is vital for proper neuronal function. This study has identified a novel role of astrocytes in regulating axonal transport in neurons through mitochondrial bioenergetics, thus, providing evidence for astrocyte metabolism as a potential ALS therapeutic target.

Appendix

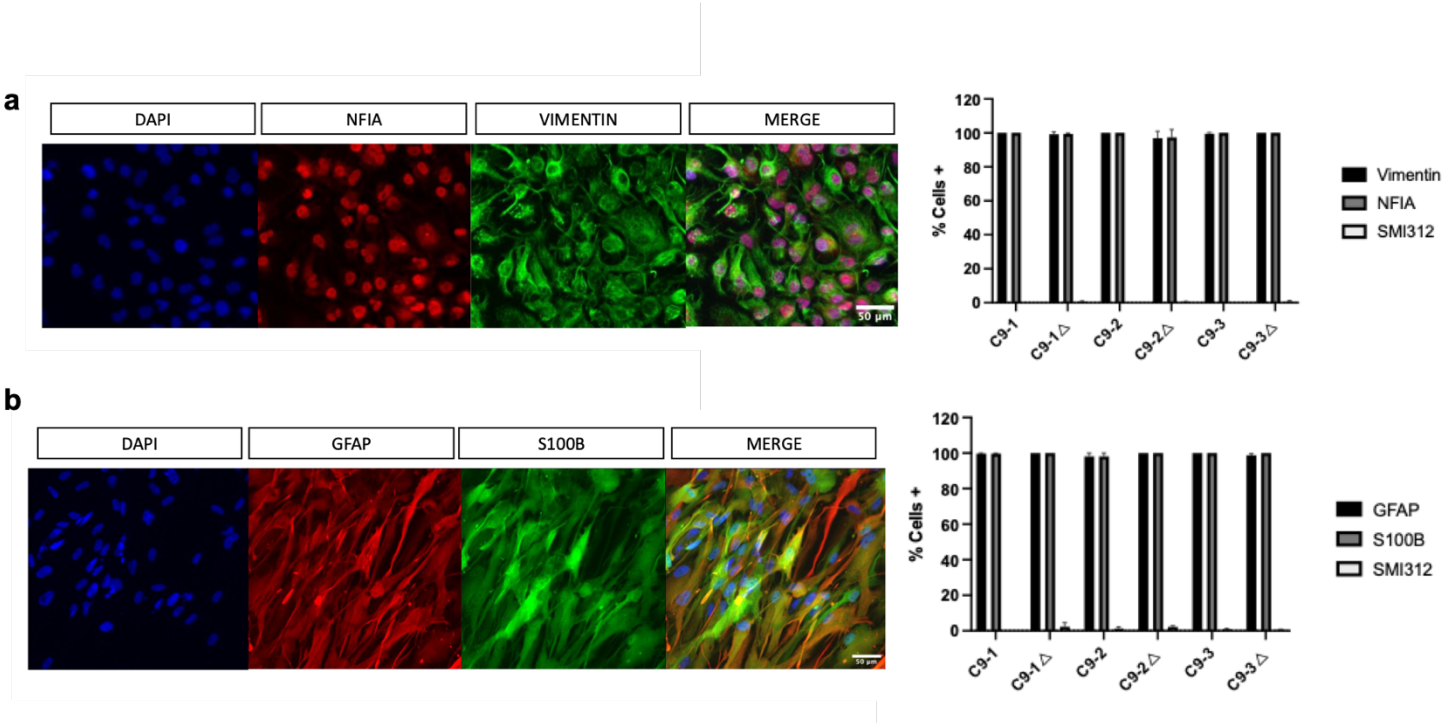

Figure 1: Generation and characterisation of astrocytes from iPSCs. (a) Representative images of vimentin and NFIA immunostaining in astrocyte progenitors (upper panel) and S100B and GFAP immunostaining in 2-week-old astrocyte cultures (lower panel). (Scale bars: 50 µm). (b) Percentage of $S100B^+$, $GFAP^+$ and $SMI312^+$ cells in 2-week-old astrocyte cultures derived from the three pairs of iPSC lines (N = 3–7, at least 400 cells per cell line per experiment, one-way ANOVA with Bonferroni correction).

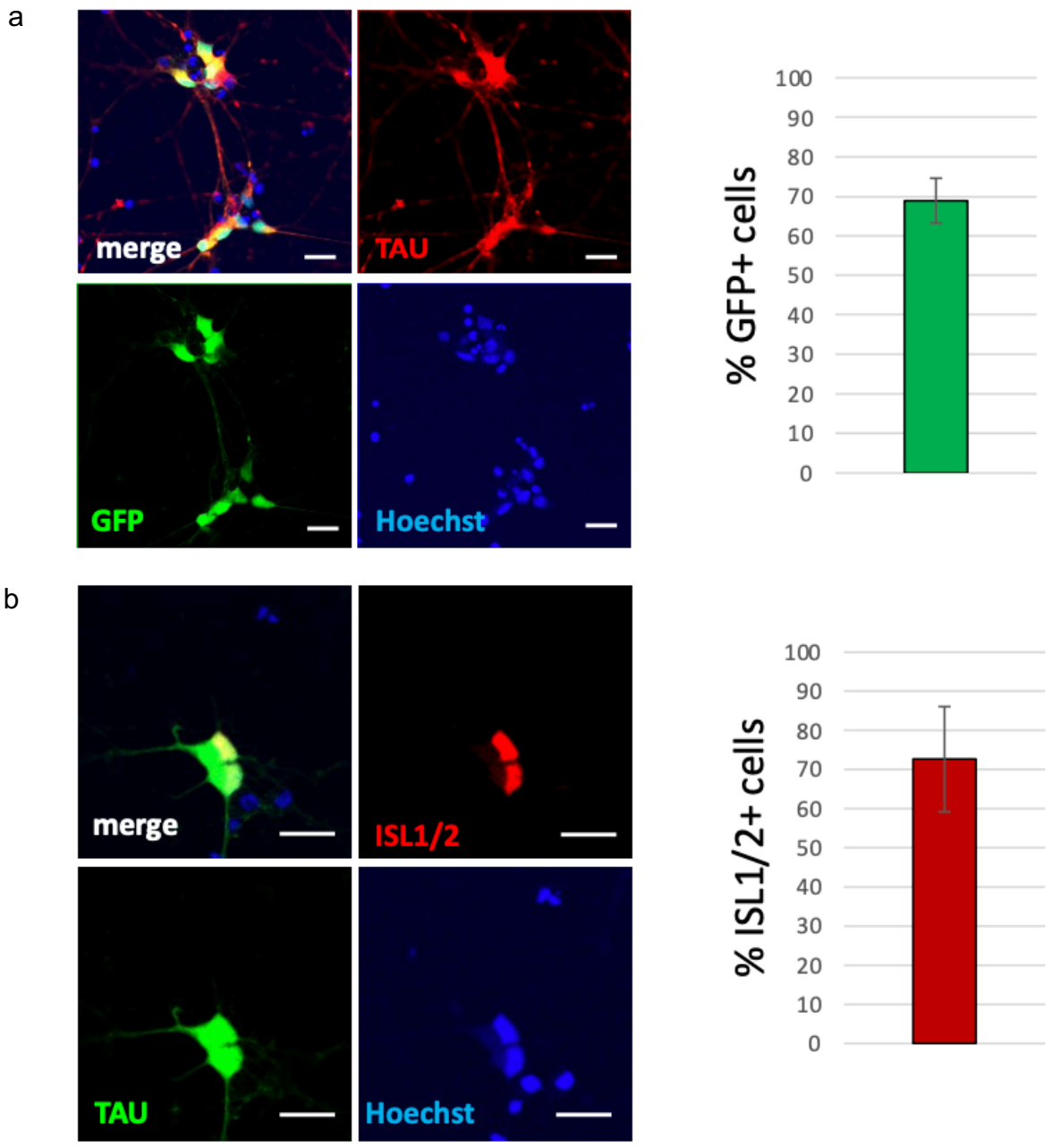

Figure 2: a. Representative images and quantification of Hb9::GFP MNs 1 week after dissociation and plate-down, stained for TAU and GFP. 69% of the TAU+ cells expressed GFP. **b.** Representative images and quantification of Hb9::GFP MNs 1 week after dissociation and plate-down, stained for TAU and ISL1/2. 73% of the TAU+ cells expressed ISL1/2. Scale bar = 20um. Image reproduced with permission from Alessandra Cardinali, Accelerated Drug Discovery for Amyotrophic Lateral Sclerosis using high-throughput phenotypic drug screening, [2023].

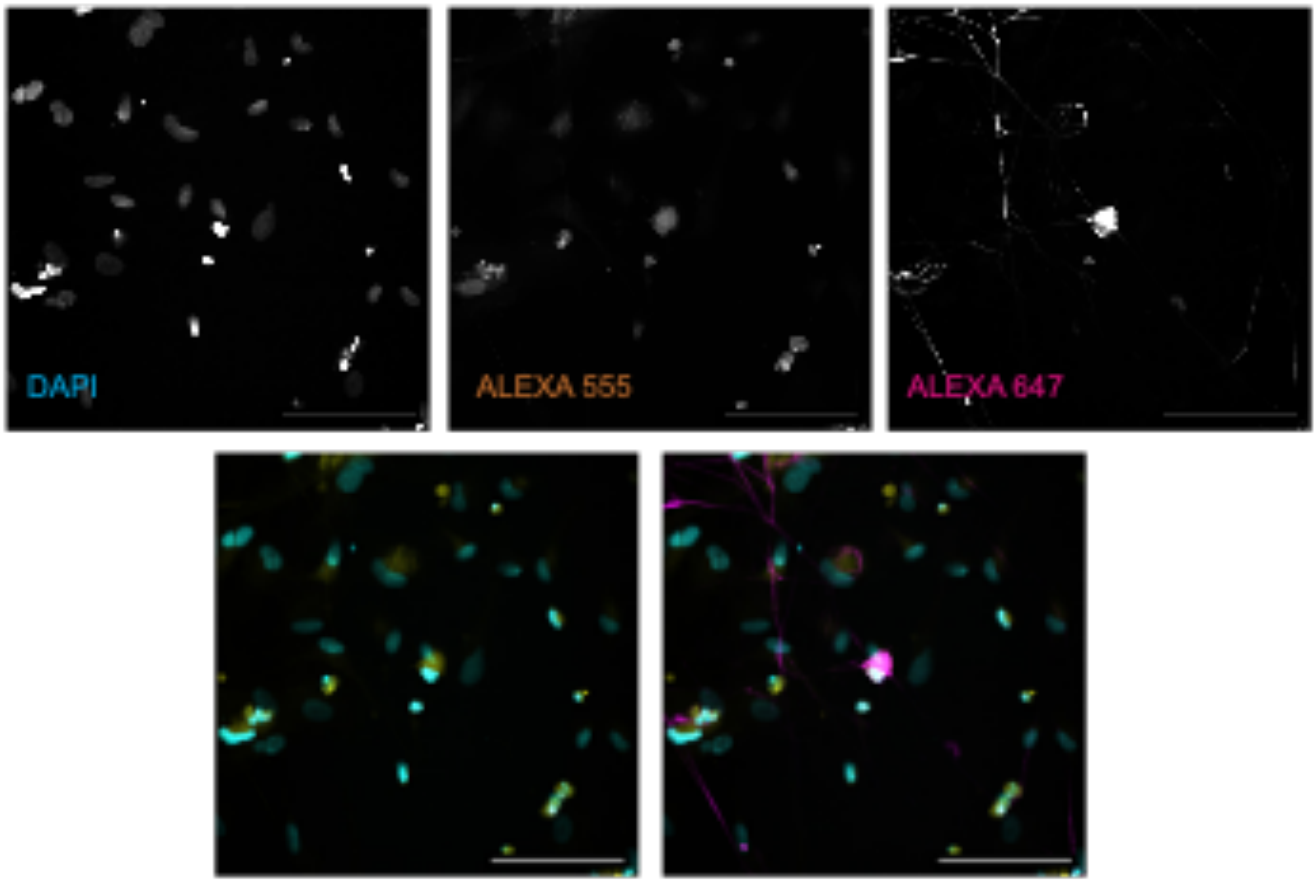

Figure 3: Representative images of astrocyte-neuronal cocultures loaded with MitoTracker Red CMXRos (mitochondrial staining; Alexa fluor 555) and immunostained with SMI312+ (Alexa fluor 647) for identification and analysis of MNs.

The Max Perutz Science Award

In October 2020, I was awarded a 3rd place (commendation) in the 2020 MRC Max Perutz Science Writing competition.

The Max Perutz Science Writing Award aims to support the career development of current MRC PhD students, helping them build their skills to become tomorrow's leaders in discovery science. It also aims to encourage and recognise outstanding written communication. Applicants, who are all MRC PhD students, were asked to write and submit an article about research in their field, discuss why it matters, and do this in a format that would hold the interest of a non-scientific reader.

Undoing the 'Straitjacket' *by Maria Stavrou*

Sandra explodes into motion like a sprinter off the blocks, seizing the bucket of ice cubes and swiftly upending it over herself. Her expression turns from anticipation to paralysed terror. Muscles taut as steel cables, body rocking stiffly as if cement fills her joints. In shivering shock, she awaits normality. As her body temp normalises, her passion follows. She screams and leaps about the garden as if tailed by a swarm of hornets.

Her father, Charles, has positioned his wheelchair for perfect viewing of this surreal sight. Guffawing and applauding, he has no need to empty a bucket of ice over himself to simulate her sensation. The Ice Bucket Challenge was rather poignant, in that regard. But unlike his daughter, Charles' racking stiffness won't fade. It only heralds the beginning of a dark descent...

Motor Neurone Disease (MND) is a devastating neurodegenerative disorder that kills 4 of every 5 patients within 5 years of diagnosis. Since first described by neurologist Jean-Martin Charcot in 1874, there has been no significant breakthrough – certainly no cure. Only Riluzole, the modifying therapy prolonging survival by months at most....

Its invisible straitjacket tightens at breakneck pace, whisking you on a frightening journey of physical decline. You lose the ability to move your arms and legs, speak, swallow and eventually, breathe altogether.

As I test the power in Charles' arms during one of our consults, I tell Charles with confidence that study into MND has never been stronger. "One day," I say, "our nervous system won't be unrepairable." His wry look echoes the less hopeful of the medical community. To change that expression means everything to me.

The brain is so complex that we cannot run tests on it as simply as on other organs. Such an approach would require a brain matter biopsy or close monitoring of specific drug effects via regular scanning. And neither of these are what you'd call 'comfortable' procedures.

"Rather than extract nerve cells from patients' brains," I tell Charles, "we take skin cells and reprogram them back in time – to default generic cells like those in embryos – then turn them into specialised brain cells like neurons and astrocytes." Stem cell reprograming was pioneered in 2006 by Shinya Yamanaka with his renowned and rather fluffy lab assistant: Dolly, the world's most famous sheep. Sorry Shaun, we still love you...

"I use these cells to create 'disease in a dish' models recapitulating MND's key aspects, to better understand its biology." Understanding is the first step to treatment, in which we compare behaviour of diseased and healthy cells to develop a fantastic approach to drug discovery. Like anything, a decent metaphor brings the narrative to life.

"Listened to any good music recently?" I ask at our next consult, knowing Charles loves a quality composition. There's a Mozart piano quartet he holds dear, a beautiful, intimate recording by a Scottish quartet. He almost drifts off as he recalls the soothing music from his vintage hi-fi. The stage – and soundtrack, no less – for my story is set. "The neurons that form the brain's building blocks don't live in isolation. They're surrounded by three other cell types called glia (from the Greek meaning 'glue'), each

vital for neuron prosperity. In harmony, these four cell types create an extraordinary symphony of electrical activity.” My narrative rallies, Charles smiles.

“This electrical activity allows us to emote, remember, move – feel every sensation there is. But if just one cell misbehaves, the tune falls flat. And if the first to decline is a neuron, MND rears its head ...”

Charles nods once more, visualising the quartet of brain cells playing his beloved Mozart, before admitting he’s never heard of glia cells. They’ve been long neglected in the field, with most emphasis upon the study of neurons.

“Though the piano is the star, the performance is incomplete without supporting players. The neurons, likewise, rely on the glia.”

I tell Charles my research focuses on one glia cell: the astrocyte. If the human brain were the night sky, astrocytes would be the stars twinkling with brightness and vitality. They regulate neurons and their environment by providing nutrients, clearing waste, and repairing brain and spinal cord damage. “Let me guess... They look like stars?”

I point to an image on my office wall. Their nomenclature receives Charles’ nod of approval. Humble questions like these, from patients like Charles, fuel my search for a cure.

In simple words carrying deep responsibility, I explain that my goal is to find medicines that not only halt brain degeneration but actively reverse it.
“Like one day I’ll be able to play my piano again, you mean?”

I speak on behalf of the entire world’s MND researchers – an especially ambitious bunch of boffins – that we will one day find a way for those suffering from MND to live longer, enjoy life and their families.

"And when will that be?” asks Charles with trademark cheek and a check of his watch. I wouldn’t lie to him – I have no answer. But the intent is there, lining each petri dish in

which I poke about, beckoning the brave face I don daily for the assurance of those like Charles...

Right now, I compare healthy astrocytes with those of patients with MND, which carry the C9orf72 mutation. To date, over 25 MND-related genes have been discovered, and C9orf72 seems the most common genetic cause. I grow healthy and MND astrocytes with human motor neurons and examine their effect on neuron health and architecture.

So far, I've found motor neurons mixed with errant astrocytes are much smaller and less branched. Is it due to direct contact of motor neurons with MND astrocytes, a consequence of toxic substances released by astrocytes, or both? By identifying genes, proteins and pathways affected, we may one day banish this cruel monster.
Charles is positioning his wheelchair to depart when my phone rings. "Dvorak's Humoresque," he muses. "Not bad at all."

Like the Czech folk composer's ponderous pieces, an undying sense of direction buoys our research. With ongoing support from institutions like the MRC, and the awe-inspiring resolve of our patients, a far light glimmer. The payoff may not be definable in this instant, yet our progress toward it will not halt.

This is not just history in the making – to visualise a better future and work towards it is one of humanity's most fundamental ideals. Only 15 years ago, our work was considered impossible. In another 15, perhaps a cure is plausible. One day, MND patients will take showers, tie shoelaces, and hug their loved ones without assistance.

Now that's music to my ears.

Bibliography

Ababneh, N. A. *et al.* (2020) 'Correction of amyotrophic lateral sclerosis related phenotypes in induced pluripotent stem cell-derived motor neurons carrying a hexanucleotide expansion mutation in C9orf72 by CRISPR/Cas9 genome editing using homology-directed repair', *Human Molecular Genetics*, 29(13), pp. 2200–2217. doi: 10.1093/hmg/ddaa106.

Abo-rady, M. *et al.* (2020) 'Knocking out C9ORF72 Exacerbates Axonal Trafficking Defects Associated with Hexanucleotide Repeat Expansion and Reduces Levels of Heat Shock Proteins', *Stem Cell Reportsts*, 14(3), p. 390-405. doi: 10.1016/j.stemcr.2020.01.010.

Abramov, A. Y., Canevari, L. and Duchen, M. R. (2004) 'β-Amyloid Peptides Induce Mitochondrial Dysfunction and Oxidative Stress in Astrocytes and Death of Neurons through Activation of NADPH Oxidase', *Journal of Neuroscience*, 24(2), pp. 565–575. doi: 10.1523/JNEUROSCI.4042-03.2004.

Addendum: Relyvrio withdrawn. (2024) *Med Lett Drugs Ther*. 66(1704), pp. 96. doi: 10.58347/tml.2024.1704e.

Agulhon, C. *et al.* (2008) 'What Is the Role of Astrocyte Calcium in Neurophysiology?', *Neuron*, 59(6), pp. 932–946. doi: 10.1016/j.neuron.2008.09.004.

Al-Chalabi, A. and Visscher, P. M. (2014) 'Common genetic variants and the heritability of ALS', *Nature Reviews Neurology*, 10(10), pp. 549–550. doi: 10.1038/nrneurol.2014.166.

Aladesuyi Arogundade, O. *et al.* (2021) 'Nucleolar stress in C9orf72 and sporadic ALS spinal motor neurons precedes TDP-43 mislocalization', *Acta Neuropathologica Communications*, 9(1), pp. 1–16. doi: 10.1186/s40478-021-01125-6.

Alexa, A., Rahnenführer, J. and Lengauer, T. (2006) 'Improved scoring of functional

groups from gene expression data by decorrelating GO graph structure', *Bioinformatics*, 22(13), pp. 1600–1607. doi: 10.1093/bioinformatics/btl140.

Allaman, I. *et al.* (2010) 'Amyloid-β aggregates cause alterations of astrocytic metabolic phenotype: Impact on neuronal viability', *Journal of Neuroscience*. 30(9), pp. 3326-38. doi: 10.1523/JNEUROSCI.5098-09.2010.

Allen, N. J. *et al.* (2012) 'Astrocyte glypicans 4 and 6 promote formation of excitatory synapses via GluA1 AMPA receptors', *Nature*. Nature Publishing Group, 486(7403), pp. 410–414. doi: 10.1038/nature11059.

Allen, N. J. (2014) 'Astrocyte regulation of synaptic behavior', *Annual Review of Cell and Developmental Biology*, 30(1), pp. 439–463. doi: 10.1146/annurev-cellbio-100913-013053.

Allen, S. P., Hall, B., Castelli, L. M., *et al.* (2019) 'Astrocyte adenosine deaminase loss increases motor neuron toxicity in amyotrophic lateral sclerosis', *Brain*, 142(3), pp. 586–605. doi: 10.1093/brain/awy353.

Allen, S. P., Hall, B., Woof, R., *et al.* (2019) 'C9orf72 expansion within astrocytes reduces metabolic flexibility in amyotrophic lateral sclerosis', *Brain*, 142(12), pp. 3771–3790. doi: 10.1093/brain/awz302.

Almad, A. A. *et al.* (2016) 'Connexin 43 in astrocytes contributes to motor neuron toxicity in amyotrophic lateral sclerosis', *Glia*, 64(7), pp. 1154–1169. doi: 10.1002/glia.22989.

Amari, L. and Germain, M. (2021) 'Mitochondrial Extracellular Vesicles – Origins and Roles', *Frontiers in Molecular Neuroscience*, 14(October), pp. 1–7. doi: 10.3389/fnmol.2021.767219.

Anderson, C. M. and Swanson, R. A. (2000) 'Astrocyte glutamate transport: Review of properties, regulation, and physiological functions', *Glia*, 32(1), pp. 1–14. doi: 10.1002/1098-1136(200010)32:1<1::AID-GLIA10>3.0.CO;2-W.

Aoki, Y. *et al.* (2017) ‘C9orf72 and RAB7L1 regulate vesicle trafficking in amyotrophic lateral sclerosis and frontotemporal dementia’, *Brain*, 140(4), pp. 887–897. doi: 10.1093/brain/awx024.

Araque, A. *et al.* (1999) ‘Tripartite synapses: Glia, the unacknowledged partner’, *Trends in Neurosciences*, 22(5), pp. 208–215. doi: 10.1016/S0166-2236(98)01349-6.

Arizono, M. *et al.* (2020) ‘Structural basis of astrocytic Ca2+ signals at tripartite synapses’, *Nature Communications*. Springer US, 11(1), pp. 1–15. doi: 10.1038/s41467-020-15648-4.

Atanasio, A. *et al.* (2016) ‘C9orf72 ablation causes immune dysregulation characterized by leukocyte expansion, autoantibody production, and glomerulonephropathy in mice’, *Scientific Reports*, 6, pp. 1–14. doi: 10.1038/srep23204.

Atassi, N. *et al.* (2014) ‘The PRO-ACT database: design, initial analyses, and predictive features’, 83(19), pp. 1719–1725. doi: 10.1212/WNL.0000000000000951.

Bak, T. H. (2010) ‘Motor neuron disease and frontotemporal dementia: One, two, or three diseases’, *Annals of Indian Academy of Neurology*, 13(SUPPL. 2), S81-8. doi: 10.4103/0972-2327.74250.

Balendra, R. and Isaacs, A. M. (2019) ' C9orf72-mediated ALS and FTD: multiple pathways to disease.', *Nature Reviews Neurology*, 14(9), pp. 544-558, doi: 10.1038/s41582-018-0047-2.

Bantle, C. M. *et al.* (2021) ‘Mitochondrial Dysfunction in Astrocytes: A Role in Parkinson’s Disease?’, *Frontiers in Cell and Developmental Biology*, 8(January), pp. 1–12. doi: 10.3389/fcell.2020.608026.

Barker, H. V. *et al.* (2017) ‘RNA misprocessing in C9orf72-linked neurodegeneration’, *Frontiers in Cellular Neuroscience*, 11(July), pp. 1–15. doi: 10.3389/fncel.2017.00195.

Barrientos, A., & Fontanesi, F., Diaz, F. (2012). 'Evaluation of the mitochondrial respiratory chain and oxidative phosphorylation system using polarography and spectrophotometric enzyme assays', Current Protocols in Human Genetics, 73, 19.3.1-19.3.14. doi: 10.1002/0471142905.hg1903s63.

Basso, M. *et al.* (2013) 'Mutant copper-zinc superoxide dismutase (SOD1) induces protein secretion pathway alterations and exosome release in astrocytes: implications for disease spreading and motor neuron pathology in amyotrophic lateral sclerosis.', *The Journal of Biological Chemistry*. United States, 288(22), pp. 15699–15711. doi: 10.1074/jbc.M112.425066.

Bazargani, N. and Attwell, D. (2016) 'Astrocyte calcium signaling: The third wave', *Nature Neuroscience*, 19(2), pp. 182–189. doi: 10.1038/nn.4201.

Beard, E. *et al.* (2022) 'Astrocytes as Key Regulators of Brain Energy Metabolism: New Therapeutic Perspectives', *Frontiers in Physiology*, 12(January):825816. doi: 10.3389/fphys.2021.825816.

Bélanger, M., Allaman, I. and Magistretti, P. J. (2011) 'Brain energy metabolism: Focus on Astrocyte-neuron metabolic cooperation', *Cell Metabolism*, 14(6), pp. 724–738. doi: 10.1016/j.cmet.2011.08.016.

Belzil, V. V. *et al.* (2013) 'Reduced C9orf72 gene expression in c9FTD/ALS is caused by histone trimethylation, an epigenetic event detectable in blood', *Acta Neuropathologica*, 126(6), pp. 895–905. doi: 10.1007/s00401-013-1199-1.

von Bernhardi, R. *et al.* (2015) 'Role of TGFβ signaling in the pathogenesis of Alzheimer's disease', *Frontiers in Cellular Neuroscience*, 9(OCTOBER), pp. 1–21. doi: 10.3389/fncel.2015.00426.

Beurdeley, M. *et al.* (2013) 'Compact designer TALENs for efficient genome engineering', *Nature Communications*. Nature Publishing Group, 4:1762. doi: 10.1038/ncomms2782.

Bezzi, P. and Volterra, A. (2001) ‘A neuron-glia signalling network in the active brain’, *Current Opinion in Neurobiology*, 11(3), pp. 387–394. doi: 10.1016/S0959-4388(00)00223-3.

Bilican, B. *et al.* (2012) ‘Mutant induced pluripotent stem cell lines recapitulate aspects of TDP-43 proteinopathies and reveal cell-specific vulnerability’, *Proceedings of the National Academy of Sciences of the United States of America*, 109(15), pp. 5803–5808. doi: 10.1073/pnas.1202922109.

Birger, A. *et al.* (2019) ‘Human iPSC-derived astrocytes from ALS patients with mutated C9ORF72 show increased oxidative stress and neurotoxicity’, *EBioMedicine*. Elsevier B.V., 50, pp. 274–289. doi: 10.1016/j.ebiom.2019.11.026.

Blacker, D. *et al.* (1998) ‘Alpha-2 macroglobulin is genetically associated with Alzheimer disease’, *Nature Genetics*, 19(4), pp. 357–360. doi: 10.1038/1243.

Blanquie, O. and Bradke, F. (2018) ‘Cytoskeleton dynamics in axon regeneration', *Curr Opin Neurobiol*. 51:60-69. doi: 10.1016/j.conb.2018.02.024.

Blinder, P. *et al.* (2013) ‘The cortical angiome: An interconnected vascular network with noncolumnar patterns of blood flow’, *Nature Neuroscience*, 16(7), pp. 889–897. doi: 10.1038/nn.3426.

van Blitterswijk, M. *et al.* (2015) ‘Novel clinical associations with specific C9ORF72 transcripts in patients with repeat expansions in C9ORF72’, *Acta Neuropathologica*, 130(6), pp. 863–876. doi: 10.1007/s00401-015-1480-6.

Bock, C. *et al.* (2011) ‘Reference maps of human es and ips cell variation enable high-throughput characterization of pluripotent cell lines’, *Cell*. Elsevier Inc., 144(3), pp. 439–452. doi: 10.1016/j.cell.2010.12.032.

Bolaños, J. P. (2016) ‘Bioenergetics and redox adaptations of astrocytes to neuronal activity’, *Journal of Neurochemistry*, 139, pp. 115–125. doi: 10.1111/jnc.13486.

Borg, R. *et al.* (2021) ‘Genetic analysis of ALS cases in the isolated island population of Malta’, *European Journal of Human Genetics*. Springer US, 29(4), pp. 604–614. doi: 10.1038/s41431-020-00767-9.

Brambilla, L. *et al.* (2016) ‘Disruption of the astrocytic TNFR1-GDNF axis accelerates motor neuron degeneration and disease progression in amyotrophic lateral sclerosis’, *Human Molecular Genetics*, 25(14), pp. 3080–3095. doi: 10.1093/hmg/ddw161.

Brown, A. and Ransom, B. (2007) ‘Astrocyte Glycogen and Brain Energy Metabolism’, *Glia*, 55(March), pp. 1263–127. doi: 10.1002/glia.

Bruijn, L. I. *et al.* (1997) ‘ALS-linked SOD1 mutant G85R mediates damage to astrocytes and promotes rapidly progressive disease with SOD1-containing inclusions’, *Neuron*, 18(2), pp. 327–338. doi: 10.1016/S0896-6273(00)80272-X.

Burberry, A. *et al.* (2020) ‘C9orf72 suppresses systemic and neural inflammation induced by gut bacteria’, *Nature*. Springer US, 582(7810), pp. 89–94. doi: 10.1038/s41586-020-2288-7.

Burk, K. and Pasterkamp, R. J. (2019) ‘Disrupted neuronal trafficking in amyotrophic lateral sclerosis’, *Acta Neuropathologica*, 137(6), pp. 859–877. doi: 10.1007/s00401-019-01964-7.

Burkhardt, M. F. *et al.* (2016) ‘A cellular model for sporadic ALS using patient-derived induced pluripotent stem cells’, *Mol Cell Neurosci*, 56 pp. 355–364. doi: 10.1016/j.mcn.2013.07.007.A.

Burrell, J. R. *et al.* (2016) ‘The frontotemporal dementia-motor neuron disease continuum’, *The Lancet*, 388(10047), pp. 919–931. doi: 10.1016/S0140-6736(16)00737-6.

Byrne, S. *et al.* (2012) ‘Cognitive and clinical characteristics of patients with amyotrophic lateral sclerosis carrying a C9orf72 repeat expansion: A population-based cohort study’, *The Lancet Neurology*. Elsevier Ltd, 11(3), pp. 232–240. doi:

10.1016/S1474-4422(12)70014-5.

Cahan, P. and Daley, G. Q. (2013) ‘Origins and implications of pluripotent stem cell variability and heterogeneity’, *Nature Reviews Molecular Cell Biology*. Nature Publishing Group, 14(6), pp. 357–368. doi: 10.1038/nrm3584.

Cahoy, J. D. *et al.* (2008) ‘A transcriptome database for astrocytes, neurons, and oligodendrocytes: A new resource for understanding brain development and function’, *Journal of Neuroscience*, 28(1), pp. 264–278. doi: 10.1523/JNEUROSCI.4178-07.2008.

Caldwell, A. L. *et al.* (2020) ‘Aberrant astrocyte protein secretion contributes to altered neuronal development in diverse disorders’, *Nat Neurosci.* 25(9):1163-1178. doi: 10.1038/s41593-022-01150-1.

Cassina, P. *et al.* (2008) ‘Mitochondrial dysfunction in SOD1G93A-bearing astrocytes promotes motor neuron degeneration: Prevention by mitochondrial-targeted antioxidants’, *Journal of Neuroscience*, 28(16), pp. 4115–4122. doi: 10.1523/JNEUROSCI.5308-07.2008.

Chen, C. *et al.* (2022) ‘Astrocytic Changes in Mitochondrial Oxidative Phosphorylation Protein Levels in Parkinson’s Disease’, *Movement Disorders*, 37(2), pp. 302–314. doi: 10.1002/mds.28849.

Chen, Q. Y. *et al.* (2021) ‘Exosomal Proteins and miRNAs as Mediators of Amyotrophic Lateral Sclerosis’, *Frontiers in Cell and Developmental Biology*, 9(September):718803. doi: 10.3389/fcell.2021.718803.

Chen, W. T. *et al.* (2020) ‘Spatial Transcriptomics and In Situ Sequencing to Study Alzheimer’s Disease’, *Cell*. 182(4), pp. 976-991. doi: 10.1016/j.cell.2020.06.038.

Cheng, X. Y. *et al.* (2020a) ‘Human iPSCs derived astrocytes rescue rotenone-induced mitochondrial dysfunction and dopaminergic neurodegeneration in vitro by donating functional mitochondria’, *Translational Neurodegeneration*, 9(1), pp. 1–14. doi:

10.1186/s40035-020-00190-6.

Cheng, X. Y. *et al.* (2020b) 'Human iPSCs derived astrocytes rescue rotenone-induced mitochondrial dysfunction and dopaminergic neurodegeneration in vitro by donating functional mitochondria', *Translational Neurodegeneration*. Translational Neurodegeneration, 9(1), pp. 1–14. doi: 10.1186/s40035-020-00190-6.

Chen, Y. *et al*. (2017) 'Kennedy disease with difficulty in differential diagnosis: A case report', *Medicine (Baltimore)*, 96(19), e6792. doi: 10.1097/MD.0000000000006792.

Chew, J. *et al.* (2015) 'C9ORF72 repeat expansions in mice cause TDP-43 pathology, neuronal loss, and behavioral deficits', *Science*, 348(6239), pp. 1151–1154. doi: 10.1126/science.aaa9344.

Chiò, A. *et al.* (2013) 'Global Epidemiology of Amyotrophic Lateral Sclerosis: a Systematic Review of the Published Literature', *Neuroepidemiology*, 41(2), pp. 118–130. doi: 10.1159/000351153.Global.

Christopherson, K. S. *et al.* (2005) 'Thrombospondins are astrocyte-secreted proteins that promote CNS synaptogenesis', *Cell*, 120(3), pp. 421–433. doi: 10.1016/j.cell.2004.12.020.

Chuang, Y. C. *et al.* (2017) 'Mitochondrial Transfer from Wharton's Jelly Mesenchymal Stem Cell to MERRF Cybrid Reduces Oxidative Stress and Improves Mitochondrial Bioenergetics', *Oxidative Medicine and Cellular Longevity*, 2017:569215. doi: 10.1155/2017/5691215.

Cleary, E. M. *et al.* (2016) 'Improved PCR based methods for detecting C9orf72 hexanucleotide repeat expansions', *Molecular and Cellular Probes*. Elsevier Ltd, 30(4), pp. 218–224. doi: 10.1016/j.mcp.2016.06.001.

Clement, A. M. *et al.* (2003) 'Wild-type nonneuronal cells extend survival of SOD1 mutant motor neurons in ALS mice.', *Science (New York, N.Y.)*. United States, 302(5642), pp. 113–117. doi: 10.1126/science.1086071.

Colombo, J. A. *et al.* (2005) ‘Development of interlaminar astroglial processes in the cerebral cortex of control and Down’s syndrome human cases’, *Experimental Neurology*, 193(1), pp. 207–217. doi: 10.1016/j.expneurol.2004.11.024.

Colombo, J. A., Quinn, B. and Puissant, V. (2002) ‘Disruption of astroglial interlaminar processes in Alzheimer’s disease’, *Brain Research Bulletin*, 58(2), pp. 235–242. doi: 10.1016/S0361-9230(02)00785-2.

Conlon, E. G. *et al.* (2016) ‘The C9ORF72 GGGGCC expansion forms RNA G-quadruplex inclusions and sequesters hnRNP H to disrupt splicing in ALS brains’, *eLife*, 5(September), pp. 1–28. doi: 10.7554/eLife.17820.

Connolly, N. M. C. *et al.* (2018) 'Guidelines on experimental methods to assess mitochondrial dysfunction in cellular models of neurodegenerative diseases', *Cell Death and Differentiation*. 25(3), pp. 542-572. doi: 10.1038/s41418-017-0020-4.

Cooper-Knock, J. *et al.* (2013) ‘Clinical/Scientific Notes C9ORF72 transcription in a frontotemporal dementia case with two expanded alleles’, *Neurology*, 81(19), pp. 1719–1721. doi: 10.1212/01.wnl.0000435295.41974.2e.

Cooper-Knock, J. *et al.* (2015) ‘Antisense RNA foci in the motor neurons of C9ORF72-ALS patients are associated with TDP-43 proteinopathy’, *Acta Neuropathologica*, 130(1), pp. 63–75. doi: 10.1007/s00401-015-1429-9.

Cornell-Bell, A.H. *et al.* (1990) ‘Glutamate induces calcium waves in cultured astrocytes: long-range glial signaling’, *Science*, 247(24), pp. 470-3. doi: 10.1126/science.1967852.

Costa, J., Swash, M. and De Carvalho, M. (2012) ‘Awaji criteria for the diagnosis of amyotrophic lateral sclerosis: A systematic review’, *Archives of Neurology*, 69(11), pp. 1410–1416. doi: 10.1001/archneurol.2012.254.

Covelo, A. and Araque, A. (2018) ‘Neuronal activity determines distinct gliotransmitter release from a single astrocyte’, *eLife*, 7, pp. 1–19. doi: 10.7554/eLife.32237.

Dafinca, R. *et al.* (2016) ‘C9orf72 Hexanucleotide Expansions Are Associated with Altered Endoplasmic Reticulum Calcium Homeostasis and Stress Granule Formation in Induced Pluripotent Stem Cell-Derived Neurons from Patients with Amyotrophic Lateral Sclerosis and Frontotemporal Demen’, *Stem Cells*, 34(8), pp. 2063–2078. doi: 10.1002/stem.2388.

Davis, C. H. O. *et al.* (2014) ‘Transcellular degradation of axonal mitochondria’, *Proceedings of the National Academy of Sciences of the United States of America*, 111(26), pp. 9633–9638. doi: 10.1073/pnas.1404651111.

Davalos, D. *et al.* (2005). ATP mediates rapid microglial response to local brain injury in vivo. Nature Neuroscience, 8(6), 752-758. doi: 10.1038/nn1472.

DeJesus-Hernandez, M. *et al.* (2011) ‘Expanded GGGGCC Hexanucleotide Repeat in Noncoding Region of C9ORF72 Causes Chromosome 9p-Linked FTD and ALS’, *Neuron*, 72(2), pp. 245–256. doi: 10.1016/j.neuron.2011.09.011.

Deng, H. X. *et al.* (2021) ‘Efficacy and long-term safety of CRISPR/Cas9 genome editing in the SOD1-linked mouse models of ALS’, *Communications Biology*, 4(1), pp. 1–11. doi: 10.1038/s42003-021-01942-4.

Desai, S. *et al.* (2024) ‘Performance of TMRM and Mitotrackers in mitochondrial morphofunctional analysis of primary human skin fibroblasts’, *Biochimica et Biophysica Acta - Bioenergetics*, 1865(2). doi: 10.1016/j.bbabio.2023.149027.

Devine, H. and Patani, R. (2017) ‘The translational potential of human induced pluripotent stem cells for clinical neurology: The translational potential of hiPSCs in neurology’, *Cell Biology and Toxicology*, 33(2), pp. 129–144. doi: 10.1007/s10565-016-9372-7.

Diaz, F. et al. (2012) 'A defect in the mitochondrial complex III, but not complex IV, triggers early ROS-dependent damage in defined brain regions', *Hum Mol Genet,* 21(23), pp. 5066-77. doi: 10.1093/hmg/dds350.

Dickinson, M. E. *et al.* (2016) ‘High-throughput discovery of novel developmental phenotypes’, *Nature*. Nature Publishing Group, 537(7621), pp. 508–514. doi: 10.1038/nature19356.

Dienel, G.A. (2019) 'Brain Glucose Metabolism: Integration of Energetics with Function', *Physiol Rev*, 99(1), pp. 949-1045. doi: 10.1152/physrev.00062.2017.

Diniz, L. P. *et al.* (2012) ‘Astrocyte-induced synaptogenesis is mediated by transforming growth factor β signaling through modulation of d-serine levels in cerebral cortex neurons’, *Journal of Biological Chemistry*, 287(49), pp. 41432–41445. doi: 10.1074/jbc.M112.380824.

Dobin, A. *et al.* (2013) ‘STAR: Ultrafast universal RNA-seq aligner’, *Bioinformatics*, 29(1), pp. 15–21. doi: 10.1093/bioinformatics/bts635.

Domènech-Estévez, E. *et al*. (2015) 'Distribution of monocarboxylate transporters in the peripheral nervous system suggests putative roles in lactate shuttling and myelination', *J Neurosci,* 35(10), pp. 4151-6. doi: 10.1523/JNEUROSCI.3534-14.2015.

Le Douce, J. *et al.* (2020) ‘Impairment of Glycolysis-Derived L-Serine Production in Astrocytes Contributes to Cognitive Deficits in Alzheimer’s Disease’, *Cell Metabolism*, 31(3), pp. 503-517.e8. doi: 10.1016/j.cmet.2020.02.004.

Douvaras, P. *et al.* (2017) ‘Directed Differentiation of Human Pluripotent Stem Cells to Microglia’, *Stem Cell Reports*. ElsevierCompany, 8(6), pp. 1516–1524. doi: 10.1016/j.stemcr.2017.04.023.

Edmond, J., Robbins, R. A., Bergstrom, J. D., Cole, R. A., & de Vellis, J. (1987) 'Capacity for substrate utilization in oxidative metabolism by neurons, astrocytes, and oligodendrocytes from developing brain in primary culture', *J Neurosci Res*. 18(4), pp. 551-61. doi: 10.1002/jnr.490180407.

Egawa, N. *et al.* (2012) ‘Drug screening for ALS using patient-specific induced

pluripotent stem cells', *Science Translational Medicine*, 4(145), pp. 1–9. doi: 10.1126/scitranslmed.3004052.

Endo, F., Komine, O. and Yamanaka, K. (2016) 'Neuroinflammation in motor neuron disease', *Clinical and Experimental Neuroimmunology*, 7(2), pp. 126–138. doi: 10.1111/cen3.12309.

Eroglu, Ç. *et al.* (2009) 'Gabapentin Receptor α2δ-1 Is a Neuronal Thrombospondin Receptor Responsible for Excitatory CNS Synaptogenesis', *Cell*, 139(2), pp. 380–392. doi: 10.1016/j.cell.2009.09.025.

Escartin, C. *et al.* (2021) 'Reactive astrocyte nomenclature, definitions, and future directions', *Nature Neuroscience*. Springer US, 24(3), pp. 312–325. doi: 10.1038/s41593-020-00783-4.

Farg, M. A. *et al.* (2014) 'C9ORF72, implicated in amytrophic lateral sclerosis and frontotemporal dementia, regulates endosomal trafficking', *Human Molecular Genetics*, 23(13), pp. 3579–3595. doi: 10.1093/hmg/ddu068.

Fawcett, J. W., Oohashi, T. and Pizzorusso, T. (2019) 'The roles of perineuronal nets and', *Nature Reviews Neuroscience*, 20(August), pp. 451–465. doi: 10.1038/s41583-019-0196-3.

Ferraiuolo, L. *et al.* (2011) 'Dysregulation of astrocyte-motoneuron cross-talk in mutant superoxide dismutase 1-related amyotrophic lateral sclerosis', *Brain*, 134(9), pp. 2627–2641. doi: 10.1093/brain/awr193.

Finkbeiner, S. (1992) 'Calcium waves in astrocytes-filling in the gaps', *Neuron*, 8(6), pp. 1101–1108. doi: 10.1016/0896-6273(92)90131-V.

Fossati, G. *et al.* (2019) 'Pentraxin 3 regulates synaptic function by inducing AMPA receptor clustering via ECM remodeling and β1-integrin', *The EMBO Journal*, 38(1), pp. 1–20. doi: 10.15252/embj.201899529.

Fossati, G., Matteoli, M. and Menna, E. (2020) ‘Astrocytic Factors Controlling Synaptogenesis: A Team Play’, *Cells*, 9(10), pp. 1–20. doi: 10.3390/cells9102173.

Fournier, C. *et al.* (2019) ‘Relations between C9orf72 expansion size in blood, age at onset, age at collection and transmission across generations in patients and presymptomatic carriers’, *Neurobiology of Aging*, 74, pp. 234.e1-234.e8. doi: 10.1016/j.neurobiolaging.2018.09.010.

Fratta, P. *et al.* (2013) ‘Homozygosity for the C9orf72 GGGGCC repeat expansion in frontotemporal dementia’, *Acta Neuropathologica*, 126(3), pp. 401–409. doi: 10.1007/s00401-013-1147-0.

Fredi, M. *et al.* (2019) ‘C9orf72 Intermediate Alleles in Patients with Amyotrophic Lateral Sclerosis, Systemic Lupus Erythematosus, and Rheumatoid Arthritis’, *NeuroMolecular Medicine*, 21(9), pp. 150–159. doi: 10.1007/s12017-019-08528-8.

Freibaum, B. D. *et al.* (2015) ‘GGGGCC repeat expansion in C9orf72 compromises nucleocytoplasmic transport’, *Nature*, 525(7567), pp. 129–133. doi: 10.1038/nature14974.

Freibaum, B. D. and Taylor, J. P. (2017) ‘The role of dipeptide repeats in C9ORF72-related ALS-FTD’, *Frontiers in Molecular Neuroscience*, 10:35. doi: 10.3389/fnmol.2017.00035.

Frick, P. et al. (2018) ‘Novel antibodies reveal presynaptic localization of C9orf72 protein and reduced protein levels in C9orf72 mutation carriers’, Acta neuropathologica communications. *Acta Neuropathologica Communications*, 6(1), p. 72. doi: 10.1186/s40478-018-0579-0.

Fritz, E. *et al.* (2013) ‘Mutant SOD1-expressing astrocytes release toxic factors that trigger motoneuron death by inducing hyperexcitability’, *Journal of Neurophysiology*, 109(11), pp. 2803–2814. doi: 10.1152/jn.00500.2012.

Fuentes-Medel, Y. *et al.* (2012) ‘Integration of a retrograde signal during synapse

formation by glia-secreted TGF-β ligand', *Current Biology*, 22(19), pp. 1831–1838. doi: 10.1016/j.cub.2012.07.063.

Fünfschilling, U., Supplie, L. M., Mahad, D., Boretius, S., Saab, A. S., Edgar, J., ... & Martini, R. (2012). Glycolytic oligodendrocytes maintain myelin and long-term axonal integrity. *Nature*, 485(7399), pp. 517-521. doi: 10.1038/nature11007.

Fujimori, K. *et al.* (2018) 'Modeling sporadic ALS in iPSC-derived motor neurons identifies a potential therapeutic agent', *Nature Medicine*. Springer US, 24(10), pp. 1579–1589. doi: 10.1038/s41591-018-0140-5.

Fumagalli, L. *et al.* (2021) 'C9orf72 -derived arginine-containing dipeptide repeats associate with axonal transport machinery and impede microtubule-based motility', (April), 7(15), pp. 19–23. doi: 10.1126/sciadv.abg3013.

Gao, L. *et al.* (2019) 'Mitochondria are dynamically transferring between human neural cells and alexander disease-associated GFAP mutations impair the astrocytic transfer', *Frontiers in Cellular Neuroscience*, 13(July), pp. 1–16. doi: 10.3389/fncel.2019.00316.

Gatto, N. *et al.* (2021) 'Directly converted astrocytes retain the ageing features of the donor fibroblasts and elucidate the astrocytic contribution to human CNS health and disease', *Aging Cell*, 20(1). doi: 10.1111/acel.13281.

Giaume, C. and Liu, X. (2012) 'From a glial syncytium to a more restricted and specific glial networking', *Journal of Physiology Paris*, 106(1–2), pp. 34–39. doi: 10.1016/j.jphysparis.2011.09.001.

Gijselinck, I. *et al.* (2016) 'The C9orf72 repeat size correlates with onset age of disease, DNA methylation and transcriptional downregulation of the promoter', *Molecular Psychiatry*, 21(8), pp. 1112–1124. doi: 10.1038/mp.2015.159.

De Giorgio, F. *et al.* (2019) 'Transgenic and physiological mouse models give insights into different aspects of amyotrophic lateral sclerosis', *DMM Disease Models and*

Mechanisms, 12(1), pp. 2013–2014. doi: 10.1242/dmm.037424.

Di Giorgio, F. P. *et al.* (2008) ‘Human Embryonic Stem Cell-Derived Motor Neurons Are Sensitive to the Toxic Effect of Glial Cells Carrying an ALS-Causing Mutation’, *Cell Stem Cell*, 3(6), pp. 637–648. doi: 10.1016/j.stem.2008.09.017.

Gao, C. et al. (2023) 'Microglia in neurodegenerative diseases: mechanism and potential therapeutic targets', *Signal Transduct Target Ther*, 8(1), pp. 359. doi: 10.1038/s41392-023-01588-0.

Goldman, S. A. *et al.* (2015) ‘Modeling cognition and disease using human glial chimeric mice’, *GLIA*, 63(8), pp. 1483–1493. doi: 10.1002/glia.22862.Modeling.

Gollihue, J. L. and Norris, C. M. (2020) ‘Astrocyte mitochondria: Central players and potential therapeutic targets for neurodegenerative diseases and injury’, *Ageing Research Reviews*, 59:101039. doi: 10.1016/j.arr.2020.101039.

Gomez-Nicola, D., & Perry, V. H. (2015). 'Microglial dynamics and role in the healthy and diseased brain: A paradigm of functional plasticity', *Neuroscientist*, 21(2), pp. 169-184. doi: 10.1177/1073858414530512.

Gomez-Suaga, P. *et al.* (2022) ‘Disruption of ER-mitochondria tethering and signalling in C9orf72-associated amyotrophic lateral sclerosis and frontotemporal dementia’, *Aging Cell*, 21(2):e13549. doi: 10.1111/acel.13549.

Gore, A. *et al.* (2011) ‘Somatic coding mutations in human induced pluripotent stem cells’, *Nature*. Nature Publishing Group, 471(7336), pp. 63–67. doi: 10.1038/nature09805.

Greenhill, C. (2023) 'Microglial inflammatory signalling improves glucose tolerance', *Nat Rev Endocrinol*, 19(10), pp. 555. doi: 10.1038/s41574-023-00892-7.

Guerra-Gomes, S. *et al.* (2018) ‘Functional roles of astrocyte calcium elevations: From synapses to behavior’, *Frontiers in Cellular Neuroscience*, 11(January), pp. 1–7. doi:

10.3389/fncel.2017.00427.

Guillaud, L. *et al.* (2020) ‘Anterograde Axonal Transport in Neuronal Homeostasis and Disease’, *Frontiers in Molecular Neuroscience*, 13(September), pp. 1–17. doi: 10.3389/fnmol.2020.556175.

Guthrie, P. B. *et al.* (1999) ‘ATP released from astrocytes mediates glial calcium waves’, *Journal of Neuroscience*, 19(2), pp. 520–528. doi: 10.1523/jneurosci.19-02-00520.1999.

Guttenplan, K. A. *et al.* (2020) ‘slows disease progression in an ALS mouse model’, *Nature Communications*, 11(2020), pp. 1–9. doi: org/10.1038/s41467-020-17514-9.

Haeusler, A. R., Donnelly, C. J. and Rothstein, J. D. (2016) ‘The expanding biology of the C9orf72 nucleotide repeat expansion in neurodegenerative disease’, *Nature Reviews Neuroscience*. Nature Publishing Group, 17(6), pp. 383–395. doi: 10.1038/nrn.2016.38.

Hafezparast, M. *et al.* (2003) ‘Mutations in dynein link motor neuron degeneration to defects in retrograde transport’, *Science*, 300(5620), pp. 808–812. doi: 10.1126/science.1083129.

Hahn, J., Wang, X. and Margeta, M. (2015) ‘Astrocytes increase the activity of synaptic GluN2B NMDA receptors’, *Frontiers in Cellular Neuroscience*, 9(APR), pp. 1–16. doi: 10.3389/fncel.2015.00117.

Haidet-Phillips, A. M. *et al.* (2011) ‘Astrocytes from familial and sporadic ALS patients are toxic to motor neurons’, *Nature Biotechnology*, 29(9), pp. 824–828. doi: 10.1038/nbt.1957.

Haidet-Phillips, A. M. *et al.* (2013) ‘Altered astrocytic expression of TDP-43 does not influence motor neuron survival’, *Experimental Neurology*. Elsevier Inc., 250, pp. 250–259. doi: 10.1016/j.expneurol.2013.10.004.

Hall, C. E. *et al.* (2017) ‘Progressive Motor Neuron Pathology and the Role of Astrocytes in a Human Stem Cell Model of VCP-Related ALS’, *Cell Reports*, 19(9), pp. 1739–1749. doi: 10.1016/j.celrep.2017.05.024.

Han, K.-S. *et al.* (2013) ‘Channel-mediated astrocytic glutamate release via Bestrophin-1 targets synaptic NMDARs’, *Molecular Brain*, 6(1):4. doi: 10.1186/1756-6606-6-4.

Han, Q. *et al.* (2020) ‘Restoring Cellular Energetics Promotes Axonal Regeneration and Functional Recovery after Spinal Cord Injury’, *Cell Metabolism*, 31(3), pp. 623-641.e8. doi: 10.1016/j.cmet.2020.02.002.

Han, S. *et al*. (2022) 'Functions and dysfunctions of oligodendrocytes in neurodegenerative diseases', *Front Cell Neurosci*, 16, pp. 1083159. doi: 10.3389/fncel.2022.1083159.

Han, X. *et al.* (2013) ‘Forebrain engraftment by human glial progenitor cells enhances synaptic plasticity and learning in adult mice’, *Cell Stem Cell*. Elsevier Inc., 12(3), pp. 342–353. doi: 10.1016/j.stem.2012.12.015.

Hao, Z. *et al.* (2019) ‘Motor dysfunction and neurodegeneration in a C9orf72 mouse line expressing poly-PR’, *Nature Communications*. Springer US, 10(1):2906. doi: 10.1038/s41467-019-10956-w.

Hardingham, G. E. and Bading, H. (2003) ‘The Yin and Yang of NMDA receptor signalling.’, *Trends in neurosciences*. England, 26(2), pp. 81–89. doi: 10.1016/S0166-2236(02)00040-1.

Harms, M. B. *et al.* (2013) ‘Lack of C9ORF72 coding mutations supports a gain of function for repeat expansions in amyotrophic lateral sclerosis’, *Neurobiology of Aging*, 34(9), pp. 2234.e13-2234.e19. doi: 10.1016/j.neurobiolaging.2013.03.006.

Hartopp, N. *et al.* (2022) ‘Disruption of the VAPB-PTPIP51 ER-mitochondria tethering proteins in post-mortem human amyotrophic lateral sclerosis’, *Frontiers in Cell and*

Developmental Biology, 10(August), pp. 1–9. doi: 10.3389/fcell.2022.950767.

Hasegawa, M. *et al.* (2008) 'Phosphorylated TDP-43 in frontotemporal lobar degeneration and amyotrophic lateral sclerosis', *Annals of Neurology*, 64(1), pp. 60–70. doi: 10.1002/ana.21425.

Hayakawa, K. *et al.* (2016) 'Transfer of mitochondria from astrocytes to neurons after stroke', *Nature*, 535(7613), pp. 551–555. doi: 10.1038/nature18928.

Herndon, R.C. *et al*. (1998) 'Quantification of white matter and gray matter volumes from three-dimensional magnetic resonance volume studies using fuzzy classifiers', *J Magn Reson Imaging*, 8(5), pp. 1097-105. doi: 10.1002/jmri.1880080515.

Iguchi, Y. *et al.* (2016) 'Exosome secretion is a key pathway for clearance of pathological TDP-43', *Brain*, 139(12), pp. 3187–3201. doi: 10.1093/brain/aww237.

Ikiz, B. *et al.* (2015) 'The Regulatory Machinery of Neurodegeneration in In Vitro Models of Amyotrophic Lateral Sclerosis', *Cell Reports*. Elsevier, 12(2), pp. 335–345. doi: 10.1016/j.celrep.2015.06.019.

Jackson, J. L. *et al.* (2020) 'Elevated methylation levels, reduced expression levels, and frequent contractions in a clinical cohort of C9orf72 expansion carriers', *Molecular Neurodegeneration*, 15(1), pp. 1–11. doi: 10.1186/s13024-020-0359-8.

Jalaludin, I., Lubman, D. M. and Kim, J. (2021) 'A guide to mass spectrometric analysis of extracellular vesicle proteins for biomarker discovery', *Mass Spectrometry Reviews*, 42(2), pp. 1–29. doi: 10.1002/mas.21749.

Jia, M. *et al.* (2015) 'Taming glutamate excitotoxicity: Strategic pathway modulation for neuroprotection', *CNS Drugs*, 29(2), pp. 153–162. doi: 10.1007/s40263-015-0225-3.

Jiang, J. *et al.* (2016) 'Gain of Toxicity from ALS/FTD-Linked Repeat Expansions in C9ORF72 Is Alleviated by Antisense Oligonucleotides Targeting GGGGCC-

Containing RNAs', *Neuron*. Elsevier Inc., 90(3), pp. 535–550. doi: 10.1016/j.neuron.2016.04.006.

Jiang, P. *et al.* (2013) 'Adenosine monophosphate-activated protein kinase overactivation leads to accumulation of α-synuclein oligomers and decrease of neurites', *Neurobiology of Aging*. 34(5), pp. 1504-1515. doi: 10.1016/j.neurobiolaging.2012.11.001.

Jiwaji, Z. *et al.* (2017) 'The role of neuronal activity in regulating metabolism in mouse and human astrocytes', *The Lancet*. Elsevier Ltd, 389, p. S51. doi: 10.1016/s0140-6736(17)30447-6.

Johnstone, M. *et al.* (2019) 'Reversal of proliferation deficits caused by chromosome 16p13.11 microduplication through targeting NFκB signaling: an integrated study of patient-derived neuronal precursor cells, cerebral organoids and in vivo brain imaging', *Molecular Psychiatry*, 24(2), pp. 294–311. doi: 10.1038/s41380-018-0292-1.

Jovičič, A. *et al.* (2015) 'Modifiers of C9orf72 dipeptide repeat toxicity connect nucleocytoplasmic transport defects to FTD/ALS', *Nature Neuroscience*, 18(9), pp. 1226–1229. doi: 10.1038/nn.4085.

Jung, Y. J. and Chung, W. S. (2018) 'Phagocytic roles of glial cells in healthy and diseased brains', *Biomolecules and Therapeutics*, 26(4), pp. 350–357. doi: 10.4062/biomolther.2017.133.

Kanekura, K. *et al.* (2016) 'Poly-dipeptides encoded by the C9ORF72 repeats block global protein translation', *Human Molecular Genetics*, 25(9), pp. 1803–1813. doi: 10.1093/hmg/ddw052.

Kanemaru, K. *et al.* (2014) 'In Vivo visualization of subtle, transient, and local activity of astrocytes using an ultrasensitive Ca2+ indicator', *Cell Reports*. The Authors, 8(1), pp. 311–318. doi: 10.1016/j.celrep.2014.05.056.

Karki, P. *et al.* (2015) 'Role of transcription factor yin yang 1 in manganese-induced

reduction of astrocytic glutamate transporters: Putative mechanism for manganese-induced neurotoxicity', *Neurochemistry International*, 88, pp. 53–59. doi: 10.1016/j.neuint.2014.08.002.

Kawamata, H. *et al.* (2014) 'Abnormal intracellular calcium signaling and SNARE dependent exocytosis contributes to SOD1G93A astrocyte- mediated toxicity in amyotrophic lateral sclerosis', *Journal of Neuroscience*, 34(6), pp. 2331–2348. doi: 10.1523/JNEUROSCI.2689-13.2014.

Kieran, D. *et al.* (2005) 'A mutation in dynein rescues axonal transport defects and extends the life span of ALS mice', *Journal of Cell Biology*, 169(4), pp. 561–567. doi: 10.1083/jcb.200501085.

Kleinstiver, B. P. *et al.* (2016) 'High-fidelity CRISPR-Cas9 nucleases with no detectable genome-wide off-target effects', *Nature*. Nature Publishing Group, 529(7587), pp. 490–495. doi: 10.1038/nature16526.

Kohli, M. A. *et al.* (2013) 'Repeat expansions in the C9ORF72 gene contribute to Alzheimer's disease in Caucasians', *Neurobiology of Aging*. Elsevier, 34(5), pp. 1519.e5-1519.e12. doi: 10.1016/j.neurobiolaging.2012.10.003.

Kortazar-Zubizarreta, I. *et al*. (2023) 'C9ORF72 Gene GGGGCC Hexanucleotide Expansion: A High Clinical Variability from Amyotrophic Lateral Sclerosis to Frontotemporal Dementia', *J Pers Med*, 13(9), pp. 1396. doi: 10.3390/jpm13091396.

Koppers, M. *et al.* (2015) 'C9orf72 ablation in mice does not cause motor neuron degeneration or motor deficits', *Annals of Neurology*, 78(3), pp. 426–438. doi: 10.1002/ana.24453.

Kreutzberg, G. W. (1996) 'Microglia: A sensor for pathological events in the CNS', *Trends in Neurosciences*, 19(8), pp. 312-318. doi: 10.1016/0166-2236(96)10049-7.

Kucukdereli, H. *et al.* (2011) 'Control of excitatory CNS synaptogenesis by astrocyte-secreted proteins hevin and SPARC', *Proceedings of the National Academy of*

Sciences of the United States of America, 108(32), pp. E440-9. doi: 10.1073/pnas.1104977108.

Kwon, I. *et al.* (2014) 'Poly-dipeptides encoded by the C9orf72 repeats bind nucleoli, impede RNA biogenesis, and kill cells', *Science*, 345(6201), pp. 1139–1145. doi: 10.1126/science.1254917.

Lagier-Tourenne, C. *et al.* (2013) 'Targeted degradation of sense and antisense C9orf72 RNA foci as therapy for ALS and frontotemporal degeneration', *Proceedings of the National Academy of Sciences of the United States of America*, 110(47), E4530-9. doi: 10.1073/pnas.1318835110.

Lampinen, R. *et al.* (2022) 'Neuron-astrocyte transmitophagy is altered in Alzheimer ' s disease', 170(May):105753. doi: 10.1016/j.nbd.2022.105753.

Larson, V.A. et al. (2018) 'Oligodendrocytes control potassium accumulation in white matter and seizure susceptibility', *Elife*, 7, e34829. doi: 10.7554/eLife.34829.

Lapasset, L. *et al.* (2011) 'Rejuvenating senescent and centenarian human cells by reprogramming through the pluripotent state', *Genes and Development*, 25(21), pp. 2248–2253. doi: 10.1101/gad.173922.111.

Lee, J. H. *et al.* (2018a) 'Advances in Patient-Specific Induced Pluripotent Stem Cells Shed Light on Drug Discovery for Amyotrophic Lateral Sclerosis', *Cell Transplantation*, 27(9), pp. 1301–1312. doi: 10.1177/0963689718785154.

Lee, Y. *et al.* (2012). Oligodendroglia metabolically support axons and contribute to neurodegeneration. *Nature*, 487(7408), pp. 443-448. doi: 10.1038/nature11314.

Lee, Y. B. *et al.* (2013) 'Hexanucleotide repeats in ALS/FTD form length-dependent RNA Foci, sequester RNA binding proteins, and are neurotoxic', *Cell Reports*, 5(5), pp. 1178–1186. doi: 10.1016/j.celrep.2013.10.049.

Lepore, A. C. *et al.* (2008) 'Focal transplantation-based astrocyte replacement is

neuroprotective in a model of motor neuron disease', *Nature Neuroscience*, 11(11), pp. 1294–1301. doi: 10.1038/nn.2210.

Li, K. *et al.* (2019) 'Reactive astrocytes in neurodegenerative diseases', *Aging and Disease*, 10(3), pp. 664–675. doi: 10.14336/AD.2018.0720.

Li, Y. X., Sibon, O. C. M. and Dijkers, P. F. (2018) 'Inhibition of NF-KB in astrocytes is sufficient to delay neurodegeneration induced by proteotoxicity in neurons', *Journal of Neuroinflammation*, 15(1), pp. 1–17. doi: 10.1186/s12974-018-1278-2.

Liao, Y., Smyth, G. K. and Shi, W. (2014) 'FeatureCounts: An efficient general purpose program for assigning sequence reads to genomic features', *Bioinformatics*, 30(7), pp. 923–930. doi: 10.1093/bioinformatics/btt656.

Liddelow, S. A. and Sofroniew, M. V. (2019) 'Astrocytes usurp neurons as a disease focus', *Nature Neuroscience*, 22(4), pp. 512–513. doi: 10.1038/s41593-019-0367-6.

Liebner, S. *et al.* (2018) 'Functional morphology of the blood–brain barrier in health and disease', *Acta Neuropathologica*. Springer Berlin Heidelberg, 135(3), pp. 311–336. doi: 10.1007/s00401-018-1815-1.

Lin, C. L. G. *et al.* (1998) 'Aberrant RNA processing in a neurodegenerative disease: The cause for absent EAAT2, a glutamate transporter, in amyotrophic lateral sclerosis', *Neuron*, 20(3), pp. 589–602. doi: 10.1016/S0896-6273(00)80997-6.

Lin, J., Handschin, C. and Spiegelman, B. M. (2005) 'Metabolic control through the PGC-1 family of transcription coactivators', *Cell Metabolism*, 1(6), pp. 361–370. doi: 10.1016/j.cmet.2005.05.004.

Lines, J. *et al.* (2020) 'Astrocytes modulate sensory-evoked neuronal network activity', *Nature Communications*. Springer US, 11(1), pp. 1–12. doi: 10.1038/s41467-020-17536-3.

Ling, S. C., Polymenidou, M. and Cleveland, D. W. (2013) 'Converging mechanisms

in als and FTD: Disrupted RNA and protein homeostasis', *Neuron*. Elsevier Inc., 79(3), pp. 416–438. doi: 10.1016/j.neuron.2013.07.033.

Liu, D. *et al.* (2021) 'Intercellular mitochondrial transfer as a means of tissue revitalization', *Signal Transduction and Targeted Therapy*. Springer US, 6(1):65. doi: 10.1038/s41392-020-00440-z.

Liu, F. *et al.* (2016) 'Identification of a novel loss-of-function C9orf72 splice site mutation in a patient with amyotrophic lateral sclerosis', *Neurobiology of Aging*, 47, pp. 219.e1-219.e5. doi: 10.1016/j.neurobiolaging.2016.07.027.

Liu, Y. *et al.* (2016) 'C9orf72 BAC Mouse Model with Motor Deficits and Neurodegenerative Features of ALS/FTD', *Neuron*. Elsevier Inc., 90(3), pp. 521–534. doi: 10.1016/j.neuron.2016.04.005.

Lopez-Gonzalez, R. *et al.* (2016) 'Poly(GR) in C9ORF72-Related ALS/FTD Compromises Mitochondrial Function and Increases Oxidative Stress and DNA Damage in iPSC-Derived Motor Neurons', Neuron, 92(2), pp. 383–391. doi: 10.1016/j.neuron.2016.09.015.

López-Doménech, G. *et al.* (2021) 'Loss of neuronal Miro1 disrupts mitophagy and induces hyperactivation of the integrated stress response', *The EMBO Journal*, 40(14), pp. 1–20. doi: 10.15252/embj.2018100715.

Love, M. I., Huber, W. and Anders, S. (2014) 'Moderated estimation of fold change and dispersion for RNA-seq data with DESeq2', *Genome Biology*, 15(12), pp. 1–21. doi: 10.1186/s13059-014-0550-8.

Ludolph, A. C. *et al.* (2020) 'Effect of High-Caloric Nutrition on Survival in Amyotrophic Lateral Sclerosis', *Annals of Neurology*, 87(2), pp. 206–216. doi: 10.1002/ana.25661.

Lutz, C. (2018) 'Mouse models of ALS: Past, present and future', *Brain Research*. Elsevier B.V., 1693, pp. 1–10. doi: 10.1016/j.brainres.2018.03.024.

Macleod, K. G., Serrels, B. and Carragher, N. O. (2017) 'Reverse phase protein arrays and drug discovery', *Methods in Molecular Biology*, 1647, pp. 153–169. doi: 10.1007/978-1-4939-7201-2_10.

Madill, M. *et al.* (2017) 'Amyotrophic lateral sclerosis patient iPSC-derived astrocytes impair autophagy via non-cell autonomous mechanisms', *Molecular Brain*, 10(1), pp. 1–12. doi: 10.1186/s13041-017-0300-4.

Madji Hounoum, B. *et al.* (2017) 'Wildtype motoneurons, ALS-Linked SOD1 mutation and glutamate profoundly modify astrocyte metabolism and lactate shuttling.', *Glia*. United States, 65(4), pp. 592–605. doi: 10.1002/glia.23114.

Magistretti, P. J. and Pellerin, L. (1999) 'Astrocytes couple synaptic activity to glucose utilization in the brain', *News in Physiological Sciences*, 14(5), pp. 177–182. doi: 10.1152/physiologyonline.1999.14.5.177.

de Majo, M. *et al.* (2020) 'An update on human astrocytes and their role in development and disease', *Glia*, 68(4), pp. 685–704. doi: 10.1002/glia.23771.

Marchetto, M. C. N. *et al.* (2008) 'Non-cell-autonomous effect of human SOD1 G37R astrocytes on motor neurons derived from human embryonic stem cells.', *Cell stem cell*. United States, 3(6), pp. 649–657. doi: 10.1016/j.stem.2008.10.001.

Martin, S. *et al.* (2017) 'The benefit of evolving multidisciplinary care in ALS: a diagnostic cohort survival comparison', *Amyotrophic Lateral Sclerosis and Frontotemporal Degeneration*, 18(7–8), pp. 569–575. doi: 10.1080/21678421.2017.1349151.

Mathiisen, T. M. *et al.* (2010) 'The perivascular astroglial sheath provides a complete covering of the brain microvessels: An electron microscopic 3D reconstruction', *Glia*, 58(9), pp. 1094–1103. doi: 10.1002/glia.20990.

Matsui, T. *et al.* (2017) 'Astrocytic glycogen-derived lactate fuels the brain during exhaustive exercise to maintain endurance capacity', *Proceedings of the National*

Academy of Sciences of the United States of America, 114(24), pp. 6358–6363. doi: 10.1073/pnas.1702739114.

Mattson, M. P. and Rychlik, B. (1990) 'Cell culture of cryopreserved human fetal cerebral cortical and hippocampal neurons: neuronal development and responses to trophic factors', *Brain Research*, 522(2), pp. 204–214. doi: 10.1016/0006-8993(90)91462-P.

Mauch, D. H. *et al.* (2001) 'CNS synaptogenesis promoted by glia-derived cholesterol', *Science*, 294(5545), pp. 1354–1357. doi: 10.1126/science.294.5545.1354.

Maury, Y. *et al.* (2015) 'Combinatorial analysis of developmental cues efficiently converts human pluripotent stem cells into multiple neuronal subtypes', *Nature Biotechnology*, 33(1), pp. 89–96. doi: 10.1038/nbt.3049.

McCauley, M. E. *et al.* (2020) 'C9orf72 in myeloid cells suppresses STING-induced inflammation', *Nature*. Springer US, 585(7823), pp. 96–101. doi: 10.1038/s41586-020-2625-x.

McConnell, H. L. *et al.* (2019) 'Astrocyte dysfunction and neurovascular impairment in neurological disorders: Correlation or causation?', *Neurochemistry International*, 128(April), pp. 70–84. doi: 10.1016/j.neuint.2019.04.005.

McMillan, C. T. *et al.* (2015) 'C9orf72 promoter hypermethylation is neuroprotective', *Neurology*, 84(16), pp. 1622–1630. doi: 10.1212/WNL.0000000000001495.

Mehta, A. R. *et al.* (2021) 'Mitochondrial bioenergetic deficits in C9orf72 amyotrophic lateral sclerosis motor neurons cause dysfunctional axonal homeostasis', *Acta Neuropathologica*, 141(2), pp. 257–279. doi: 10.1007/s00401-020-02252-5.

Meyer, K. *et al.* (2014a) 'Direct conversion of patient fibroblasts demonstrates non-cell autonomous toxicity of astrocytes to motor neurons in familial and sporadic ALS', *Proceedings of the National Academy of Sciences of the United States of America*, 111(2), pp. 829–832. doi: 10.1073/pnas.1314085111.

Meyer, K. *et al.* (2014b) ‘Direct conversion of patient fibroblasts demonstrates non-cell autonomous toxicity of astrocytes to motor neurons in familial and sporadic ALS’, *Proceedings of the National Academy of Sciences of the United States of America*, 111(2), pp. 829–832. doi: 10.1073/pnas.1314085111.

Miller, J. D. *et al.* (2013) ‘Human iPSC-based modeling of late-onset disease via progerin-induced aging’, *Cell Stem Cell*. Elsevier Inc., 13(6), pp. 691–705. doi: 10.1016/j.stem.2013.11.006.

Miller T. *et al.* (2020) 'Phase 1-2 Trial of Antisense Oligonucleotide Tofersen for SOD1 ALS', *N Engl J Med*, 383(2), pp. 109-119. doi: 10.1056/NEJMoa2003715.

Miller T. *et al*. (2022) 'Trial of Antisense Oligonucleotide Tofersen for SOD1 ALS', *N Engl J Med*, 387(12), pp. 1099-1110. doi: 10.1056/NEJMoa2204705.

Miller, Z. A. *et al.* (2016) ‘Increased prevalence of autoimmune disease within C9 and FTD/MND cohorts Completing the picture’, *Neurology: Neuroimmunology and NeuroInflammation*, 3(6), pp. 1–8. doi: 10.1212/NXI.0000000000000301.

De Miranda, B. R. *et al.* (2018) ‘Astrocyte-specific DJ-1 overexpression protects against rotenone-induced neurotoxicity in a rat model of Parkinson’s disease’, *Neurobiology of Disease*, 115, pp. 101–114. doi: 10.1016/j.nbd.2018.04.008.

Mishra, A. *et al.* (2016) ‘Astrocytes mediate neurovascular signaling to capillary pericytes but not to arterioles’, *Nature Neuroscience*, 19(12), pp. 1619–1627. doi: 10.1038/nn.4428.

Mizielinska, S. *et al.* (2013) ‘C9orf72 frontotemporal lobar degeneration is characterised by frequent neuronal sense and antisense RNA foci’, *Acta Neuropathologica*, 126(6), pp. 845–857. doi: 10.1007/s00401-013-1200-z.

Mizielinska, S. and Isaacs, A. M. (2014) ‘C9orf72 amyotrophic lateral sclerosis and frontotemporal dementia: Gain or loss of function?’, *Current Opinion in Neurology*, 27(5), pp. 515–523. doi: 10.1097/WCO.0000000000000130.

Moens, T. G. *et al.* (2019) 'C9orf72 arginine-rich dipeptide proteins interact with ribosomal proteins in vivo to induce a toxic translational arrest that is rescued by eIF1A', *Acta Neuropathologica*, 137(3), pp. 487–500. doi: 10.1007/s00401-018-1946-4.

Mora, J. S. *et al.* (2021) 'Long-term survival analysis of masitinib in amyotrophic lateral sclerosis', *Therapeutic Advances in Neurological Disorders*, 14(Ci), pp. 1–16. doi: 10.1177/17562864211030365.

Morales, I. *et al.* (2020) 'Neuroglial transmitophagy and Parkinson's disease', *Glia*, 68(11), pp. 2277–2299. doi: 10.1002/glia.23839.

Mordes, D. A. *et al.* (2020) 'Absence of Survival and Motor Deficits in 500 Repeat C9ORF72 BAC Mice', *Neuron*, 108(4), pp. 775-783.e4. doi: 10.1016/j.neuron.2020.08.009.

Van Mossevelde, S. *et al.* (2017) 'Clinical evidence of disease anticipation in families segregating a C9 orf 72 repeat expansion', *JAMA Neurology*, 74(4), pp. 445–452. doi: 10.1001/jamaneurol.2016.4847.

Mouton-Liger, F. *et al.* (2018) 'Parkin deficiency modulates NLRP3 inflammasome activation by attenuating an A20-dependent negative feedback loop', *Glia*, 66(8), pp. 1736–1751. doi: 10.1002/glia.23337.

Münch, C. *et al.* (2004) 'Point mutations of the p150 subunit of dynactin (DCTN1) gene in ALS', *Neurology*, 63, pp. 724-6. doi: 10.1212/01.wnl.0000134608.83927.b1.
Murphy, N. A. *et al.* (2017) 'Age-related penetrance of the C9orf72 repeat expansion', *Scientific Reports*, 7(1), pp. 1–7. doi: 10.1038/s41598-017-02364-1.

Nagai, M. *et al.* (2007a) 'Astrocytes expressing ALS-linked mutated SOD1 release factors selectively toxic to motor neurons', *Nature Neuroscience*, 10(5), pp. 615–622. doi: 10.1038/nn1876.

Nagai, M. *et al.* (2007b) 'Astrocytes expressing ALS-linked mutated SOD1 release

factors selectively toxic to motor neurons', *Nature Neuroscience*, 10(5), pp. 615–622. doi: 10.1038/nn1876.

Nett, W. J., Oloff, S. H. and Mccarthy, K. D. (2002) 'Hippocampal astrocytes in situ exhibit calcium oscillations that occur independent of neuronal activity', *Journal of Neurophysiology*, 87(1), pp. 528–537. doi: 10.1152/jn.00268.2001.

Nguyen, L. *et al.* (2020) 'Survival and motor phenotypes in FVB C9-500 ALS/FTD BAC transgenic mice reproduced by multiple labs', *Neuron*, 108(4), pp. 784–796. doi: 10.1016/j.neuron.2020.09.009.Survival.

Nicolas, A. *et al.* (2018) 'Genome-wide Analyses Identify KIF5A as a Novel ALS Gene', *Neuron*, 97(6), pp. 1268-1283.e6. doi: 10.1016/j.neuron.2018.02.027.

Norris, R. P. (2021) 'Transfer of mitochondria and endosomes between cells by gap junction internalization', *Traffic*, 22(6), pp. 174–179. doi: 10.1111/tra.12786.

Nualart-marti, A., Solsona, C. and Fields, R. D. (2013) 'Gap Junction Communication in Myelinating Glia', *Biochim Biophys Acta.*, 1828(1), pp. 69–78. doi: 10.1016/j.bbamem.2012.01.024.Gap.

Nuria, M.-F. *et al.* (2022) 'Restoring synapse integrity and memory in Alzheimer's disease by downregulation of the Wnt antagonist Dickkopf-3', *Biorvix Preprint*. doi: https://doi.org/10.1101/2022.06.16.495307

O'Rourke, J. G. *et al.* (2016) 'C9orf72 is required for proper macrophage and microglial function in mice', *Science*, 351(6279), pp. 1324–1329. doi: 10.1126/science.aaf1064.

Oberheim, N. A. *et al.* (2009) 'Uniquely hominid features of adult human astrocytes', *Journal of Neuroscience*, 29(10), pp. 3276–3287. doi: 10.1523/JNEUROSCI.4707-08.2009.

Oki, R. *et al.* (2022) 'Efficacy and Safety of Ultrahigh-Dose Methylcobalamin in Early-Stage Amyotrophic Lateral Sclerosis: A Randomized Clinical Trial', *JAMA Neurology*,

79(6), pp. 575–583. doi: 10.1001/jamaneurol.2022.0901.

Onesto, E. *et al.* (2016) ‘Gene-specific mitochondria dysfunctions in human TARDBP and C9ORF72 fibroblasts’, *Acta neuropathologica communications*, 4(1), p. 47. doi: 10.1186/s40478-016-0316-5.

Opie-Martin, S. *et al.* (2021) ‘Motor Neuron Disease Register for England, Wales and Northern Ireland—an analysis of incidence in England’, *Amyotrophic Lateral Sclerosis and Frontotemporal Degeneration*. Taylor & Francis, 22(1–2), pp. 86–93. doi: 10.1080/21678421.2020.1812661.

Ortinski, P. I. *et al.* (2010) ‘Selective induction of astrocytic gliosis generates deficits in neuronal inhibition’, *Nature Neuroscience*. Nature Publishing Group, 13(5), pp. 584–591. doi: 10.1038/nn.2535.

Paganoni, S. *et al.* (2020) ‘Trial of Sodium Phenylbutyrate–Taurursodiol for Amyotrophic Lateral Sclerosis’, *New England Journal of Medicine*, 383(10), pp. 919–930. doi: 10.1056/nejmoa1916945.

Papadeas, S. T. *et al.* (2011) ‘Astrocytes carrying the superoxide dismutase 1 (SOD1 G93A) mutation induce wild-type motor neuron degeneration in vivo’, *Proceedings of the National Academy of Sciences of the United States of America*, 108(43), pp. 17803–17808. doi: 10.1073/pnas.1103141108.

Pardo, A. C. *et al.* (2006) ‘Loss of the astrocyte glutamate transporter GLT1 modifies disease in SOD1G93A mice’, *Experimental Neurology*, 201(1), pp. 120–130. doi: 10.1016/j.expneurol.2006.03.028.

Pasti, L. *et al.* (1997) ‘Intracellular calcium oscillations in astrocytes: A highly plastic, bidirectional form of communication between neurons and astrocytes in situ’, *Journal of Neuroscience*, 17(20), pp. 7817–7830. doi: 10.1523/jneurosci.17-20-07817.1997.

Patterson, M. *et al.* (2012) ‘Defining the nature of human pluripotent stem cell progeny’, *Cell Research*, 22(1), pp. 178–193. doi: 10.1038/cr.2011.133.

Pellerin, L. & Magistretti, P.J. (2012) 'Sweet sixteen for ANLS', *J Cereb Blood Flow Metab,* 32(7), pp. 1152-66. doi: 10.1038/jcbfm.2011.149.

Perea, G. and Araque, A. (2005) 'Properties of synaptically evoked astrocyte calcium signal reveal synaptic information processing by astrocytes', *Journal of Neuroscience*, 25(9), pp. 2192–2203. doi: 10.1523/JNEUROSCI.3965-04.2005.

Pereira, J. D. *et al.* (2021) 'Human sensorimotor organoids derived from healthy and amyotrophic lateral sclerosis stem cells form neuromuscular junctions', *Nature Communications*. Springer US, 12(1):4744. doi: 10.1038/s41467-021-24776-4.

Pereira, J. X. *et al.* (2019) 'Galectin-3 Regulates the Expression of Tumor Glycosaminoglycans and Increases the Metastatic Potential of Breast Cancer', *Journal of Oncology*, 2019. doi: 10.1155/2019/9827147.

Peppiatt, C. M. *et al*. (2006) 'Bidirectional control of CNS capillary diameter by pericytes', *Nature*, 443(7112), pp. 700-704. doi: 10.1038/nature05193.

Phatnani, H. and Maniatis, T. (2015) 'Astrocytes in neurodegenerative disease', *Cold Spring Harbor Perspectives in Biology*, 7(6), pp. 1–18. doi: 10.1101/cshperspect.a020628.

Philips, T. and Rothstein, J. D. (2015) 'Rodent models of amyotrophic lateral sclerosis', *Current Protocols in Pharmacology*, 2015(June), pp. 5.67.1-5.67.21. doi: 10.1002/0471141755.ph0567s69.

Picher-Martel, V. *et al.* (2016) 'From animal models to human disease: A genetic approach for personalized medicine in ALS', *Acta Neuropathologica Communications*, 4(1), pp. 1–29. doi: 10.1186/s40478-016-0340-5.

Presa, J. L. *et al.* (2020) 'Vasculo-Neuronal Coupling and Neurovascular Coupling at the Neurovascular Unit: Impact of Hypertension', *Frontiers in Physiology*, 11(September), pp. 1–19. doi: 10.3389/fphys.2020.584135.

Proudfoot, M. *et al.* (2014) ‘Early dipeptide repeat pathology in a frontotemporal dementia kindred with C9ORF72 mutation and intellectual disability’, *Acta Neuropathologica*, 127(3), pp. 451–458. doi: 10.1007/s00401-014-1245-7.

Prudencio, M. *et al.* (2015) ‘Distinct brain transcriptome profiles in C9orf72-associated and sporadic ALS’, *Nature Neuroscience*, 18(8), pp. 1175–1182. doi: 10.1038/nn.4065.

Qian, K. *et al.* (2017) ‘Sporadic ALS Astrocytes Induce Neuronal Degeneration In Vivo’, *Stem Cell Reports*. ElsevierCompany, 8(4), pp. 843–855. doi: 10.1016/j.stemcr.2017.03.003.

Qiu, J. *et al.* (2018) ‘Mixed-species RNA-seq for elucidation of non-cell-autonomous control of gene transcription’, *Nature Protocols*, 13(10), pp. 2176–2199. doi: 10.1038/s41596-018-0029-2.

Ramírez-Jarquín, U. N. *et al.* (2017) ‘Chronic infusion of SOD1G93A astrocyte-secreted factors induces spinal motoneuron degeneration and neuromuscular dysfunction in healthy rats’, *Journal of Cellular Physiology*, 232(10), pp. 2610–2615. doi: 10.1002/jcp.25827.

Ran, F. A. *et al.* (2013) ‘Genome engineering using the CRISPR-Cas9 system’, *Nature Protocols*, 8(11), pp. 2281–2308. doi: 10.1038/nprot.2013.143.

Renton, A. E. *et al.* (2011) ‘A hexanucleotide repeat expansion in C9ORF72 is the cause of chromosome 9p21-linked ALS-FTD’, *Neuron*, 72(2), pp. 257–268. doi: 10.1016/j.neuron.2011.09.010.

Richard, J.-P. and Maragakis, N. J. (2015) ‘Induced pluripotent stem cells from ALS patients for disease modeling’, *Brain Research*, 1607, pp. 15-25. doi: 10.1016/j.brainres.2014.09.017.

Rinholm, J.E. *et al*. (2011) 'Regulation of oligodendrocyte development and myelination by glucose and lactate', *J Neurosci*, 31(2), pp. 538-48. doi:

10.1523/JNEUROSCI.3516-10.2011.

Rizzu, P. *et al.* (2016) 'C9orf72 is differentially expressed in the central nervous system and myeloid cells and consistently reduced in C9orf72, MAPT and GRN mutation carriers', *Acta Neuropathologica Communications*, 4(1), p. 37. doi: 10.1186/s40478-016-0306-7.

Rohrer, J. D. *et al.* (2015) 'C9orf72 expansions in frontotemporal dementia and amyotrophic lateral sclerosis', *The Lancet Neurology*, 14(3), pp. 291–301. doi: 10.1016/S1474-4422(14)70233-9.

Rojas, F. *et al.* (2014) 'Astrocytes expressing mutant SOD1 and TDP43 trigger motoneuron death that is mediated via sodium channels and nitroxidative stress', *Frontiers in Cellular Neuroscience*, 8(FEB), pp. 1–15. doi: 10.3389/fncel.2014.00024.

Rose, J. *et al.* (2020) 'Mitochondrial Metabolism in Astrocytes Regulates Brain Bioenergetics, Neurotransmission and Redox Balance', *Frontiers in Neuroscience*, 14(November), pp. 1–20. doi: 10.3389/fnins.2020.536682.

Rothstein, J. D. *et al.* (1995) 'Selective loss of glial glutamate transporter GLT-1 in amyotrophic lateral sclerosis', *Annals of Neurology*, 38(1), pp. 73–84. doi: 10.1002/ana.410380114.

Rouach, N. *et al.* (2008) 'Astroglial Metabolic Networks Sustain Hippocampal Synaptic Transmission', *Science (New York, N.Y.)*, 322(December), pp. 1551–1555. doi: 10.1126/science.1164022

Rowland, L. P. and Shneider, N. A. (2001) 'Amyotrophic lateral sclerosis', *The New England Journal of Medicine*, 344, pp. 1688–1700. doi: 10.5177/ntvt.2010.08.10122.

Russo, I. *et al.* (2019) 'Transcriptome analysis of LRRK2 knock-out microglia cells reveals alterations of inflammatory- and oxidative stress-related pathways upon treatment with α-synuclein fibrils', *Neurobiology of Disease*, 129, pp. 67–78. doi: 10.1016/j.nbd.2019.05.012.Transcriptome.

Ryan, M. *et al.* (2019) ‘Lifetime Risk and Heritability of Amyotrophic Lateral Sclerosis’, *JAMA Neurology*, 76(11), pp. 1367–1374. doi: 10.1001/jamaneurol.2019.2044.

Saab, A. S., Tzvetanova, I. D., & Nave, K. A. (2016). The role of myelin and oligodendrocytes in axonal energy metabolism. *Current Opinion in Neurobiology*, 23(6), pp. 1065-72. doi: 10.1016/j.conb.2013.09.008.

Saberi, S. *et al.* (2018) ‘Sense-encoded poly-GR dipeptide repeat proteins correlate to neurodegeneration and uniquely co-localize with TDP-43 in dendrites of repeat-expanded C9orf72 amyotrophic lateral sclerosis’, *Acta Neuropathologica*. Springer Berlin Heidelberg, 135(3), pp. 459–474. doi: 10.1007/s00401-017-1793-8.

Sander, J. D. and Joung, J. K. (2014) ‘CRISPR-Cas systems for editing, regulating and targeting genomes’, *Nature Biotechnology*. Nature Publishing Group, 32(4), pp. 347–350. doi: 10.1038/nbt.2842.

Sandoe, J. and Eggan, K. (2013) ‘Opportunities and challenges of pluripotent stem cell neurodegenerative disease models’, *Nature Neuroscience*. Nature Publishing Group, 16(7), pp. 780–789. doi: 10.1038/nn.3425.

Sarvi, S. *et al.* (2018) ‘Kindlin-1 promotes pulmonary breast cancer metastasis’, *Cancer Research*, 78(6), pp. 1484–1496. doi: 10.1158/0008-5472.CAN-17-1518.

Sasabe, J. *et al.* (2012) ‘D-Amino acid oxidase controls motoneuron degeneration through D-serine’, *Proceedings of the National Academy of Sciences of the United States of America*, 109(2), pp. 627–632. doi: 10.1073/pnas.1114639109.

Sasaki, S. and Iwata, M. (1996) ‘Impairment of fast axonal transport in the proximal axons of anterior horn neurons in amyotrophic lateral sclerosis.’, *Neurology*. United States, 47(2), pp. 535–540. doi: 10.1212/wnl.47.2.535.

Savage, J. C. *et al*. (2019) 'Nuclear receptors license phagocytosis by trem2+ myeloid cells in mouse models of Alzheimer's disease', *Journal of Neuroscience*, 35(16), pp. 6532-43. doi: 10.1523/JNEUROSCI.4586-14.2015.

Scemes, E. and Giaume, C. (2006) ‘Astrocyte Calcium Waves’, *Glia*, 54(203), pp. 716–725. doi: 10.1002/glia.20374.Astrocyte.

Schmidt, S. *et al.* (2011) ‘Genetic mouse models for Parkinson’s disease display severe pathology in glial cell mitochondria’, *Human Molecular Genetics*, 20(6), pp. 1197-211. doi: 10.1093/hmg/ddq564.

Sellier, C. *et al.* (2016) ‘ Loss of C9 ORF 72 impairs autophagy and synergizes with polyQ Ataxin-2 to induce motor neuron dysfunction and cell death ’, *The EMBO Journal*, 35(12), pp. 1276–1297. doi: 10.15252/embj.201593350.

Selvaraj, B. T. *et al.* (2012) ‘Local axonal function of STAT3 rescues axon degeneration in the pmn model of motoneuron disease’, *Journal of Cell Biology*, 199(3), pp. 437–451. doi: 10.1083/jcb.201203109.

Selvaraj, B. T. *et al.* (2018) ‘C9ORF72 repeat expansion causes vulnerability of motor neurons to Ca2+-permeable AMPA receptor-mediated excitotoxicity’, *Nature Communications*. Springer US, 9(1):347 doi: 10.1038/s41467-017-02729-0.

Serio, A. *et al.* (2013) ‘Astrocyte pathology and the absence of non-cell autonomy in an induced pluripotent stem cell model of TDP-43 proteinopathy’, *Proceedings of the National Academy of Sciences of the United States of America*, 110(12), pp. 4697–4702. doi: 10.1073/pnas.1300398110.

Shao, Q. *et al.* (2019) ‘C9orf72 deficiency promotes motor deficits of a C9ALS/FTD mouse model in a dose-dependent manner’, *Acta Neuropathologica Communications*, 7(1), p. 32. doi: 10.1186/s40478-019-0685-7.

Shi, Y. *et al.* (2018) ‘Haploinsufficiency leads to neurodegeneration in C9ORF72 ALS/FTD human induced motor neurons’, *Nature Medicine*. Nature Publishing Group, 24(3), pp. 313–325. doi: 10.1038/nm.4490.

Shibata, N. (2001) ‘Transgenic mouse model for familial amyotrophic lateral sclerosis with superoxide dismutase-1 mutatione’, *Neuropathology*. 21(1), pp. 82-92. doi:

10.1046/j.1440-1789.2001.00361.x.

Siebert, J. R., Conta Steencken, A. and Osterhout, D. J. (2014) 'Chondroitin Sulfate Proteoglycans in the Nervous System: Inhibitors to Repair', *BioMed Research International*, 2014:845323. doi: 10.1155/2014/845323

Silva, C. A. P. *et al.* (2021) 'Activity-dependent regulation of mitochondrial motility in developing cortical dendrites', *eLife*, 10, pp. 1–19. doi: 10.7554/eLife.62091.

Sivadasan, R. *et al.* (2016) 'C9ORF72 interaction with cofilin modulates actin dynamics in motor neurons', *Nature Neuroscience*, 19(12), pp. 1610–1618. doi: 10.1038/nn.4407.

Slanzi, A. *et al.* (2020) 'In vitro Models of Neurodegenerative Diseases', *Frontiers in Cell and Developmental Biology*, 8(May):328 doi: 10.3389/fcell.2020.00328.

Sleigh, J. N. *et al.* (2019) 'Axonal transport and neurological disease', *Nature Reviews Neurology*. Springer US, 15(12), pp. 691–703. doi: 10.1038/s41582-019-0257-2.

Sliter, D. A. *et al.* (2018) 'Parkin and PINK1 mitigate STING-induced inflammation', *Nature*. Springer US, 561(7722), pp. 258–262. doi: 10.1038/s41586-018-0448-9.

Sloan, S. A. *et al.* (2018) 'Human Astrocyte Maturation Captured in 3D Cerebral Cortical Spheroids Derived from Pluripotent Stem Cells', 95(4), pp. 779–790. doi: 10.1016/j.neuron.2017.07.035.Human.

Smeyers, J., Banchi, E. G. and Latouche, M. (2021) 'C9ORF72: What It Is, What It Does, and Why It Matters', *Frontiers in Cellular Neuroscience*, 15(May), pp. 1–16. doi: 10.3389/fncel.2021.661447.

Smith, B. N. *et al.* (2014) 'Exome-wide rare variant analysis identifies TUBA4A mutations associated with familial ALS', *Neuron*, 84(2), pp. 324–331. doi: 10.1016/j.neuron.2014.09.027.

Smith, M. P. *et al.* (2017) ‘Targeting endothelin receptor signalling overcomes heterogeneity driven therapy failure’, *EMBO Molecular Medicine*, 9(8), pp. 1011–1029. doi: 10.15252/emmm.201607156.

Snowden, J. S. *et al.* (2012) ‘Distinct clinical and pathological characteristics of frontotemporal dementia associated with C9ORF72 mutations’, *Brain*, 135(3), pp. 693–708. doi: 10.1093/brain/awr355.

Song, S. W. *et al.* (2016) ‘Major histocompatibility complex class I molecules protect motor neurons from astrocyte-induced toxicity in amyotrophic lateral sclerosis’, *Nature Medicine*. Nature Publishing Group, 22(4), pp. 397–403. doi: 10.1038/nm.4052.

Spees, J. L. *et al.* (2006) ‘Mitochondrial transfer between cells can rescue aerobic respiration’, *Proceedings of the National Academy of Sciences of the United States of America*, 103(5), pp. 1283–1288. doi: 10.1073/pnas.0510511103.

Stackhouse, T. L. and Mishra, A. (2021) ‘Neurovascular Coupling in Development and Disease: Focus on Astrocytes’, *Frontiers in Cell and Developmental Biology*, 9(July), pp. 1–20. doi: 10.3389/fcell.2021.702832.

Stenmark, H. (2009) ‘Rab GTPases as coordinators of vesicle traffic’, *Nature Reviews Molecular Cell Biology*. Nature Publishing Group, 10(8), pp. 513–525. doi: 10.1038/nrm2728.

Stobart, J. L. *et al.* (2018) ‘Cortical Circuit Activity Evokes Rapid Astrocyte Calcium Signals on a Similar Timescale to Neurons’, *Neuron*, 98(4), pp. 726-735.e4. doi: 10.1016/j.neuron.2018.03.050.

Stogsdill, J. A. *et al.* (2017) ‘Astrocytic neuroligins control astrocyte morphogenesis and synaptogenesis’, *Nature*. Nature Publishing Group, 551(7679), pp. 192–197. doi: 10.1038/nature24638.

Su, X. W. *et al.* (2014) ‘Genetic heterogeneity of amyotrophic lateral sclerosis: Implications for clinical practice and research’, *Muscle and Nerve*, 49(6), pp. 786–803.

doi: 10.1002/mus.24198.

Sudria-Lopez, E. *et al.* (2016) 'Full ablation of C9orf72 in mice causes immune system-related pathology and neoplastic events but no motor neuron defects', *Acta Neuropathologica*. Springer Berlin Heidelberg, 132(1), pp. 145–147. doi: 10.1007/s00401-016-1581-x.

Sullivan, P. M. *et al.* (2016) 'The ALS/FTLD associated protein C9orf72 associates with SMCR8 and WDR41 to regulate the autophagy-lysosome pathway', *Acta Neuropathologica Communications*, 4(1), p. 51. doi: 10.1186/s40478-016-0324-5.

Supplie, L. M. *et al.* (2017) 'Respiration-deficient astrocytes survive as glycolytic cells in vivo', *Journal of Neuroscience*, 37(16), pp. 4231–4242. doi: 10.1523/JNEUROSCI.0756-16.2017.

Swinnen, B. *et al.* (2018) 'A zebrafish model for C9orf72 ALS reveals RNA toxicity as a pathogenic mechanism', *Acta Neuropathologica*, 135(3), pp. 427–443. doi: 10.1007/s00401-017-1796-5.

Swinnen, B. and Robberecht, W. (2014) 'The phenotypic variability of amyotrophic lateral sclerosis', *Nature Reviews Neurology*. Nature Publishing Group, 10(11), pp. 661–670. doi: 10.1038/nrneurol.2014.184.

Talbot, K. (2009) 'Motor neuron disease', *Practical Neurology*, 9(5), pp. 303–309. doi: 10.1136/jnnp.2009.188151.

Taylor, J. P., Brown, R. H. and Cleveland, D. W. (2016) 'Decoding ALS: From genes to mechanism', *Nature*, 539(7628), pp. 197–206. doi: 10.1038/nature20413.

Tefera, T. W. and Borges, K. (2016) 'Metabolic Dysfunctions in Amyotrophic Lateral Sclerosis Pathogenesis and Potential Metabolic Treatments.', *Frontiers in neuroscience*. Switzerland, 10, p. 611. doi: 10.3389/fnins.2016.00611.

Teuling, E. *et al.* (2008) 'A novel mouse model with impaired dynein/dynactin function

develops amyotrophic lateral sclerosis (ALS)-like features in motor neurons and improves lifespan in SOD1-ALS mice', *Human Molecular Genetics*, 17(18), pp. 2849–2862. doi: 10.1093/hmg/ddn182.

Therrien, M. *et al.* (2013) 'Deletion of C9ORF72 results in motor neuron degeneration and stress sensitivity in C. elegans', *PLoS ONE*, 8(12), pp. 1–10. doi: 10.1371/journal.pone.0083450.

Tong, J. *et al.* (2013) 'Expression of ALS-linked TDP-43 mutant in astrocytes causes non-cell-autonomous motor neuron death in rats', *EMBO Journal*, 32(13), pp. 1917–1926. doi: 10.1038/emboj.2013.122.

Tosolini, A. P. and Sleigh, J. N. (2017) 'Motor neuron gene therapy: Lessons from spinal muscular atrophy for amyotrophic lateral sclerosis', *Frontiers in Molecular Neuroscience*, 10(December):405. doi: 10.3389/fnmol.2017.00405.

Tran, A. P. *et al.* (2020) 'Regulation of Autophagy by inhibitory CSPG interactions with Receptor PTPσ and its Impact on Plasticity and Regeneration after Spinal Cord Injury', 328, pp. 1–25. doi: 10.1016/j.expneurol.2020.113276.Regulation.

Tran, A. P. *et al.* (2018) 'The Biology of Regeneration Failure and Success After Spinal Cord Injury', *Physiol Rev*, 98(2), pp. 881-917. doi: 10.1016/j.expneurol.2020.113276.

Tran, C. H. T., Peringod, G. and Gordon, G. R. (2018) 'Astrocytes Integrate Behavioral State and Vascular Signals during Functional Hyperemia', *Neuron*. Elsevier Inc., 100(5), pp. 1133-1148.e3. doi: 10.1016/j.neuron.2018.09.045.

Tripathi, P. *et al.* (2017) 'Reactive Astrocytes Promote ALS-like Degeneration and Intracellular Protein Aggregation in Human Motor Neurons by Disrupting Autophagy through TGF-β1', *Stem Cell Reports*. ElsevierCompany, 9(2), pp. 667–680. doi: 10.1016/j.stemcr.2017.06.008.

Ullian, E. *et al.* (2001) 'Control of Synapse Number by Glia', *Science*, 291, pp. 657-61. doi: 10.1126/science.291.5504.657.

Umoh, M. E. *et al.* (2016) 'Comparative analysis of C9orf72 and sporadic disease in an ALS clinic population', *Neurology*, 87(10), pp. 1024–1030. doi: 10.1212/WNL.0000000000003067.

Varcianna, A. *et al.* (2019) 'Micro-RNAs secreted through astrocyte-derived extracellular vesicles cause neuronal network degeneration in C9orf72 ALS', *EBioMedicine*. Elsevier B.V., 40, pp. 626–635. doi: 10.1016/j.ebiom.2018.11.067.

Vasile, F., Dossi, E. and Rouach, N. (2017) 'Human astrocytes: structure and functions in the healthy brain', *Brain Structure and Function*. Springer Berlin Heidelberg, 222(5), pp. 2017–2029. doi: 10.1007/s00429-017-1383-5.

Vasta, R. *et al.* (2022) 'Unraveling the complex interplay between genes, environment, and climate in ALS', *eBioMedicine*, 75, pp. 1–12. doi: 10.1016/j.ebiom.2021.103795.

Vatsavayai, S. C. *et al.* (2016) 'Timing and significance of pathological features in C9orf72 expansion-associated frontotemporal dementia', *Brain*, 139(12), pp. 3202–3216. doi: 10.1093/brain/aww250.

Verkhratsky, A. and Nedergaard, M. (2018) 'Physiology of astroglia', *Physiological Reviews*, 98(1), pp. 239–389. doi: 10.1152/physrev.00042.2016.

Victor, M. B. *et al.* (2018) 'Striatal neurons directly converted from Huntington's disease patient fibroblasts recapitulate age-associated disease phenotypes', *Nature Neuroscience*. Springer US, 21(3), pp. 341–352. doi: 10.1038/s41593-018-0075-7.

Volkenhoff, A. *et al.* (2015) 'Glial glycolysis is essential for neuronal survival in drosophila', *Cell Metabolism*, 22(3), pp. 437–447. doi: 10.1016/j.cmet.2015.07.006.

De Vos, K. J. and Hafezparast, M. (2017) 'Neurobiology of axonal transport defects in motor neuron diseases: Opportunities for translational research?', *Neurobiology of Disease*, 105, pp. 283–299. doi: 10.1016/j.nbd.2017.02.004.

Wang, B., Guo, W. T. and Huang, Y. (2012) 'Thrombospondins and synaptogenesis',

Neural Regeneration Research, 7(22), pp. 1737–1743. doi: 10.3969/j.issn.1673-5374.
Wang, L., Gutmann, D. H. and Roos, R. P. (2011) 'Astrocyte loss of mutant SOD1 delays ALS disease onset and progression in G85R transgenic mice', *Human Molecular Genetics*, 20(2), pp. 286–293. doi: 10.1093/hmg/ddq463.

Wang, R., Yang, B. and Zhang, D. (2011) 'Activation of interferon signaling pathways in spinal cord astrocytes from an ALS mouse model', *Glia*, 59(6), pp. 946–958. doi: 10.1002/glia.21167.

Wang, T. *et al.* (2021) 'C9orf72 regulates energy homeostasis by stabilizing mitochondrial complex I assembly', *Cell Metabolism*. Elsevier Inc., 33(3), pp. 531-546.e9. doi: 10.1016/j.cmet.2021.01.005.

Wang, W. *et al.* (2013) 'The ALS disease-associated mutant TDP-43 impairs mitochondrial dynamics and function in motor neurons', *Human Molecular Genetics*, 22(23), pp. 4706–4719. doi: 10.1093/hmg/ddt319.

Wang, X. and Gerdes, H. H. (2015) 'Transfer of mitochondria via tunneling nanotubes rescues apoptotic PC12 cells', *Cell Death and Differentiation*. Nature Publishing Group, 22(7), pp. 1181–1191. doi: 10.1038/cdd.2014.211.

Warburg, O. (1956) 'On the origin of cancer cells', *Science*, 123(3191), pp. 309-314. doi: 10.1126/science.123.3191.309.

Webster, C. P. *et al.* (2016) ' The C9orf72 protein interacts with Rab1a and the ULK 1 complex to regulate initiation of autophagy ', *The EMBO Journal*, 35(15), pp. 1656–1676. doi: 10.15252/embj.201694401.

Westergard, T. *et al.* (2016) 'Cell-to-Cell Transmission of Dipeptide Repeat Proteins Linked to C9orf72-ALS/FTD', *Cell Reports*, 17(3), pp. 645–652. doi: 10.1016/j.celrep.2016.09.032.

Wiese, S. *et al.* (2010) 'Isolation and enrichment of embryonic mouse motoneurons from the lumbar spinal cord of individual mouse embryos', *Nature Protocols*, 5(1), pp.

31–38. doi: 10.1038/nprot.2009.193.
Williams, T.L. (2013) 'Motor neurone disease: diagnostic pitfalls' *Clin Med (Lond)*, 13(1), pp. 97-100. doi: 10.7861/clinmedicine.13-1-97.

Williamson, T. L. and Cleveland, D. W. (1999) 'Slowing of axonal transport is a very early event in the toxicity of ALS-linked SOD1 mutants to motor neurons', *Nature Neuroscience*, 2(1), pp. 50–56. doi: 10.1038/4553.

Wong, C. *et al.* (2021) 'Clinical trials in amyotrophic lateral sclerosis: a systematic review and perspective', *Brain Communications*, 3(4):fcab242. doi: 10.1093/braincomms/fcab242.

Wu, D. and Smyth, G. K. (2012) 'Camera: A competitive gene set test accounting for inter-gene correlation', *Nucleic Acids Research*, 40(17), pp. 1–12. doi: 10.1093/nar/gks461.

Wu, Z. *et al.* (1999) 'Mechanisms controlling mitochondrial biogenesis and respiration through the thermogenic coactivator PGC-1', *Cell*, 98(1), pp. 115–124. doi: 10.1016/S0092-8674(00)80611-X.

Xi, Z. *et al.* (2015) 'The C9orf72 repeat expansion itself is methylated in ALS and FTLD patients', *Acta Neuropathologica*, 129(5), pp. 715–727. doi: 10.1007/s00401-015-1401-8.

Xiao, S. *et al.* (2015) 'Isoform-specific antibodies reveal distinct subcellular localizations of C9orf72 in amyotrophic lateral sclerosis', *Annals of Neurology*, 78(4), pp. 568–583. doi: 10.1002/ana.24469.

Xu, Z. *et al.* (2013) 'Expanded GGGGCC repeat RNA associated with amyotrophic lateral sclerosis and frontotemporal dementia causes neurodegeneration', *Proceedings of the National Academy of Sciences of the United States of America*, 110(19), pp. 7778–7783. doi: 10.1073/pnas.1219643110.

Yamanaka, K. *et al.* (2008) 'Mutant SOD1 in cell types other than motor neurons and

oligodendrocytes accelerates onset of disease in ALS mice', *Proceedings of the National Academy of Sciences of the United States of America*, 105(21), pp. 7594–7599. doi: 10.1073/pnas.0802556105.

Yamanaka, K. and Komine, O. (2018) 'The multi-dimensional roles of astrocytes in ALS', *Neuroscience Research*, 126, pp. 31–38. doi: 10.1016/j.neures.2017.09.011.

Yang, M. *et al.* (2016) 'A C9ORF72/SMCR8-containing complex regulates ULK1 and plays a dual role in autophagy', *Science Advances*, 2(9), pp. 1–18. doi: 10.1126/sciadv.1601167.

Yang, Q., Jiao, B. and Shen, L. (2020) 'The Development of C9orf72-Related Amyotrophic Lateral Sclerosis and Frontotemporal Dementia Disorders', *Frontiers in Genetics*, 11(September), pp. 1–11. doi: 10.3389/fgene.2020.562758.

Yi, M., Weaver, D. and Hajnóczky, G. (2004) 'Control of mitochondrial motility and distribution by the calcium signal: A homeostatic circuit', *Journal of Cell Biology*, 167(4), pp. 661–672. doi: 10.1083/jcb.200406038.

Zala, D. *et al.* (2013) 'Vesicular glycolysis provides on-board energy for fast axonal transport', *Cell*, 152(3), pp. 479–491. doi: 10.1016/j.cell.2012.12.029.

Zhang, K. *et al.* (2015) 'The C9orf72 repeat expansion disrupts nucleocytoplasmic transport', *Nature*, 525(7567), pp. 56–61. doi: 10.1038/nature14973.

Zhang, K. *et al.* (2018) 'Stress Granule Assembly Disrupts Nucleocytoplasmic Transport', *Cell*. Elsevier Inc., 173(4), pp. 958-971.e17. doi: 10.1016/j.cell.2018.03.025.

Zhang, X. H. *et al.* (2015) 'Off-target effects in CRISPR/Cas9-mediated genome engineering', *Molecular Therapy - Nucleic Acids*. Official Journal of the American Society of Gene & Cell Therapy, 4(11): e264. doi: 10.1038/mtna.2015.37.

Zhang, Y. *et al.* (2014) 'An RNA-sequencing transcriptome and splicing database of

glia, neurons, and vascular cells of the cerebral cortex', *Journal of Neuroscience*, 34(36), pp. 11929–11947. doi: 10.1523/JNEUROSCI.1860-14.2014.

Zhang, Y. J. *et al.* (2014) 'Aggregation-prone c9FTD/ALS poly(GA) RAN-translated proteins cause neurotoxicity by inducing ER stress', *Acta Neuropathologica*, 128(4), pp. 505–524. doi: 10.1007/s00401-014-1336-5.

Zhang, Y. J. *et al.* (2018) 'Poly(GR) impairs protein translation and stress granule dynamics in C9orf72-associated frontotemporal dementia and amyotrophic lateral sclerosis', *Nature Medicine*. Springer US, 24(8), pp. 1136–1142. doi: 10.1038/s41591-018-0071-1.

Zhao, C. *et al.* (2020) 'Mutant C9orf72 human iPSC-derived astrocytes cause non-cell autonomous motor neuron pathophysiology', *GLIA*, 68(5). doi: 10.1002/glia.23761.

Zhou, Y. *et al.* (2020) 'Human and mouse single-nucleus transcriptomics reveal TREM2-dependent and TREM2-independent cellular responses in Alzheimer's disease', *Nature Medicine*, 26(1), pp. 131-142 doi: 10.1038/s41591-019-0695-9.

Zhu, W., Smith, J. W. and Huang, C. M. (2010) 'Mass spectrometry-based label-free quantitative proteomics', *Journal of Biomedicine and Biotechnology*, 2010: 840518. doi: 10.1155/2010/840518.

Zu, T. *et al.* (2013) 'RAN proteins and RNA foci from antisense transcripts in C9ORF72 ALS and frontotemporal dementia', *Proceedings of the National Academy of Sciences of the United States of America*, 110(51), pp. E4968-4977. doi: 10.1073/pnas.1315438110.